General Disclaimer

One or more of the Following Statements may affect this Document

- This document has been reproduced from the best copy furnished by the organizational source. It is being released in the interest of making available as much information as possible.

- This document may contain data, which exceeds the sheet parameters. It was furnished in this condition by the organizational source and is the best copy available.

- This document may contain tone-on-tone or color graphs, charts and/or pictures, which have been reproduced in black and white.

- This document is paginated as submitted by the original source.

- Portions of this document are not fully legible due to the historical nature of some of the material. However, it is the best reproduction available from the original submission.

NASA CR 137578

THEORETICAL PREDICTION OF THICK WING AND PYLON-FUSELAGE-FANPOD-NACELLE AERODYNAMIC CHARACTERISTICS AT SUBCRITICAL SPEEDS

PART I - THEORY AND RESULTS

By J.R. Tulinius

July 24, 1974

Prepared under Contract No. NAS2-7904 by

LOS ANGELES AIRCRAFT DIVISION
ROCKWELL INTERNATIONAL
International Airport
Los Angeles, California 90009

for

AMES RESEARCH CENTER
NATIONAL AERONAUTICS AND SPACE ADMINISTRATION

NASA CR 137578

ERRATA SHEET

PAGE

42. THIRD SENTENSE - REMOVE PERIOD AFTER " APPENDIX F "

50 THIRD PARAGRAPH — REMOVE LAST SENTENSE, ENDING WITH " EQUATIONS 137 AND 138."

80 REMOVE " , SQ FT " AFTER " AREA"

156 THE EQUATION JUST AHEAD OF EQUATION (5) SHOULD READ:

$$\hat{N}(\infty A' Q) = \left\{ \frac{z^*}{\sqrt{\quad}} \right\} \hat{j} - \left\{ \frac{y^* + y_T}{\sqrt{\quad}} \right\} \hat{k}_w$$

(ADD THE $\hat{j}$)

NASA CR 137578

THEORETICAL PREDICTION OF THICK WING AND PYLON-FUSELAGE-FANPOD-NACELLE AERODYNAMIC CHARACTERISTICS AT SUBCRITICAL SPEEDS

PART I - THEORY AND RESULTS

By J.R. Tulinius

July 24, 1974

Prepared under Contract No. NAS2-7904 by

LOS ANGELES AIRCRAFT DIVISION
ROCKWELL INTERNATIONAL
International Airport
Los Angeles, California 90009

for

AMES RESEARCH CENTER
NATIONAL AERONAUTICS AND SPACE ADMINISTRATION

TABLE OF CONTENTS

THEORETICAL PREDICTION OF THICK WING AND PYLON-FUSELAGE-FANPOD-NACELLE AERODYNAMIC CHARACTERISTICS AT SUBCRITICAL SPEEDS

PART I - THEORY AND RESULTS

By J.R. Tulinius
Los Angeles Aircraft Division
Rockwell International

SUMMARY

This report describes the theoretical development and the comparison of results with data of a thick wing and pylon-fuselage-fanpod-nacelle analysis. The analysis utilizes potential flow theory to compute the surface velocities and pressures, section lift and center of pressure, and the total configuration lift, moment, and vortex drag. The skin friction drag is also estimated in the analysis.

The perturbation velocities induced by the wing and pylon, fuselage and fanpod, and nacelle are represented by source and vortex lattices, quadrilateral vortices, and source frustums, respectively. The strengths of these singularities are solved for simultaneously including all interference effects.

The wing and pylon planforms, twists, cambers, and thickness distributions, and the fuselage and fanpod geometries can be arbitrary in shape, provided the surface gradients are smooth. The flow through nacelle is assumed to be axisymmetric. An axisymmetric center engine hub can also be included. The pylon and nacelle can be attached to the wing, fuselage, or fanpod.

The wing can have both leading and trailing edge plain flaps of either the full or partial span type. Subcritical compressibility is accounted for by means of the second order correction developed by Labrujere.

INTRODUCTION

In order to improve the cruise efficiency of V/STOL aircraft with fanpods, pylons, and nacelles it is necessary to locally shape the configuration to minimize component induced adverse pressure gradients which cause premature shock induced separation. The wing-fanpod juncture must be contoured to minimize fanpod on wing interference. Also, the nacelle and pylon must be located such as to minimize pylon and nacelle interference on the wing and fanpod. If the surface velocities and pressure coefficients can be computed, with all interference effects included, then the optimum location and shape of the pylon, fanpod, and nacelle can be determined.

In this analysis the surface velocities and pressure coefficients are computed for a thick wing and pylon-fuselage-fanpod-nacelle combination. The wing and pylon induced flow fields are represented by source and vortex lattices. The source lattice induces flow due to airfoil thickness and the vortex lattice induces flow due to lift. The flow induced by the wing and pylon thickness can be computed directly since the source lattices are placed on the chordal planes, which allows the source strengths to be defined by the local slopes of the distribution of wing and pylon thickness. The wing and pylon vortex strengths, however, must be determined simultaneously along with the quadrilateral vortex strengths for the fanpod and fuselage and the source frustum strengths for the nacelle.

In order to determine the wing, pylon, fuselage, and fanpod vortex strengths and the nacelle source frustum strengths a system of aerodynamic influence equations is developed and solved. The equations are developed by computing the amount of velocity induced by each of the vortices and source frustums, of unit strength, normal to the surface of each component at a series of control points. This set of influence equations is reduced in size by constraining the strengths of the vortices in the chordwise direction by a vorticity series. The equations are then solved by partitioning the matrix into two sets of equations: 1) that due to the vortex strengths, which is overdetermined, and therefore solved by a least squares technique and 2) that due to the source frustums. Both inversions in the solution of these two sets of simultaneous equations are done by Householder's procedure. The program has options which allow the smaller interference influence matrices to be neglected in the solution, in order to save computer time. If these influence matrices are to be neglected they are neither computed nor manipulated in the solution of the influence equations.

In this analysis advantage is taken of the similarities between the source and vortex induced flow fields. The influence equations for the source and vortex lattices have been formulated in terms of the same expressions. This permits the velocity induced by the source lattice and that induced by the vortex lattice to be computed and summed simultaneously, saving approximately 50 percent of the computing time that would otherwise be required to calculate the wing and pylon influence matrices. Also, since quadrilateral vortices are used on the fanpod and fuselage, it was possible to neglect the contribution of those vortices which are more than a given distance from a control point. The induced flow from a quadrilateral vortex decreases rapidly

as the control point is moved away from the vortex. This is due to the cancelling effect of adjacent parallel sides. The induced flow decreases proportional to $(\frac{\Delta}{r})^2$ where Δ is the perpendicular distance between two adjacent parallel sides and r is the distance between the centroid of the vortex and the control point. A similar effect is obtained in the spanwise direction on the wing and pylon due to the cancelling effect of adjacent trailing vortex legs. Because of these effects, limits were put into the program which define the significant area of influence of a vortex element and contributions are computed only for those control points which fall within this area of influence. The limits are given as input data. This concept has produced a considerable savings of computer time with no significant change in accuracy.

LIST OF SYMBOLS

A consistant set of units is assumed throughout this report except for the skin friction drag equations derived in Appendix K, which assumes the units specified in that appendix.

A	Aerodynamic influence matrix
A	Incremental area
α	Angle of attack
b	Span
β	Pylon angle of cant or compressibility factor
C	Chord
C_d	Section drag coefficient
C_D	Total drag coefficient
C_ℓ	Section lift coefficient
C_L	Total lift coefficient
C_N	Section normal force coefficient
C_m	Section pitching moment coefficient
C_M	Total pitching moment coefficient
C_P	Pressure coefficient
γ	Vorticity, ratio of specific heats, or pylon dihedral angle
ΔS	Fanpod, fuselage, or root section vortex grid length or width
∇S	Freestream plus source lattice flow normal to component surface
E	Influence function
F	Wing or pylon chordwise vorticity series coefficient
h	Pylon height

Θ	Fanpod or fuselage polar angle measured from the X-Z plane about the X axis. The positive direction is clockwise when looking from the fanpod tail end to the nose.
K	Discrete vortex strength
M_∞	Freestream Mach number
$\vec{N}$	Unit vector normal to surface
N_i	Number of vortices and sources in chordwise direction on the wing or pylon
N_u	Number of terms in the chordwise vorticity series on the wing or pylon
η	$2Y_W/b_W$ or Y_P/h
P	Special spanwise load shape or $\sqrt{1+\frac{1}{2}\cos^2\phi}$
ϕ	Chordwise polar coordinate equal to $\cos^{-1}(1-2x/c)$ or sweep angle
S	Influence matrix due to source lattice
σ	Surface source strength
$\vec{T}$	Unit vector tangent to surface
u	Perturbation velocity in X direction
V	Total velocity
V_∞	Freestream velocity
v	Perturbation velocity in Y direction
W	Perturbation velocity in Z direction or width
y_s	Spanwise source lattice spacing
y_v	Spanwise vortex lattice spacing
Z_c	Camber line ordinate
Z_t	Wing or pylon thickness

AR	Aspect ratio b^2/S_w
δ	Flap deflection
ϵ	Wing twist
ϕ_w	Local sweepback angle of constant % chordlines
	Velocity components in equations (129) through (138)
$v_{m_{www}}$	Total surface perturbation velocity in chordwise direction including lift and thickness interaction
$v_{T_{www}}$	Total surface perturbation velocity in spanwise direction including lift and thickness interactions
u_{w_L}	Chordwise component of perturbation velocity due to lift
v_{w_L}	Spanwise component of perturbation velocity due to lift
u_{w_T}	Chordwise component of perturbation velocity due to thickness
u'_{w_T}	Additional thickness perturbation velocity term which does influence lift
v_{w_T}	Spanwise component of perturbation velocity due to thickness
v'_{w_T}	Additional thickness perturbation velocity term which does influence lift

Subscript	Definition
B	Fuselage
BB	Fuselage on fuselage
BF	Fanpod on fuselage
BN	Nacelle on fuselage
BP	Pylon on fuselage
BW	Wing on fuselage
C	Chord or camber
F	Fanpod
f	Flap
FB	Fuselage on fanpod
FF	Fanpod on fanpod
FN	Nacelle on fanpod
FP	Pylon on fanpod
FW	Wing on fanpod
i	Source or vortex location in chordwise direction, inboard lattice panel, or incompressible coordinate.
∞	Freestream direction
J	Control point location
NF	Fanpod on nacelle
NN	Nacelle on nacelle
NP	Pylon on nacelle
NW	Wing on nacelle
PF	Fanpod on pylon
PN	Nacelle on pylon
PP	Pylon on pylon

PW	Wing on pylon
WF	Fanpod on wing
WN	Nacelle on wing
WP	Pylon on wing
WW	Wing on wing
K	Leading edge flap or span location index
L	Spanwise location of source or vortex
L.E.	Leading edge
M	Longitudinal direction
N	Nacelle, normal direction, chordwise load shape
O	Outboard lattice panel
P	Pylon
T	Lateral direction
t	Thickness
u	X direction perturbation velocity
v	Y direction perturbation velocity
w	Z direction perturbation velocity
(X_F, Y_F, Z_F)	Fanpod coordinate system
(X_N, Y_N)	Nacelle coordinate system
(X_P, Y_P, Z_P)	Pylon coordinate system
(X_W, Y_W, Z_W)	Wing coordinate system
(X_B, Y_B, Z_B)	Fuselage coordinate system

CONFIGURATION REPRESENTATION

The theory discussed in this report is capable of predicting surface velocities and static pressure coefficients, section loads, and total loads and moments for a configuration of the type shown in figure 1.

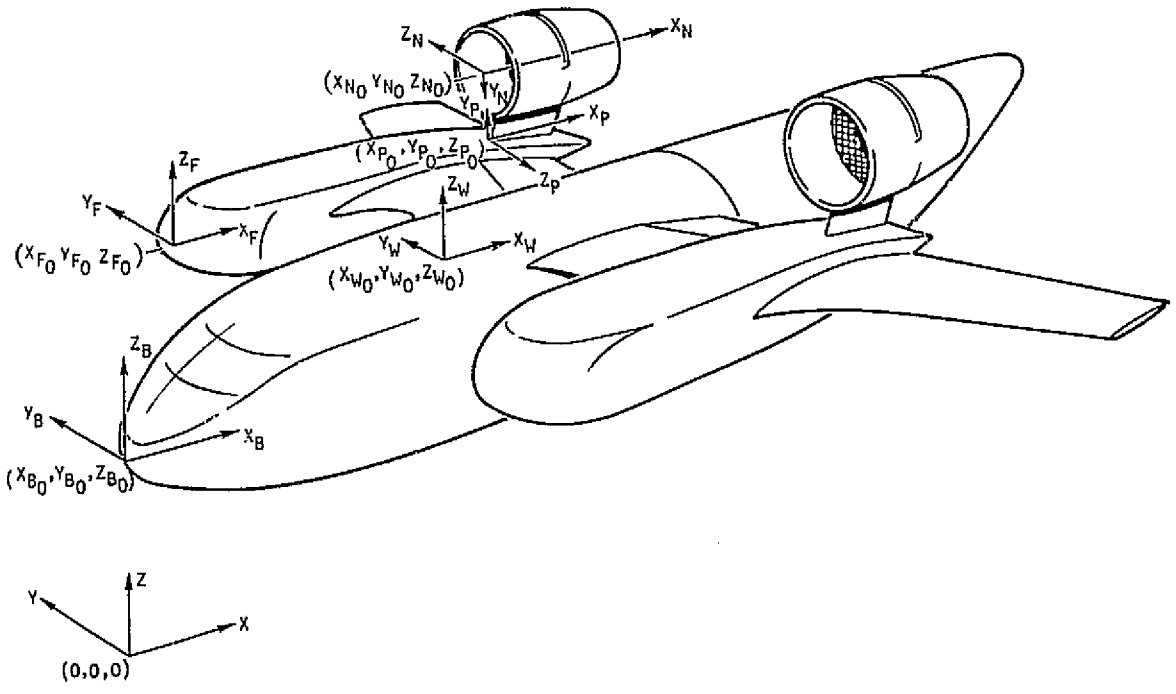

Figure 1. Thick Wing and Pylon-Fuselage-Fanpod-Nacelle Configuration

In general, the fanpod and fuselage can be arbitrary in shape. The fanpod can be placed anywhere on the wing except at the wing tip. The fanpod and fuselage do not have to have straight juncture lines where the wing and pylon are attached. This allows the fanpod and fuselage to be shaped in any desired manner, in the juncture region, to produce a favorable induced effect on the wing and pylon. In order to do this the wing and pylon have been divided into two sections; the basic wing or pylon panel and the root section. The basic wing or pylon panel is assumed to be near planar.

The root section is a transition region from the basic panel to the juncture line where the wing or pylon is attached.

The wing and pylon can be arbitrary in planform shape and can have any desired twist, camber, and thickness distribution. The wing can have either full or partial span leading or trailing edge flaps.

The nacelle is assumed to be axisymmetric and is attached to the pylon. A center engine hub can also be included with the nacelle. Also, different mass flow ratios can be simulated by blocking different amounts of flow going through the nacelle.

The perturbation velocity induced by the fanpod and fuselage is produced by a grid of quadrilateral vortices on the external surface of the fanpod and fuselage. A quadrilateral vortex is a line vortex of constant strength bent into the shape of a quadrilateral. As shown in figure 2 vortex lines are placed both collinear with and perpendicular to meridian lines. The strengths of these lines are assumed to be constant around each of the quadrilaterals formed by the intersection of longitudinal and lateral grid lines. The strength of any one vortex segment is equal to the sum of the strengths of the two adjacent quadrilateral vortices. The direction of the circulation due to a vortex segment is defined by the right hand rule when applied about the segment. The positive direction is assumed to be clockwise around the perimeter of the quadrilateral when looking at its external surface.

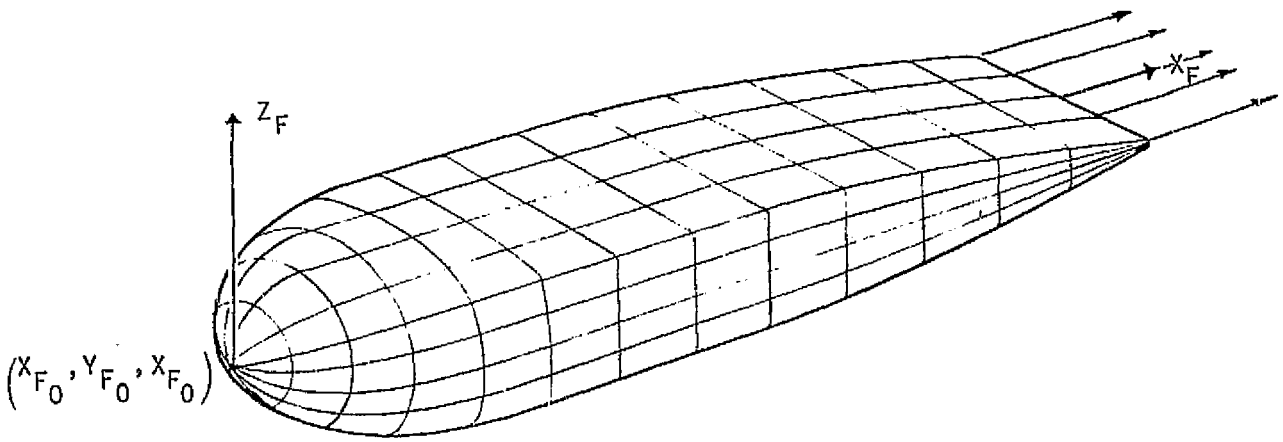

Figure 2. Fanpod Quadrilateral Vortex Grid

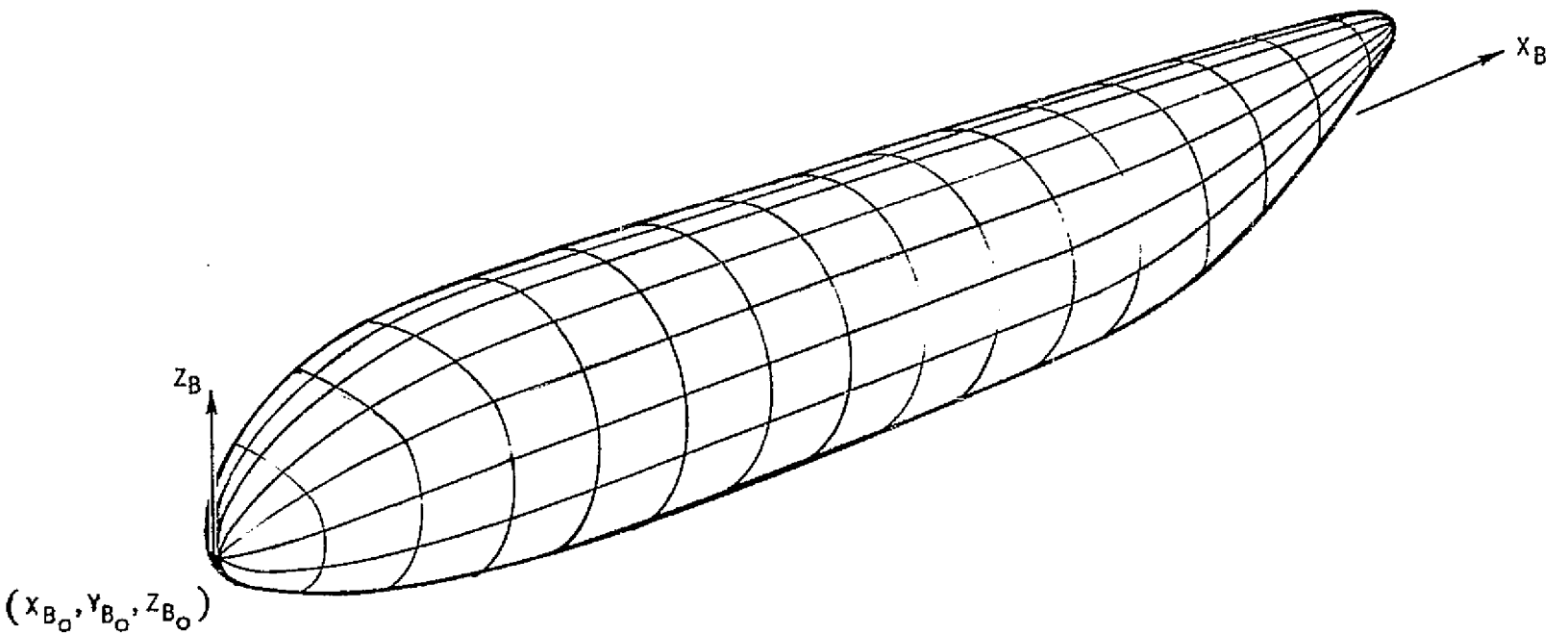

Figure 3. Fuselage Quadrilateral Vortex Grid

The flow induced by the basic panels of the wing and pylon is produced by source and vortex lattices placed on the wing and pylon chordal planes. As shown in figures 3 and 4 the bound vortex and source lines are skewed and collinear with each other. The trailing vortex lines are in the free-stream direction. The bound vortex and source lines are spaced at equal increments of Θ_w or Θ_p, where $\Theta_w = \cos^{-1}[1 - 2(x_w - x_{w_{L.E.}})/c_w]$ and $\Theta_p = \cos^{-1}[1 - 2(x_p - x_{p_{L.E.}})/c_p]$. This type of spacing places more singularities near the leading edge where the source and vortex strengths vary most rapidly. The trailing vortex lines are evenly spaced.

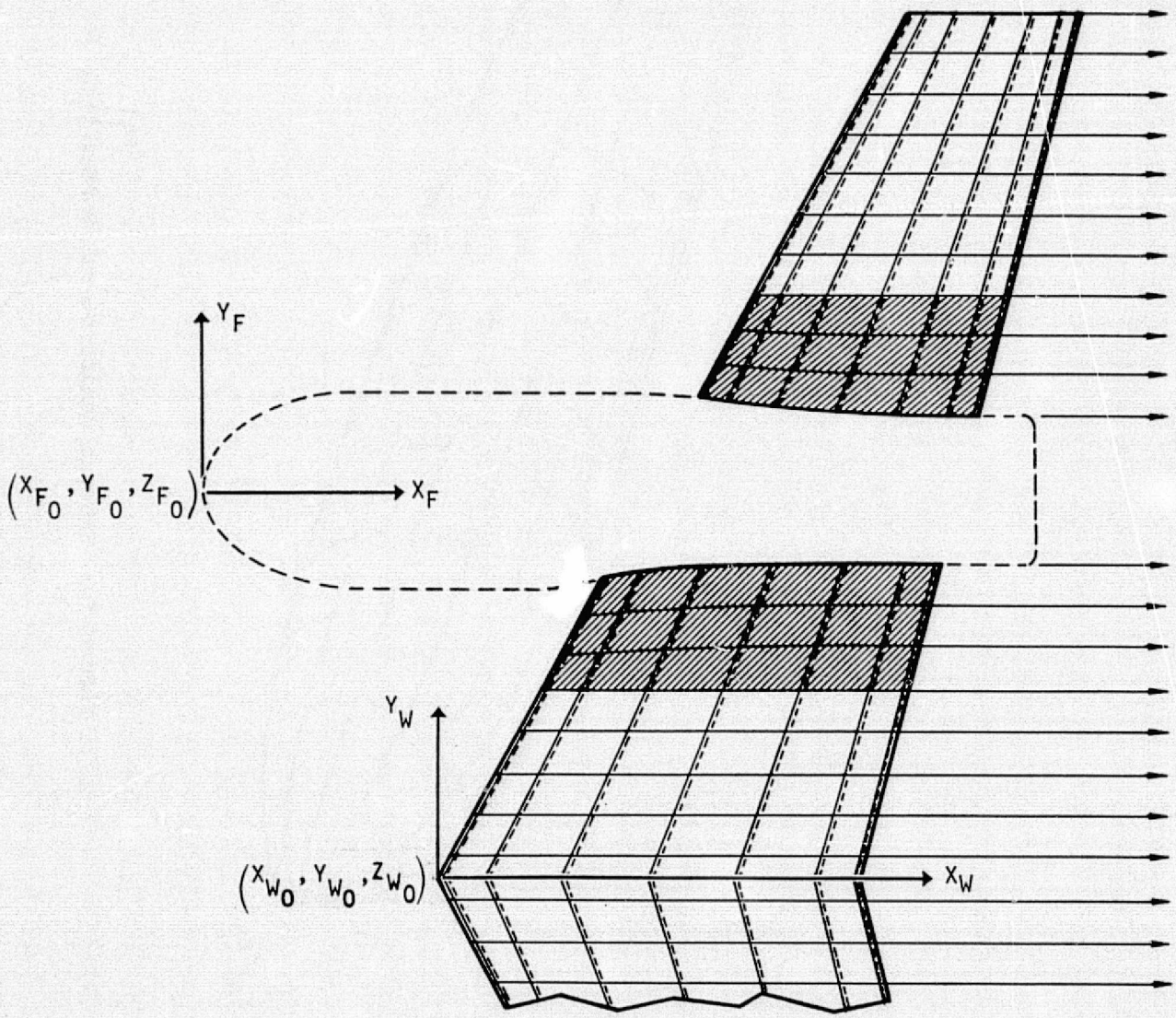

Figure 4. Wing Source-Vortex Lattice

The flow induced by the wing and pylon root sections is produced by quadrilateral vortices and skewed source lines. As with the basic panel, the vortex and source lines produce flows which are antisymmetric and symmetric about the mean camber surface, respectively. The antisymmetric flow represents the solution due to lift and the symmetric flow represents that due to thickness. The quadrilateral vortices in the root section are formed by the intersection of lines equally spaced between the juncture line and the basic panel, and lines spaced at equal increments of Θ_W or Θ_P in the chordwise direction. The skewed source lines are collinear with the bound vortex lines as in the basic panel.

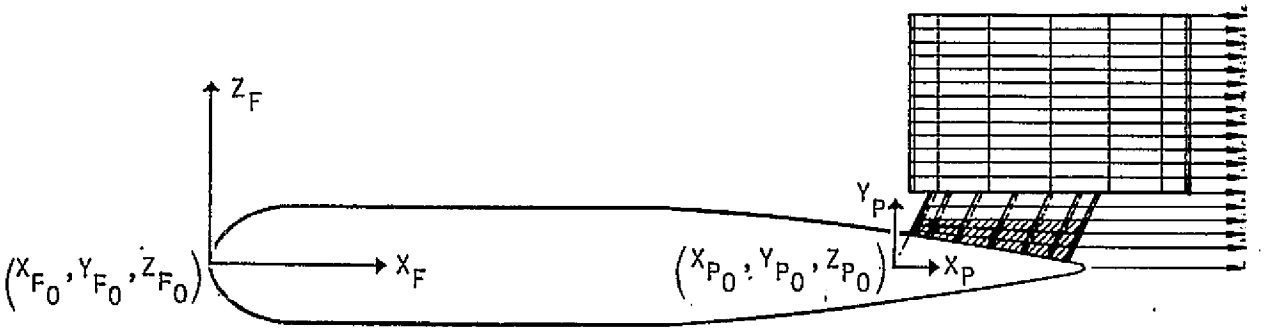

Figure 5. Pylon Source-Vortex Lattice

The pylon vortex lattice extends up into the nacelle in order to satisfy the boundary condition of no cross flow through the nacelle. This is necessary since the nacelle is assumed to be axisymmetric, which makes it possible to satisfy the nacelle boundary conditions at only one lateral station. These are satisfied at the lateral station closest to the surface where the pylon is attached, to ensure the best possible representation of the nacelle interference within the axisymmetric nacelle assumption.

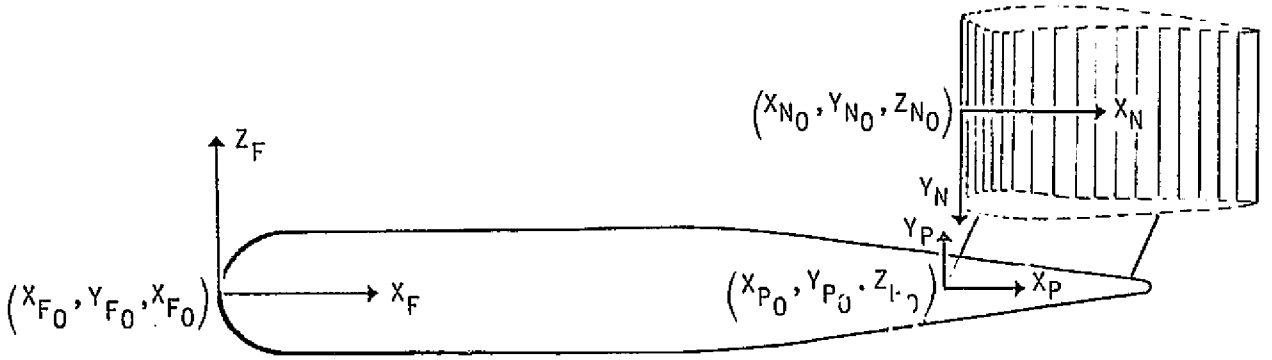

Figure 6. Flow Through Nacelle Source Frustum Representation

The nacelle induced flow is produced by a distribution of source frustums as shown in figure 6. The frustums are distributed around the inner and outer surfaces of a flow through nacelle or over the external surface of any desired axisymmetric shape. A center engine hub or other body used to block mass flow can also be represented by source frustums along with the nacelle.

INFLUENCE EQUATIONS

Each of the skewed sources, source frustums, quadrilateral vortices, and skewed vortices induce flow at control points distributed over the surface of the thick wing and pylon-fuselage-fanpod-nacelle configuration. Their strengths are solved for simultaneously such that the flow induced by them plus the freestream, is a minimum normal to the configuration surface at the control points. In order to obtain the singularity strengths a set of aerodynamic influence equations is developed by computing the flow induced normal to the surface at each control point due to a unit strength of each singularity. These are then multiplied by their respective unknown coefficients, summed along with the component of freestream velocity normal to the surface, and set equal to zero at each control point. This results in a system of equations where the number of unknowns are equal to the number of singularities and the number of equations are equal to the number of control points.

The number of unknowns can be reduced by constraining the singularity strengths by a set of finite series. When this is done, the number of unknowns becomes equal to the number of terms in the series times the number of series used. In this analysis the skewed vortices on the wing and pylon and the quadrilateral vortices on the fuselage and the fanpod are constrained in the chordwise direction. Also, there is the option of constraining the skewed vortices in the spanwise direction on the wing. When these singularity strengths are constrained the aerodynamic influence equations described above are linearly transformed such that the unknowns are then the coefficients of the terms in the finite series. This results in a system of equations which is overdetermined. The equations are solved using a least squares technique.

WING ON WING

The influence of the wing on itself is divided into two parts; the influence of the vortices and the influence of the sources. The sources are assumed to lie on a plane and can therefore only produce velocity normal to that plane at their respective locations. Because of this fact, the wing sources cannot affect the strength of each other nor can they affect the strength of the wing vortices. Their influence can therefore be omitted from the wing on wing influence equations.

The velocity induced by the wing vortices normal to the wing mean camber surface is given by;

$$\left\{\frac{V_{W_{WW}}}{V_\infty}\right\} = \left[N_{W_{X_W}} A_{WW_{X_W}} + N_{W_{Y_W}} A_{WW_{Y_W}} + N_{W_{Z_W}} A_{WW_{Z_W}}\right]\left\{\frac{K_W}{V_\infty}\right\} \qquad (1)$$

Where $N_{W_{X_W}}$ and $N_{W_{Z_W}}$ are defined in the following sketch.

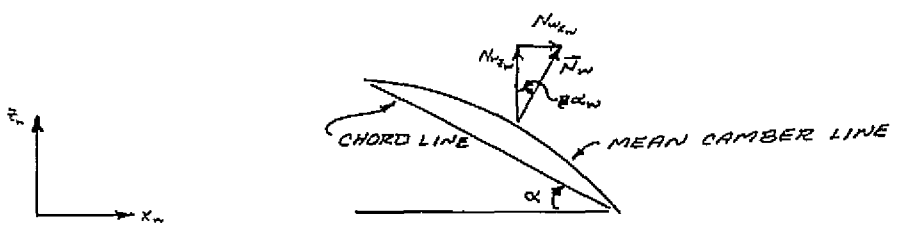

The local angle α_W is assumed small and the wing dihedral zero, so that, $N_{W_{X_W}} = \alpha_W$, $N_{W_{Y_W}} = 0$ and $N_{W_{Z_W}} \approx 1$.

Therefore;

$$\left\{\frac{V_{W_{WW}}}{V_\infty}\right\} = \left\{\left[\alpha_W\right]\left[A_{WW_{X_W}}\right] + \left[A_{WW_{Z_W}}\right]\right\}\left\{\frac{K_W}{V_\infty}\right\} \qquad (2)$$

Since; both α_W and $A_{WW_{X_W}}$ are small the product $\left[\alpha_W\right]\left[A_{WW_{X_W}}\right]$ will be omitted.

Therefore;

$$\left\{\frac{V_{W_{WW}}}{V_\infty}\right\} = \left[A_{WW_{Z_W}}\right]\left\{\frac{K_W}{V_\infty}\right\} \qquad (3)$$

The elements of $A_{WW_{Z_W}}$ are computed with equations for the velocity induced by skewed and quadrilateral vortices, defined in Appendices C and D, respectively.

FANPOD ON WING

The fanpod is represented by a grid of quadrilateral vortices on the fanpod surface. The velocity induced by the fanpod quadrilateral vortices normal to the wing mean camber surface is given by

$$\left\{\frac{V_{N_{WF}}}{V_\infty}\right\} = \left[N_{x_w} A_{WF_{x_w}} + N_{y_w} A_{WF_{y_w}} + N_{z_w} A_{WF_{z_w}} \right]\left\{\frac{K_F}{V_\infty}\right\} \tag{4}$$

The influence matrices $A_{WF_{z_w}}$, $A_{WF_{y_w}}$, and $A_{WF_{z_w}}$ are defined as:

$$\left[A_{WF_{x_w}}\right] = \left[\cos\beta\alpha_{FW}\right]\left[A_{WF_{x_F}}\right] + \left[\sin\beta\alpha_{FW}\right]\left[A_{WF_{z_F}}\right] \tag{5}$$

$$\left[A_{WF_{y_w}}\right] = \left[A_{WF_{y_F}}\right] \tag{6}$$

$$\left[A_{WF_{z_w}}\right] = -\left[\sin\beta\alpha_{FW}\right]\left[A_{WF_{x_F}}\right] + \left[\cos\beta\alpha_{FW}\right]\left[A_{WF_{z_F}}\right] \tag{7}$$

Where $\beta\alpha_{FW}$ is defined in the following sketch.

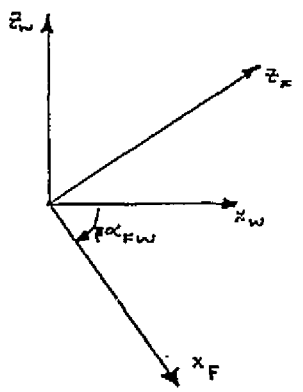

The angle α_{FW} and the matrix $A_{WF_{x_F}}$ are assumed small, so that $\cos\beta\alpha_{FW} \approx 1$, $\sin\beta\alpha_{FW} \approx \beta\alpha_{FW}$ and the product $\left[\sin\beta\alpha_{FW}\right]\left[A_{WF_{x_F}}\right]$ is omitted.

Therefore:

$$\left\{\frac{V_{N_{WF}}}{V_\infty}\right\} = \left\{\left[\beta\alpha_w\right]\left[A_{WF_{x_F}}\right] + \left[\beta\alpha_w\right]\left[\beta\alpha_{FW}\right]\left[A_{WF_{z_F}}\right] + \left[A_{WF_{z_F}}\right]\right\}\left\{\frac{K_F}{V_\infty}\right\} \tag{8}$$

In addition, since $[\beta\alpha_w]$, $[\beta\alpha_{FW}]$, and $[A_{WF_{x_F}}]$ are small, the products $[\beta\alpha_w][A_{WF_{x_F}}]$ and $[\beta\alpha_w][\beta\alpha_{FW}][A_{WF_{z_F}}]$ are omitted.

Therefore;

$$\left\{\frac{V_{N_{WF}}}{V_\infty}\right\} = \left[A_{WF_{z_F}}\right]\left\{\frac{k_F}{V_\infty}\right\} \tag{9}$$

The elements of $A_{WF_{z_F}}$ are computed with equations defined in Appendix D.

FUSELAGE ON WING

The influence equation for the fuselage on the wing is analogous to that for the fanpod on the wing. Therefore;

$$\left\{\frac{V_{N_{WB}}}{V_\infty}\right\} = \left[A_{WB_{z_B}}\right]\left\{\frac{k_B}{V_\infty}\right\} \tag{10}$$

The elements of $A_{WB_{z_B}}$ are computed with equations defined in Appendix D.

PYLON ON WING

The influence of the pylon on the wing is due to the vortex and source lattices on the pylons. The velocity induced by these lattices normal to the wing mean camber surface is given by;

$$\left\{\frac{V_{N_{WP}}}{V_\infty}\right\} = \left[N_{W_{x_W}} A_{WP_{x_W}} + N_{W_{y_W}} A_{WP_{y_W}} + N_{W_{z_W}} A_{WP_{z_W}}\right]\left\{\frac{k_P}{V_\infty}\right\}$$

$$+\left[N_{W_{x_W}} S_{WP_{x_W}} + N_{W_{y_W}} S_{WP_{y_W}} + N_{W_{z_W}} S_{WP_{z_W}}\right]\left\{\frac{\sigma_P}{V_\infty}\right\} \tag{11}$$

Where the matrices $A_{WP_{x_W}}$, $A_{WP_{y_W}}$, and $A_{WP_{z_W}}$ are due to the vortex influences and the matrices $S_{WP_{z_W}}$, $S_{WP_{y_W}}$, and $S_{WP_{z_W}}$ are due to the source influences.

The pylon can be rotated by an angle γ and positioned at any point $(X_{P_0}, Y_{P_0}, Z_{P_0})$ as shown in the following sketch.

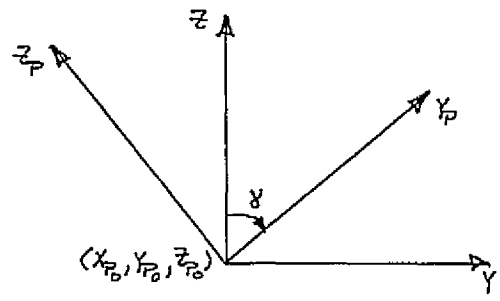

The influence mattrices $A_{WP_{X_W}}$, $A_{WP_{Y_W}}$, $A_{WP_{Z_W}}$, $S_{WP_{X_W}}$, $S_{WP_{Y_W}}$, and $S_{WP_{Z_W}}$ are given by:

$$\left[A_{WP_{X_W}}\right] = \left[A_{WP_{X_P}}\right] \tag{12}$$

$$\left[A_{WP_{Y_W}}\right] = \left[\sin\gamma\right]\left[A_{WP_{Y_P}}\right] - \left[\cos\gamma\right]\left[A_{WP_{Z_P}}\right] \tag{13}$$

$$\left[A_{WP_{Z_W}}\right] = \left[\cos\gamma\right]\left[A_{WP_{Y_P}}\right] + \left[\sin\gamma\right]\left[A_{WP_{Z_P}}\right] \tag{14}$$

$$\left[S_{WP_{X_W}}\right] = \left[S_{WP_{X_P}}\right] \tag{15}$$

$$\left[S_{WP_{Y_W}}\right] = \left[\sin\gamma\right]\left[S_{WP_{Y_P}}\right] - \left[\cos\gamma\right]\left[S_{WP_{Z_P}}\right] \tag{16}$$

$$\left[S_{WP_{Z_W}}\right] = \left[\cos\gamma\right]\left[S_{WP_{Y_P}}\right] + \left[\sin\gamma\right]\left[S_{WP_{Z_P}}\right] \tag{17}$$

Since $[B\alpha_w]$, $[A_{WP_{xp}}]$, and $[S_{WP_{xp}}]$ are small, the products $[B\alpha_w][A_{WP_{xp}}]$ and $[B\alpha_w][S_{WP_{xp}}]$ are omitted. Also, since the wing has no dihedral, $N_{W_{y_w}} = 0$

Therefore;

$$\left\{\frac{V_{W_{WP}}}{V_\infty}\right\} = \left\{ [\cos\gamma][A_{WP_{yp}}] + [\sin\gamma][A_{WP_{zp}}] \right\}\left\{\frac{K_p}{V_\infty}\right\}$$

$$+ \left\{ [\cos\gamma][S_{WP_{yp}}] + [\sin\gamma][S_{WP_{zp}}] \right\}\left\{\frac{\sigma_p}{V_\infty}\right\} \qquad (18)$$

The elements of $A_{WP_{y_p}}$, $A_{WP_{z_p}}$, $S_{WP_{y_p}}$, and $S_{WP_{z_p}}$ are computed with equations defined in Appendices B, C, and D. The port pylon influence is computed by moving the control point to its image location on the port side, computing the influence of the starboard pylon at that point, and then changing the sign of the "Y" component.

NACELLE ON WING

The flow through nacelle is represented by a system of source frustums as shown in figure 5. The velocity induced by the nacelle frustums normal to the wing mean camber surface is given by;

$$\left\{\frac{V_{W_{WN}}}{V_\infty}\right\} = \left[N_{W_{x_w}} A_{WN_{x_w}} + N_{W_{y_w}} A_{WN_{y_w}} + N_{W_{z_w}} A_{WN_{z_w}} \right]\left\{\frac{\sigma_w}{V_\infty}\right\} \qquad (19)$$

The influence matrices $A_{WN_{x_w}}$, $A_{WN_{y_w}}$, and $A_{WN_{z_w}}$ are defined as;

$$[A_{WN_{x_w}}] = [A_{WN_{x_N}}] \qquad (20)$$

$$[A_{WN_{y_w}}] = -[\sin(\gamma - \theta_{WN})][A_{WN_{y_N}}] \qquad (21)$$

$$[A_{WN_{z_w}}] = -[\cos(\gamma - \theta_{WN})][A_{WN_{y_N}}] \qquad (22)$$

$$\theta_{WN} = \tan^{-1}\left[\frac{(Y_{W_g} - Y_{N_o})\cos\gamma - (Z_{W_g} - Z_{N_o})\sin\gamma}{-(Y_{W_g} - Y_{N_o})\sin\gamma - (Z_{W_g} - Z_{N_o})\cos\gamma}\right] \qquad (23)$$

$$\left\{\frac{V_{W_{WN}}}{V_\infty}\right\} = \left\{ [B\alpha_w][A_{WN_{x_N}}] - [\cos(\gamma - \theta_{WN})][A_{WN_{y_N}}] \right\}\left\{\frac{\sigma_w}{V_\infty}\right\} \qquad (24)$$

Again since $[B\alpha_W]$ and $[A_{WW_{YW}}]$ are small, their product is omitted.

Therefore:

$$\left\{\frac{V_{WW\alpha}}{V_\infty}\right\} = -\left[\cos(\gamma - \theta_{WW}) \coprod A_{WW_{YW}}\right]\left\{\frac{\sigma_W}{V_\infty}\right\} \tag{25}$$

The elements of $A_{WW_{YW}}$ are computed with equations derived in Appendix E. The influence of the port nacelle is computed by moving the control point to its image location on the port side, computing the influence of the starboard nacelle on that point, and then changing the sign of the "Y" component.

FREESTREAM ON WING

$$\left\{\frac{V_{W\infty}}{V_\infty}\right\} = \left\{ N_{W_{XW}} \frac{V_{\infty X_W}}{V_\infty} + N_{W_{YW}} \frac{V_{\infty Y_W}}{V_\infty} + N_{W_{ZW}} \frac{V_{\infty Z_W}}{V_\infty} \right\} \tag{26}$$

where $\frac{V_{\infty X_W}}{V_\infty} = 1$, $\frac{V_{\infty Y_W}}{V_\infty} = 0$, AND $\frac{V_{\infty Z_W}}{V_\infty} = 0$

Therefore;

$$\left\{\frac{V_{W\infty}}{V_\infty}\right\} = \left[B\alpha_W\right]\left\{1\right\} = \left\{B\alpha_W\right\} \tag{27}$$

WING ON PYLON

The influence of the wing on the pylon is due to the source and vortex lattices on the wing. The velocity induced by these lattices normal to the pylon mean camber surface is given by the following expression.

$$\left\{\frac{V_{WP}}{V_\infty}\right\} = \left[N_{P_{XP}} A_{PW_{XP}} + N_{P_{YP}} A_{PW_{YP}} + N_{P_{ZP}} A_{PW_{ZP}} \right]\left\{\frac{K_W}{V_\infty}\right\}$$

$$+ \left[N_{P_{XP}} S_{PW_{XP}} + N_{P_{YP}} A_{PW_{YP}} + N_{P_{ZP}} A_{PW_{ZP}} \right]\left\{\frac{\sigma_W}{V_\infty}\right\} \tag{28}$$

Where $N_{P_{X_P}}$ and $N_{P_{Z_P}}$ are defined in the following sketch.

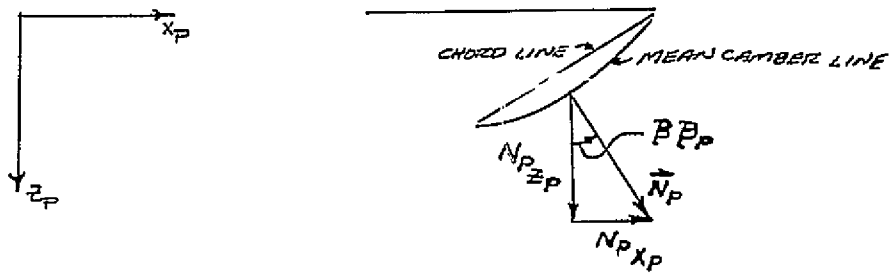

If the local angle $\beta\beta_P$ is assumed small and the pylon cant zero, then $N_{P_{X_P}} \approx \beta\beta_P$, $N_{P_{Y_P}} = 0$, and $N_{P_{Z_P}} = 1.0$.

$$\left\{\frac{V_{INDW}}{V_\infty}\right\} = \left\{\left[\beta\beta_P\right]\left[A_{PW_{X_P}}\right] + \left[A_{PW_{Z_P}}\right]\right\}\left\{\frac{K_W}{V_\infty}\right\} + \left\{\left[\beta\beta_P\right]\left[S_{PW_{X_P}}\right] + \left[S_{PW_{Z_P}}\right]\right\}\left\{\frac{\sigma_W}{V_\infty}\right\} \tag{29}$$

Since $\left[\beta\beta_P\right]$, $\left[A_{PW_{X_P}}\right]$, and $\left[S_{PW_{X_P}}\right]$ are small, the products $\left[\beta\beta_P\right]\left[A_{PW_{X_P}}\right]$ and $\left[\beta\beta_P\right]\left[S_{PW_{X_P}}\right]$ are omitted.

Then considering the difference in orientation between the wing and pylon coordinate frames:

$$\left[A_{PW_{Z_P}}\right] = -\left[\cos\gamma\right]\left[A_{PW_{Y_W}}\right] + \left[\sin\gamma\right]\left[A_{PW_{Z_W}}\right] \tag{30}$$

$$\left[S_{PW_{Z_P}}\right] = -\left[\cos\gamma\right]\left[S_{PW_{Y_W}}\right] + \left[\sin\gamma\right]\left[S_{PW_{Z_W}}\right] \tag{31}$$

Therefore;

$$\left\{\frac{V_{INDW}}{V_\infty}\right\} = \left\{-\left[\cos\gamma\right]\left[A_{PW_{Y_W}}\right] + \left[\sin\gamma\right]\left[A_{PW_{Z_W}}\right]\right\}\left\{\frac{K_W}{V_\infty}\right\} + \left\{-\left[\cos\gamma\right]\left[S_{PW_{Y_W}}\right] + \left[\sin\gamma\right]\left[S_{PW_{Z_W}}\right]\right\}\left\{\frac{\sigma_W}{V_\infty}\right\} \tag{32}$$

The elements of the matrices $A_{PW_{Y_W}}$, $A_{PW_{Z_W}}$, $S_{PW_{Y_W}}$, and $S_{PW_{Z_W}}$ are computed with equations defined in Appendices B, C, and D.

FANPOD ON PYLON

The velocity induced by the fanpod quadrilateral vortices normal to the pylon mean camber surface is given by:

$$\left\{\frac{V_{N_{PF}}}{V_\infty}\right\} = \left[N_{P_{XP}} A_{PF_{XP}} + N_{P_{YP}} A_{PF_{YP}} + N_{P_{ZP}} A_{PF_{ZP}} \right]\left\{\frac{K_F}{V_\infty}\right\} \tag{33}$$

After taking into account the difference in orientation of the pylon and fanpod

$$\left[A_{PF_{XP}} \right] = \left[A_{PF_{XF}} \right] \tag{34}$$

$$\left[A_{PF_{YP}} \right] = \left[\sin\gamma \right]\left[A_{PF_{YF}} \right] + \left[\cos\gamma \right]\left[A_{PF_{ZF}} \right] \tag{35}$$

$$\left[A_{PF_{ZP}} \right] = -\left[\cos\gamma \right]\left[A_{PF_{YF}} \right] + \left[\sin\gamma \right]\left[A_{PF_{ZF}} \right] \tag{36}$$

Therefore, since

$$\left\{\frac{V_{N_{PF}}}{V_\infty}\right\} = \left\{\left[\beta_{E_P} \right]\left[A_{PF_{XF}} \right] - \left[\cos\gamma \right]\left[A_{PF_{YF}} \right] + \left[\sin\gamma \right]\left[A_{PF_{ZF}} \right]\right\}\left\{\frac{K_F}{V_\infty}\right\} \tag{37}$$

Since both β_{E_P} and $A_{PF_{XF}}$ are small, their product is omitted.

$$\left\{\frac{V_{N_{PF}}}{V_\infty}\right\} = \left\{-\left[\cos\gamma \right]\left[A_{PF_{YF}} \right] + \left[\sin\gamma \right]\left[A_{PF_{ZF}} \right]\right\}\left\{\frac{K_F}{V_\infty}\right\} \tag{38}$$

The elements of $A_{PF_{YF}}$ and $A_{PF_{ZF}}$ are computed with equations defined in Appendix D.

FUSELAGE ON PYLON

The influence equation for the fuselage on the pylon is analogous to that for the fanpod on the pylon. Therefore;

$$\left\{\frac{V_{N_{PB}}}{V_\infty}\right\} = \left\{-\left[\cos\gamma \right]\left[A_{PB_{YB}} \right] + \left[\sin\gamma \right]\left[A_{PB_{ZB}} \right]\right\}\left\{\frac{K_B}{V_\infty}\right\} \tag{39}$$

The elements of $A_{PB_{y_B}}$ and $A_{BB_{z_B}}$ are computed with equations defined in Appendix D.

PYLON ON PYLON

The influence of the pylon on itself is computed in the same manner as the influence of the wing on itself except for the influence of the port pylon on the starboard pylon.

$$\left\{\frac{V_{N_{PP}}}{V_\infty}\right\} = \left[N_{B_{KP}} A_{PP_{KP}} + N_{B_{YP}} A_{PP_{YP}} + N_{B_{ZP}} A_{PP_{ZP}} \right]\left\{\frac{K_P}{V_\infty}\right\}$$

$$+ \left[N_{B_{KP}} S_{PP_{KP}} + N_{B_{YP}} S_{PP_{YP}} + N_{B_{ZP}} S_{PP_{ZP}} \right]\left\{\frac{\sigma_P}{V_\infty}\right\} \qquad (40)$$

Both the source and vortex lattices of the port pylon contribute to the starboard pylon. Only the vortex lattice of the starboard pylon contributes to the starboard pylon influence equations.

Since; $N_{B_{KP}} \approx B_{EP}$, $N_{B_{YP}} = 0$, $N_{B_{ZP}} \approx 1.0$ and $[B_{EB_P}]$, $[A_{PP_{KP}}]$, and $[S_{PP_{KP}}]$ are small

$$\left\{\frac{V_{N_{PP}}}{V_\infty}\right\} = \left\{ - \left[\cos\delta\right]\left[A_{PB_Y}\right] + \left[\sin\gamma\right]\left[A_{PP_Z}\right] \right.$$

$$\left. + \left[A_{PP_{ZP}}\right]\right\}\left\{\frac{K_P}{V_\infty}\right\} + \left\{ - \left[\cos\gamma\right]\left[S_{PP_Y}\right] \right.$$

$$\left. + \left[\sin\gamma\right]\left[S_{PP_Y}\right]\right\}\left\{\frac{\sigma_P}{V_\infty}\right\} \qquad (41)$$

where A_{PP_Y}, A_{PP_Z}, S_{PP_Y}, and S_{PP_Z} are influences of the port pylon onto the starboard pylon.

The five level subscript notation in equations (42) through (45) indicates: Levels 1 and 2) PPp influence of port pylon on starboard pylon; Levels 3, 4, and 5) X_{P_P} coordinate of vortex segment located on port pylon.

$$\left[A_{PP_Y}\right] = -\left[\sin\gamma\right]\left[A_{PP_{Y_{IP}}}\right] + \left[\cos\gamma\right]\left[A_{PP_{Z_{IP}}}\right] \tag{42}$$

$$\left[A_{PP_Z}\right] = \left[\cos\gamma\right]\left[A_{PP_{Y_{IP}}}\right] - \left[\sin\gamma\right]\left[A_{PP_{Z_{IP}}}\right] \tag{43}$$

$$\left[S_{PP_Y}\right] = -\left[\sin\gamma\right]\left[S_{PP_{Y_{IP}}}\right] + \left[\cos\gamma\right]\left[S_{PP_{Z_{IP}}}\right] \tag{44}$$

and

$$\left[S_{PP_Z}\right] = \left[\cos\gamma\right]\left[S_{PP_{Y_{IP}}}\right] - \left[\sin\gamma\right]\left[S_{PP_{Z_{IP}}}\right] \tag{45}$$

The elements of $A_{PP_{Y_{IP}}}$, $A_{PP_{Z_{IP}}}$, $A_{PP_{IP}}$, $S_{PP_{Y_{IP}}}$, and $S_{PP_{Z_{IP}}}$ are computed with equations defined in Appendices B, C, and D. The influence of the port pylon is obtained by moving the control point to its image location on the port side and then computing the influence of the starboard pylon at that point. When this procedure is used, the sign on the "Y" component of velocity must be changed. This sign change is applied in equations (42) and (44).

NACELLE ON PYLON

The expression for the velocity induced by the nacelle normal to the pylon mean camber surface is given by the following expression

$$\left\{\frac{V_{N_{IP}}}{V_\infty}\right\} = \left[N_{P_{IP}} A_{PN_{IP}} + N_{P_{YP}} A_{PN_{YP}} + N_{P_{ZP}} A_{PN_{ZP}}\right]\left\{\frac{\sigma_N}{V_\infty}\right\} \tag{46}$$

Since the nacelle produces an axisymmetric flow field, no contribution to $A_{PN_{ZP}}$ is obtained from the starboard nacelle on the starboard pylon. However, both nacelles contribute to $A_{PN_{YP}}$ and $A_{PN_{YP}}$. Since $N_{P_{YP}}$ and $A_{PN_{YP}}$ are small and since $N_{P_{YP}} = 0$;

$$\left\{\frac{V_{N_{IP}}}{V_\infty}\right\} = \left[A_{PN_{ZP}}\right]\left\{\frac{\sigma_N}{V_\infty}\right\} \tag{47}$$

Where

$$\left[A_{PNP_{ZF}}\right] = -\left[\cos\delta\right]\left[A_{PNP_Y}\right] + \left[\sin\delta\right]\left[A_{PNP_Z}\right] \tag{48}$$

and

$$\left[A_{PNP_Y}\right] = \left[\sin(\delta-\theta)\right]\left[A_{PNP_{YNP}}\right] \tag{49}$$

$$\left[A_{PNP_Z}\right] = -\left[\cos(\delta-\theta)\right]\left[A_{PNP_{YNP}}\right] \tag{50}$$

The elements of $A_{PNP_{YNP}}$ are computed from equations derived in Appendix E. The influence of the nacelle on the port side is determined by moving the control point to the port side and computing the influence of the starboard nacelle at that point and then changing the sign on the "Y" component.

FREESTREAM ON PYLON

$$\left\{\frac{V_{N_{PNP}}}{V_\infty}\right\} = \left\{N_{P_{XP}}\frac{V_{\infty XP}}{V_\infty} + N_{P_{YP}}\frac{V_{\infty YP}}{V_\infty} + N_{P_{ZP}}\frac{V_{\infty ZP}}{V_\infty}\right\} \tag{51}$$

Where

$$N_{P_{XP}} \approx BB_P \quad , \quad N_{P_{YP}} = 0 \quad , \quad N_{P_{ZP}} = 1 \quad , \quad \frac{V_{\infty XP}}{V_\infty} \approx 1.0$$

and $\frac{V_{\infty ZP}}{V_\infty} \approx \alpha \sin\gamma$

Therefore:

$$\left\{\frac{V_{N_{PNP}}}{V_\infty}\right\} = \left[BB_P\right]\left\{1\right\} + \left[-1\right]\left\{\alpha\sin\gamma\right\} \tag{52}$$

WING ON FANPOD

The wing influences the fanpod quadrilateral vortex strengths with the flow induced by the wing source and vortex lattices. The component of this flow normal to the fanpod surface is given by the following expression.

$$\left\{\frac{V_{N_{FW}}}{V_\infty}\right\} = \left[N_{F_{XF}}A_{FW_{XF}} + N_{F_{YF}}A_{FW_{YF}} + N_{F_{ZF}}A_{FW_{ZF}}\right]\left\{\frac{K_W}{V_\infty}\right\} \tag{53}$$

$$+\left[N_{F_{XF}}S_{FW_{XF}} + N_{F_{YF}}S_{FW_{YF}} + N_{F_{ZF}}S_{FW_{ZF}}\right]\left\{\frac{\sigma_W}{V_\infty}\right\}$$

where

$$\left[A_{FW_{XF}}\right] = \left[\cos\beta\alpha_{FW}\right]\left[A_{FW_{XW}}\right] - \left[\sin\beta\alpha_{FW}\right]\left[A_{FW_{ZW}}\right] \tag{54}$$

$$\left[A_{FW_{YF}}\right] = \left[A_{FW_{YW}}\right] \tag{55}$$

$$\left[A_{FW_{ZF}}\right] = \left[\sin\beta\alpha_{FW}\right]\left[A_{FW_{XW}}\right] + \left[\cos\beta\alpha_{FW}\right]\left[A_{FW_{ZW}}\right] \tag{56}$$

$$\left[S_{FW_{XF}}\right] = \left[\cos\beta\alpha_{FW}\right]\left[S_{FW_{XW}}\right] - \left[\sin\beta\alpha_{FW}\right]\left[S_{FW_{ZW}}\right] \tag{57}$$

$$\left[S_{FW_{YF}}\right] = \left[S_{FW_{YW}}\right] \tag{58}$$

$$\left[S_{FW_{ZF}}\right] = \left[\sin\beta\alpha_{FW}\right]\left[S_{FW_{XW}}\right] + \left[\cos\beta\alpha_{FW}\right]\left[S_{FW_{ZW}}\right] \tag{59}$$

Since $\left[\beta\alpha_{FW}\right]$, $\left[A_{FW_{XW}}\right]$, and $\left[S_{FW_{XW}}\right]$ are small;

$$\left\{\frac{V_{WFW}}{V_\infty}\right\} = \left\{\left[N_{F_{XF}}\right]\left[A_{FW_{XW}}\right] - \left[N_{F_{XF}}\right]\left[\beta\alpha_{FW}\right]\left[A_{FW_{ZW}}\right] + \left[N_{F_{YF}}\right]\left[A_{FW_{YW}}\right] + \left[N_{F_{ZF}}\right]\left[A_{FW_{ZW}}\right]\right\}\left\{\frac{K_W}{V_\infty}\right\}$$

$$+ \left\{\left[N_{F_{XF}}\right]\left[S_{FW_{XW}}\right] + \left[N_{F_{YF}}\right]\left[S_{FW_{YW}}\right] + \left[N_{F_{ZF}}\right]\left[S_{FW_{ZW}}\right]\right\}\left\{\frac{\sigma_W}{V_\infty}\right\} \tag{60}$$

Also, since the product $\left[N_{F_{XF}}\right]\left[\beta\alpha_{FW}\right]$ is small;

$$\left\{\frac{V_{WFW}}{V_\infty}\right\} = \left\{\left[N_{F_{XF}}\right]\left[A_{FW_{XW}}\right] + \left[N_{F_{YF}}\right]\left[A_{FW_{YW}}\right] + \left[N_{F_{ZF}}\right]\left[A_{FW_{ZW}}\right]\right\}\left\{\frac{K_W}{V_\infty}\right\}$$

$$+ \left\{\left[N_{F_{XF}}\right]\left[S_{FW_{XW}}\right] + \left[N_{F_{YF}}\right]\left[S_{FW_{YW}}\right] + \left[N_{F_{ZF}}\right]\left[S_{FW_{ZW}}\right]\right\}\left\{\frac{\sigma_W}{V_\infty}\right\} \tag{61}$$

The elements of $A_{FW_{XW}}$, $A_{FW_{YW}}$, and $A_{FW_{ZW}}$ and of $S_{FW_{XW}}$, $S_{FW_{YW}}$, and $S_{FW_{ZW}}$ are computed with equations derived in Appendices C, B, and D.

The components of the unit vector normal to the fanpod surface are computed from the coordinates of the vortex grid.

$$N_{F_{X_F}} = T_{FM_{Y_{F_i}}} T_{FT_{Z_{F_i}}} - T_{FM_{Z_{F_i}}} T_{FT_{Y_{F_i}}} \tag{62}$$

$$N_{F_{Y_F}} = T_{FT_{X_{F_i}}} T_{FM_{Z_{F_i}}} - T_{FT_{Z_{F_i}}} T_{FM_{X_{F_i}}} \tag{63}$$

and

$$N_{F_{Z_F}} = T_{FM_{X_{F_i}}} T_{FT_{Y_{F_i}}} - T_{FM_{Y_{F_i}}} T_{FT_{X_{F_i}}} \tag{64}$$

where

$$T_{FM_{X_{F_i}}} = (X_{F_2} - X_{F_1} + X_{F_4} - X_{F_3}) / \Delta S_{FM_i} \tag{65}$$

$$T_{FM_{Y_{F_i}}} = \beta (Y_{F_2} - Y_{F_1} + Y_{F_4} - Y_{F_3}) / \Delta S_{FM_i} \tag{66}$$

$$T_{FM_{Z_{F_i}}} = \beta (Z_{F_2} - Z_{F_1} + Z_{F_4} - Z_{F_3}) / \Delta S_{FM_i} \tag{67}$$

$$T_{FT_{X_{F_i}}} = (X_{F_3} - X_{F_1} + X_{F_4} - X_{F_2}) / \Delta S_{FT_i} \tag{68}$$

$$T_{FT_{Y_{F_i}}} = \beta (Y_{F_3} - Y_{F_1} + Y_{F_4} - Y_{F_2}) / \Delta S_{FT_i} \tag{69}$$

and

$$T_{FT_{Z_{F_i}}} = \beta (Z_{F_3} - Z_{F_1} + Z_{F_4} - Z_{F_2}) / \Delta S_{FT_i} \tag{70}$$

Also where;

$$\Delta S_{FM_i} = \left[(X_{F_2} - X_{F_1} + X_{F_4} - X_{F_3})^2 + \beta^2 (Y_{F_2} - Y_{F_1} + Y_{F_4} - Y_{F_3})^2 + \beta^2 (Z_{F_2} - Z_{F_1} + Z_{F_4} - Z_{F_3})^2 \right]^{1/2} \tag{71}$$

and

$$\Delta S_{F_{T_i}} = \left[(X_{F_3} - X_{F_1} + X_{F_4} - X_{F_2})^2 + \beta^2 (Y_{F_3} - Y_{F_1} + Y_{F_4} - Y_{F_2}) \right.$$

$$\left. + \beta^2 (Z_{F_3} - Z_{F_1} + Z_{F_4} - Z_{F_2}) \right]^{1/2} \qquad (72)$$

Where the indices refer to the corners of the quadrilateral vortex as shown in the following sketch.

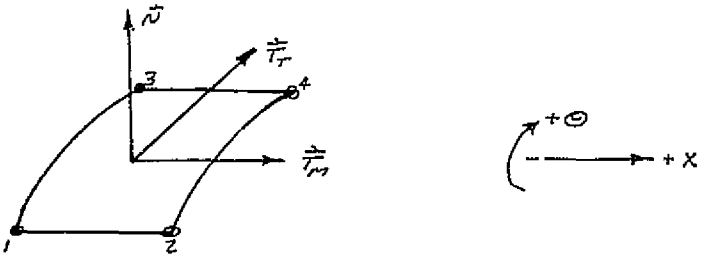

The $'$ subscript indicates that the unit vectors are for the equivalent incompressible fanpod obtained from the Gothert compressibility transformation.

FANPOD ON FANPOD

The influence of the fanpod on itself is due to the velocity induced by the fanpod quadrilateral vortices normal to the fanpod surface. This component of velocity is given by;

$$\left\{ \frac{V_{N_{FF}}}{V_\infty} \right\} = \left[N_{F_{X_F}} A_{FF_{X_F}} + N_{F_{Y_F}} A_{FF_{Y_F}} + N_{F_{Z_F}} A_{FF_{Z_F}} \right] \left\{ \frac{K_F}{V_\infty} \right\} \qquad (73)$$

The elements of $A_{FF_{X_F}}$, $A_{FF_{Y_F}}$, and $A_{FF_{Z_F}}$ are computed from equations defined in Appendix D.

FUSELAGE ON FANPOD

The influence of the fuselage on the fanpod is analogous to the influence of the fanpod on itself.

Therefore;

$$\left\{\frac{V_{N_{FB}}}{V_\infty}\right\} = \left[N_{F_{XF}} A_{FB_{XB}} + N_{F_{YF}} A_{FB_{YB}} + N_{F_{YF}} A_{FB_{ZB}} \right]\left\{\frac{K_B}{V_\infty}\right\} \tag{74}$$

Where the elements of $A_{FB_{XB}}$, $A_{FB_{YB}}$, and $A_{FB_{ZB}}$ are computed with equations defined in Appendix D.

PYLON ON FANPOD

The influence of the pylon on the fanpod is due to the pylon source and vortex lattices. These lattices induce a velocity normal to the fanpod surface which is given by;

$$\left\{\frac{V_{N_{FP}}}{V_\infty}\right\} = \left[N_{F_{XF}} A_{FP_{XF}} + N_{F_{YF}} A_{FP_{YF}} + N_{F_{ZF}} A_{FP_{ZF}} \right]\left\{\frac{K_P}{V_\infty}\right\} + \left[N_{F_{XF}} S_{FP_{XF}} + N_{F_{YF}} S_{FP_{YF}} + N_{F_{ZF}} S_{FP_{ZF}} \right]\left\{\frac{\sigma_P}{V_\infty}\right\} \tag{75}$$

When the difference in pylon and fanpod coordinate frame orientation is taken into account,

$$\begin{aligned}\left\{\frac{V_{N_{FP}}}{V_\infty}\right\} = {} & \left\{ \left[N_{F_{XF}}\right]\left[A_{FP_{XP}}\right] + \left[N_{F_{YF}}\right]\left\{\left[\sin\gamma\right]\left[A_{FP_{YP}}\right] - \left[\cos\gamma\right]\left[A_{FP_{ZP}}\right]\right\} + \left[N_{F_{ZF}}\right]\left\{\left[\cos\gamma\right]\left[A_{FP_{YP}}\right] + \left[\sin\gamma\right]\left[A_{FP_{ZP}}\right]\right\}\right\}\left\{\frac{K_P}{V_\infty}\right\} \\ & + \left\{ \left[N_{F_{XF}}\right]\left[S_{FP_{XP}}\right] + \left[N_{F_{YF}}\right]\left\{\left[\sin\gamma\right]\left[S_{FP_{YP}}\right] - \left[\cos\gamma\right]\left[S_{FP_{ZP}}\right]\right\} + \left[N_{F_{ZF}}\right]\left\{\left[\cos\gamma\right]\left[S_{FP_{YP}}\right] + \left[\sin\gamma\right]\left[S_{FP_{ZP}}\right]\right\}\right\}\left\{\frac{\sigma_P}{V_\infty}\right\}\end{aligned} \tag{76}$$

The elements of $A_{FP_{XP}}$, $A_{FP_{YP}}$, $A_{FP_{ZP}}$, $S_{FP_{XP}}$, $S_{FP_{YP}}$, and $S_{FP_{ZP}}$ are computed with equations defined in Appendices B, C, and D. The influence of the port pylon is computed by moving the control point to its image location on the port side, computing the influence of the starboard pylon at that point, and then changing the sign on the "Y" component.

NACELLE ON FANPOD

The velocity induced normal to the fanpod surface by the nacelle source frustums is given by:

$$\left\{\frac{V_{N_{FN}}}{V_\infty}\right\} = \left[N_{F_{XF}} A_{FN_{XF}} + N_{F_{YF}} A_{FN_{YF}} + N_{F_{ZF}} A_{FN_{ZF}} \right]\left\{\frac{\sigma_N}{V_\infty}\right\} \tag{77}$$

The influence matrices $A_{FN_{XF}}$, $A_{FN_{YF}}$, and $A_{FN_{ZF}}$ are defined as:

$$\left[A_{FN_{XF}}\right] = \left[A_{FN_{XN}}\right] \tag{78}$$

$$\left[A_{FN_{YF}}\right] = -\left[\sin(\gamma-\theta_{FN})\right]\left[A_{FN_{YN}}\right] \tag{79}$$

$$\left[A_{FN_{ZF}}\right] = -\left[\cos(\gamma-\theta_{FN})\right]\left[A_{FN_{YN}}\right] \tag{80}$$

where

$$\theta_{FN} = \tan^{-1}\left[\frac{(Y_{F_g}-Y_{N_0})\cos\gamma - (Z_{F_g}-Z_{N_0})\sin\gamma}{-(Y_{F_g}-Y_{N_0})\sin\gamma - (Z_{F_g}-Z_{N_0})\cos\gamma}\right] \tag{81}$$

Therefore;

$$\left\{\frac{V_{N_{FN}}}{V_\infty}\right\} = \left\{\left[N_{F_{XF}}\right]\left[A_{FN_{XN}}\right] - \left[N_{F_{YF}}\right]\left[\sin(\gamma-\theta_{FN})\right]\left[A_{FN_{YN}}\right] - \left[N_{F_{ZF}}\right]\left[\cos(\gamma-\theta_{FN})\right]\left[A_{FN_{YN}}\right]\right\}\left\{\frac{\sigma_N}{V_\infty}\right\} \tag{82}$$

The influence matrices $A_{FN_{X_N}}$ and $A_{FN_{Y_N}}$ are computed with equations defined in Appendix E. The influence of the port nacelle is computed by moving the control point to its image location on the port side, computing the influence of the starboard nacelle at that point, and then changing the sign of the "Y" component.

FREESTREAM ON FANPOD

$$\left\{\frac{V_{N_{F\infty}}}{V_\infty}\right\} = \left\{ N_{F_{XF}} \frac{V_{\infty XF}}{V_\infty} + N_{F_{YF}} \frac{V_{\infty YF}}{V_\infty} + N_{F_{ZF}} \frac{V_{\infty ZF}}{V_\infty} \right\} \tag{83}$$

Therefore;

$$\left\{\frac{V_{N_{F\infty}}}{V_\infty}\right\} = \left[N_{F_{XF}}\right]\left[\cos\alpha_F\right]\{1\} + \left[N_{F_{XF}}\right]\left[\sin\alpha_F\right]\{1\} \tag{84}$$

WING ON FUSELAGE

The influences of the different components on the fuselage are computed in a manner analogous to that for the fanpod. Therefore;

$$\left\{\frac{V_{N_{BW}}}{V_\infty}\right\} = \left\{\left[N_{B_{X_B}}\right]\left[A_{BW_{X_W}}\right] + \left[N_{B_{Y_B}}\right]\left[A_{BW_{Y_W}}\right] + \left[N_{B_{Z_B}}\right]\left[A_{BW_{Z_W}}\right]\right\}\left\{\frac{K_\omega}{V_\infty}\right\}$$

$$+ \left\{\left[N_{B_{X_B}}\right]\left[S_{BW_{X_W}}\right] + \left[N_{B_{Y_B}}\right]\left[S_{BW_{Y_W}}\right] + \left[N_{B_{Z_B}}\right]\left[S_{BW_{Z_W}}\right]\right\}\left\{\frac{\sigma_W}{V_\infty}\right\} \tag{85}$$

The elements of $A_{BW_{X_W}}$, $A_{BW_{Y_W}}$, $A_{BW_{Z_W}}$, $S_{BW_{X_W}}$, $S_{BW_{Y_W}}$, and $S_{BW_{Z_W}}$ are computed with equations derived in Appendices C, B, and D.

The surface unit vectors $(N_{B_{X_B}}, N_{B_{Y_B}}, N_{B_{Z_B}})$, $(T_{B_{M_{X_B}}}, T_{B_{M_{Y_B}}}, T_{B_{M_{Z_B}}})$ and $(T_{B_{T_{X_B}}}, T_{B_{T_{Y_B}}}, T_{B_{T_{Z_B}}})$ are computed the same as those for the fanpod and defined by equations (47) through (55).

FANPOD ON FUSELAGE

$$\left\{\frac{V_{N_{BF}}}{V_\infty}\right\} = \left[N_{B_{X_B}} A_{BF_{X_F}} + N_{B_{Y_B}} A_{BF_{Y_F}} + N_{B_{Z_B}} A_{BF_{Z_F}}\right]\left\{\frac{K_F}{V_\infty}\right\} \tag{86}$$

The elements of $A_{BF_{X_F}}$, $A_{BF_{Y_F}}$, and $A_{BF_{Z_F}}$ are computed from equations defined in Appendix D.

FUSELAGE ON FUSELAGE

$$\left\{\frac{V_{N_{BB}}}{V_\infty}\right\} = \left[N_{B_{X_B}} A_{BB_{X_B}} + N_{B_{Y_B}} A_{BB_{Y_B}} + N_{B_{Z_B}} A_{BB_{Z_B}} \right]\left\{\frac{K_B}{V_\infty}\right\} \qquad (87)$$

The elements of $A_{BB_{X_B}}$, $A_{BB_{Y_B}}$, and $A_{BB_{Z_B}}$ are computed from equations defined in Appendix D.

PYLON ON FUSELAGE

$$\begin{aligned}\left\{\frac{V_{N_{BP}}}{V_\infty}\right\} = \Big\{ &\left[N_{B_{X_B}}\right]\left[A_{BP_{X_P}}\right] + \left[N_{B_{Y_B}}\right]\Big\{\left[\sin\gamma\right]\left[A_{BP_{Y_P}}\right] \\ &- \left[\cos\gamma\right]\left[A_{BP_{Z_P}}\right]\Big\} + \left[N_{B_{Z_B}}\right]\Big\{\left[\cos\gamma\right]\left[A_{BP_{Y_P}}\right] \\ &+ \left[\sin\gamma\right]\left[A_{BP_{Z_P}}\right]\Big\}\Big\}\left\{\frac{K_P}{V_\infty}\right\} + \Big\{\left[N_{B_{X_B}}\right]\left[S_{BP_{X_P}}\right] \\ &+ \left[N_{B_{Y_B}}\right]\Big\{\left[\sin\gamma\right]\left[S_{BP_{Y_P}}\right] - \left[\cos\gamma\right]\left[S_{BP_{Z_P}}\right]\Big\} \\ &+ \left[N_{B_{Z_B}}\right]\Big\{\left[\cos\gamma\right]\left[S_{BP_{Y_P}}\right] + \left[\sin\gamma\right]\left[S_{BP_{Z_P}}\right]\Big\}\Big\}\left\{\frac{\sigma_P}{V_\infty}\right\}\end{aligned} \qquad (88)$$

The elements of $A_{BP_{X_P}}$, $A_{BP_{Y_P}}$, $A_{BP_{Z_P}}$, $S_{BP_{X_P}}$, $S_{BP_{Y_P}}$, and $S_{BP_{Z_P}}$ are computed with equations defined in Appendices B, C, and D. The influence of the port pylon is computed by moving the control point to its image location on the port side, computing the influence of the starboard pylon at that point, and then changing the sign on the "Y" component.

NACELLE ON FUSELAGE

$$\left\{\frac{V_{N_{BN}}}{V_\infty}\right\} = \left\{\left[N_{B_{X_B}}\right]\left[A_{BN_{X_N}}\right] - \left[N_{B_{Y_B}}\right]\left[\sin(\gamma-\theta_{BN})\right]\left[A_{BN_{Y_N}}\right]\right.$$

$$\left. - \left[N_{B_{Z_B}}\right]\left[\cos(\gamma-\theta_{BN})\right]\left[A_{BN_{Y_N}}\right]\right\}\left\{\frac{\sigma_B}{V_\infty}\right\} \qquad (89)$$

where

$$\theta_{BN} = \tan^{-1}\left[\frac{(Y_{B_g}-Y_{N_o})\cos\gamma - (Z_{B_g}-Z_{N_o})\sin\gamma}{-(Y_{B_g}-Y_{N_o})\sin\gamma - (Z_{B_g}-Z_{N_o})\cos\gamma}\right] \qquad (90)$$

The influence matrices $A_{BN_{X_N}}$ and $A_{BN_{Y_N}}$ are computed with equations defined in Appendix E. The influence of the port nacelle is computed as in the case of the nacelle on fanpod.

FREESTREAM ON FUSELAGE

$$\left\{\frac{V_{N_{B\infty}}}{V_\infty}\right\} = \left[N_{B_{X_B}}\right]\left[\cos\alpha_B\right]\left\{1\right\} + \left[N_{B_{Z_B}}\right]\left[\sin\alpha_B\right]\left\{1\right\} \qquad (91)$$

WING ON NACELLE

The flow induced normal to the nacelle surface by the wing source and vortex lattices is given by the following equation:

$$\left\{\frac{V_{N_{WN}}}{V_\infty}\right\} = \left[N_{N_{X_W}} A_{NW_{X_N}} + N_{N_{Y_N}} A_{NW_{Y_N}}\right]\left\{\frac{K_W}{V_\infty}\right\}$$

$$+ \left[N_{N_{X_N}} S_{NW_{X_N}} + N_{N_{Y_N}} S_{NW_{Y_N}}\right]\left\{\frac{\sigma_W}{V_\infty}\right\} \qquad (92)$$

After transforming the influence matrices to the wing coordinate system:

$$\left\{\frac{V_{NWN}}{V_\infty}\right\} = \left\{\left[N_{N_{X_N}}\right]\left[A_{NW_{X_W}}\right] - \left[N_{N_{Y_N}}\right]\left\{\left[\sin\gamma\right]\left[A_{NW_{Y_W}}\right] + \left[\cos\gamma\right]\left[A_{NW_{Z_W}}\right]\right\}\right\}\left\{\frac{k_W}{V_\infty}\right\} + \left\{\left[N_{N_{X_N}}\right]\left[S_{NW_{X_W}}\right] - \left[N_{N_{Y_N}}\right]\left\{\left[\sin\gamma\right]\left[S_{NW_{Y_W}}\right] + \left[\cos\gamma\right]\left[S_{NW_{Z_W}}\right]\right\}\right\}\left\{\frac{\sigma_W}{V_\infty}\right\} \tag{93}$$

The influence matrices $A_{NW_{X_W}}$, $A_{NW_{Y_W}}$, and $A_{NW_{Z_W}}$ are computed with equations defined in Appendices C and D, and the matrices $S_{NW_{X_W}}$, $S_{NW_{Y_W}}$, and $S_{NW_{Z_W}}$ are computed with equations defined in Appendix B. Also, $N_{N_{X_N}} = -\sin\alpha_{N_i}$ and $N_{N_{Y_N}} = \cos\alpha_{N_i}$ where α_{N_i} is defined in Appendix E.

PYLON ON NACELLE

The flow induced normal to the nacelle surface by the pylon source and vortex lattices is given by the following equations.

$$\left\{\frac{V_{NWP}}{V_\infty}\right\} = \left[N_{N_{X_N}} A_{NP_{X_N}} + N_{N_{Y_N}} A_{NP_{Y_N}}\right]\left\{\frac{k_P}{V_\infty}\right\} + \left[N_{N_{X_N}} S_{NP_{X_N}} + N_{N_{Y_N}} S_{NP_{Y_N}}\right]\left\{\frac{\sigma_P}{V_\infty}\right\} \tag{94}$$

After transforming the influence matrices to the pylon coordinate system:

$$\left\{\frac{V_{NWP}}{V_\infty}\right\} = \left\{\left[N_{N_{X_N}}\right]\left[A_{NP_{X_P}}\right] - \left[N_{N_{Y_N}}\right]\left[A_{NP_{Y_P}}\right]\right\}\left\{\frac{k_P}{V_\infty}\right\} + \left\{\left[N_{N_{X_N}}\right]\left[S_{NP_{X_P}}\right] - \left[N_{N_{Y_N}}\right]\left[S_{NP_{Y_P}}\right]\right\}\left\{\frac{\sigma_P}{V_\infty}\right\} \tag{95}$$

where

$$\left[A_{NP_{Y_P}}\right] = \left[\sin\delta\right]\left\{-\left[\sin\delta\right]\left[A_{NP_{X_P}}\right] + \left[\cos\delta\right]\left[A_{NP_{Z_P}}\right]\right\} + \left[\cos\delta\right]\left\{\left[\cos\delta\right]\left[A_{NP_{Y_P}}\right] + \left[\sin\gamma\right]\left[A_{NP_{Z_P}}\right]\right\} + \left[A_{NP_{S_{Y_P}}}\right] \tag{96}$$

$$\left[S_{NB_{YP}}\right] = \left[\sin\gamma\right]\left\{-\left[\sin\gamma\right]\left[S_{NB_{YP}}\right] + \left[\cos\gamma\right]\left[S_{NB_{ZP}}\right]\right\}$$

$$+\left[\cos\gamma\right]\left\{\left[\cos\gamma\right]\left[S_{NB_{YP}}\right] + \left[\sin\gamma\right]\left[S_{NB_{ZP}}\right]\right\} \qquad (97)$$

$$+\left[S_{NB_{YP}}\right]$$

The influence matrices $A_{NB_{YP}}$, $A_{NB_{ZP}}$, $S_{NB_{YP}}$, and $S_{NB_{ZP}}$ are due to the port pylon and $A_{NB_{YP}}$ and $S_{NB_{YP}}$ are due to the starboard pylon. The influence of the port pylon is computed by moving the control point to its image location on the port side, computing the influence at that point, and then changing the sign on the "Y" component.

The influence matrices $A_{NB_{XP}}$ and $A_{NB_{YP}}$ are computed from equations defined in Appendices C and D, and the matrices $S_{NB_{XP}}$ and $S_{NB_{YP}}$ are computed with equations defined in Appendix B.

FANPOD ON NACELLE

The flow induced by the fanpod quadrilateral vortices normal to the nacelle surface is given by:

$$\left\{\frac{V_{N_{NF}}}{V_\infty}\right\} = \left[N_{N_N} A_{NF_N} + N_{N_W} A_{NF_W}\right]\left\{\frac{K_F}{V_\infty}\right\} \qquad (98)$$

After transforming the influence matrices A_{NF_N} and A_{NF_W} to the fanpod coordinate frame;

$$\left\{\frac{V_{N_{NF}}}{V_\infty}\right\} = \left\{\left[N_{N_N}\right]\left[A_{NF_F}\right] - \left[N_{N_N}\right]\left\{\left[\sin\gamma\right]\left[A_{NF_F}\right] + \left[\cos\gamma\right]\left[A_{NF_{ZF}}\right]\right\}\right\}\left\{\frac{K_F}{V_\infty}\right\} \qquad (99)$$

The influence matrices $A_{NF_{XF}}$, $A_{NF_{YF}}$, and $A_{NF_{ZF}}$ are computed with equations defined in Appendix D.

FUSELAGE ON NACELLE

$$\left\{\frac{V_{W_{NB}}}{V_\infty}\right\} = \left\{\left[N_{N_{X_W}}\right]\left[A_{NB_{X_B}}\right] - \left[N_{N_{Y_W}}\right]\left\{\left[\sin\gamma\right]\left[A_{NB_{Y_B}}\right] + \left[\cos\gamma\right]\left[A_{NB_{Z_B}}\right]\right\}\right\}\left\{\frac{V_B}{V_\infty}\right\} \tag{100}$$

The influence matrices $A_{NB_{X_B}}$, $A_{NB_{Y_B}}$, and $A_{NB_{Z_B}}$ are computed with equations defined in Appendix D.

NACELLE ON NACELLE

The flow induced by the nacelle frustums normal to the nacelle surface is given by:

$$\left\{\frac{V_{W_{NN}}}{V_\infty}\right\} = \left[N_{N_{X_N}} A_{NN_{X_N}} + N_{N_{Y_N}} A_{NN_{Y_N}}\right]\left\{\frac{\sigma_N}{V_\infty}\right\} \tag{101}$$

$$\left\{\frac{V_{W_{NN}}}{V_\infty}\right\} = \left\{-\left[\sin\alpha_{N_i}\right]\left[A_{NN_{X_N}}\right] + \left[\cos\alpha_{N_i}\right]\left\{\left[\sin\gamma\right]\left[\sin(\gamma-\theta_{NM_P})\right]\left[\hat{A}_{NNP_{Y_N}}\right] + \left[\cos\gamma\right]\left[\cos(\gamma-\theta_{NM_P})\right]\right\}\left[A_{NP_{Y_N}}\right] + \left[\cos\alpha_{N_i}\right]\left[A_{NN_{S_{Y_N}}}\right]\right\}\left\{\frac{\sigma_N}{V_\infty}\right\} \tag{102}$$

where

$$\theta_{NM_P} = \tan^{-1}\left[\frac{(Y_{N_S} - Y_{N_P})\cos\gamma - (Z_{N_S} - Z_{N_P})\sin\gamma}{-(Y_{N_S} - Y_{N_P})\sin\gamma - (Z_{N_S} - Z_{N_P})\sin\gamma}\right] \tag{103}$$

The second subscript N_P and N_S refer to the port and starboard nacelles, respectively. The port nacelle influence is computed by moving the control point to its image location on the port side, computing the influence at that point, and then changing the sign of the "Y" component.

The matrices A_{NN_P} and A_{NN_P} are computed with equations defined in Appendix E.

FREESTREAM ON NACELLE

$$\left\{\frac{V_{N_{\infty}}}{V_{\infty}}\right\} = \left[\; N_{N_P} \;\right]\left\{\frac{V_{\infty_P}}{V_{\infty}}\right\} + \left[\; N_{N_S} \;\right]\left\{\frac{V_{\infty_S}}{V_{\infty}}\right\} \tag{104}$$

$$\left\{\frac{V_{N_{\infty}}}{V_{\infty}}\right\} = \left[\cos\alpha_{N_i}\right]\{1\} + \left[\sin\alpha_{N_i}\right]\left[\cos\gamma\right]\{\beta\alpha\} \tag{105}$$

Combined influence equations

$$\frac{V_{N_{BB}}}{V_{\infty}} + \frac{V_{N_{BF}}}{V_{\infty}} + \frac{V_{N_{BW}}}{V_{\infty}} + \frac{V_{N_{BP}}}{V_{\infty}} + \frac{V_{N_{BN}}}{V_{\infty}} = 0$$

$$\frac{V_{N_{FB}}}{V_{\infty}} + \frac{V_{N_{FF}}}{V_{\infty}} + \frac{V_{N_{FW}}}{V_{\infty}} + \frac{V_{N_{FP}}}{V_{\infty}} + \frac{V_{N_{FN}}}{V_{\infty}} = 0$$

$$\frac{V_{N_{WB}}}{V_{\infty}} + \frac{V_{N_{WF}}}{V_{\infty}} + \frac{V_{N_{WW}}}{V_{\infty}} + \frac{V_{N_{WP}}}{V_{\infty}} + \frac{V_{N_{WN}}}{V_{\infty}} = 0$$

$$\frac{V_{N_{PB}}}{V_{\infty}} + \frac{V_{N_{PF}}}{V_{\infty}} + \frac{V_{N_{PW}}}{V_{\infty}} + \frac{V_{N_{PP}}}{V_{\infty}} + \frac{V_{N_{PN}}}{V_{\infty}} = 0$$

$$\frac{V_{N_{NB}}}{V_{\infty}} + \frac{V_{N_{NF}}}{V_{\infty}} + \frac{V_{N_{NW}}}{V_{\infty}} + \frac{V_{N_{NP}}}{V_{\infty}} + \frac{V_{N_{NN}}}{V_{\infty}} = 0$$

Therefore, the discrete influence equation is;

$$\begin{bmatrix} \bar{A}_{BB} & \bar{A}_{BF} & \bar{A}_{BW} & \bar{A}_{BP} & \bar{A}_{BN} \\ \bar{A}_{FB} & \bar{A}_{FF} & \bar{A}_{FW} & \bar{A}_{FP} & \bar{A}_{FN} \\ \bar{A}_{WB} & \bar{A}_{WF} & \bar{A}_{WW} & \bar{A}_{WP} & \bar{A}_{WN} \\ \bar{A}_{PB} & \bar{A}_{PF} & \bar{A}_{PW} & \bar{A}_{PP} & \bar{A}_{PN} \\ \bar{A}_{NB} & \bar{A}_{NF} & \bar{A}_{NW} & \bar{A}_{NP} & \bar{A}_{NN} \end{bmatrix} \begin{bmatrix} K_B/V_{\infty} \\ K_F/V_{\infty} \\ K_W/V_{\infty} \\ K_P/V_{\infty} \\ \sigma_N/V_{\infty} \end{bmatrix} = \begin{bmatrix} \nabla S_B \\ \nabla S_F \\ \nabla S_W \\ \nabla S_P \\ \nabla S_N \end{bmatrix} \tag{106}$$

CONSTRAINT EQUATIONS

The discrete matrix influence equation can be transformed to reduce the number of unknowns by letting the discrete vortex strengths on the wing and pylon be defined by:

$$\frac{K_i}{V_\infty} = 4\pi b \bar{\rho} \left[\left(K'_{oi}/V_\infty \right) F_o + \left(K'_{fi}/V_\infty \right) F_f + \left(K'_{ki}/V_\infty \right) F_k + \sum_{N=1}^{N_w-3} \left(K'_{wi}/V_\infty \right) F_w \right] \tag{107}$$

Where F_o , F_f , F_k , and F_w and K'_{oi} , K'_{fi} , K'_{ki} , and K'_{wi} are defined in Appendices F and G, respectively. Equation 107 can be written in matrix notation as:

$$\left\{ \frac{K}{V_\infty} \right\} = \left[\quad T \quad \right] \left\{ F \right\} \tag{108}$$

Also, due to the definition of $\{F\}$ in equation 51 of Appendix F.

$$\left\{ \frac{K}{V_\infty} \right\} = \left[T(\tfrac{x}{c}) \right] \left[T(\eta) \right] \left\{ a \right\} = \left[\quad S \quad \right] \left\{ a \right\} \tag{109}$$

The pylon vortex strengths are constrained in the chordwise direction only, therefore, they are defined by an expression of the form;

$$\left\{ \frac{K_p}{V_\infty} \right\} = \left[\quad T_p \quad \right] \left\{ F_p \right\} \tag{110}$$

The form of the expression used to define the K's on the wing can be either that of equation 108 or that of equation 109, depending on whether just the chordwise variation of vortex strengths is constrained or both the chordwise and spanwise variations of vortex strengths are constrained. If just the chordwise direction is constrained, the wing vortex strengths are defined by;

$$\left\{ \frac{K_w}{V_\infty} \right\} = \left[\quad T_w \quad \right] \left\{ F_w \right\} \tag{111}$$

If both the chordwise and spanwise directions of the wing are constrained;

$$\left\{ \frac{K_w}{V_\infty} \right\} = \left[\quad S_w \quad \right] \left\{ a_w \right\} \tag{112}$$

A matrix constraint equation for the fanpod and fuselage vortex strengths is derived in Appendix H. This equation has the form:

$$\left\{\frac{K}{V_\infty}\right\} = \left[\quad R L \phi \quad\right]\left\{F\right\} \tag{113}$$

After combining equations 110 , 112 , and 113 , the transformation matrix by which the discrete influence matrix is post multiplied, to obtain the constrained influence matrix, is given by;

$$\begin{bmatrix} [(RL\phi)_B] & [0] & [0] & [0] & [0] \\ [0] & [(RL\phi)_F] & [0] & [0] & [0] \\ [0] & [0] & [S_W] & [0] & [0] \\ [0] & [0] & [0] & [T_P] & [0] \\ [0] & [0] & [0] & [0] & [1] \end{bmatrix} \tag{114}$$

Therefore, the constrained influence matrix is;

$$\begin{bmatrix} A_{BB} & A_{BF} & A_{BW} & A_{BP} & A_{BN} \\ A_{FB} & A_{FF} & A_{FW} & A_{FP} & A_{FN} \\ A_{WB} & A_{WF} & A_{WW} & A_{WP} & A_{WN} \\ A_{PB} & A_{PF} & A_{PW} & A_{PP} & A_{PN} \\ A_{NB} & A_{NF} & A_{NW} & A_{NP} & A_{NN} \end{bmatrix} = \begin{bmatrix} \bar{A}_{BB} & \bar{A}_{BF} & \bar{A}_{BW} & \bar{A}_{BP} & \bar{A}_{BN} \\ \bar{A}_{FB} & \bar{A}_{FF} & \bar{A}_{FW} & \bar{A}_{FP} & \bar{A}_{FN} \\ \bar{A}_{WB} & \bar{A}_{WF} & \bar{A}_{WW} & \bar{A}_{WP} & \bar{A}_{WN} \\ \bar{A}_{PB} & \bar{A}_{PF} & \bar{A}_{PW} & \bar{A}_{PP} & \bar{A}_{PN} \\ \bar{A}_{NB} & \bar{A}_{NF} & \bar{A}_{NW} & \bar{A}_{NP} & \bar{A}_{NN} \end{bmatrix} \begin{bmatrix} (RL\phi)_B & 0 & 0 & 0 & 0 \\ 0 & (RL\phi)_F & 0 & 0 & 0 \\ 0 & 0 & S_W & 0 & 0 \\ 0 & 0 & 0 & T_P & 0 \\ 0 & 0 & 0 & 0 & 1 \end{bmatrix} \tag{115}$$

SOLUTION OF INFLUENCE EQUATIONS

To solve the constrained influence equation the unknowns are divided into two sets; (1) those which define the strengths of the singularities on the wing, pylon, fuselage and fanpod, and (2) those which define the source strength of the nacelle. When this is done, the influence matrix equation is partitioned as follows;

$$\left[\begin{array}{cccc|c} A_{BB} & A_{BF} & A_{BW} & A_{BP} & A_{BN} \\ A_{FB} & A_{FF} & A_{FW} & A_{FP} & A_{FN} \\ A_{WB} & A_{WF} & A_{WW} & A_{WP} & A_{WN} \\ A_{PB} & A_{PF} & A_{PW} & A_{PP} & A_{PN} \\ \hline A_{NB} & A_{NF} & A_{NW} & A_{NP} & A_{NN} \end{array}\right]\left[\begin{array}{c} F_B \\ F_F \\ a_W \\ a_P \\ \hline \Phi_i/4\pi \end{array}\right] = \left[\begin{array}{c} \nabla S_B \\ \nabla S_F \\ \nabla S_W \\ \nabla S_P \\ \hline \nabla S_N \end{array}\right] \tag{116}$$

This matrix can then be represented by

$$\left[\begin{array}{cc} A_{11} & A_{12} \\ A_{21} & A_{22} \end{array}\right]\left[\begin{array}{c} a_1 \\ a_2 \end{array}\right] = \left[\begin{array}{c} \nabla S_1 \\ \nabla S_2 \end{array}\right] \tag{117}$$

where

$$A_{11} = \left[\begin{array}{ccc} A_{WW} & A_{WP} & A_{WF} \\ A_{PW} & A_{PP} & A_{PF} \\ A_{FW} & A_{FP} & A_{FF} \end{array}\right] \tag{118}$$

$$A_{12} = \left[\begin{array}{c} A_{WN} \\ A_{PN} \\ A_{FN} \end{array}\right] \tag{119}$$

$$A_{21} = \left[\begin{array}{ccc} A_{NW} & A_{NP} & A_{NF} \end{array}\right] \tag{120}$$

and

$$A_{22} = A_{NN} \tag{121}$$

The solution to equation 117 is then found as follows;

$$A_{11} a_1 + A_{12} a_2 = \nabla S_1 \tag{122}$$

$$A_{21} a_1 + A_{22} a_2 = \nabla S_2 \tag{123}$$

$$A_{22}^{-1} A_{21} a_1 + a_2 = A_{22}^{-1} \nabla S_2 \tag{124}$$

$$A_{12} A_{22}^{-1} A_{21} a_1 + A_{12} a_2 = A_{12} A_{22}^{-1} \nabla S_2 \tag{125}$$

Then after subtracting equation 125 from equation 122;

$$[A_{11} - A_{12}(A_{22}^{-1} A_{21})] a_1 = \nabla S_1 - A_{12}(A_{22}^{-1} \nabla S_2) \tag{126}$$

Since $[A_{11} - A_{12} A_{22}^{-1} A_{21}]$ is not square, equation 126 is solved using Householder's triangulation procedure discussed in Appendix A. This solution will be denoted by;

$$a_1 = [A_{11} - A_{12}(A_{22}^{-1} A_{21})]^{-1} [\nabla S_1 - A_{12}(A_{22}^{-1} \nabla S_2)] \tag{127}$$

Equation 127 is then substituted back into equation 123 to obtain a_2.

$$a_2 = A_{22}^{-1} [\nabla S_2 - A_{21} a_1] \tag{128}$$

SURFACE VELOCITIES AND PRESSURES

In order to compute the surface velocities, the component influence matrices are multiplied by the components of the surface tangent unit vector, in a scalar product, and then in turn post multiplied by the unknown coefficients obtained in the simultaneous influence equation solution. This is done for the influence of the wing, pylon, fuselage, fanpod, and nacelle on the wing, pylon, fuselage, and fanpod. The components of the surface resultant velocity due to each of the configuration components are then summed to obtain the total surface velocity at each of the control points. This velocity is then substituted into the Bernoulli equation to obtain the surface static pressures.

WING ON WING

The velocity ratio components on the wing due to the wing vorticity and source density are given by the following expressions.

$$\frac{V_{W_W W}}{V_\infty} = \frac{\frac{u_{W_C}}{V_\infty} \pm \left(\frac{u_{W_L}}{V_\infty}\right)_{N=0} \left\{1 + \sqrt{1+\tau A N^2 \phi_W}\left[\frac{u_{W_C}}{V_\infty} - \frac{u'_{W_C}}{V_\infty}\right]\right\} \pm \left(\frac{u_{W_L}}{V_\infty}\right)_{N=1,2,\cdots,N_W-3,\,f,\,K}}{\left\{1 + \left(1 + \tau A N^2 \phi_W\right)\left(\frac{dz_{W_C}}{dx_W} \pm \frac{dz_{W_L}}{dx_W}\right)^2\right\}^{1/2}} \tag{129}$$

$$\frac{V_{T_W W}}{V_\infty} = \frac{\frac{v_{W_C}}{V_\infty} \pm \left(\frac{v_{W_L}}{V_\infty}\right)_{N=0} \left\{1 + \sqrt{1+\tau A N^2 \phi_W}\left[\frac{v_{W_C}}{V_\infty} - \frac{v'_{W_C}}{V_\infty}\right]\right\} \pm \left(\frac{v_{W_L}}{V_\infty}\right)_{N=1,2,\cdots,N_W-3,\,f,\,K}}{\left\{1 + \left(1 + \tau A N^2 \phi_W\right)\left(\frac{dz_{W_C}}{dx_W} \pm \frac{dz_{W_L}}{dx_W}\right)^2\right\}^{1/2}} \tag{130}$$

Where the upper sign is applied to the upper surface calculation and the lower sign to the lower surface, also;

$$\left(\frac{u_{W_L}}{V_\infty}\right)_{N=0} = \frac{2 b_W}{c_W \beta} F_{0_W} \cot \theta_{1/2} \tag{131}$$

$$\left(\frac{u_{W_L}}{V_\infty}\right)_{N=1,2,\cdots,N_W-3,\,f,\,K} = \frac{2 b_W}{c_W \beta}\left\{\sum_{N=1}^{N_W-3} F_{N_W} \sin N\theta_W + F_f \log_e \left|\frac{\sin\frac{1}{2}(\theta_W + \theta_f)}{\sin\frac{1}{2}(\theta_W - \theta_f)}\right| + F_K \log_e \left|\frac{\sin\frac{1}{2}(\theta_W + \theta_c)}{\sin\frac{1}{2}(\theta_W - \theta_c)}\right|\right\} \tag{132}$$

$$\left(\frac{v_{W_L}}{V_\infty}\right)_{N=0} = 2\left\{\frac{1}{\beta}\frac{\partial F_{0_W}}{\partial \eta_W}(\sin\theta_W + \theta_W) - \frac{2 b_W}{c_W} F_{0_W} \cot\theta_{1/2}\left[\tau A N \phi^*_{W_{L.E.}} + \frac{1}{2}\left(\tau A N \phi^*_{W_{L.E.}} - \tau A N \phi^*_{W_{L.E.}}\right)(1 - \cos\theta_W)\right]\right\} \tag{133}$$

and

$$\left(\frac{v_{w_L}}{V_\infty}\right)_{N=1,2,\cdots,N_w-3,f,K} = \frac{2}{B}\left\{\frac{\partial F_{1w}}{\partial \eta_w}\left(\frac{\theta_w}{2} - \frac{1}{4}\sin 2\theta_w\right) + \sum_{N=2}^{N_w-3}\frac{\partial F_{Nw}}{\partial \eta_w}\left[\frac{\sin(N-1)\theta_w}{2(N-1)}\right.\right.$$

$$\left. - \frac{\sin(N+1)\theta_w}{2(N+1)}\right] + \frac{\partial F_f}{\partial \eta_w}\left[\left(\cos\theta_w\right.\right.$$

$$\left. - \cos\theta_f\right)\log_e\left|\frac{\sin\frac{1}{2}(\theta_w-\theta_f)}{\sin\frac{1}{2}(\theta_w+\theta_f)}\right| + \theta_w\sin\theta_f$$

$$\left. + \frac{\partial F_K}{\partial \eta_w}\left[\left(\cos\theta_w - \cos\theta_K\right)\log_e\left|\frac{\sin\frac{1}{2}(\theta_w-\theta_K)}{\sin\frac{1}{2}(\theta_w+\theta_K)}\right| + \theta_w\sin\theta_K\right]\right\}$$

$$- \frac{2b_w}{c_w}\left\{\sum_{N=1}^{N_w-3} F_{Nw}\sin N\theta_w + F_f\log_e\left|\frac{\sin\frac{1}{2}(\theta_w+\theta_f)}{\sin\frac{1}{2}(\theta_w-\theta_f)}\right|\right.$$

$$\left. + F_K\log_e\left|\frac{\sin\frac{1}{2}(\theta_w+\theta_K)}{\sin\frac{1}{2}(\theta_w-\theta_K)}\right|\right\}\left\{\tan\phi^*_{L.E.}\right.$$

$$\left. + \frac{1}{2}\left(\tan\phi^*_{T.E.} - \tan\phi^*_{L.E.}\right)\left(1-\cos\theta_w\right)\right\} \qquad (134)$$

where $\tan\phi^*_{L.E.}$ and $\tan\phi^*_{T.E.}$ and the derivatives $\frac{\partial F_{0w}}{\partial \eta_w}$, $\frac{\partial F_{1w}}{\partial \eta_w}$, $\frac{\partial F_{Nw}}{\partial \eta_w}$, $\frac{\partial F_f}{\partial \eta_w}$, and $\frac{\partial F_K}{\partial \eta_w}$ are defined in Appendix J,

Also;

$$\frac{u_{w_L}}{V_\infty} = \frac{1}{2N_{i_w}\gamma_{s_w}B^2}\left\{\sum_{L=1}^{N_w}\sum_{i=1}^{N_{i_w}} c_{w_L}\left[\left(\frac{x_{w_{s_i}} - x_{w_{L.E._L}}}{c_{w_L}}\right) - \left(\frac{x_{w_{s_i}} - x_{w_{L.E._L}}}{c_{w_L}}\right)^2\right]^{1/2}\left(\frac{dz_w}{dx_w}\right)_{i_L}\right.\left[\right.$$

$$\left.\left.\frac{E_{u_{w_{o_{i_L}}}}T_{w_{o_{i_L}}} - E_{v_{w_{o_{i_L}}}}}{P^2_{w_{o_{i_L}}}} - \frac{E_{u_{w_{i_{i_L}}}}T_{w_{i_{i_L}}} - E_{v_{w_{i_{i_L}}}}}{P^2_{w_{i_{i_L}}}}\right]\right\} \qquad (135)$$

$$\frac{v_{w_t}}{V_\infty} = \frac{1}{2 N_{i_w} \gamma_{s_w} \bar{e}} \left\{ \sum_{L=1}^{N_{L_w}} \sum_{i=1}^{N_{i_w}} c_{w_L} \left[\left(\frac{x_{w_{s_i}} - x_{w_{L.E._L}}}{c_{w_L}} \right) - \left(\frac{x_{w_{s_L}} - x_{w_{L.E._L}}}{c_{w_L}} \right) \right]^{1/2} \left(\frac{d\bar{z}_{w_t}}{d x_w} \right) \left[\right.\right.$$

$$\left. \left. \frac{E_{v_{w_{oLL}}} T_{w_{oLL}} + E_{u_{w_{oLL}}}}{P^2_{w_{oLL}}} - \frac{E_{v_{w_{iLL}}} T_{w_{iLL}} + E_{u_{w_{iLL}}}}{P^2_{w_{iLL}}} \right] \right\} \qquad (136)$$

$$\frac{u'_{w_t}}{V_\infty} = \frac{1}{2 N_{i_w} \gamma_{s_w} \bar{e}} \left\{ \sum_{L=1}^{N_{L_w}} \sum_{i=1}^{N_{i_w}} c_{w_L} \left[\left(\frac{x_{w_{s_i}} - x_{w_{L.E._L}}}{c_{w_L}} \right) - \left(\frac{x_{w_{s_L}} - x_{w_{L.E._L}}}{c_{w_L}} \right)^2 \right]^{1/2} \left[\frac{2 \left(\frac{\bar{z}_{w_t}}{c_{w_L}} \right)_{LL}}{\sin^2 \theta_{w_i}} \right] \right.\left[\right.$$

$$\left. \left. \frac{E_{u_{w_{oLL}}} T_{w_{oLL}} - E_{v_{w_{oLL}}}}{P^2_{w_{oLL}}} - \frac{E_{u_{w_{iLL}}} T_{w_{iLL}} - E_{v_{w_{iLL}}}}{P^2_{w_{iLL}}} \right] \right\} \qquad (137)$$

and

$$\frac{v'_{w_t}}{V_\infty} = \frac{1}{2 N_{i_w} \gamma_{s_w} \bar{e}} \left\{ \sum_{L=1}^{N_{L_w}} \sum_{i=1}^{N_{i_w}} c_{w_L} \left[\left(\frac{x_{w_{s_i}} - x_{w_{L.E._L}}}{c_{w_L}} \right) - \left(\frac{x_{w_{s_L}} - x_{w_{L.E._L}}}{c_{w_L}} \right)^2 \right]^{1/2} \left[\frac{2 \left(\frac{\bar{z}_{w_t}}{c_{w_L}} \right)_{LL}}{\sin^2 \theta_{w_i}} \right] \right.\left[\right.$$

$$\left. \left. \frac{E_{v_{w_{oLL}}} T_{w_{oLL}} + E_{u_{w_{oLL}}}}{P^2_{w_{oLL}}} - \frac{E_{v_{w_{iLL}}} T_{w_{iLL}} + E_{u_{w_{iLL}}}}{P^2_{w_{iLL}}} \right] \right\} \qquad (138)$$

See list of symbols for definition of these velocity components.

$$E_{u w_{i i L}} = \frac{1}{\sqrt{(\bar{X}_{w_i} + \bar{T}_{w_{i i L}})^2 + (\bar{Y}_{w_L} + 1)^2}} - \frac{1}{\sqrt{\bar{X}_{w_i}^2 + \bar{Y}_{w_L}^2}} \tag{139}$$

$$E_{u w_{o i L}} = \frac{1}{\sqrt{(\bar{X}_{w_i} - \bar{T}_{w_{o i L}})^2 + (\bar{Y}_{w_L} - 1)^2}} - \frac{1}{\sqrt{\bar{X}_{w_i}^2 + \bar{Y}_{w_L}^2}} \tag{140}$$

$$E_{v w_{i i L}} = \frac{1}{(\bar{X}_{w_i} - \bar{Y}_{w_L} \bar{T}_{w_{i i L}})} \left\{ \frac{(\bar{Y}_{w_L} + \bar{X}_{w_i} \bar{T}_{w_{i i L}}) + \bar{T}_{w_{i i L}}^2}{\sqrt{(\bar{X}_{w_i} + \bar{T}_{w_{i i L}})^2 + (\bar{Y}_{w_L} + 1)^2}} - \frac{(\bar{Y}_{w_L} + \bar{X}_{w_i} \bar{T}_{w_{i i L}})}{\sqrt{\bar{X}_{w_i}^2 + \bar{Y}_{w_L}^2}} \right\} \tag{141}$$

and

$$E_{v w_{o i L}} = \frac{1}{(\bar{X}_{w_i} - \bar{Y}_{w_L} \bar{T}_{w_{o i L}})} \left\{ \frac{(\bar{Y}_{w_L} + \bar{X}_{w_i} \bar{T}_{w_{o i L}}) - \bar{T}_{w_{o i L}}^2}{\sqrt{(\bar{X}_{w_i} - \bar{T}_{w_{o i L}})^2 + (\bar{Y}_w - 1)^2}} - \frac{(\bar{Y}_{w_L} + \bar{X}_{w_i} \bar{T}_{w_{o i L}})}{\sqrt{\bar{X}_{w_i}^2 + \bar{Y}_{w_i}^2}} \right\} \tag{142}$$

where $\bar{X}_{w_i} = \dfrac{X_{w_\delta} - X_{w_{Si}}}{\beta\, y_{s_w}}$, $\bar{Y}_{w_L} = \dfrac{Y_{w_\delta} - Y_{w_{Si}}}{y_{s_w}}$, $T_{w_{b_{ii}}} = \frac{1}{\beta}\tan\phi_0$

$$T_{w_{i_{ii}}} = \frac{1}{\beta}\tan\phi_{w_i} \;,\quad P_{w_{o_{ii}}} = \left[1 + \left(\frac{\tan\phi_{w_o}}{\beta}\right)^2\right]^{1/2} \;,\quad P_{w_{i_{ii}}} = \left[1 + \left(\frac{\tan\phi_{w_i}}{\beta}\right)^2\right]^{1/2}$$

The indices i and ℓ refer to the chordwise and spanwise source line locations, respectively.

The bracketed terms of equations 141 and 142 are seen to be identical to the third and fourth bracketed terms of equation 14 in Appendix C, respectively. Because of this, the velocity due to thickness and the induced velocity due to the bound vortex segments can be computed simultaneously saving a considerable amount of computer time.

It is noted that equations 139 and 136 are the same as equations 137 and 138 , respectively, except for $2(\bar{\gamma}/c_{w_i})_{i_L}/\sin^2\phi_i$ being substituted in for $(d\bar{z}_w/dx_w)_{i_L}$. Also, the last terms in equations 141 and 142 are omitted when substituted into equations 137 and 138 .

FANPOD ON WING

The velocity induced tangent to the wing surface by the fanpod quadrilateral vortices is given by;

$$\left\{\frac{V_{M_{WF}}}{V_\infty}\right\} = \left[\frac{1}{\beta^2} T_{W_{M_{X_W}}} A_{WF_{X_W}} + \frac{1}{\beta^2} T_{W_{M_{Y_W}}} A_{WF_{Y_W}} + \frac{1}{\beta} T_{W_{M_{Z_W}}} A_{WF_{Z_W}}\right]\left\{\frac{K_F}{V_\infty}\right\} \quad (143)$$

where

$$\left[A_{WF_{X_W}}\right] = \left[\cos\alpha_{F_W}\right]\left[A_{WF_{X_F}}\right] + \left[\sin\alpha_{F_W}\right]\left[A_{WF_{Z_F}}\right] \quad (144)$$

$$\left[A_{WF_{Y_W}}\right] = \left[A_{WF_{Y_F}}\right] \quad (145)$$

$$\left[A_{WF_{Z_W}}\right] = -\left[\sin\alpha_{F_W}\right]\left[A_{WF_{X_F}}\right] + \left[\cos\alpha_{F_W}\right]\left[A_{WF_{Z_F}}\right] \quad (146)$$

$$\left[T_{W_{M_{X_W}}}\right] = \left[\frac{1}{\left\{1 + (1+\tan^2\phi_W)\left(\frac{d\bar{z}_{w_T}}{dx_w} \pm \frac{d\bar{z}_{w_C}}{dx_w}\right)^2\right\}^{1/2}}\right] \quad (147)$$

$$\left[T_{W_{M_{Y_W}}}\right] = \left[0\right] \quad (148)$$

$$\left[T_{W_{M_{Z_W}}} \right] = \left[\begin{array}{c} \\ 0 \\ \\ \end{array} \right] \tag{149}$$

since α_{FW} is small;

$$\left\{ \frac{V_{M_{WF}}}{V_\infty} \right\} = \left[\begin{array}{c} \\ \dfrac{1}{\beta^2 \left\{ 1 + (1+\tau_{AW}^2 \phi_W^2)\left(\frac{dz_{WC}}{dx_W} \pm \frac{dz_{We}}{dx_W} \right)^2 \right\}^{1/2}} \\ \\ \end{array} \right] \left[A_{WF_{X_F}} \right] \left\{ \frac{K_F}{V_\infty} \right\} \tag{150}$$

Also,

$$\left\{ \frac{V_{T_{WF}}}{V_\infty} \right\} = \left[\frac{1}{\beta^2} T_{W_{T_{X_W}}} A_{WF_{X_W}} + \frac{1}{\beta^2} T_{W_{T_{Y_W}}} A_{WF_{Y_W}} + \frac{1}{\beta^2} T_{W_{T_{Z_W}}} A_{WF_{Z_W}} \right] \left\{ \frac{K_F}{V_\infty} \right\} \tag{151}$$

where

$$\left[T_{W_{T_{X_W}}} \right] = \left[\begin{array}{c} \\ 0 \\ \\ \end{array} \right] \tag{152}$$

$$\left[T_{W_{T_{Y_W}}} \right] = \left[\begin{array}{c} \\ \dfrac{1}{\left\{ 1 + (1+\tau_{AW}^2 \phi_W^2)\left(\frac{dz_{WC}}{dx_W} \pm \frac{dz_{We}}{dx_W} \right)^2 \right\}^{1/2}} \\ \\ \end{array} \right] \tag{153}$$

and

$$\left[T_{W_{T_{Z_W}}} \right] = \left[\begin{array}{c} \\ 0 \\ \\ \end{array} \right] \tag{154}$$

Therefore:

$$\left\{ \frac{V_{T_{WF}}}{V_\infty} \right\} = \left[\begin{array}{c} \\ \dfrac{1}{\beta \left\{ 1 + (1+\tau_{AW}^2 \phi_W^2)\left(\frac{dz_{WC}}{dx_W} \pm \frac{dz_{We}}{dx_W} \right)^2 \right\}^{1/2}} \\ \\ \end{array} \right] \left[A_{WF_{Y_F}} \right] \left\{ \frac{K_F}{V_\infty} \right\} \tag{155}$$

The influence matrices $A_{WF_{X_F}}$ and $A_{WF_{Y_F}}$ are computed with equations derived in Appendix D.

FUSELAGE ON WING

The velocity induced tangent to the wing surface by the fuselage quadrilateral vortices is given by:

$$\left\{ \frac{V_{M_{WB}}}{V_\infty} \right\} = \left[\frac{1}{\beta^2} T_{W_{M_{X_W}}} A_{WB_{X_W}} + \frac{1}{\beta^2} T_{W_{M_{Y_W}}} A_{WB_{Y_W}} + \frac{1}{\beta^2} T_{W_{M_{Z_W}}} A_{WB_{Z_W}} \right] \left\{ \frac{K_B}{V_\infty} \right\} \tag{156}$$

Therefore, since $T_{W_{M_{Y_W}}} = T_{W_{M_{Z_W}}} = 0$;

$$\left\{\frac{V_{M_{WB}}}{V_\infty}\right\} = \left[\frac{1}{\beta^2\left\{1+(1+\tau A R^2 \phi_W)\left(\frac{dz_{WC}}{dx_W} \pm \frac{dz_{WC}}{dx_W}\right)^2\right\}^{1/2}}\right]\left[\; A_{WB_{X_B}} \;\right]\left\{\frac{K_B}{V_\infty}\right\} \qquad (157)$$

Also;

$$\left\{\frac{V_{T_{WB}}}{V_\infty}\right\} = \left[\frac{1}{\beta^2} T_{W_{T_{X_W}}} A_{WB_{X_W}} + \frac{1}{\beta} T_{W_{T_{Y_W}}} A_{WB_{Y_W}} + \frac{1}{\beta} T_{W_{T_{Z_W}}} A_{WB_{Z_W}}\right]\left\{\frac{K_B}{V_\infty}\right\} \qquad (158)$$

since $T_{W_{T_{X_W}}} = T_{W_{T_{Z_W}}} = 0$

$$\left\{\frac{V_{T_{WB}}}{V_\infty}\right\} = \left[\frac{1}{\beta\left\{1+(1+\tau A R^2 \phi_W)\left(\frac{dz_{WC}}{dx_W} \pm \frac{dz_{WC}}{dx_W}\right)^2\right\}^{1/2}}\right]\left[\; A_{WB_{Y_B}} \;\right]\left\{\frac{K_B}{V_\infty}\right\} \qquad (159)$$

The influence matrices $A_{WB_{X_B}}$ and $A_{WB_{Y_B}}$ are computed with equations derived in Appendix D.

PYLON ON WING

The velocity induced tangent to the wing surface by the pylon vortex and source lattices is given by;

$$\left\{\frac{V_{M_{WP}}}{V_\infty}\right\} = \left[\frac{1}{\beta^2} T_{W_{M_{X_W}}} A_{WP_{X_W}} + \frac{1}{\beta} T_{W_{M_{Y_W}}} A_{WP_{Y_W}} + \frac{1}{\beta} T_{W_{M_{Z_W}}} A_{WP_{Z_W}}\right]\left\{\frac{K_P}{V_\infty}\right\}$$

$$+ \left[\frac{1}{\beta^2} T_{W_{M_{X_W}}} S_{WP_{X_W}} + \frac{1}{\beta} T_{W_{M_{Y_W}}} S_{WP_{Y_W}} + \frac{1}{\beta} T_{W_{M_{Z_W}}} S_{WP_{Z_W}}\right]\left\{\frac{\sigma_W}{V_\infty}\right\} \qquad (160)$$

where

$$\left[A_{WP_{x_W}}\right] = \left[A_{WP_{x_P}}\right] \tag{161}$$

$$\left[A_{WP_{y_W}}\right] = \left[\sin\gamma\right]\left[A_{WP_{y_P}}\right] - \left[\cos\gamma\right]\left[A_{WP_{z_P}}\right] \tag{162}$$

$$\left[A_{WP_{z_W}}\right] = \left[\cos\gamma\right]\left[A_{WP_{y_P}}\right] + \left[\sin\gamma\right]\left[A_{WP_{z_P}}\right] \tag{163}$$

$$\left[S_{WP_{x_W}}\right] = \left[S_{WP_{x_P}}\right] \tag{164}$$

$$\left[S_{WP_{y_W}}\right] = \left[\sin\gamma\right]\left[S_{WP_{y_P}}\right] - \left[\cos\gamma\right]\left[S_{WP_{z_P}}\right] \tag{165}$$

and

$$\left[S_{WP_{z_W}}\right] = \left[\cos\gamma\right]\left[S_{WP_{y_P}}\right] + \left[\sin\gamma\right]\left[S_{WP_{z_P}}\right] \tag{166}$$

Therefore;

$$\left\{\frac{V_{MWP}}{V_\infty}\right\} = \left[\frac{1}{\beta^2\left\{1+(1+\tau A N^2\phi_W)\left(\frac{dz_{WU}}{dx_W} \pm \frac{dz_{WL}}{dx_W}\right)^2\right\}^{1/2}}\right]\left\{\left[A_{WP_{x_P}}\right]\left\{\frac{K_P}{V_\infty}\right\} + \left[S_{WP_{x_P}}\right]\left\{\frac{\alpha_P}{V_\infty}\right\}\right\}$$

and

$$\left\{\frac{V_{TWP}}{V_\infty}\right\} = \left[\frac{1}{\beta^2}T_{W_{T_{x_W}}}A_{WP_{x_W}} + \frac{1}{\beta}T_{W_{T_{y_W}}}A_{WP_{y_W}} + \frac{1}{\beta}T_{W_{T_{z_W}}}A_{WP_{z_W}}\right]\left\{\frac{K_P}{V_\infty}\right\} + \left[\frac{1}{\beta^2}T_{W_{T_{x_W}}}S_{WP_{x_W}} + \frac{1}{\beta}T_{W_{T_{y_W}}}S_{WP_{y_W}} + \frac{1}{\beta}T_{W_{T_{z_W}}}S_{WP_{z_W}}\right]\left\{\frac{\alpha_P}{V_\infty}\right\} \tag{167}$$

since

$$\left[T_{W_{T_{X_W}}}\right] = \left[0\right] \tag{168}$$

$$\left[T_{W_{T_{Y_W}}}\right] = \left[\frac{1}{\left\{1+(1+\tau A N^2 \phi_W)\left(\frac{dz_{W_C}}{dx_W} \pm \frac{dz_{W_t}}{dx_W}\right)^2\right\}^{1/2}}\right] \tag{169}$$

$$\left[T_{W_{T_{Z_W}}}\right] = \left[0\right] \tag{170}$$

then

$$\left\{\frac{V_{T_{WP}}}{V_\infty}\right\} = -\left[\frac{1}{\beta\left\{1+(1+\tau A N^2 \phi_W)\left(\frac{dz_{W_C}}{dx_W} \pm \frac{dz_{W_t}}{dx_W}\right)^2\right\}^{1/2}}\right]\left\{\left\{\left[\sin\gamma\right]\left[A_{WP_{Y_P}}\right] - \left[\cos\gamma\right]\left[A_{WP_{Z_P}}\right]\right\}\left\{\frac{K_P}{V_\infty}\right\} + \left\{\left[\sin\gamma\right]\left[S_{WP_{Y_P}}\right] - \left[\cos\gamma\right]\left[S_{WP_{Z_P}}\right]\right\}\left\{\frac{\sigma_P}{V_\infty}\right\}\right\} \tag{171}$$

The influence matrices $A_{WP_{X_P}}$, $A_{WP_{Y_P}}$ and $A_{WP_{Z_P}}$ are computed from equations defined in Appendices C and D. The matrices $S_{WP_{X_P}}$, $S_{WP_{Y_P}}$, and $S_{WP_{Z_P}}$ are computed from equations defined in Appendix B.

NACELLE ON WING

The velocity induced tangent to the wing surface by the nacelle source frustums is given by;

$$\left\{\frac{V_{N_W}}{V_\infty}\right\} = \left[\frac{1}{\beta^2} T_{W_{N_{X_W}}} A_{WN_{X_W}} + \frac{1}{\beta} T_{W_{N_{Y_W}}} A_{WN_{Y_W}} + \frac{1}{\beta} T_{W_{N_{Z_W}}} A_{WN_{Z_W}}\right]\left\{\frac{\sigma_N}{V_\infty}\right\} \tag{172}$$

since

$$\left[A_{WW_{X_W}}\right] = \left[A_{WW_{X_W}}\right] \tag{173}$$

$$\left[A_{WW_{Y_W}}\right] = -\left[\sin(\gamma-\theta_{WW})\right]\left[A_{WW_{Y_W}}\right] \tag{174}$$

and

$$\left[A_{WW_{Z_W}}\right] = -\left[\cos(\gamma-\theta_{WW})\right]\left[A_{WW_{Y_W}}\right] \tag{175}$$

then

$$\left\{\frac{V_{m_{WW}}}{V_\infty}\right\} = \left[\frac{1}{\beta^2\left[1+(1+\tau A N^2\phi_W)\left(\frac{dz_{WC}}{dx_W}\pm\frac{dz_{WC}}{dx_W}\right)^2\right]^{1/2}}\right]\left[A_{WW_{X_W}}\right]\left\{\frac{\sigma_W}{V_\infty}\right\} \tag{176}$$

Also;

$$\left\{\frac{V_{T_{WW}}}{V_\infty}\right\} = \left[\frac{1}{\beta^2}T_{W_{T_{X_W}}}A_{WW_{X_W}} + \frac{1}{\beta}T_{W_{T_{Y_W}}}A_{WW_{Y_W}} + \frac{1}{\beta}T_{W_{T_{Z_W}}}A_{WW_{Z_W}}\right]\left\{\frac{\sigma_W}{V_\infty}\right\} \tag{177}$$

then

$$\left\{\frac{V_{T_{WW}}}{V_\infty}\right\} = \left[\frac{1}{\beta\left\{1+(1+\tau A N^2\phi_W)\left(\frac{dz_{WC}}{dx_W}\pm\frac{dz_{WC}}{dx_W}\right)^2\right]^{1/2}}\right]\left[\sin\theta_{WW}\right]\left[A_{WW_{Y_W}}\right]\left\{\frac{\sigma_W}{V_\infty}\right\} \tag{178}$$

The influence matrices $A_{WW_{X_W}}$ and $A_{WW_{Y_W}}$ are calculated with equations defined in Appendix E.

FREESTREAM ON WING

Expressions for the velocity tangent to the wing surface due to the freestream were given in reference .

$$\frac{V_{TW\infty}}{V_\infty} = \frac{1+\tau A N^2\phi_W\left[1+(1+\tau A N^2\phi_W)\left(\frac{dz_{WC}}{dx_W}\pm\frac{dz_{WC}}{dx_W}\right)^2\right]^{1/2}}{\left[1+\tau A N^2\phi_W\right]\left[1+(1+\tau A N^2\phi_W)\left(\frac{dz_{WC}}{dx_W}\pm\frac{dz_{WC}}{dx_W}\right)^2\right]^{1/2}} \tag{179}$$

and

$$\frac{V_{T_{W\infty}}}{V_\infty} = -\frac{\tau A N\phi_W\left\{1-\left[1+(1+\tau A N^2\phi_W)\left(\frac{dz_{WC}}{dx_W}\pm\frac{dz_{WC}}{dx_W}\right)^2\right]^{1/2}\right\}}{\left[1+\tau A N^2\phi_W\right]\left[1+(1+\tau A N^2\phi_W)\left(\frac{dz_{WC}}{dx_W}\pm\frac{dz_{WC}}{dx_W}\right)^2\right]^{1/2}} \tag{180}$$

WING ON PYLON

The velocity induced tangent to the pylon surface by the wing source and vortex lattices is given by the following expressions.

$$\left\{\frac{V_{IPW}}{V_\infty}\right\} = \left[\frac{1}{\beta^2} T_{PM_{XP}} A_{PW_{XP}} + \frac{1}{\beta} T_{PM_{YP}} A_{PW_{YP}} + \frac{1}{\beta} T_{PM_{ZP}} A_{PW_{ZP}}\right]\left\{\frac{K_W}{V_\infty}\right\}$$

$$+ \left[\frac{1}{\beta^2} T_{PM_{XP}} S_{PW_{XP}} + \frac{1}{\beta} T_{PM_{YP}} S_{PW_{YP}} + \frac{1}{\beta} T_{PM_{ZP}} S_{PW_{ZP}}\right]\left\{\frac{\sigma_W}{V_\infty}\right\} \tag{181}$$

where

$$\left[T_{PM_{XP}}\right] = \left[\frac{1}{\left\{1 + (1+\tan^2\phi_p)\left(\frac{dz_{PT}}{dx_p} \pm \frac{dz_{PC}}{dx_p}\right)^2\right\}^{1/2}}\right] \tag{182}$$

$$\left[T_{PM_{YP}}\right] = \left[0\right] \tag{183}$$

$$\left[T_{PM_{ZP}}\right] = \left[0\right] \tag{184}$$

$$\left[A_{PW_{XP}}\right] = \left[A_{PW_{XW}}\right] \tag{185}$$

$$\left[A_{PW_{YP}}\right] = \left[\sin\gamma\right]\left[A_{PW_{YW}}\right] + \left[\cos\gamma\right]\left[A_{PW_{ZW}}\right] \tag{186}$$

$$\left[A_{PW_{ZP}}\right] = -\left[\cos\gamma\right]\left[A_{PW_{YW}}\right] + \left[\sin\gamma\right]\left[A_{PW_{ZW}}\right] \tag{187}$$

$$\left[S_{PW_{XP}}\right] = \left[S_{PW_{XW}}\right] \tag{188}$$

$$\left[S_{PW_{YP}}\right] = \left[\sin\gamma\right]\left[S_{PW_{YW}}\right] + \left[\cos\gamma\right]\left[S_{PW_{ZW}}\right] \tag{189}$$

$$\left[S_{PW_{ZP}}\right] = -\left[\cos\gamma\right]\left[S_{PW_{YW}}\right] + \left[\sin\gamma\right]\left[S_{PW_{ZW}}\right] \tag{190}$$

Therefore;

$$\left\{\frac{V_{TPW}}{V_\infty}\right\} = \left[\frac{1}{\beta^2\left\{1+(1+\tau A_W^2\phi_P)\left(\frac{d\bar{z}_{PT}}{d\bar{x}_P} \pm \frac{d\bar{z}_{PC}}{d\bar{x}_P}\right)^2\right\}^{1/2}}\right]\left\{\left[A_{PW_{XW}}\right]\left\{\frac{K_W}{V_\infty}\right\} + \left[S_{PW_{XW}}\right]\left\{\frac{\sigma_W}{V_\infty}\right\}\right\} \tag{191}$$

Also;

$$\left\{\frac{V_{TPW}}{V_\infty}\right\} = \left[\frac{1}{\beta^2}T_{PT_{XP}}A_{PW_{XP}} + \frac{1}{\beta^2}T_{PT_{YP}}A_{PW_{YP}} + \frac{1}{\beta^2}T_{PT_{ZP}}A_{PW_{ZP}}\right]\left\{\frac{K_W}{V_\infty}\right\} + \left[\frac{1}{\beta^2}T_{PT_{XP}}S_{PW_{XP}} + \frac{1}{\beta^2}T_{PT_{YP}}S_{PW_{YP}} + \frac{1}{\beta^2}T_{PT_{ZP}}S_{PW_{ZP}}\right]\left\{\frac{\sigma_W}{V_\infty}\right\} \tag{192}$$

since

$$\left[T_{PT_{XP}}\right] = \left[0\right] \tag{193}$$

$$\left[T_{PT_{YP}}\right] = \left[\frac{1}{\left\{1+(1+\tau A_W^2\phi_P)\left(\frac{d\bar{z}_{PT}}{d\bar{x}_P} \pm \frac{d\bar{z}_{PC}}{d\bar{x}_P}\right)^2\right\}^{1/2}}\right] \tag{194}$$

and

$$\left[T_{PT_{ZP}}\right] = \left[0\right] \tag{195}$$

Therefore;

$$\left\{\frac{V_{TPW}}{V_\infty}\right\} = \left[\frac{1}{\beta\left\{1+(1+\tau A_W^2\phi_P)\left(\frac{d\bar{z}_{PT}}{d\bar{x}_P} \pm \frac{d\bar{z}_{PC}}{d\bar{x}_P}\right)^2\right\}^{1/2}}\right]\left\{\left[A_{PW_{YP}}\right]\left\{\frac{K_W}{V_\infty}\right\} + \left[S_{PW_{YP}}\right]\left\{\frac{\sigma_W}{V_\infty}\right\}\right\} \tag{196}$$

The influence matrices $A_{PW_{XW}}$, $A_{PW_{YW}}$, and $A_{PW_{ZW}}$ are computed by equations defined in Appendices C and D. The matrices $S_{PW_{XW}}$, $S_{PW_{YW}}$, and $S_{PW_{ZW}}$ are computed by equations in Appendix B.

FANPOD ON PYLON

The flow induced by the fanpod quadrilateral vortices tangent to the pylon surface is given by the following expressions.

$$\left\{\frac{V_{INDF}}{V_\infty}\right\} = \left[\frac{1}{\ell^2} T_{PM_{XP}} A_{PF_{XP}} + \frac{1}{\ell} T_{PM_{YP}} A_{PF_{YP}} + \frac{1}{\ell} T_{PM_{ZP}} A_{PF_{ZP}}\right]\left\{\frac{K_F}{V_\infty}\right\} \tag{197}$$

where

$$\left[A_{PF_{XP}}\right] = \left[A_{PF_{XF}}\right] \tag{198}$$

$$\left[A_{PF_{YP}}\right] = \left[\sin\delta\right]\left[A_{PF_{YF}}\right] + \left[\cos\delta\right]\left[A_{PF_{ZF}}\right] \tag{199}$$

and

$$\left[A_{PF_{ZP}}\right] = -\left[\cos\delta\right]\left[A_{PF_{YF}}\right] + \left[\sin\delta\right]\left[A_{PF_{ZF}}\right] \tag{200}$$

Therefore;

$$\left\{\frac{V_{INDF}}{V_\infty}\right\} = \left[\frac{1}{\ell^2\left\{1+(1+\tan^2\phi_P)\left(\frac{dZ_{PT}}{dX_P} \pm \frac{dZ_{PC}}{dX_P}\right)^2\right\}^{1/2}}\right]\left[A_{PF_{XF}}\right]\left\{\frac{K_F}{V_\infty}\right\} \tag{201}$$

also;

$$\left\{\frac{V_{TPF}}{V_\infty}\right\} = \left[\frac{1}{\ell^2} T_{PT_{XP}} A_{PF_{XP}} + \frac{1}{\ell} T_{PT_{YP}} A_{PF_{YP}} + \frac{1}{\ell} T_{PT_{ZP}} A_{PF_{ZP}}\right]\left\{\frac{K_F}{V_\infty}\right\} \tag{202}$$

or

$$\left\{\frac{V_{TPF}}{V_\infty}\right\} = \left[\frac{1}{\ell^2\left\{1+(1+\tan^2\psi_P)\left(\frac{dZ_{PT}}{dX_P} \pm \frac{dZ_{PC}}{dX_P}\right)^2\right\}^{1/2}}\right]\left[A_{PF_{YP}}\right]\left\{\frac{K_F}{V_\infty}\right\} \tag{203}$$

The influence matrices $A_{PF_{XF}}$; $A_{PF_{YF}}$ and $A_{PF_{ZF}}$ are computed from equations defined in Appendix D.

FUSELAGE ON PYLON

The flow induced by the fuselage quadrilateral vortices tangent to the pylon surface is given by equations analogous to those for the fanpod on the pylon.

Therefore;

$$\left\{\frac{V_{M_{PB}}}{V_\infty}\right\} = \left[\frac{1}{\beta^2\left\{1+(1+\tau\tan^2\alpha_P)\left(\frac{dz_{PL}}{dx_P} \pm \frac{dz_{PC}}{dx_P}\right)^2\right\}^{1/2}}\right]\left[A_{PB_{X_B}}\right]\left\{\frac{K_B}{V_\infty}\right\} \qquad (204)$$

and

$$\left\{\frac{V_{T_{PB}}}{V_\infty}\right\} = \left[\frac{1}{\beta\left\{1+(1+\tau\tan^2\phi_P)\left(\frac{dz_{PL}}{dx_P} \pm \frac{dz_{PC}}{dx_P}\right)^2\right\}^{1/2}}\right]\left[A_{PB_{Y_P}}\right]\left\{\frac{K_B}{V_\infty}\right\} \qquad (205)$$

where

$$\left[A_{PB_{Y_P}}\right] = \left[\sin\delta\right]\left[A_{PB_{Y_B}}\right] + \left[\cos\delta\right]\left[A_{PB_{Z_B}}\right] \qquad (206)$$

The influence matrices $A_{PB_{X_B}}$, $A_{PB_{Y_B}}$, and $A_{PB_{Z_B}}$ are computed from equations defined in Appendix D.

PYLON ON PYLON

The flow induced by the port and starboard pylons vortex and source lattices onto the starboard pylon is given by the following equations.

$$\left\{\frac{V_{m_{PP}}}{V_\infty}\right\} = \left\{\frac{\frac{u_{P_T}}{V_\infty} \pm \left(\frac{u_{P_L}}{V_\infty}\right)_{N=0}\left\{1+\sqrt{1+\tau^2 M^2 \phi_P}\left[\frac{u_{P_T}}{V_\infty} - \frac{u'_{P_T}}{V_\infty}\right]\right\} \pm \left(\frac{u_{P_L}}{V_\infty}\right)_{N=1,2,\cdots,N_{W_P}-1}}{\left[1+\left(1+\tau^2 M^2 \phi_P\right)\left(\frac{dz_{P_T}}{dx_P} \pm \frac{dz_{P_C}}{dx_P}\right)^2\right]^{1/2}}\right\}$$

$$+ \left[\frac{1}{\beta^2} T_{P_{M_{x_P}}} A_{PP_{x_P}} + \frac{1}{\beta} T_{P_{M_{y_P}}} A_{PP_{y_P}} + \frac{1}{\beta} T_{P_{M_{z_P}}} A_{PP_{z_P}}\right]\left\{\frac{K_P}{V_\infty}\right\}$$

$$+ \left[\frac{1}{\beta^2} T_{P_{M_{x_P}}} S_{PP_{x_P}} + \frac{1}{\beta} T_{P_{M_{y_P}}} S_{PP_{y_P}} + \frac{1}{\beta} T_{P_{M_{z_P}}} A_{PP_{z_P}}\right]\left\{\frac{\sigma_P}{V_\infty}\right\} \qquad (207)$$

Therefore;

$$\left\{\frac{V_{m_{PP}}}{V_\infty}\right\} = \left\{\frac{\frac{u_{P_T}}{V_\infty} \pm \left(\frac{u_{P_L}}{V_\infty}\right)_{N=0}\left\{1+\sqrt{1+\tau^2 M^2 \phi_P}\left[\frac{u_{P_T}}{V_\infty} - \frac{u'_{P_T}}{V_\infty}\right]\right\} \pm \left(\frac{u_{P_L}}{V_\infty}\right)_{N=1,2,\cdots,N_{W_P}-1}}{\left[1+\left(1+\tau^2 M^2 \phi_P\right)\left(\frac{dz_{P_T}}{dx_P} \pm \frac{dz_{P_C}}{dx_P}\right)^2\right]^{1/2}}\right\}$$

$$+ \left[\frac{1}{\beta^2\left\{1+\left(1+\tau^2 M^2 \phi_P\right)\left(\frac{dz_{P_T}}{dx_P} \pm \frac{dz_{P_C}}{dx_P}\right)^2\right\}^{1/2}}\right]\left\{\left[A_{PP_{x_P}}\right]\left\{\frac{K_P}{V_\infty}\right\}\right.$$

$$\left. + \left[S_{PP_{x_P}}\right]\left\{\frac{\sigma_P}{V_\infty}\right\}\right\} \qquad (208)$$

also;

$$\left\{\frac{v_{T_{PP}}}{V_\infty}\right\} = \left\{\frac{\frac{v_{P_T}}{V_\infty} \pm \left(\frac{v_{P_L}}{V_\infty}\right)_{N=0}\left\{1+\sqrt{1+\tau^2 M^2 \phi_P}\left[\frac{v_{P_T}}{V_\infty} - \frac{v'_{P_T}}{V_\infty}\right]\right\} \pm \left(\frac{v_{P_L}}{V_\infty}\right)_{N=1,2,\cdots,N_{W_P}-1}}{\left[1+\left(1+\tau^2 M^2 \phi_P\right)\left(\frac{dz_{P_T}}{dx_P} \pm \frac{dz_{P_C}}{dx_P}\right)^2\right]^{1/2}}\right\}$$

$$+ \left[\frac{1}{\beta^2} T_{P_{T_{x_P}}} A_{PP_{x_P}} + \frac{1}{\beta} T_{P_{T_{y_P}}} A_{PP_{y_P}} + \frac{1}{\beta} T_{P_{T_{z_P}}} A_{PP_{z_P}}\right]\left\{\frac{K_P}{V_\infty}\right\}$$

$$+ \left[\frac{1}{\beta^2} T_{P_{T_{x_P}}} S_{PP_{x_P}} + \frac{1}{\beta} T_{P_{T_{y_P}}} S_{PP_{y_P}} + \frac{1}{\beta} T_{P_{T_{z_P}}} S_{PP_{z_P}}\right]\left\{\frac{\sigma_P}{V_\infty}\right\} \qquad (209)$$

and

$$\left\{\frac{V_{T_{PP}}}{V_\infty}\right\} = \left\{\frac{\frac{v_{P_R}}{V_\infty} \pm \left(\frac{v_{P_R}}{V_\infty}\right)_{N=0}\left\{1+\sqrt{1+\tan^2\phi_P}\left[\frac{v_{P_T}}{V_\infty} - \frac{v_{P_R}'}{V_\infty}\right]\right\} \pm \left(\frac{v_{P_R}}{V_\infty}\right)_{N=1,2,\cdots,N_{W_P}-1}}{\left[1+\left(1+\tan^2\phi_P\right)\left(\frac{d\varepsilon_{P_T}}{dx_P} \pm \frac{d\varepsilon_{P_R}}{dx_P}\right)^2\right]^{1/2}}\right\}$$

$$+\left[\frac{1}{\beta\left\{1+\left(1+\tan^2\phi_P\right)\left(\frac{d\varepsilon_{P_T}}{dx_P} \pm \frac{d\varepsilon_{P_R}}{dx_P}\right)^2\right\}^{1/2}}\right]\left\{\left[A_{PP_{YP}}\right]\left\{\frac{k_P}{V_\infty}\right\}\right.$$

$$\left.+\left[S_{PP_{YP}}\right]\left\{\frac{q_P}{V_\infty}\right\}\right\} \tag{210}$$

where

$$\left[A_{PB_{YP}}\right] = \left[\sin\gamma\right]\left[A_{PB_Y}\right] + \left[\cos\gamma\right]\left[A_{PB_Z}\right] \tag{211}$$

$$\left[S_{PB_{YP}}\right] = \left[\sin\gamma\right]\left[S_{PB_Y}\right] + \left[\cos\gamma\right]\left[S_{PB_Z}\right] \tag{212}$$

where A_{PB_Y}, A_{PB_Z}, S_{PB_Y}, and S_{PB_Z} are in equations (42), (43), (44), and (45).

where

$$\left(\frac{v_{P_R}}{V_\infty}\right)_{N=0} = \frac{4h_P}{c_P\beta} F_{0P} \cot\theta_P/2 \tag{213}$$

$$\left(\frac{v_{P_R}}{V_\infty}\right)_{N=1,2,\cdots,N_{W_P}-1} = \frac{4h_P}{c_P\beta}\sum_{N=1}^{N_{W_P}} F_{NP}\sin N\theta_P \tag{214}$$

$$\left(\frac{v_{P_R}}{V_\infty}\right)_{N=0} = 2\left\{\frac{1}{2\pi}\frac{\Delta F_{0P}}{\Delta\eta_P}\left(\sin\theta_P+\theta_P\right) - \frac{4h_P}{c_P}F_{0P}\cot\theta_P/2\left[\tan\phi^*_{P_{L.E.}}\right.\right.$$

$$\left.\left.+\frac{1}{2}\left(\tan\phi^*_{P_{T.E.}} - \tan\phi^*_{P_{L.E.}}\right)\left(1-\cos\theta_P\right)\right]\right\} \tag{215}$$

and

$$\left(\frac{v_{P_R}}{V_\infty}\right)_{N=1,2,\cdots,N_{W_P}-1} = \frac{2}{\beta}\left\{\frac{\Delta F_{1P}}{\Delta\eta_P}\left(\frac{\theta_P}{2} - \frac{1}{4}\sin 2\theta_P\right) + \sum_{N=2}^{N_{W_P}-1}\frac{\Delta F_{NP}}{\Delta\eta_P}\left[\frac{\sin(N-1)\theta_P}{2(N-1)}\right.\right.$$

$$\left.\left.-\frac{\sin(N+1)\theta_P}{2(N+1)}\right]\right\} - \frac{4h_P}{c_P}\left\{\sum_{N=1}^{N_{W_P}-1}F_{NP}\sin N\theta_P\right\}\left\{\tan\phi^*_{P_{L.E.}}\right.$$

$$\left.+\frac{1}{2}\left(\tan\phi^*_{P_{T.E.}} - \tan\phi^*_{P_{L.E.}}\right)\left(1-\cos\theta_P\right)\right\} \tag{216}$$

where $\tan\phi^*_{P_{L.E.}}$ and $\tan\phi^*_{P_{T.E.}}$ are defined in Appendix I

The slopes $\frac{\Delta F_{0P}}{\Delta\eta_P}$, $\frac{\Delta F_{1P}}{\Delta\eta_P}$, and $\frac{\Delta F_{NP}}{\Delta\eta_P}$ are determined numerically from the spanwise variation of the coefficients F_{0P}, F_{1P}, and F_{NP} obtained in the simultaneous solution of the influence equations.

The expressions for $\frac{u_{pt}}{V_\infty}$, $\frac{v_{pt}}{V_\infty}$, $\frac{u'_{pt}}{V_\infty}$, and $\frac{v'_{pt}}{V_\infty}$ are the same as for the wing except that the subscript p is substituted for w. The equivalent wing expressions are given in equations 135, 136, 137, and 138.

The matrices $A_{PP_{x_p}}$ and $S_{PP_{z_p}}$ are due to the port pylon and are computed from equations defined in Appendices C and B, respectively.

NACELLE ON PYLON

The flow induced on the pylon surface by the nacelles is given by the following expressions.

$$\left\{\frac{V_{M_{PN}}}{V_\infty}\right\} = \left[\frac{1}{\beta^2} T_{PM_{x_P}} A_{PN_{x_P}} + \frac{1}{\beta} T_{PM_{y_P}} A_{PN_{y_P}} + \frac{1}{\beta} T_{PM_{z_P}} A_{PN_{z_P}}\right]\left\{\frac{\sigma_N}{V_\infty}\right\} \quad (217)$$

where

$$\left[A_{PN_{x_P}}\right] = \left[A_{PN_{x_N}}\right] \quad (218)$$

$$\left[A_{PN_{y_P}}\right] = \left[\sin\gamma\right]\left[A_{PN_{y_P}}\right] + \left[\cos\gamma\right]\left[A_{PN_{z_P}}\right] - \left[A_{PN_{y_N}}\right] \quad (219)$$

and

$$\left[A_{PN_{z_P}}\right] = -\left[\cos\gamma\right]\left[A_{PN_{y_P}}\right] + \left[\sin\gamma\right]\left[A_{PN_{z_P}}\right] \quad (220)$$

where $A_{PN_{y_P}}$ and $A_{PN_{z_P}}$ are defined by equations (49) and (50), respectively.

therefore;

$$\left\{\frac{V_{M_{PN}}}{V_\infty}\right\} = \left[\frac{1}{\beta^2\left\{1+(1+\tan^2\phi_P)\left(\frac{dz_{P_t}}{dx_P} \pm \frac{dz_{P_c}}{dx_P}\right)^2\right\}^{1/2}}\right]\left[A_{PN_{x_N}}\right]\left\{\frac{\sigma_N}{V_\infty}\right\} \quad (221)$$

and

$$\left\{\frac{V_{T_{PN}}}{V_\infty}\right\} = \left[\frac{1}{\beta^2} T_{PT_{x_P}} A_{PN_{x_P}} + \frac{1}{\beta} T_{PT_{y_P}} A_{PN_{y_P}} + \frac{1}{\beta} T_{PT_{z_P}} A_{PN_{z_P}}\right]\left\{\frac{\sigma_N}{V_\infty}\right\} \quad (222)$$

then

$$\left\{\frac{V_{T_{PN}}}{V_\infty}\right\} = -\left[\frac{1}{\beta^2\left\{1+(1+\tan^2\phi_P)\left(\frac{dz_{P_t}}{dx_P} \pm \frac{dz_{P_c}}{dx_P}\right)^2\right\}^{1/2}}\right]\left[A_{PN_{y_P}}\right]\left\{\frac{\sigma_N}{V_\infty}\right\} \quad (223)$$

The matrices $A_{PN_{x_N}}$ and $A_{PN_{y_N}}$ are computed from equations defined in Appendix E.

FREESTREAM ON PYLON

The expressions for the velocity tangent to the pylon surface due to the freestream are the same as for the velocity tangent to the wing surface due to the freestream except for the substitution of the subscript P for W.

$$\frac{V_{M_{P\infty}}}{V_\infty} = \frac{1 + t_{AN}^2\phi_P \left[1 + (1+t_{AN}^2\phi_P)\left(\frac{dz_{Pc}}{dx_P} \pm \frac{dz_{Pc}}{dx_P}\right)^2\right]^{1/2}}{\left[1+t_{AN}^2\phi_P\right]\left[1 + (1+t_{AN}^2\phi_P)\left(\frac{dz_{Pc}}{dx_P} \pm \frac{dz_{Pc}}{dx_P}\right)^2\right]^{1/2}} \tag{224}$$

and

$$\frac{V_{T_{P\infty}}}{V_\infty} = -\frac{t_{AN}\phi_P \left[1 - \left[1 + (1+t_{AN}^2\phi_P)\frac{dz_{Pc}}{dx_P} \pm \frac{dz_{Pc}}{dx_P}\right]^2\right]^{1/2}}{\left[1+t_{AN}^2\phi_P\right]\left[1 + (1+t_{AN}^2\phi_P)\left(\frac{dz_{Pc}}{dx_P} \pm \frac{dz_{Pc}}{dx_P}\right)^2\right]^{1/2}} \tag{225}$$

WING ON FANPOD

The velocity induced by the wing source and vortex lattices tangent to the fanpod surface is given by the following expressions.

$$\left\{\frac{V_{M_{FW}}}{V_\infty}\right\} = \left[\frac{1}{\ell^2} T_{FM_{XF}} A_{FW_{XF}} + \frac{1}{\ell} T_{FM_{YF}} A_{FW_{YF}} + \frac{1}{\ell} T_{FM_{ZF}} A_{FW_{ZF}}\right]\left\{\frac{K_W}{V_\infty}\right\}$$

$$+ \left[\frac{1}{\ell^2} T_{FM_{XF}} S_{FW_{XF}} + \frac{1}{\ell} T_{FM_{YF}} S_{FW_{YF}} + \frac{1}{\ell} T_{FM_{ZF}} S_{FW_{ZF}}\right]\left\{\frac{\sigma_W}{V_\infty}\right\} \tag{226}$$

and

$$\left\{\frac{V_{T_{FW}}}{V_\infty}\right\} = \left[\frac{1}{\ell^2} T_{FT_{XF}} A_{FW_{XF}} + \frac{1}{\ell} T_{FT_{YF}} A_{FW_{YF}} + \frac{1}{\ell} T_{FT_{ZF}} A_{FW_{ZF}}\right]\left\{\frac{K_W}{V_\infty}\right\}$$

$$+ \left[\frac{1}{\ell^2} T_{FT_{XF}} S_{FW_{XF}} + \frac{1}{\ell} T_{FT_{YF}} S_{FW_{YF}} + \frac{1}{\ell} T_{FT_{ZF}} S_{FW_{ZF}}\right]\left\{\frac{\sigma_W}{V_\infty}\right\} \tag{227}$$

Since the wing and fanpod coordinate frames are oriented the same direction;

$$\left\{\frac{V_{MFW}}{V_\infty}\right\} = \left[\frac{1}{\beta^2} T_{FM_{X_F}} A_{FW_{X_W}} + \frac{1}{\beta} T_{FM_{Y_F}} A_{FW_{Y_W}} + \frac{1}{\beta} T_{FM_{Z_F}} A_{FW_{Z_W}}\right]\left\{\frac{K_W}{V_\infty}\right\}$$

$$+ \left[\frac{1}{\beta^2} T_{FM_{X_F}} S_{FW_{X_W}} + \frac{1}{\beta} T_{FM_{Y_F}} S_{FW_{Y_W}} + \frac{1}{\beta} T_{FM_{Z_F}} S_{FW_{Z_W}}\right]\left\{\frac{\sigma_W}{V_\infty}\right\} \quad (228)$$

and

$$\left\{\frac{V_{TFW}}{V_\infty}\right\} = \left[\frac{1}{\beta^2} T_{FT_{X_F}} A_{FW_{X_W}} + \frac{1}{\beta} T_{FT_{Y_F}} A_{FW_{Y_W}} + \frac{1}{\beta} T_{FT_{Z_F}} A_{FW_{Z_W}}\right]\left\{\frac{K_W}{V_\infty}\right\}$$

$$+ \left[\frac{1}{\beta^2} T_{FT_{X_F}} S_{FW_{X_W}} + \frac{1}{\beta} T_{FT_{Y_F}} S_{FW_{Y_W}} + \frac{1}{\beta} T_{FT_{Z_F}} S_{FW_{Z_W}}\right]\left\{\frac{\sigma_W}{V_\infty}\right\} \quad (229)$$

The influence matrices $A_{FW_{X_W}}$, $A_{FW_{Y_W}}$, and $A_{FW_{Z_W}}$ are computed using equations defined in Appendices C and D. Also; the influence matrices $S_{FW_{X_W}}$, $S_{FW_{Y_W}}$, and $S_{FW_{Z_W}}$ are computed using equations defined in Appendix B.

The unit vectors $\vec{T}_{FM}$ and $\vec{T}_{FT}$ tangent to the actual fanpod surface are determined from the unit vectors $\vec{T}_{FM_i}$ and $\vec{T}_{FT_i}$, tangent to the fanpod surface obtained by the Gothert transformation, in the following manner.

$$T_{FM_{X_F}} = T_{FM_{X_{F_i}}} \frac{\Delta S_{FM_i}}{\Delta S_{FM}} \quad (230)$$

$$T_{FM_{Y_F}} = \frac{1}{\beta} T_{FM_{Y_{F_i}}} \frac{\Delta S_{FM_i}}{\Delta S_{FM}} \quad (231)$$

$$T_{FM_{Z_F}} = \frac{1}{\beta} T_{FM_{Z_{F_i}}} \frac{\Delta S_{FM_i}}{\Delta S_{FM}} \quad (232)$$

$$T_{FT_{X_F}} = T_{FT_{X_{F_i}}} \frac{\Delta S_{FT_i}}{\Delta S_{FT}} \quad (233)$$

$$T_{FT_{Y_F}} = \frac{1}{\beta} T_{FT_{Y_{F_i}}} \frac{\Delta S_{FT_i}}{\Delta S_{FT}} \quad (234)$$

and

$$T_{F_{T_{Z_F}}} = \frac{1}{\beta} T_{F_{T_{Z_{F_i}}}} \frac{\Delta S_{F_{T_i}}}{\Delta S_{F_T}} \tag{235}$$

where $\frac{\Delta S_{FM_i}}{\Delta S_{FM}}$ and $\frac{\Delta S_{F_{T_i}}}{\Delta S_{F_T}}$ are obtained as follows;

$$T^2_{FM_{X_F}} + T^2_{FM_{Y_F}} + T^2_{FM_{Z_F}} = 1 \tag{236}$$

Then from equations 230, 231, 232, and 236;

$$\frac{\Delta S_{FM_i}}{\Delta S_{FM}} = 1 \Big/ \sqrt{T^2_{FM_{X_{F_i}}} + \frac{1}{\beta^2} T^2_{FM_{Y_{F_i}}} + \frac{1}{\beta^2} T^2_{FM_{Z_{F_i}}}} \tag{237}$$

Similarly,

$$T^2_{F_{T_{X_F}}} + T^2_{F_{T_{Y_F}}} + T^2_{F_{T_{Z_F}}} = 1 \tag{238}$$

and after substituting equations 233, 234 and 235 into equation 238.

$$\frac{\Delta S_{F_{T_i}}}{\Delta S_{F_T}} = 1 \Big/ \sqrt{T^2_{F_{T_{X_{F_i}}}} + \frac{1}{\beta^2} T^2_{F_{T_{Y_{F_i}}}} + \frac{1}{\beta^2} T^2_{F_{T_{Z_{F_i}}}}} \tag{239}$$

FANPOD ON FANPOD

The velocity induced by the fanpod quadrilateral vortices tangent to the surface of the starboard fanpod is given by the following expressions.

$$\left\{\frac{V_{M_{FF}}}{V_\infty}\right\} = \left[\frac{1}{\beta^2} T_{FM_{X_F}} A_{FF_{X_F}} + \frac{1}{\beta} T_{FM_{Y_F}} A_{FF_{Y_F}} + \frac{1}{\beta} T_{FM_{Z_F}} A_{FF_{Z_F}}\right]\left\{\frac{K_F}{V_\infty}\right\}$$

$$+ \frac{\gamma_{FM}/V_\infty}{2\beta\sqrt{\beta^2 T^2_{FM_{X_{F_i}}} + T^2_{FM_{Y_{F_i}}} + T^2_{FM_{Z_{F_i}}}}} \tag{240}$$

and

$$\left\{\frac{V_{T_{FF}}}{V_\infty}\right\} = \left[\frac{1}{\beta^2} T_{F_{T_{X_F}}} A_{FF_{X_F}} + \frac{1}{\beta} T_{F_{T_{Y_F}}} A_{FF_{Y_F}} + \frac{1}{\beta} T_{F_{T_{Z_F}}} A_{FF_{Z_F}}\right]\left\{\frac{K_F}{V_\infty}\right\}$$

$$+ \frac{\gamma_{F_T}/V_\infty}{2\beta\sqrt{\beta^2 T^2_{F_{T_{X_{F_i}}}} + T^2_{F_{T_{Y_{F_i}}}} + T^2_{F_{T_{Z_{F_i}}}}}} \tag{241}$$

where γ_{F_M} and γ_{F_T} are the values of the surface vorticity along and perpendicular to the meridian lines, respectively. The vorticity is determined by dividing the average of the two adjacent vortex strengths by the average perpendicular distance between the two adjacent vortices.

The influence matrices $A_{FF_{X_F}}$, $A_{FF_{Y_F}}$, and $A_{FF_{Z_F}}$ are computed with equations defined in Appendix D. The components of the unit tangent vectors $\vec{T}_{F_M}$ and $\vec{T}_{F_T}$ are computed from the vortex grid coordinates.

PYLON ON FANPOD

The velocity induced by the pylons tangent to the fanpod surface is given by;

$$\left\{\frac{V_{M_{FP}}}{V_\infty}\right\} = \left[\frac{1}{\beta^2} T_{FM_{X_F}} A_{FP_{X_F}} + \frac{1}{\beta} T_{FM_{Y_F}} A_{FP_{Y_F}} + \frac{1}{\beta} T_{FM_{Z_F}} A_{FP_{Z_F}}\right]\left\{\frac{K_P}{V_\infty}\right\}$$

$$+ \left[\frac{1}{\beta^2} T_{FM_{X_F}} S_{FP_{X_F}} + \frac{1}{\beta} T_{FM_{Y_F}} S_{FP_{Y_F}} + \frac{1}{\beta} T_{FM_{Z_F}} S_{FP_{Z_F}}\right]\left\{\frac{\sigma_P}{V_\infty}\right\} \qquad (242)$$

and

$$\left\{\frac{V_{T_{FP}}}{V_\infty}\right\} = \left[\frac{1}{\beta^2} T_{FT_{X_F}} A_{FP_{X_F}} + \frac{1}{\beta} T_{FT_{Y_F}} A_{FP_{Y_F}} + \frac{1}{\beta} T_{FT_{Z_F}} A_{FP_{Z_F}}\right]\left\{\frac{K_P}{V_\infty}\right\}$$

$$+ \left[\frac{1}{\beta^2} T_{FT_{X_F}} S_{FP_{X_F}} + \frac{1}{\beta} T_{FT_{Y_F}} S_{FP_{Y_F}} + \frac{1}{\beta} T_{FT_{Z_F}} S_{FP_{Z_F}}\right]\left\{\frac{\sigma_P}{V_\infty}\right\} \qquad (243)$$

where

$$\left[A_{FP_{X_F}}\right] = \left[A_{FP_{X_P}}\right] \qquad (244)$$

$$\left[A_{FP_{Y_F}}\right] = \left[\sin\gamma\right]\left[A_{FP_{Y_P}}\right] - \left[\cos\gamma\right]\left[A_{FP_{Z_P}}\right] \qquad (245)$$

$$\left[A_{FP_{Z_F}}\right] = \left[\cos\gamma\right]\left[A_{FP_{Y_P}}\right] + \left[\sin\gamma\right]\left[A_{FP_{Z_P}}\right] \qquad (246)$$

$$\left[S_{FP_{X_F}}\right] = \left[S_{FP_{X_P}}\right] \qquad (247)$$

$$\left[S_{FP_{Y_F}} \right] = \left[\sin\gamma \right] \left[S_{FP_{Y_P}} \right] - \left[\cos\gamma \right] \left[S_{FP_{Z_P}} \right] \tag{248}$$

$$\left[S_{FP_{Z_F}} \right] = \left[\cos\gamma \right] \left[S_{FP_{Y_P}} \right] + \left[\sin\gamma \right] \left[S_{FP_{Z_P}} \right] \tag{249}$$

The influence matrices $A_{FP_{X_P}}$, $A_{FP_{Y_P}}$, and $A_{FP_{Z_P}}$ are computed with equations from Appendices C and D. Also; the influence matrices $S_{FP_{X_P}}$, $S_{FP_{Y_P}}$, and $S_{FP_{Z_P}}$ are computed with equations from Appendix B.

NACELLE ON FANPOD

The velocity induced by the nacelle tangent to the fanpod surface is given by;

$$\left\{ \frac{V_{M_{FN}}}{V_\infty} \right\} = \left[\frac{1}{\beta^2} T_{FM_{X_F}} A_{FN_{X_F}} + \frac{1}{\beta} T_{FM_{Y_F}} A_{FN_{Y_F}} + \frac{1}{\beta} T_{FM_{Z_F}} A_{FN_{Z_F}} \right] \left\{ \frac{\sigma_N}{V_\infty} \right\} \tag{250}$$

and

$$\left\{ \frac{V_{T_{FN}}}{V_\infty} \right\} = \left[\frac{1}{\beta^2} T_{FT_{X_F}} A_{FN_{X_F}} + \frac{1}{\beta} T_{FT_{Y_F}} A_{FN_{Y_F}} + \frac{1}{\beta} T_{FT_{Z_F}} A_{FN_{Z_F}} \right] \left\{ \frac{\sigma_N}{V_\infty} \right\} \tag{251}$$

where

$$\left[A_{FN_{X_F}} \right] = \left[A_{FN_{X_N}} \right] \tag{252}$$

$$\left[A_{FN_{Y_F}} \right] = - \left[\sin(\gamma - \Theta_{FN}) \right] \left[A_{FN_{Y_N}} \right] \tag{253}$$

$$\left[A_{FN_{Z_F}} \right] = - \left[\cos(\gamma - \Theta_{FN}) \right] \left[A_{FN_{Y_N}} \right] \tag{254}$$

The influence matrices $A_{FN_{X_N}}$ and $A_{FN_{Y_N}}$ are computed with equations from Appendix E.

FREESTREAM ON FANPOD

The components of the freestream velocity tangent to the surface of the fanpod are given by:

$$\left\{\frac{V_{M_{FB}}}{V_\infty}\right\} = \left[T_{FM_{X_F}}\right]\left\{\cos\alpha_F\right\} + \left[T_{FM_{Z_F}}\right]\left\{\sin\alpha_F\right\} \qquad (255)$$

and

$$\left\{\frac{V_{T_{FB}}}{V_\infty}\right\} = \left[T_{FT_{X_F}}\right]\left\{\cos\alpha_F\right\} + \left[T_{FT_{Z_F}}\right]\left\{\sin\alpha_F\right\} \qquad (256)$$

WING ON FUSELAGE

The velocity induced by the wing source and vortex lattices tangent to the fuselage surface is given by the following expressions

$$\left\{\frac{V_{M_{BW}}}{V_\infty}\right\} = \left[\frac{1}{\beta^2}T_{BM_{X_B}}A_{BW_{X_W}} + \frac{1}{\beta}T_{BM_{Y_B}}A_{BW_{Y_W}} + \frac{1}{\beta}T_{BM_{Z_B}}A_{BW_{Z_W}}\right]\left\{\frac{K_W}{V_\infty}\right\} \qquad (257)$$

$$+\left[\frac{1}{\beta^2}T_{BM_{X_B}}S_{BW_{X_W}} + \frac{1}{\beta}T_{BM_{Y_B}}S_{BW_{Y_W}} + \frac{1}{\beta}T_{BM_{Z_B}}S_{BW_{Z_W}}\right]\left[\frac{\sigma_W}{V_\infty}\right] \qquad (258)$$

$$\left\{\frac{V_{T_{BW}}}{V_\infty}\right\} = \left[\frac{1}{\beta^2}T_{BT_{X_B}}A_{BW_{K_W}} + \frac{1}{\beta}T_{BT_{Y_B}}A_{BW_{Y_W}} + \frac{1}{\beta}T_{BT_{Z_B}}A_{BW_{Z_W}}\right]\left\{\frac{K_W}{V_\infty}\right\} \qquad (259)$$

$$+\left[\frac{1}{\beta^2}T_{BT_{X_B}}S_{BW_{X_W}} + \frac{1}{\beta}T_{BT_{Y_B}}S_{BW_{Y_W}} + \frac{1}{\beta}T_{BT_{Z_B}}S_{BW_{Z_W}}\right]\left\{\frac{\sigma_W}{V_\infty}\right\} \qquad (260)$$

The influence matrices $A_{BW_{X_W}}$, $A_{BW_{Y_W}}$, and $A_{BW_{Z_W}}$ are computed using equations defined in Appendices C and D. Also the influence matrices $S_{BW_{X_W}}$, $S_{BW_{Y_W}}$, and $S_{BW_{Z_W}}$ are computed using equations defined in Appendix B.

The unit vecotrs ($T_{BM_{X_B}}$, $T_{BM_{Y_B}}$, $T_{BM_{Z_B}}$) and ($T_{BT_{X_B}}$, $T_{BT_{Y_B}}$, $T_{BT_{Z_B}}$) are computed in the same manner as those for the fanpod.

FANPOD ON FUSELAGE

The velocity induced by the fanpod quadrilateral vortices tangent to the surface of the fuselage is given by the following equations.

$$\left\{\frac{V_{M_{BF}}}{V_\infty}\right\} = \left[\frac{1}{\beta^2} T_{BM_{X_B}} A_{BF_{X_F}} + \frac{1}{\beta} T_{BM_{Y_B}} A_{BF_{Y_F}} + \frac{1}{\beta} T_{BM_{Z_B}} A_{BF_{Z_F}}\right]\left\{\frac{K_F}{V_\infty}\right\} \quad (261)$$

and

$$\left\{\frac{V_{T_{BF}}}{V_\infty}\right\} = \left[\frac{1}{\beta^2} T_{BT_{X_B}} A_{BF_{X_F}} + \frac{1}{\beta} T_{BT_{Y_B}} A_{BF_{Y_F}} + \frac{1}{\beta} T_{BT_{Z_B}} A_{BF_{Z_F}}\right]\left\{\frac{K_F}{V_\infty}\right\} \quad (262)$$

where the influence matrices $A_{BF_{X_F}}$, $A_{BF_{Y_F}}$, and $A_{BF_{Z_F}}$ are computed with equations derived in Appendix D.

FUSELAGE ON FUSELAGE

The velocity induced by the fuselage quadrilateral vortices tangent to the surface of the fuselage is given by the following expressions

$$\left\{\frac{V_{M_{BB}}}{V_\infty}\right\} = \left[\frac{1}{\beta^2} T_{BM_{X_B}} A_{BB_{X_B}} + \frac{1}{\beta} T_{BM_{Y_B}} A_{BB_{Y_B}} + \frac{1}{\beta} T_{BM_{Z_B}} A_{BB_{Z_B}}\right]\left\{\frac{K_B}{V_\infty}\right\} \quad (263)$$

$$+ \frac{\gamma_{B_M} / V_\infty}{2\beta\sqrt{\beta^2 T_{BM_{X_{B_i}}}^2 + T_{BM_{Y_{B_i}}}^2 + T_{BM_{Z_{B_i}}}^2}}$$

$$\left\{\frac{V_{T_{BB}}}{V_\infty}\right\} = \left[\frac{1}{\beta^2} T_{BT_{X_B}} A_{BB_{X_B}} + \frac{1}{\beta} T_{BT_{Y_B}} A_{BB_{Y_B}} + \frac{1}{\beta} T_{BT_{Z_B}} A_{BB_{Z_B}}\right]\left\{\frac{K_B}{V_\infty}\right\} \quad (264)$$

$$+ \frac{\gamma_{B_T} / V_\infty}{2\beta\sqrt{\beta^2 T_{BT_{X_{B_i}}}^2 + T_{BT_{Y_{B_i}}}^2 + T_{BT_{Z_{B_i}}}^2}}$$

Where γ_{B_M} and γ_{B_T} are the values of the surface vorticity along and perpendicular to the meridian lines, respectively. The vorticity is determined by dividing the average of the two adjacent vortex strengths by the average perpendicular distance between the two adjacent vortices.

The influence matrices $A_{BB_{X_B}}$, $A_{BB_{Y_B}}$, and $A_{BB_{Z_B}}$ are computed with equations defined in Appendix D.

PYLON ON FUSELAGE

The velocity induced by the pylons tangent to the fuselage surface is given by;

$$\left\{\frac{V_{m_{BP}}}{V_\infty}\right\} = \left[\frac{1}{\ell^2} T_{BM_{X_B}} A_{BP_{X_B}} + \frac{1}{\ell} T_{BM_{Y_B}} A_{BP_{Y_B}} + \frac{1}{\ell} T_{BM_{Z_B}} A_{BP_{Z_B}}\right]\left\{\frac{K_P}{V_\infty}\right\}$$

$$+\left[\frac{1}{\ell^2} T_{BM_{X_B}} S_{BP_{X_B}} + \frac{1}{\ell} T_{BM_{Y_B}} S_{BP_{Y_B}} + \frac{1}{\ell} T_{BM_{Z_B}} S_{BP_{Z_B}}\right]\left\{\frac{\sigma_P}{V_\infty}\right\} \tag{265}$$

and

$$\left\{\frac{V_{T_{BP}}}{V_\infty}\right\} = \left[\frac{1}{\ell^2} T_{BT_{X_B}} A_{BP_{X_B}} + \frac{1}{\ell} T_{BT_{Y_B}} A_{BP_{Y_B}} + \frac{1}{\ell} T_{BT_{Z_B}} A_{BP_{Z_B}}\right]\left\{\frac{K_P}{V_\infty}\right\}$$

$$+\left[\frac{1}{\ell^2} T_{BT_{X_B}} S_{BP_{X_B}} + \frac{1}{\ell} T_{BT_{Y_B}} S_{BP_{Y_B}} + \frac{1}{\ell} T_{BT_{Z_B}} S_{BP_{Z_B}}\right]\left\{\frac{\sigma_P}{V_\infty}\right\} \tag{266}$$

where

$$\left[A_{BP_{X_B}}\right] = \left[A_{BP_{X_P}}\right] \tag{267}$$

$$\left[A_{BP_{Y_B}}\right] = \left[\sin\gamma\right]\left[A_{BP_{Y_P}}\right] - \left[\cos\gamma\right]\left[A_{BP_{Z_P}}\right] \tag{268}$$

$$\left[A_{BP_{Z_B}}\right] = \left[\cos\gamma\right]\left[A_{BP_{Y_P}}\right] + \left[\sin\gamma\right]\left[A_{BP_{Z_P}}\right] \tag{269}$$

$$\left[S_{BP_{X_B}}\right] = \left[S_{BP_{X_P}}\right] \tag{270}$$

$$\left[S_{BP_{Y_B}}\right] = \left[\sin\gamma\right]\left[S_{BP_{Y_P}}\right] - \left[\cos\gamma\right]\left[S_{BP_{Z_P}}\right] \tag{271}$$

$$\left[S_{BP_{Z_B}}\right] = \left[\cos\gamma\right]\left[S_{BP_{Y_P}}\right] + \left[\sin\gamma\right]\left[S_{BP_{Z_P}}\right] \tag{272}$$

The influence matrices $A_{BP_{X_P}}$, $A_{BP_{Y_P}}$, and $A_{BP_{Z_P}}$ are computed with equations from Appendices C and D. Also, the influence matrices $S_{BP_{X_P}}$, $S_{BP_{Y_P}}$, and $S_{BP_{Z_P}}$ are computed with equations from Appendix B.

NACELLE ON FUSELAGE

The velocity induced by the nacelle tangent to the fuselage surface is given by;

$$\left\{\frac{V_{M_{BN}}}{V_\infty}\right\} = \left[\frac{1}{\beta^2} T_{BM_{X_B}} A_{BN_{X_B}} + \frac{1}{\beta} T_{BM_{Y_B}} A_{BN_{Y_B}} + \frac{1}{\beta} T_{BM_{Z_B}} A_{BN_{Z_B}}\right]\left\{\frac{\sigma_N}{V_\infty}\right\} \quad (273)$$

and

$$\left\{\frac{V_{T_{BO}}}{V_\infty}\right\} = \left[\frac{1}{\beta^2} T_{BT_{X_B}} A_{BN_{X_B}} + \frac{1}{\beta} T_{BT_{Y_B}} A_{BN_{Y_B}} + \frac{1}{\beta} T_{BT_{Z_B}} A_{BN_{Z_B}}\right]\left\{\frac{\sigma_N}{V_\infty}\right\} \quad (274)$$

where

$$\left[A_{BN_{X_B}}\right] = \left[A_{BN_{X_N}}\right] \quad (275)$$

$$\left[A_{BN_{Y_B}}\right] = -\left[\sin(\gamma - \phi_{BN})\right]\left[A_{BN_{Y_N}}\right] \quad (276)$$

$$\left[A_{BN_{Z_B}}\right] = -\left[\cos(\gamma - \phi_{BN})\right]\left[A_{BN_{Y_N}}\right] \quad (277)$$

The influence matrices $A_{BN_{X_N}}$ and $A_{BN_{Y_N}}$ are computed with equations from Appendix E.

FREESTREAM ON FUSELAGE

The components of the freestream velocity tangent to the surface of the fanpod are given by;

$$\left\{\frac{V_{M_{B\infty}}}{V_\infty}\right\} = \left[T_{BM_{X_B}}\right]\left\{\cos\alpha_B\right\} + \left[T_{BM_{Z_B}}\right]\left\{\sin\alpha_B\right\} \quad (278)$$

and

$$\left\{\frac{V_{T_{B\infty}}}{V_\infty}\right\} = \left[T_{BT_{X_B}}\right]\left\{\cos\alpha_B\right\} + \left[T_{BT_{Z_B}}\right]\left\{\sin\alpha_B\right\} \quad (279)$$

COMBINED WING VELOCITY EQUATIONS

When the velocity induced by all the configuration components is summed; the following expressions are obtained.

In the chordwise direction,

$$\left\{\frac{\bar{V}_{i_M}}{V_\infty}\right\} = \left\{\frac{V_{M_{WB}}}{V_\infty}\right\} + \left\{\frac{V_{M_{WF}}}{V_\infty}\right\} + \left\{\frac{V_{M_{WW}}}{V_\infty}\right\} + \left\{\frac{V_{M_{WP}}}{V_\infty}\right\} + \left\{\frac{V_{M_{WN}}}{V_\infty}\right\} \qquad (280)$$

and in the spanwise direction

$$\left\{\frac{\bar{V}_{W_T}}{V_\infty}\right\} = \left\{\frac{V_{T_{WB}}}{V_\infty}\right\} + \left\{\frac{V_{T_{WF}}}{V_\infty}\right\} + \left\{\frac{V_{T_{WW}}}{V_\infty}\right\} + \left\{\frac{V_{T_{WP}}}{V_\infty}\right\} + \left\{\frac{V_{T_{WN}}}{V_\infty}\right\} \qquad (281)$$

If $\left\{\frac{\Delta V_{M_W}}{V_\infty}\right\}$ and $\left\{\frac{\Delta V_{T_W}}{V_\infty}\right\}$ are defined by;

$$\left\{\frac{\Delta V_{M_W}}{V_\infty}\right\} = \left[\left\{1+(1+\tau\tan^2\phi_W)\left(\frac{dz_{W_C}}{dx_W} \pm \frac{dz_{W_C}}{dx_W}\right)^2\right\}^{1/2} - 1\right]\left\{\frac{\bar{V}_{W_M}}{V_\infty}\right\}$$

$$- \left\{\frac{1+\tau\tan^2\phi_W\left[1+(1+\tau\tan^2\phi_W)\left(\frac{dz_{W_T}}{dx_W} \pm \frac{dz_{W_C}}{dx_W}\right)^2\right]^{1/2}}{\left[1+\tau\tan^2\phi_W\right]}\right\} \qquad (282)$$

and

$$\left\{\frac{\Delta V_{T_W}}{V_\infty}\right\} = \left[\left\{1+(1+\tau\tan^2\phi_W)\left(\frac{dz_{W_T}}{dx_W} \pm \frac{dz_{W_C}}{dx_W}\right)^2\right\}^{1/2} - 1\right]\left\{\frac{\bar{V}_{W_T}}{V_\infty}\right\}$$

$$+ \left\{\frac{\tau\tan\phi_W\left\{1-\left[1+(1+\tau\tan^2\phi_W)\left(\frac{dz_{W_C}}{dx_W} \pm \frac{dz_{W_C}}{dx_W}\right)^2\right]^{1/2}\right\}}{\left[1+\tau\tan^2\phi_W\right]}\right\} \qquad (283)$$

Then, the velocity components in the chordwise and spanwise directions, corrected for compressibility by the method of Labrujere, are given by;

$$\left\{\frac{V_{M_w}}{V_\infty}\right\} = \left\{ \frac{B_w \cos^2\phi_w + \left(B^2 \frac{\Delta V_{M_w}}{V_\infty}\cos^2\phi_w - B\frac{\Delta V_{T_w}}{V_\infty}\sin\phi_w\cos\phi_w\right)/\sqrt{1-M_\infty^2\cos^2\phi_w}}{\left[B_w^2 + (1+\tan^2\phi_w)\left(\frac{dz_{w_c}}{dx_w} \pm \frac{dz_{w_c}}{dx_w}\right)^2\right]^{1/2}} \right.$$

$$\left. + \left(1 + \frac{\Delta V_{M_w}}{V_\infty}\right)\sin^2\phi_w + \frac{\Delta V_{T_w}}{V_\infty}\sin\phi_w\cos\phi_w \right\} \tag{284}$$

and

$$\left\{\frac{V_{T_w}}{V_\infty}\right\} = \left\{ \frac{-B_w \cos\phi_w\sin\phi_w + \left(B^2 \frac{\Delta V_{M_w}}{V_\infty}\sin\phi_w\cos\phi_w - B\frac{\Delta V_{T_w}}{V_\infty}\sin^2\phi_w\right)/\sqrt{1-M_\infty^2\cos^2\phi_w}}{\left[B_w^2 + (1+\tan^2\phi_w)\left(\frac{dz_{w_c}}{dx_w} \pm \frac{dz_{w_c}}{dx_w}\right)^2\right]^{1/2}} \right.$$

$$\left. + \left(1 + \frac{\Delta V_{M_w}}{V_\infty}\right)\sin\phi_w\cos\phi_w + \frac{\Delta V_{T_w}}{V_\infty}\cos^2\phi_w \right\} \tag{285}$$

where

$$B_w = \sqrt{1-M_\infty^2\cos^2\phi_w\,(1 - C_{P_i}\cdot M_\infty\cos\phi_w)} \tag{286}$$

and where

$$C_{P_i} = \frac{C_p'\sqrt{1-M_\infty^2\cos^2\phi_w}}{\left[1 - \frac{C_p'}{2}\left(1-\sqrt{1-M_\infty^2\cos^2\phi_w}\right)\right]} \tag{287}$$

and

$$C_p' = \frac{1}{.7M_\infty^2}\left[\left\{1 + .2M_\infty^2\left[1-\left(\frac{V_{M_w}}{V_\infty}\right)^2 - \left(\frac{V_{T_w}}{V_\infty}\right)^2\right]\right\}^{3.5} - 1\right] \qquad \text{FOR } M_\infty > .01 \tag{288}$$

$$C_p' = 1 - \left(\frac{V_{M_w}}{V_\infty}\right)^2 - \left(\frac{V_{T_w}}{V_\infty}\right)^2 + \frac{M_\infty^2}{4}\left[1-\left(\frac{V_{M_w}}{V_\infty}\right)^2 - \left(\frac{V_{T_w}}{V_\infty}\right)^2\right] \qquad \text{FOR } M_\infty < .01 \tag{289}$$

COMBINED PYLON VELOCITY EQUATIONS

The sum of the velocity, induced by all of the configuration components, on the pylon is given by:

$$\left\{\frac{\bar{V}_{P_M}}{V_\infty}\right\} = \left\{\frac{V_{M_{PB}}}{V_\infty}\right\} + \left\{\frac{V_{M_{PF}}}{V_\infty}\right\} + \left\{\frac{V_{M_{PW}}}{V_\infty}\right\} + \left\{\frac{V_{M_{PP}}}{V_\infty}\right\} + \left\{\frac{V_{M_{PN}}}{V_\infty}\right\} \tag{290}$$

in the chordwise direction, and

$$\left\{\frac{\bar{V}_{P_T}}{V_\infty}\right\} = \left\{\frac{V_{T_{PB}}}{V_\infty}\right\} + \left\{\frac{V_{T_{PF}}}{V_\infty}\right\} + \left\{\frac{V_{T_{PW}}}{V_\infty}\right\} + \left\{\frac{V_{T_{PP}}}{V_\infty}\right\} + \left\{\frac{V_{T_{PN}}}{V_\infty}\right\} \tag{291}$$

If $\left\{\frac{\Delta V_{MP}}{V_\infty}\right\}$ and $\left\{\frac{\Delta V_{TP}}{V_\infty}\right\}$ are defined by:

$$\left\{\frac{\Delta V_{MP}}{V_\infty}\right\} = \left[\left\{1+(1+\tan^2\phi_P)\left(\frac{dz_{P_t}}{dx_P} \pm \frac{dz_{P_c}}{dx_P}\right)^2\right\}^{1/2} - 1\right]\left\{\frac{\bar{V}_{P_M}}{V_\infty}\right\} - \left\{\frac{1+\tan^2\phi_P\left[1+(1+\tan^2\phi_P)\left(\frac{dz_{P_t}}{dx_P} \pm \frac{dz_{P_c}}{dx_P}\right)^2\right]^{1/2}}{\left[1+\tan^2\phi_P\right]}\right\} \tag{292}$$

and

$$\left\{\frac{\Delta V_{TP}}{V_\infty}\right\} = \left[\left\{1+(1+\tan^2\phi_P)\left(\frac{dz_{P_t}}{dx_P} \pm \frac{dz_{P_c}}{dx_P}\right)^2\right\}^{1/2} - 1\right]\left\{\frac{\bar{V}_{P_T}}{V_\infty}\right\} + \left\{\frac{\tan\phi_P\left\{1-\left[1+(1+\tan^2\phi_P)\left(\frac{dz_{P_t}}{dx_P} \pm \frac{dz_{P_c}}{dx_P}\right)^2\right]^{1/2}\right\}}{\left[1+\tan^2\phi_P\right]}\right\} \tag{293}$$

then, the velocity componerts in the chordwise and spanwise directions, corrected for compressibility by the method of Labrujere, are given by;

$$\left\{\frac{V_{M_P}}{V_\infty}\right\} = \left\{\frac{B_W\cos^2\phi_P + \left(B^2\frac{\Delta V_{MP}}{V_\infty}\cos^2\phi_P - B\frac{\Delta V_{TP}}{V_\infty}\sin\phi_P\cos\phi_P\right)/\sqrt{1-M_\infty^2\cos^2\phi_P}}{\left[B_W^2+(1+\tan^2\phi_P)\left(\frac{dz_{P_t}}{dx_P} \pm \frac{dz_{P_c}}{dx_P}\right)^2\right]^{1/2}} + \left(1+\frac{\Delta V_{MP}}{V_\infty}\right)\sin^2\phi_P + \frac{\Delta V_{TP}}{V_\infty}\sin\phi_P\cos\phi_P\right\} \tag{294}$$

and

$$\left\{\frac{V_{TP}}{V_\infty}\right\} = \left\{ - \frac{B_W \cos\phi_P \sin\phi_P + \left(B^2 \frac{\Delta V_{MP}}{V_\infty} \sin\phi_P \cos\phi_P - B \frac{\Delta V_{TP}}{V_\infty} \sin^2\phi_P\right)\sqrt{1 - M_\infty^2 \cos^2\phi_P}}{\left[B_W^2 + \left(1 + \tan^2\phi_P\right)\left(\frac{dz_{PT}}{dx_P} \pm \frac{dz_{PC}}{dx_P}\right)^2\right]^{1/2}} \right.$$

$$\left. + \left(1 + \frac{\Delta V_{MP}}{V_\infty}\right)\sin\phi_P \cos\phi_P + \frac{\Delta V_{TP}}{V_\infty} \cos^2\phi_P \right\} \qquad (295)$$

where B_W is defined the same as on the wing except that ϕ_P is used instead of ϕ_W.

COMBINED FANPOD VELOCITY EQUATIONS

The sum of the velocity induced on the fanpod surface by all of the components is given by;

$$\left\{\frac{V_{MF}}{V_\infty}\right\} = \left\{\frac{V_{MFB}}{V_\infty}\right\} + \left\{\frac{V_{MFF}}{V_\infty}\right\} + \left\{\frac{V_{MFW}}{V_\infty}\right\} + \left\{\frac{V_{MFP}}{V_\infty}\right\} + \left\{\frac{V_{MF\infty}}{V_\infty}\right\} \qquad (296)$$

along the meridian lines and

$$\left\{\frac{V_{TF}}{V_\infty}\right\} = \left\{\frac{V_{TFB}}{V_\infty}\right\} + \left\{\frac{V_{TFF}}{V_\infty}\right\} + \left\{\frac{V_{TFW}}{V_\infty}\right\} + \left\{\frac{V_{TFP}}{V_\infty}\right\} + \left\{\frac{V_{TF\infty}}{V_\infty}\right\} \qquad (297)$$

perpendicular to the meridian lines.

COMBINED FUSELAGE VELOCITY EQUATIONS

The sum of the velocity induced on the fuselage surface by all of the components is given by;

$$\left\{\frac{V_{MB}}{V_\infty}\right\} = \left\{\frac{V_{MBB}}{V_\infty}\right\} + \left\{\frac{V_{MBF}}{V_\infty}\right\} + \left\{\frac{V_{MBW}}{V_\infty}\right\} + \left\{\frac{V_{MBP}}{V_\infty}\right\} + \left\{\frac{V_{MB\infty}}{V_\infty}\right\} \qquad (298)$$

along the meridian lines and

$$\left\{\frac{V_{T_B}}{V_\infty}\right\} = \left\{\frac{V_{T_{BB}}}{V_\infty}\right\} + \left\{\frac{V_{T_{BF}}}{V_\infty}\right\} + \left\{\frac{V_{T_{BW}}}{V_\infty}\right\} + \left\{\frac{V_{T_{BP}}}{V_\infty}\right\} + \left\{\frac{V_{T_{BN}}}{V_\infty}\right\} \tag{299}$$

perpendicular to the meridian lines.

The compressibility correction for the fuselage and fannod is that due to Gothert and is already included in the above equations. Due to the assumption of axisymmetric flow for the nacelle, no velocities or pressures are computed on the nacelle.

The surface pressure coefficient is then computed at each of the control point locations using the following expression.

$$C_p = \frac{2}{\gamma M_\infty^2}\left[\left\{1 + \frac{\gamma-1}{2} M_\infty^2\left[1 - \left(\frac{V_m}{V_\infty}\right)^2 - \left(\frac{V_t}{V_\infty}\right)^2\right]\right\}^{\gamma/(\gamma-1)} - 1\right] \tag{300}$$

where γ is the ratio of specific heats.

SECTION AND TOTAL LOADS AND MOMENTS

The section loads on the fuselage and fanpods are computed by summing the products of the surface pressures and directed incremental areas at each longitudinal station.

The section drag is given by;

$$\left(\frac{C_d w}{w_{AVG.}}\right) = -\frac{1}{A_z \Delta(x/c)_k} \sum_i C_{p_{ik}} \Delta A_{x_{ik}} \tag{301}$$

and the section lift by;

$$\left(\frac{C_N w}{w_{AVG.}}\right) = -\frac{1}{A_z \Delta(x/c)_k} \sum_i C_{p_{ik}} \Delta A_{z_{ik}} \tag{302}$$

where i is indexed over all subareas at the longitudinal station k, and

$$A_z = \frac{1}{2} \sum_k \sum_i |\Delta A_{z_{ik}}| \tag{303}$$

is the fuselage or fanpod reference area.

$$w_{AVG.} = A_z/c \tag{304}$$

The fuselage or fanpod total lift, drag, and pitching moment are computed as follows.

$$C_L = \sum_k \left(\frac{C_N w}{w_{AVG.}}\right)_k \Delta(x/c)_k \tag{305}$$

$$C_D = \sum_k \left(\frac{C_d w}{w_{AVG.}}\right)_k \Delta(x/c)_k \tag{306}$$

and

$$C_M = -\frac{1}{A_z \bar{c}} \sum_k \sum_i \left[z_{ik} \Delta A_{x_{ik}} - x_{ik} \Delta A_{z_{ik}} \right] C_{p_{ik}} \tag{307}$$

The section loads and moments on the wing and pylons are computed by the following equations at a series of span stations.

The section lift is given by;

$$\frac{C_l c}{C_{AVG.}} = \frac{c\,AR}{2b} \int_0^{\pi} \frac{\Delta S}{\Delta S_{L.E.}} (C_{R_L} - C_{R_U}) \sin\phi \sin\gamma \, d\phi \tag{308}$$

the section drag by;

$$\frac{C_d c}{C_{AVG.}} = \frac{c\,AR}{2b} \int_0^{\pi} \frac{\Delta S}{\Delta S_{L.E.}} \left[C_{R_L} \tan\alpha_L - C_{R_U} \tan\alpha_U \right] \sin\phi \, d\phi \tag{309}$$

and the section moment by;

$$\frac{C_m c}{C_{AVG.}} = -\frac{AR\,c}{2b\bar{c}} \int_0^{\pi} \frac{\Delta S}{\Delta S_{L.E.}} (x - x_{L.E.})(C_{R_L} - C_{R_U}) \sin\phi \sin\gamma \, d\phi \tag{310}$$

where

$$\tan\alpha = \frac{\tan\delta \mp \frac{dz_L}{dx} - \frac{dz_c}{dx} + \varepsilon}{1 - \left(\mp \frac{dz_L}{dx} - \frac{dz_c}{dx} + \varepsilon\right)\tan\delta} \tag{311}$$

and

$$\phi = \cos^{-1}(1 - 2x/c)$$

NOTE; γ is equal to 90 degrees on the wing.

The section center of pressure is given by;

$$\left(x/c\right)_{c.p.} = -\frac{\frac{C_m c}{C_{AVG.}}}{\frac{C_l c}{C_{AVG.}}} \tag{312}$$

The wing and pylon total loads and moments are computed by numerical integration of the section loads.

In addition to the drag computed from equations 301 and 309 , the program also computes the skin friction and vortex drags for the complete configuration. The equations for these calculations are given in Appendices J and K.

EXPERIMENTAL COMPARISONS

Two configurations were run to demonstrate successful program operation: Case I - The wing-body configuration shown in figure 7 was run at 0.6 Mach number and zero and four degrees angle of attack. Case I comparisons are shown on figures 8 through 27. Case II - The V/STOL lift fan transport model (less tail surfaces) shown in figure 1 on page 13 was run at 0.6 Mach number and at zero and three degrees angle of attack with and without the fanpod. Case II comparisons are shown on figures 28 through 57.

WING-BODY CONFIGURATION

The wing-body configuration run as Case I is defined in RM L51F07. Comparison of results from the program with data are shown in figures 8 through 27. Figures 8 through 12 show comparisons of pressure coefficients at zero degrees angle of attack at the 20, 40, 60, 80, and 95 percent semi-span wing stations.

Figures 13 through 16 show both the body alone and wing-body pressure coefficients at the 45, 75, 105, and 135 body roll stations at zero angle of attack. These figures show the increment in pressure induced on the fuselage by the wing thickness.

Figures 17 through 21 compare results of the program with data at the 20, 40, 60, 80, and 95 percent wing semi-span stations for four degrees angle of attack. Figures 22 through 25 show both the body alone and wing-body pressures at the 45, 75, 105, and 135 body roll stations at four degrees angle of attack. These figures show the pressure induced on the body due to thickness and lift of the wing.

Figure 26 shows the comparison of theoretical to experimental span load. Figure 27 shows the comparison of theoretical to experimental longitudinal loading on the fuselage with the wing at four degrees angle of attack.

All of the results for Case I are considered to be in excellent agreement with the test data.

WING DETAILS

AIRFOIL SECTION (PARALLEL TO PLANE OF SYMMETRY)	NACA 65A006
AREA, SQ FT	1
ASPECT RATIO	4
TAPER RATIO	0.6
INCIDENCE, DEG	0
DIHEDRAL, DEG	0
GEOMETRIC TWIST, DEG	0

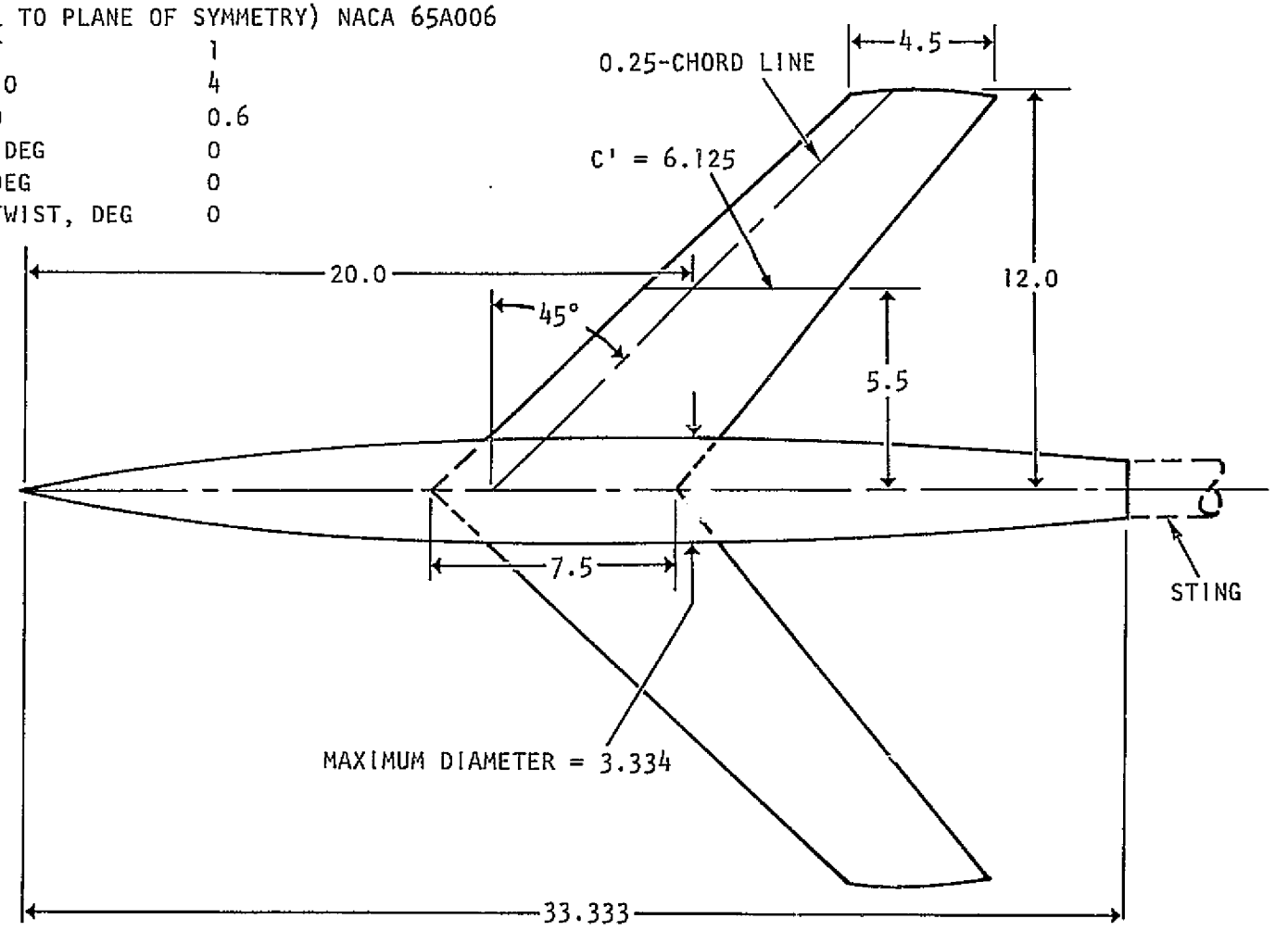

Figure 7. Wind Tunnel Model.

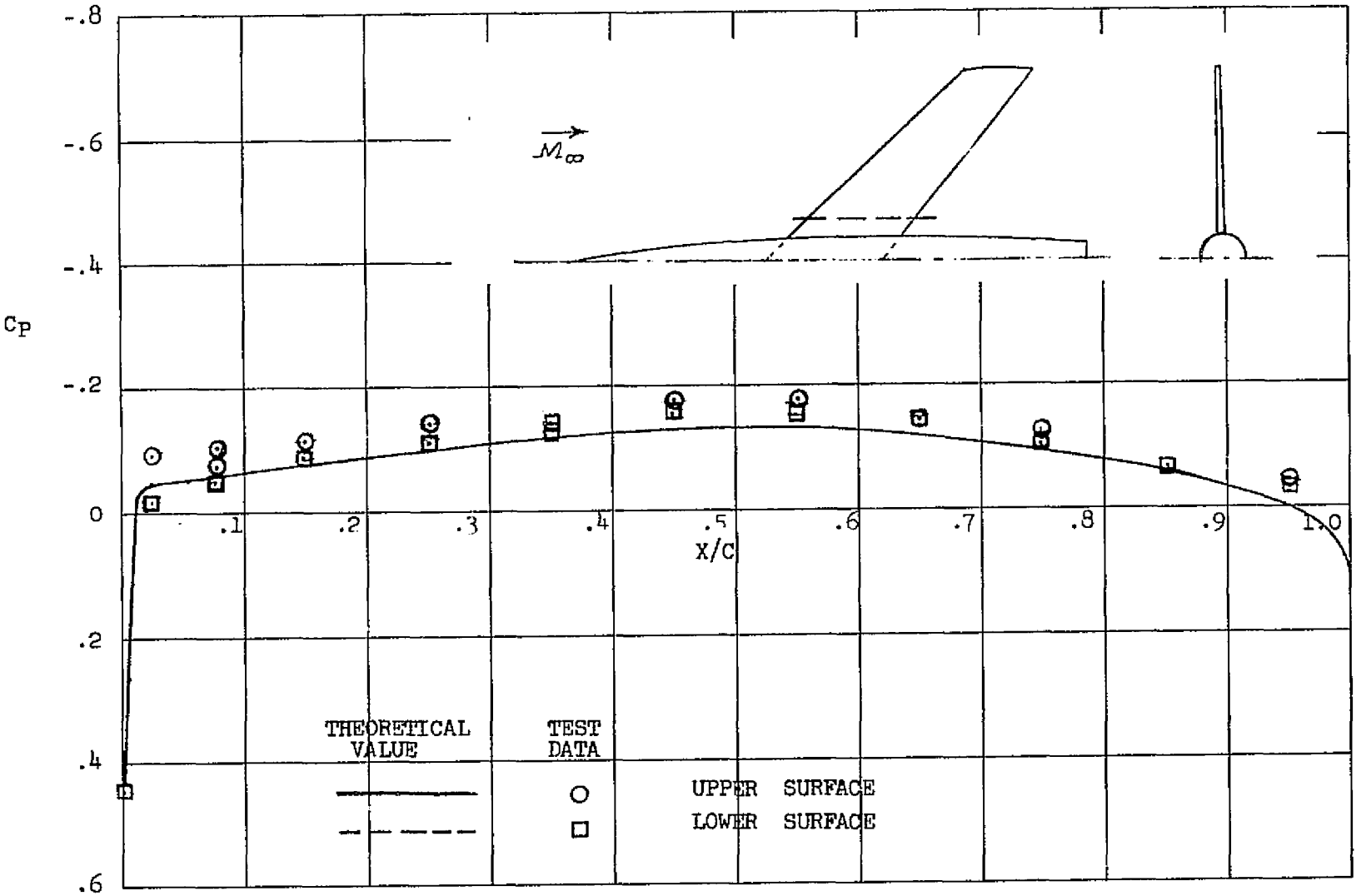

FIGURE 8. CHORDWISE PRESSURE DISTRIBUTION AT THE WING 20 PERCENT SEMI-SPAN STATION. $M_\infty = .6$, $\alpha = 0$ DEGREES

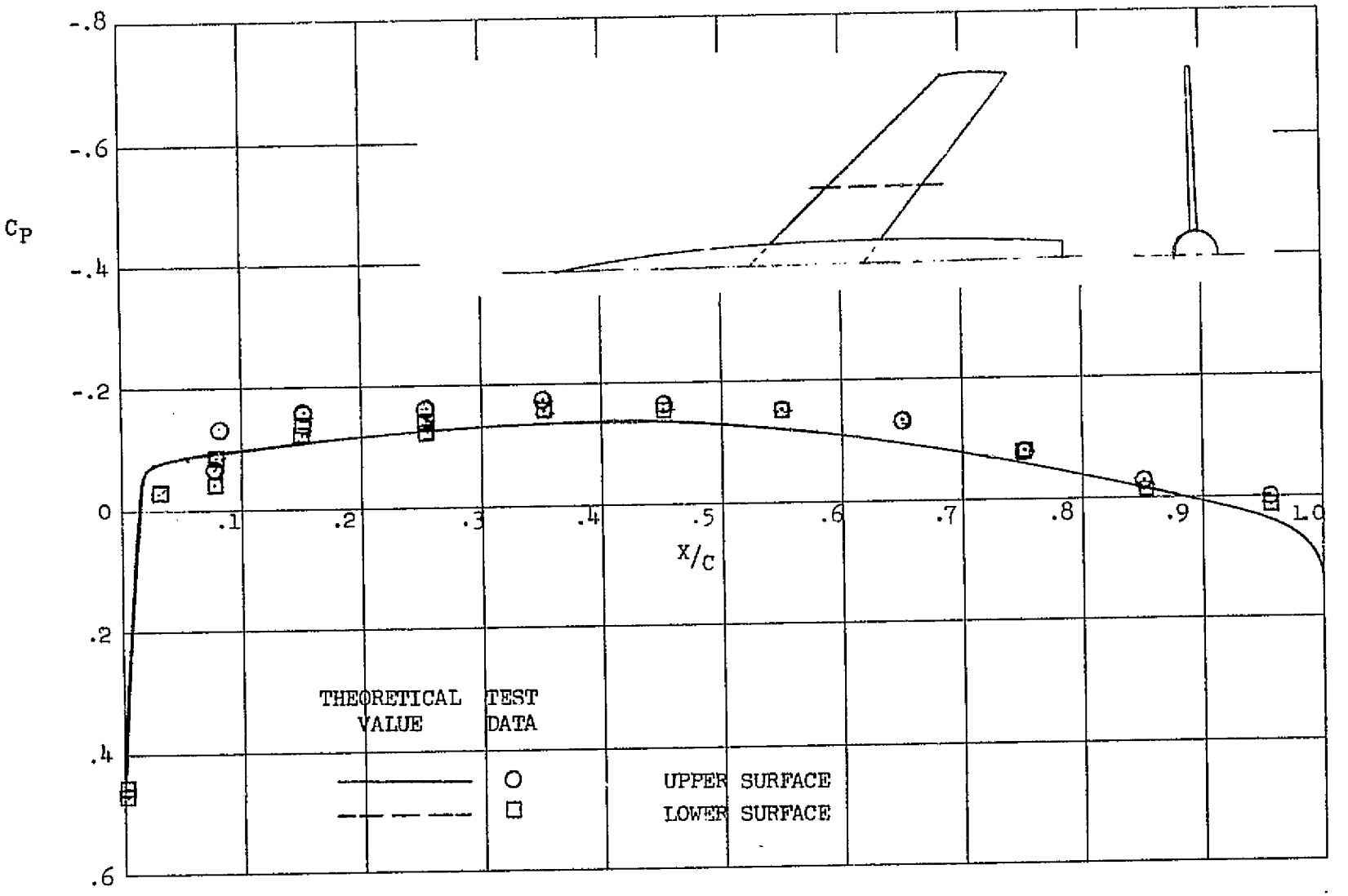

FIGURE 9. CHORDWISE PRESSURE DISTRIBUTION AT THE WING 40 PERCENT SEMI-SPAN STATION. $M_\infty = .6$, $\alpha = 0$ DEGREES

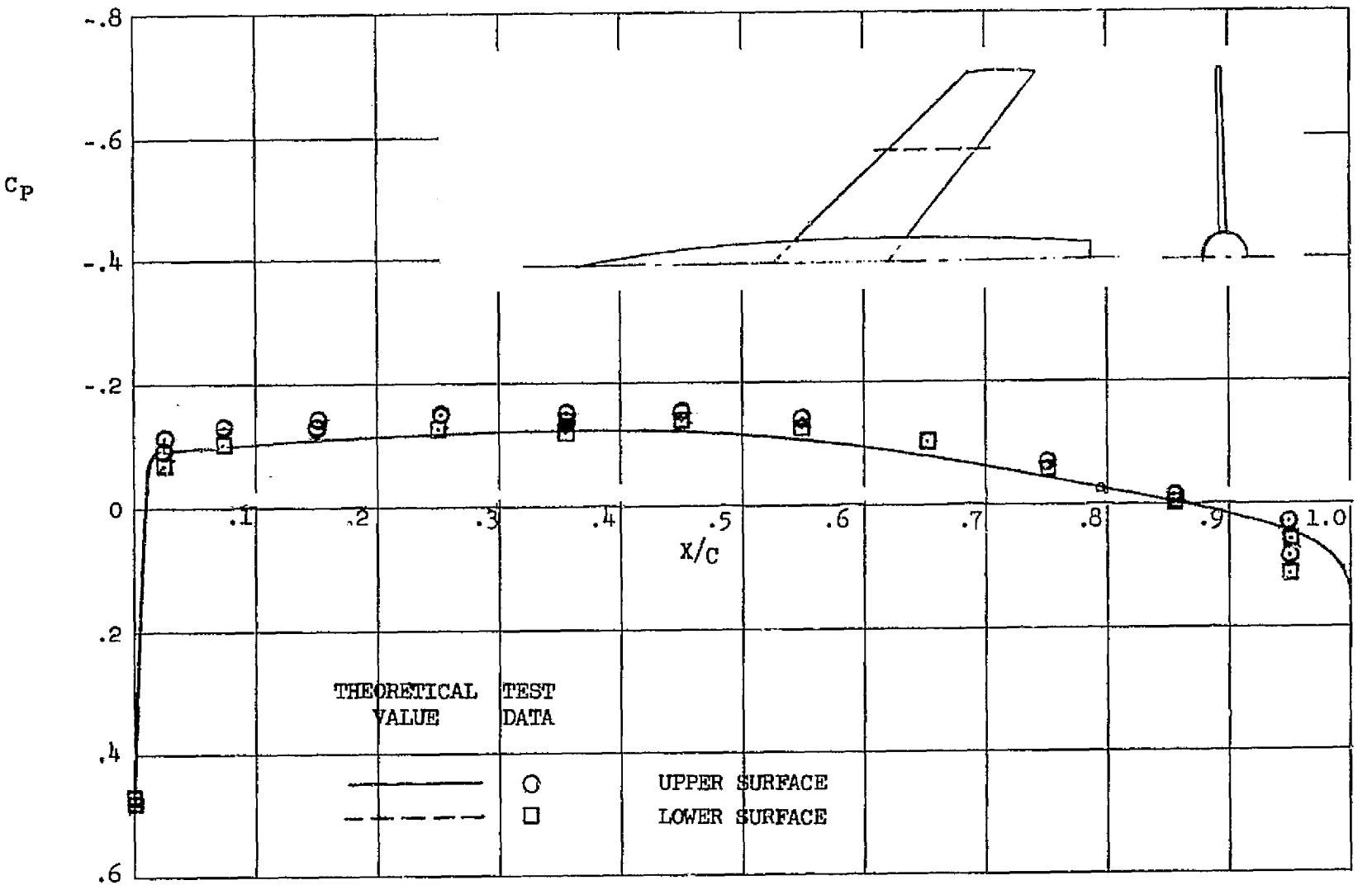

FIGURE 10. CHORDWISE PRESSURE DISTRIBUTION AT THE WING 60 PERCENT SEMI-SPAN STATION. $M_\infty = .6$, $\alpha = 0$ DEGREES

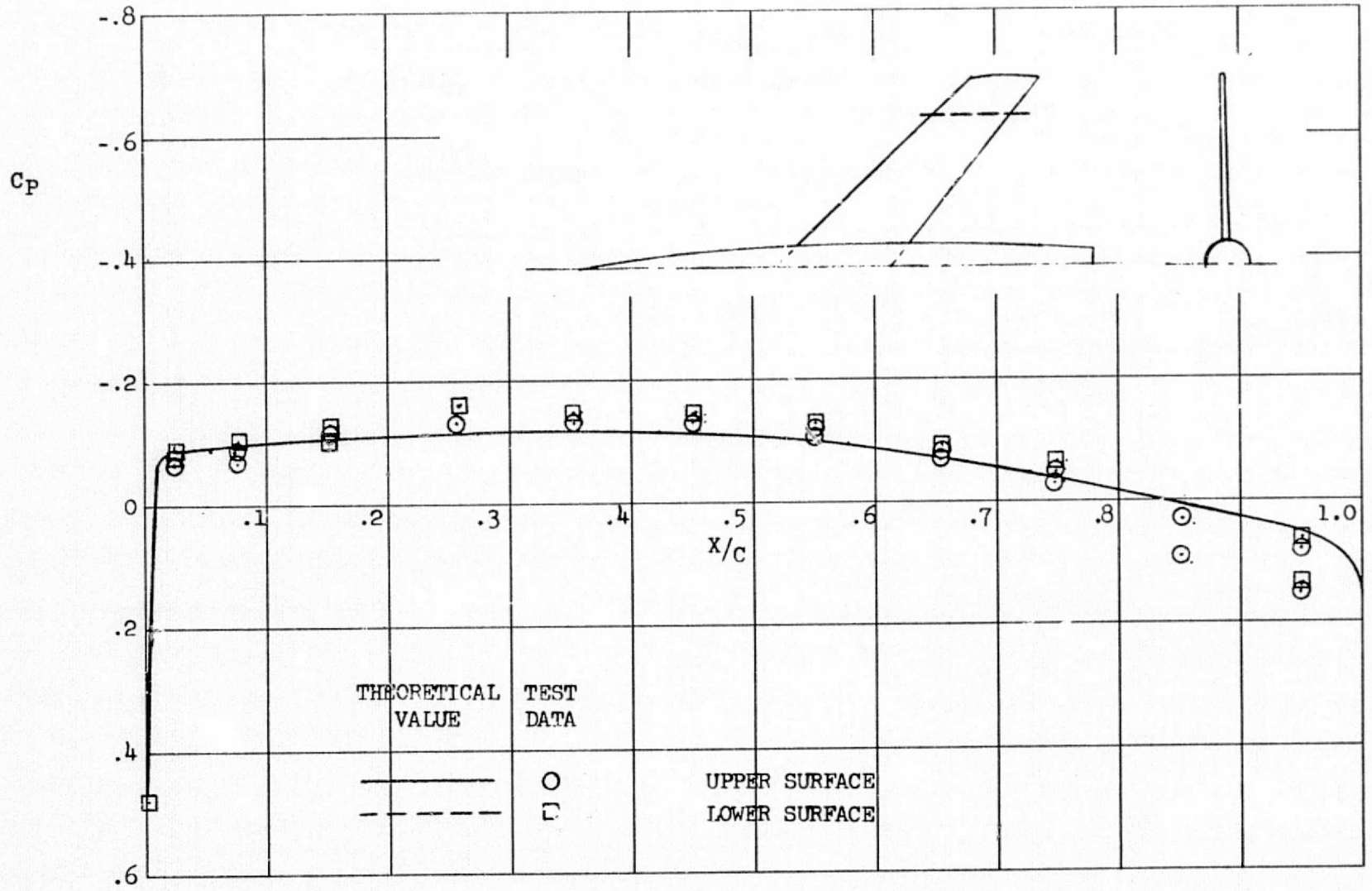

FIGURE 11. CHORDWISE PRESSURE DISTRIBUTION AT THE WING 80 PERCENT SEMI-SPAN STATION. $M_\infty = .6$, $\alpha = 0$ DEGREES

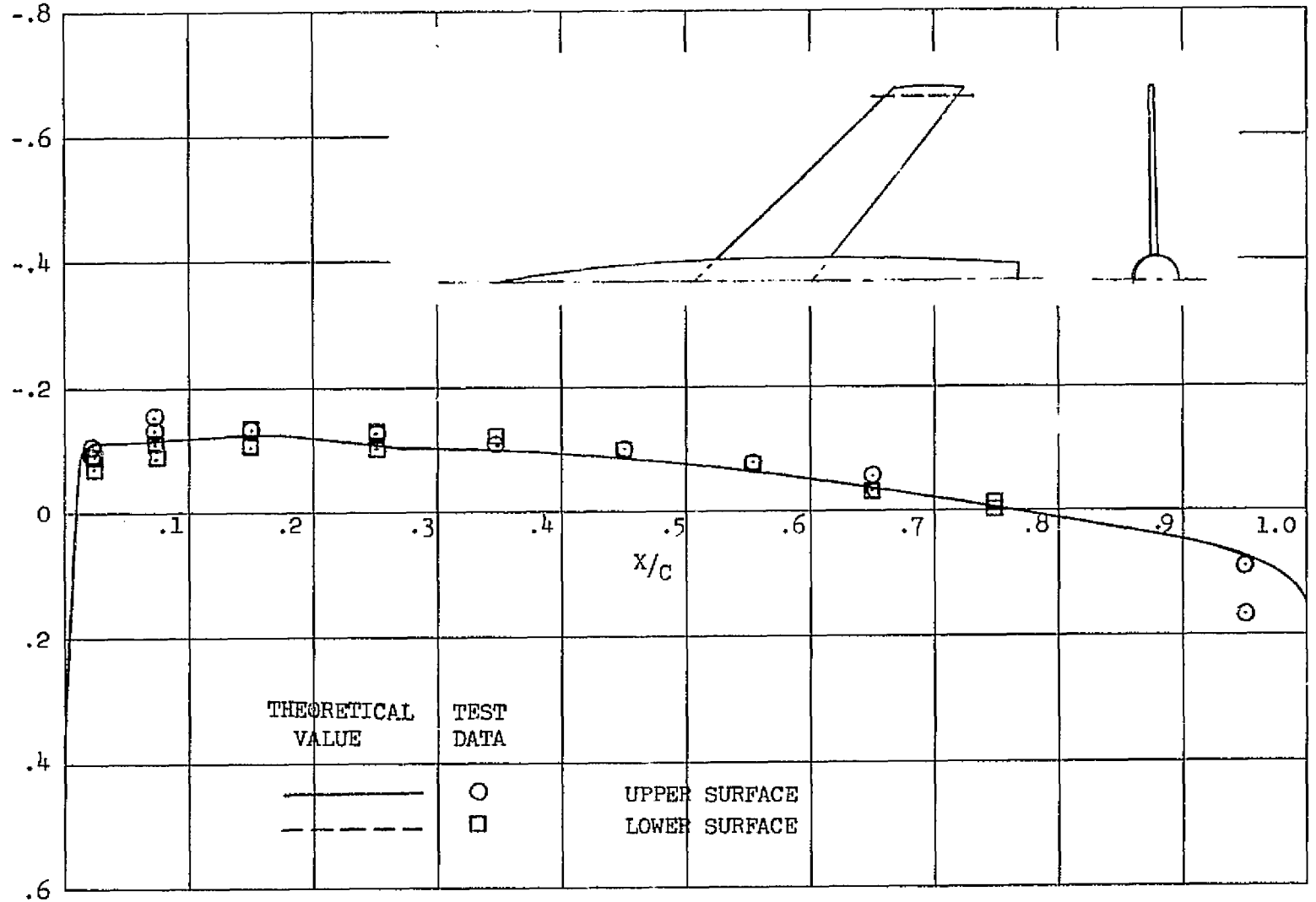

FIGURE 12. CHORDWISE PRESSURE DISTRIBUTION AT THE WING 95 PERCENT SEMI-SPAN STATION. $M_\infty = .6$, $\alpha = 0$ DEGREES

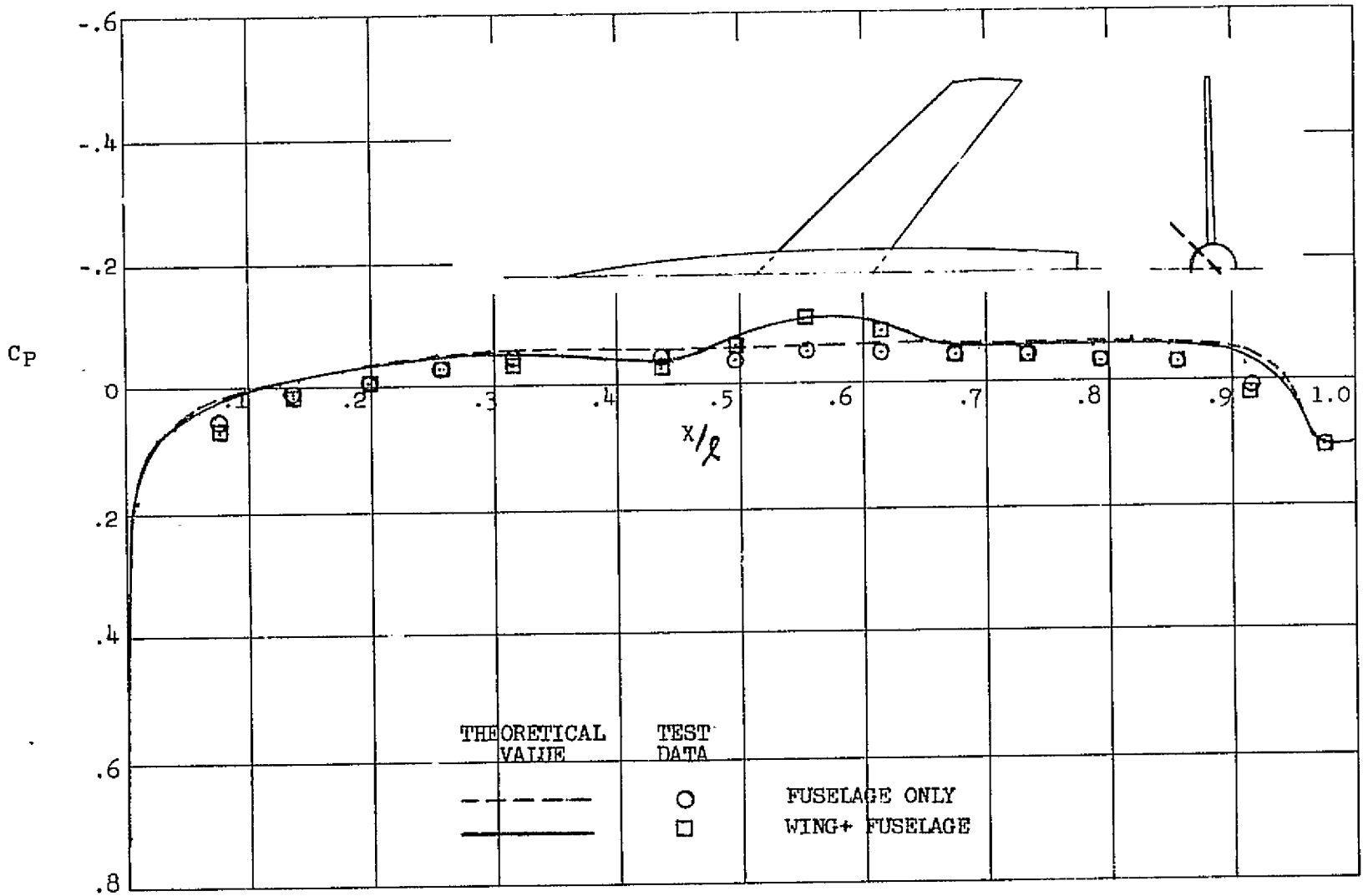

FIGURE 13. CHORDWISE PRESSURE DISTRIBUTION AT THE FUSELAGE 45 DEGREE ROLL STATION. $M_\infty = .6$, $\alpha = 0$ DEGREES

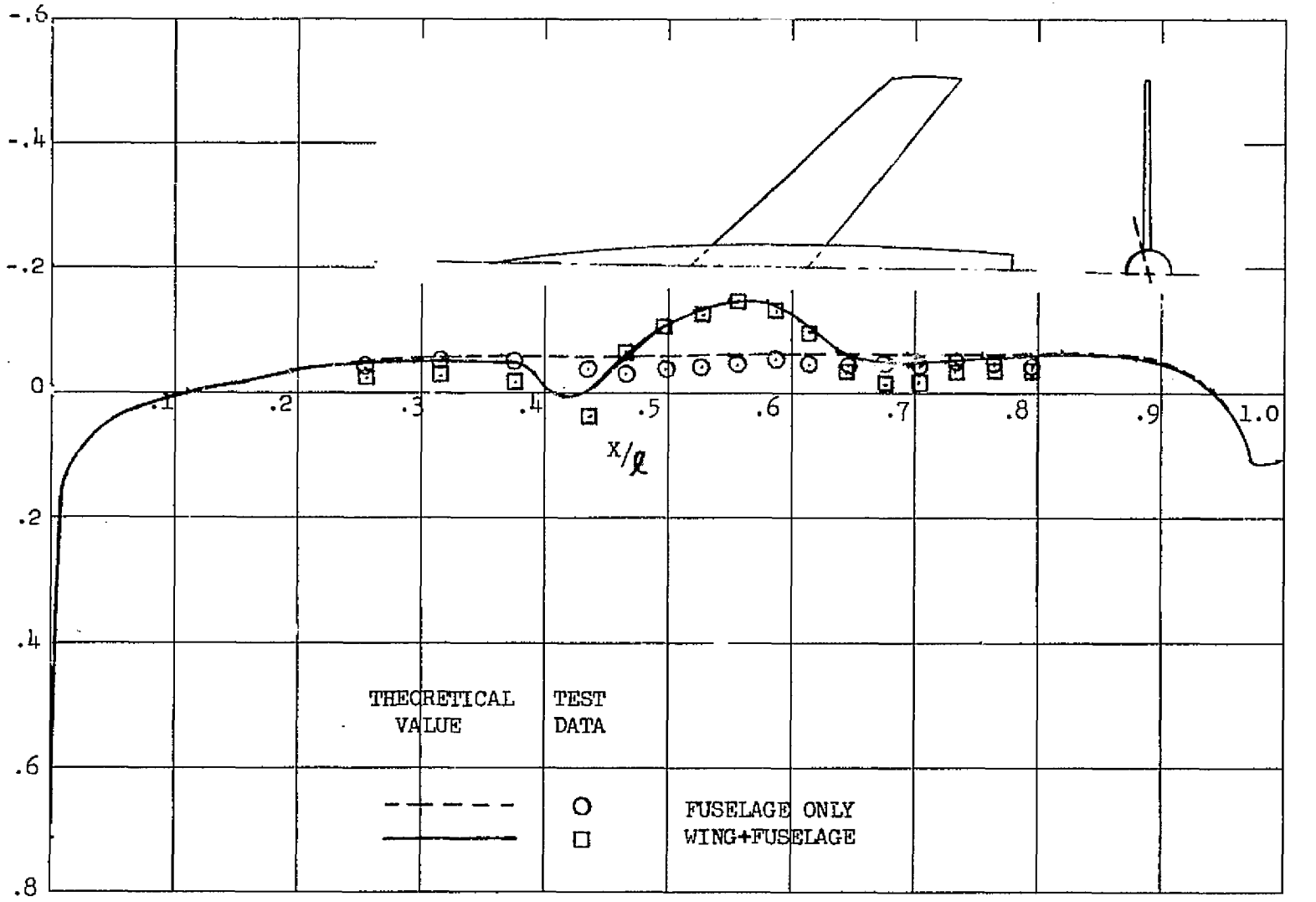

FIGURE 14. CHORDWISE PRESSURE DISTRIBUTION AT THE FUSELAGE 75 DEGREE ROLL STATION. $M_\infty = .6$, $\alpha = 0$ DEGREES

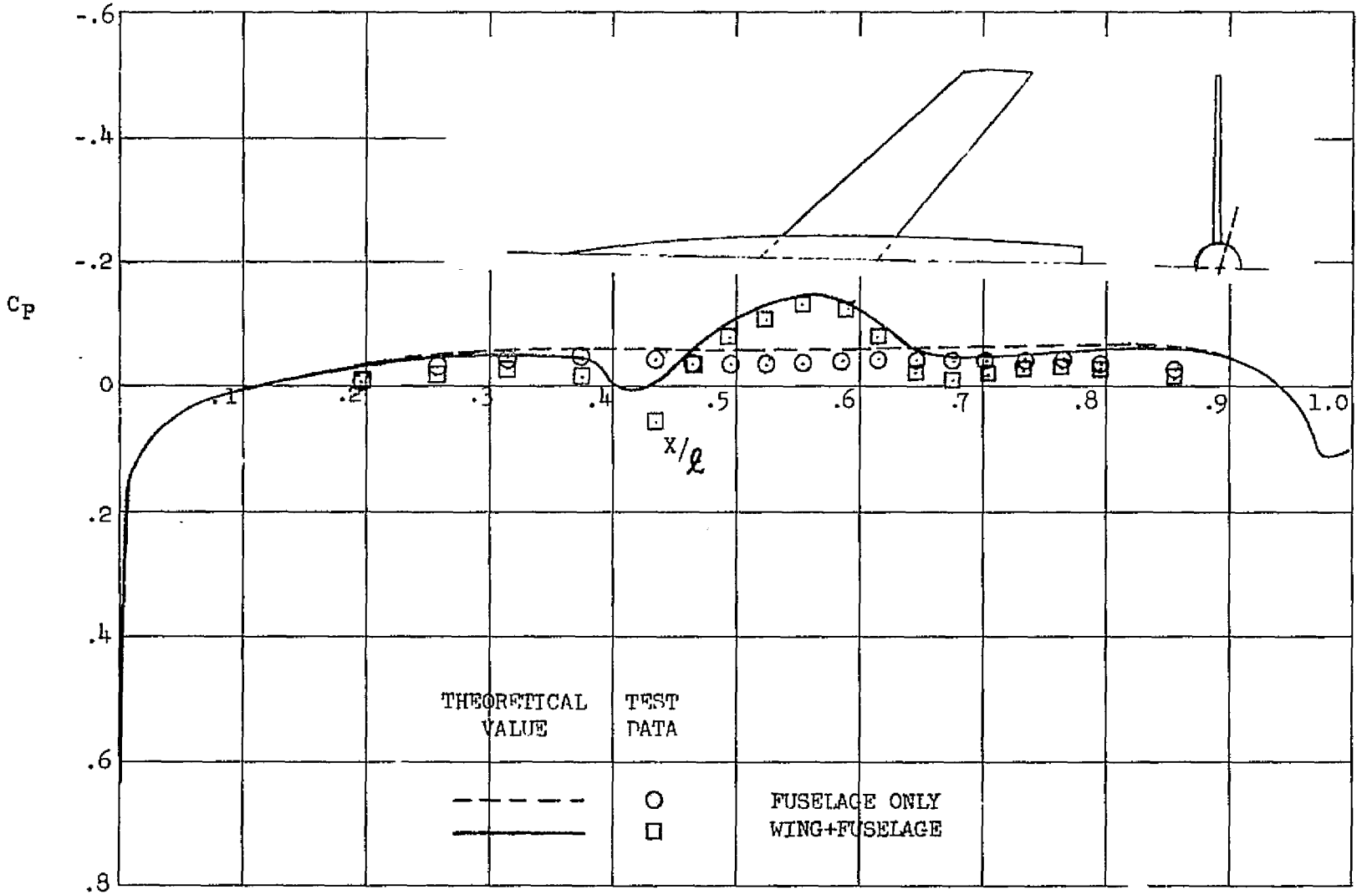

FIGURE 15. CHORDWISE PRESSURE DISTRIBUTION AT THE FUSELAGE 105 DEGREE ROLL STATION. $M_\infty = .6$, $\alpha = 0$ DEGREES

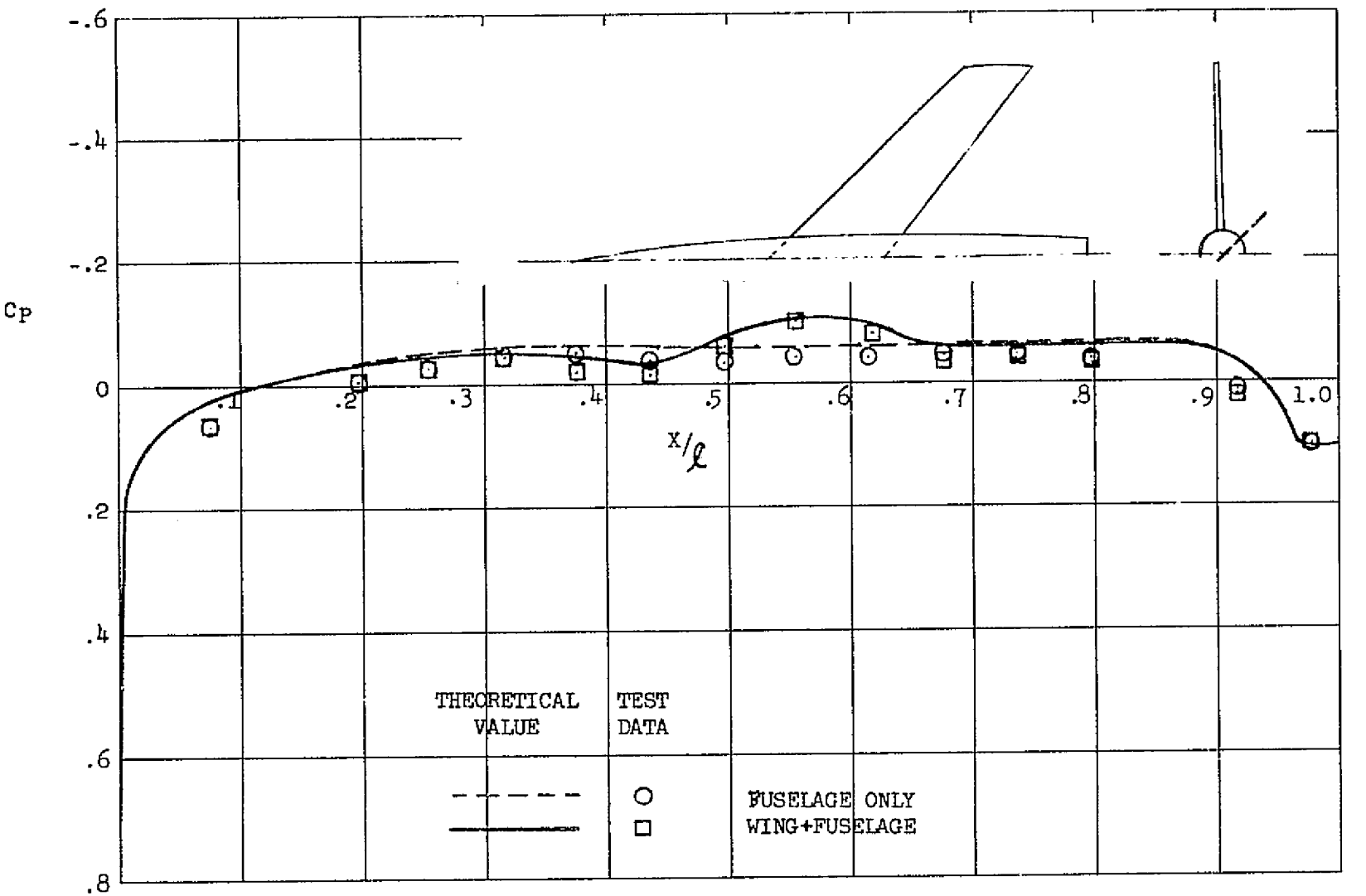

FIGURE 16. CHORDWISE PRESSURE DISTRIBUTION AT THE FUSELAGE 135 DEGREE ROLL STATION. $M_\infty = .6$, $\alpha = 0$ DEGREES

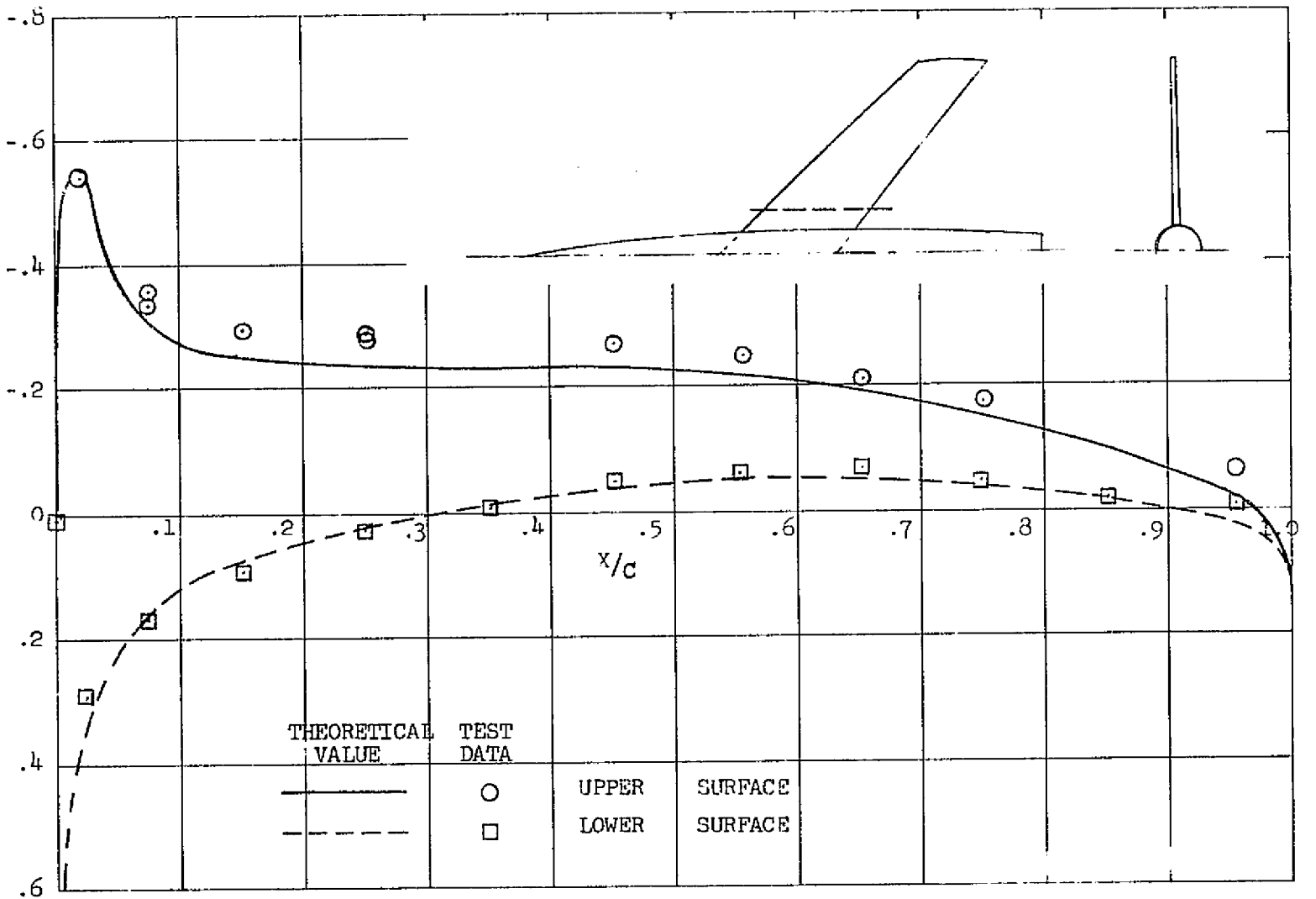

FIGURE 17. CHORDWISE PRESSURE DISTRIBUTION AT THE WING 20 PERCENT SEMI-SPAN STATION. $M_\infty = .6$, $\alpha = 4$ DEGREES

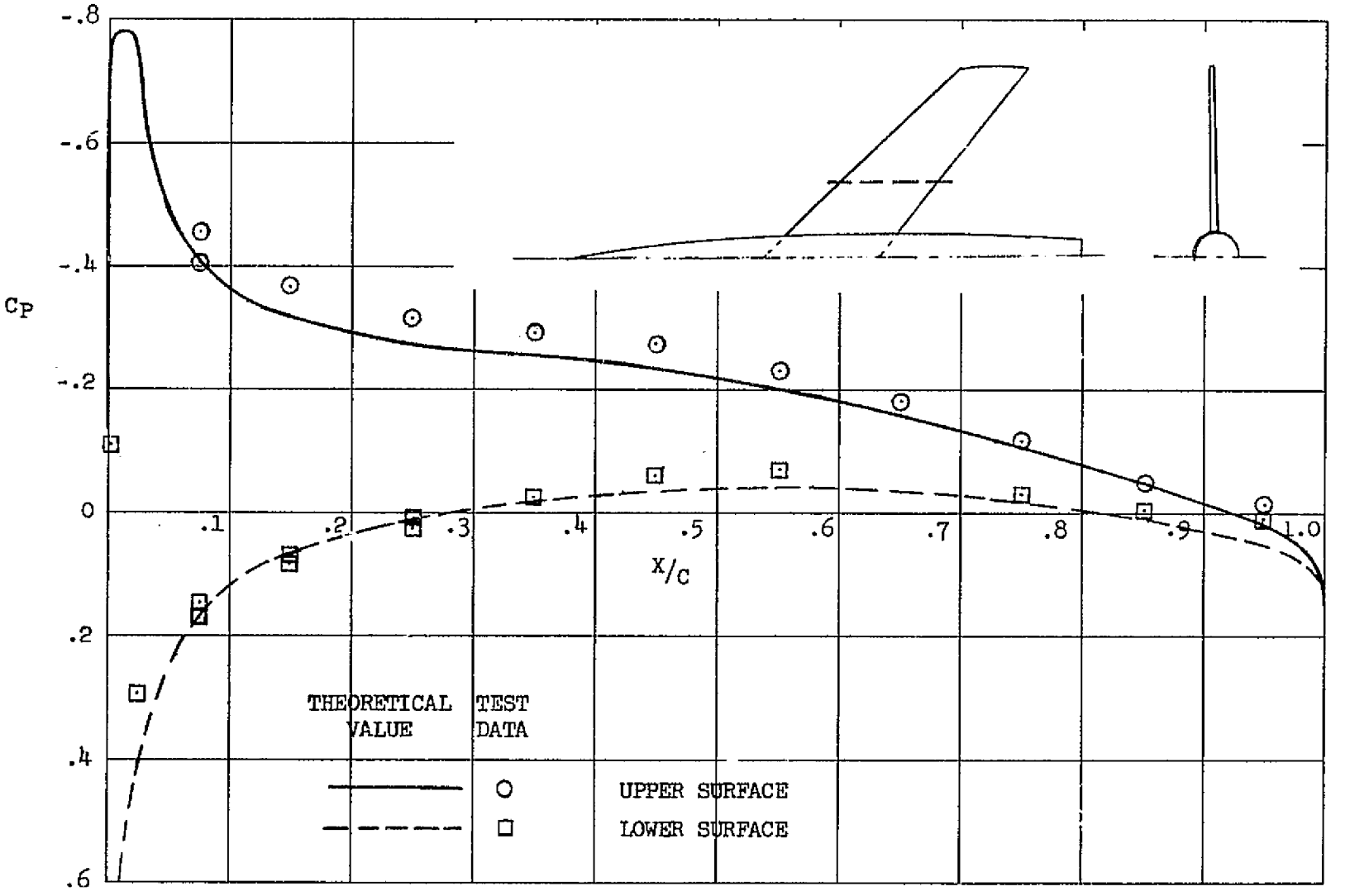

FIGURE 18. CHORDWISE PRESSURE DISTRIBUTION AT THE WING 40 PERCENT SEMI-SPAN STATION. $M_\infty = .6$, $\alpha = 4$ DEGREES

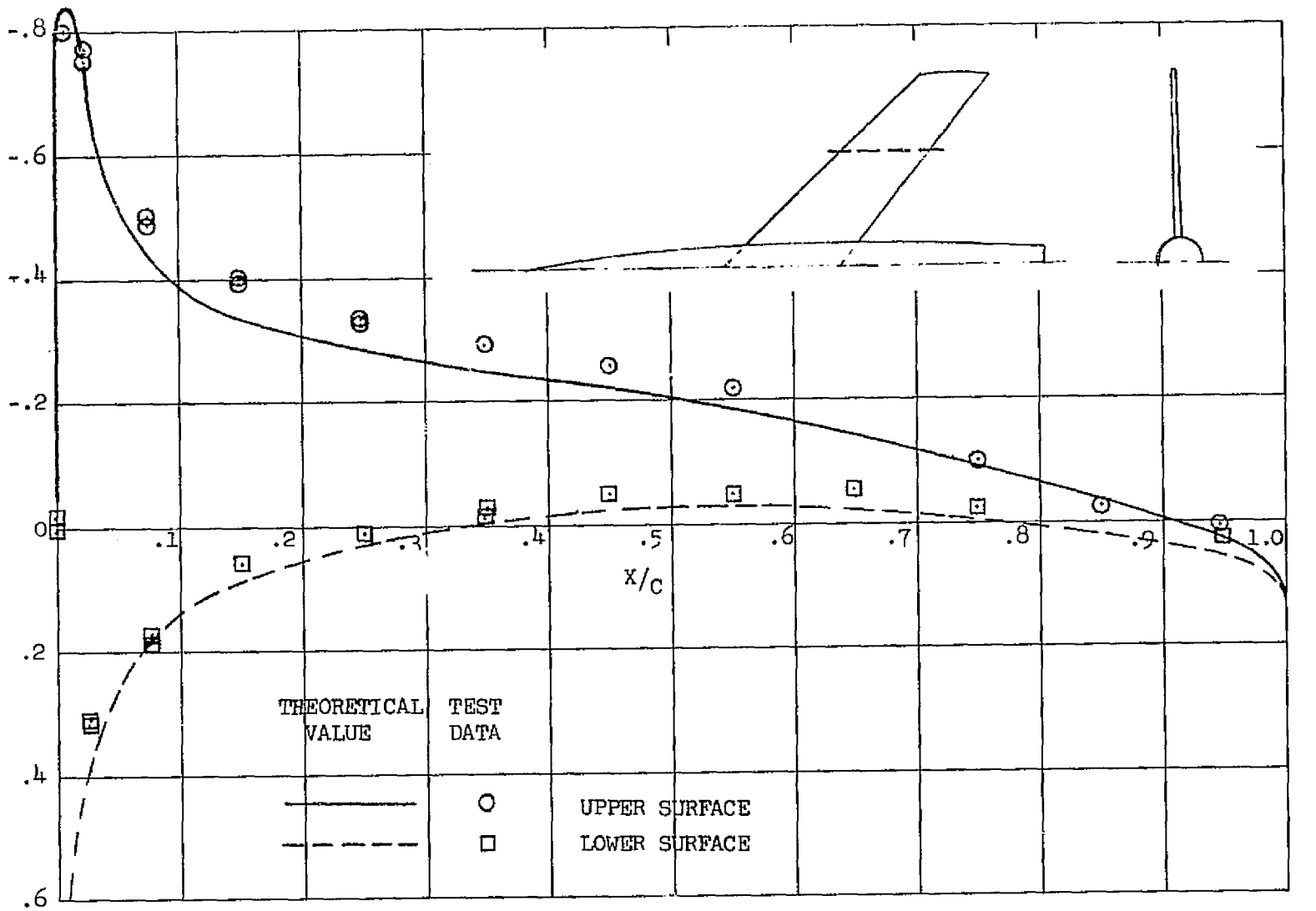

FIGURE 19. CHORDWISE PRESSURE DISTRIBUTION AT THE WING 60 PERCENT SEMI-SPAN STATION. $M_\infty = .6$, $\alpha = 4$ DEGREES

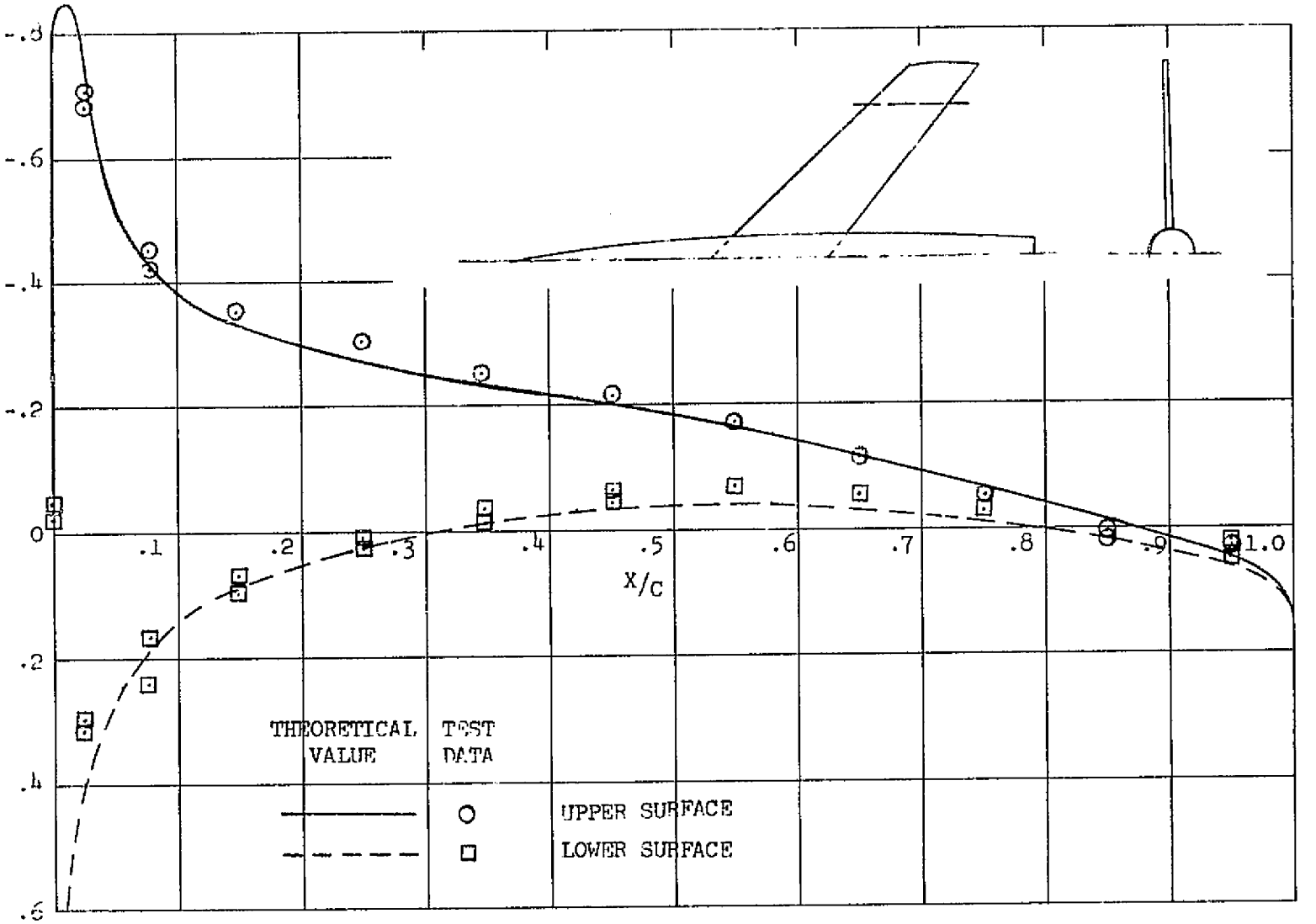

FIGURE 20. CHORDWISE PRESSURE DISTRIBUTION AT THE WING 80 PERCENT SEMI-SPAN STATION. $M_\infty = .6$, $\alpha = 4$ DEGREES

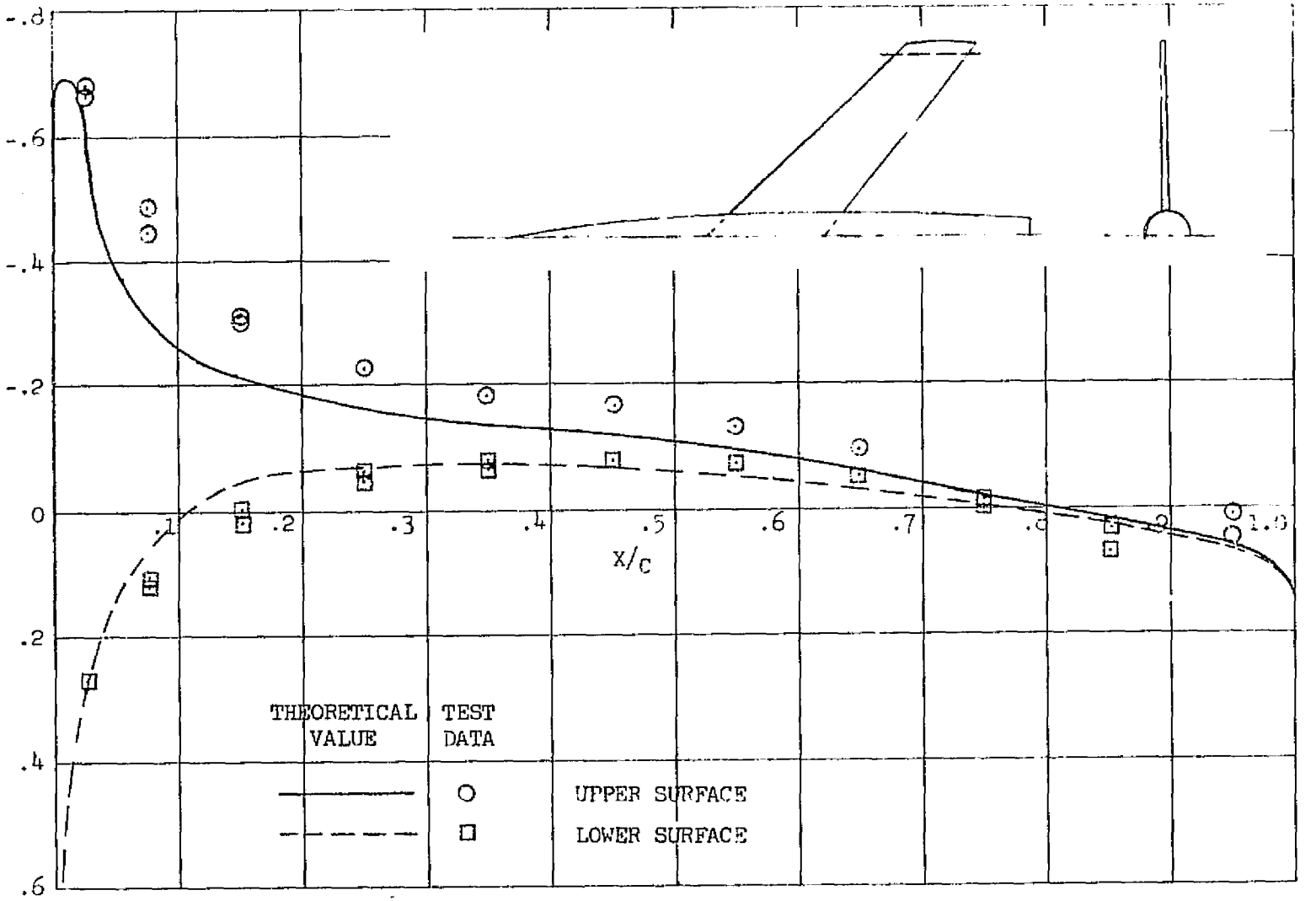

FIGURE 21. CHORDWISE PRESSURE DISTRIBUTION AT THE WING 95 PERCENT SEMI-SPAN STATION. $M_\infty = .6$, $\alpha = 4$ DEGREES

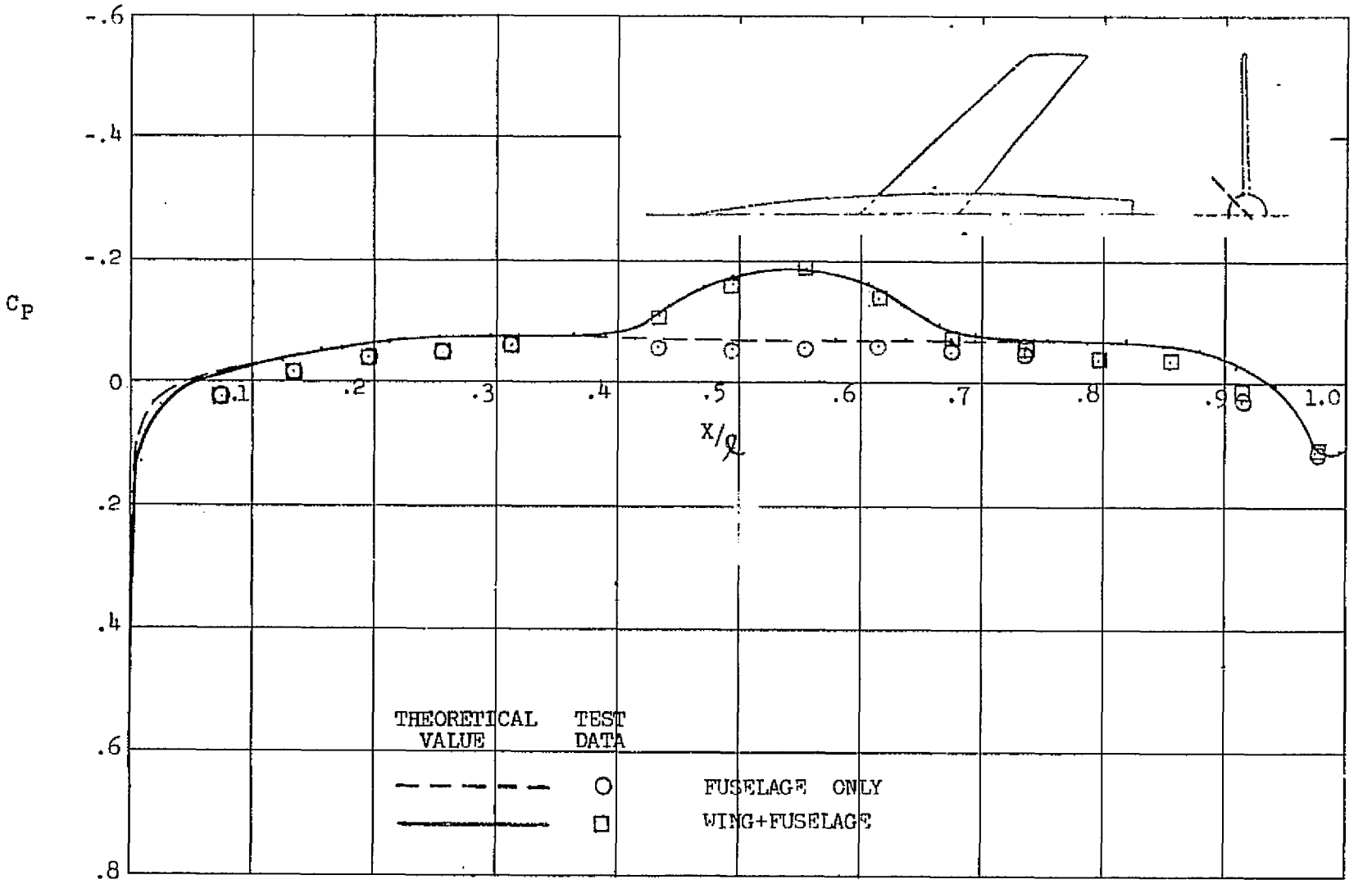

FIGURE 22. CHORDWISE PRESSURE DISTRIBUTION AT THE FUSELAGE 45 DEGREE ROLL STATION. $M_\infty = .6$, $\alpha = 4$ DEGREES

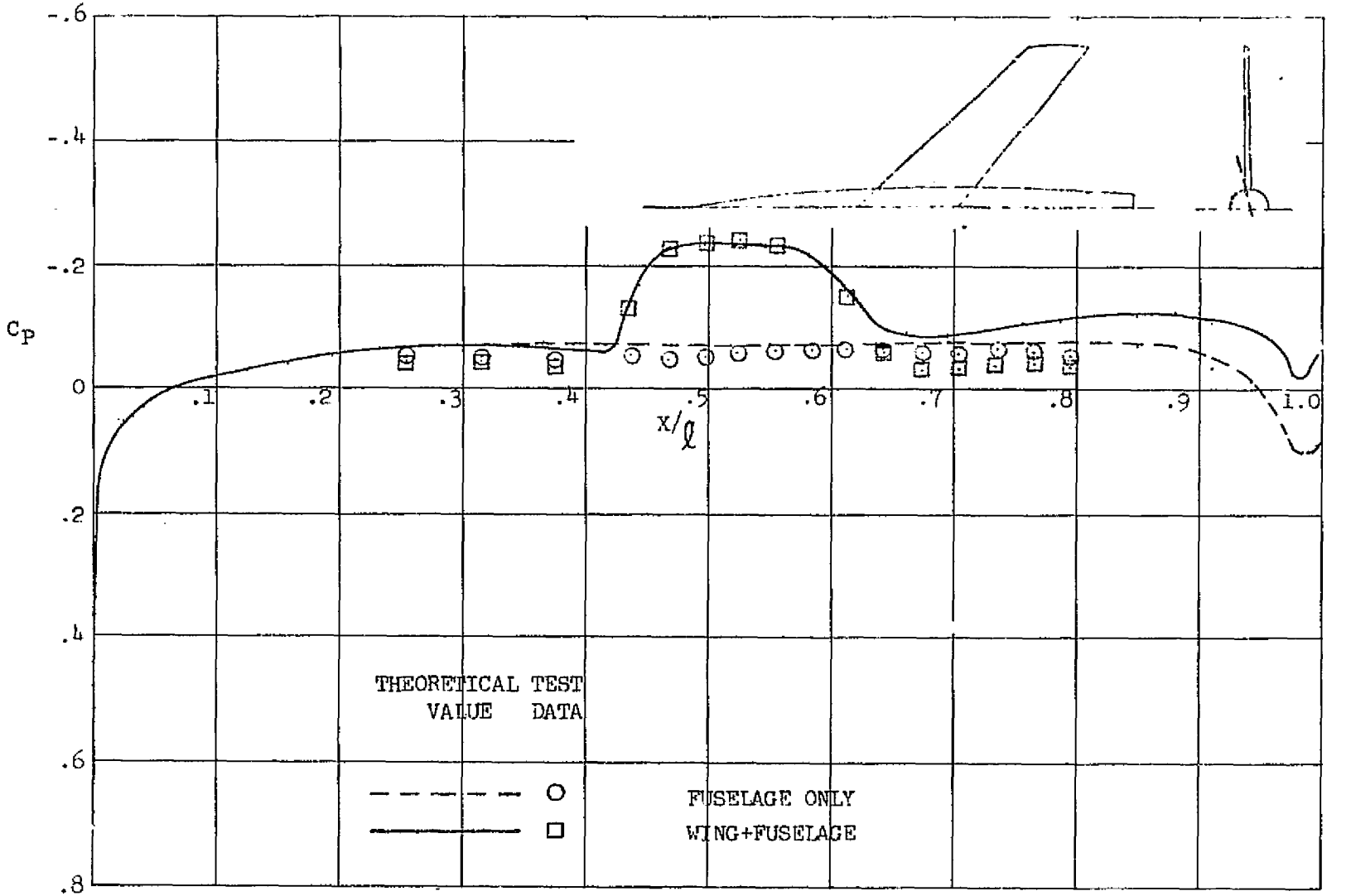

FIGURE 23. CHORDWISE PRESSURE DISTRIBUTION AT THE FUSELAGE 75 DEGREE ROLL STATION. $M_\infty = .6$, $\alpha = 4$ DEGREES

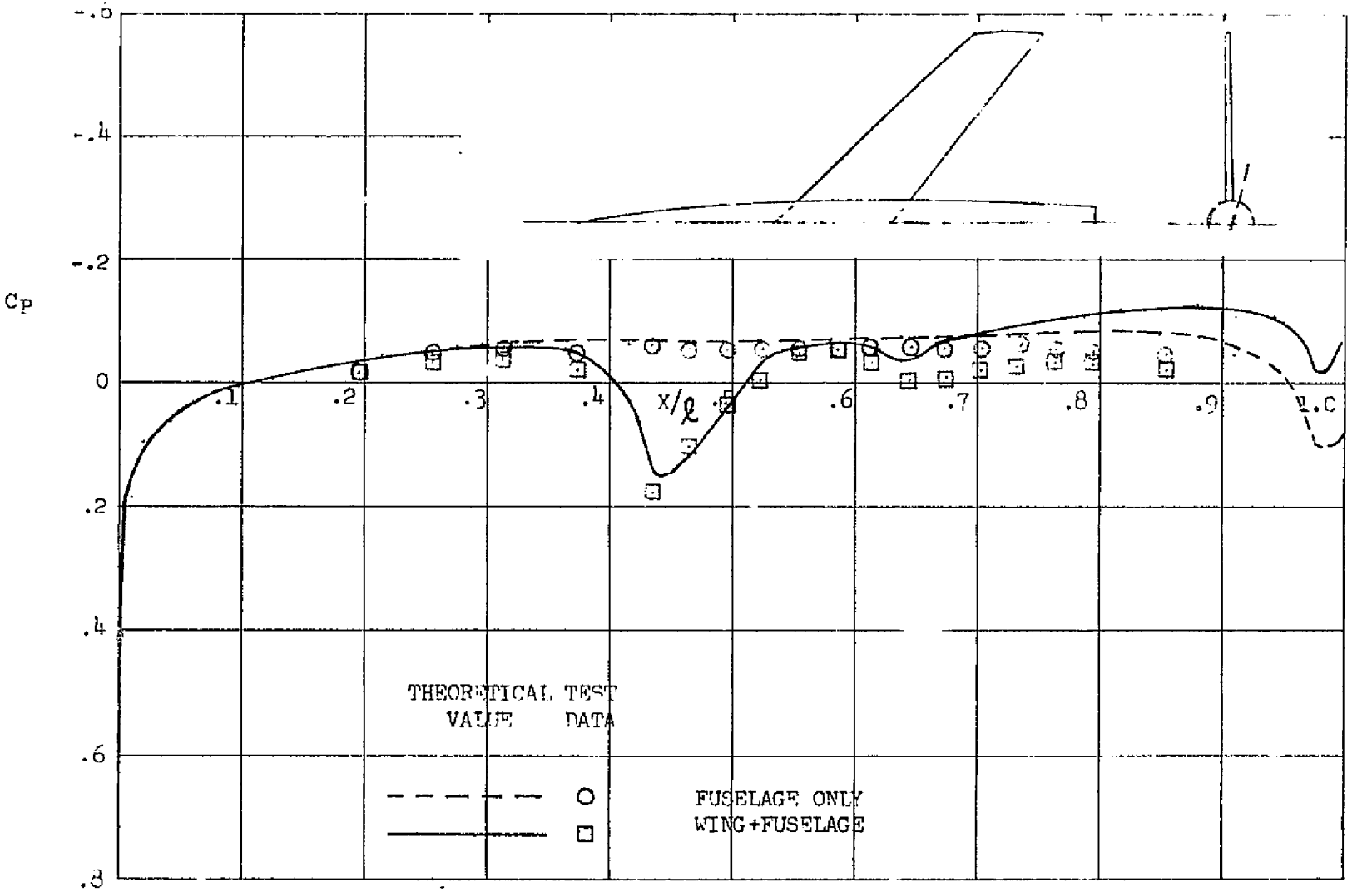

FIGURE 24. CHORDWISE PRESSURE DISTRIBUTION AT THE FUSELAGE 105 DEGREE ROLL STATION. $M_\infty = .6$, $\alpha = 4$ DEGREES

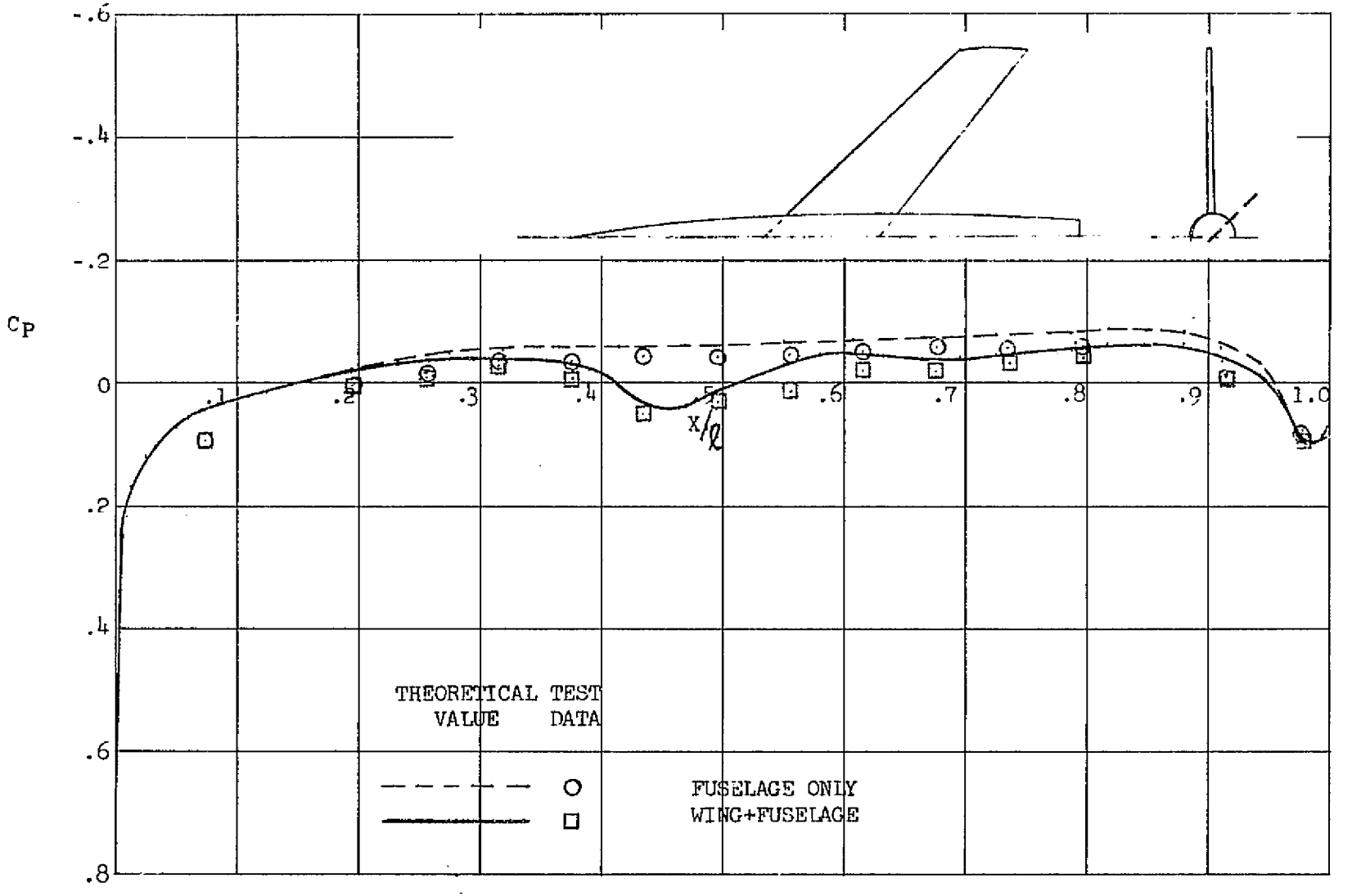

FIGURE 25. CHORDWISE PRESSURE DISTRIBUTION AT THE FUSELAGE 135 DEGREE ROLL STATION. $M_\infty = .6$, $\alpha = 4$ DEGREES

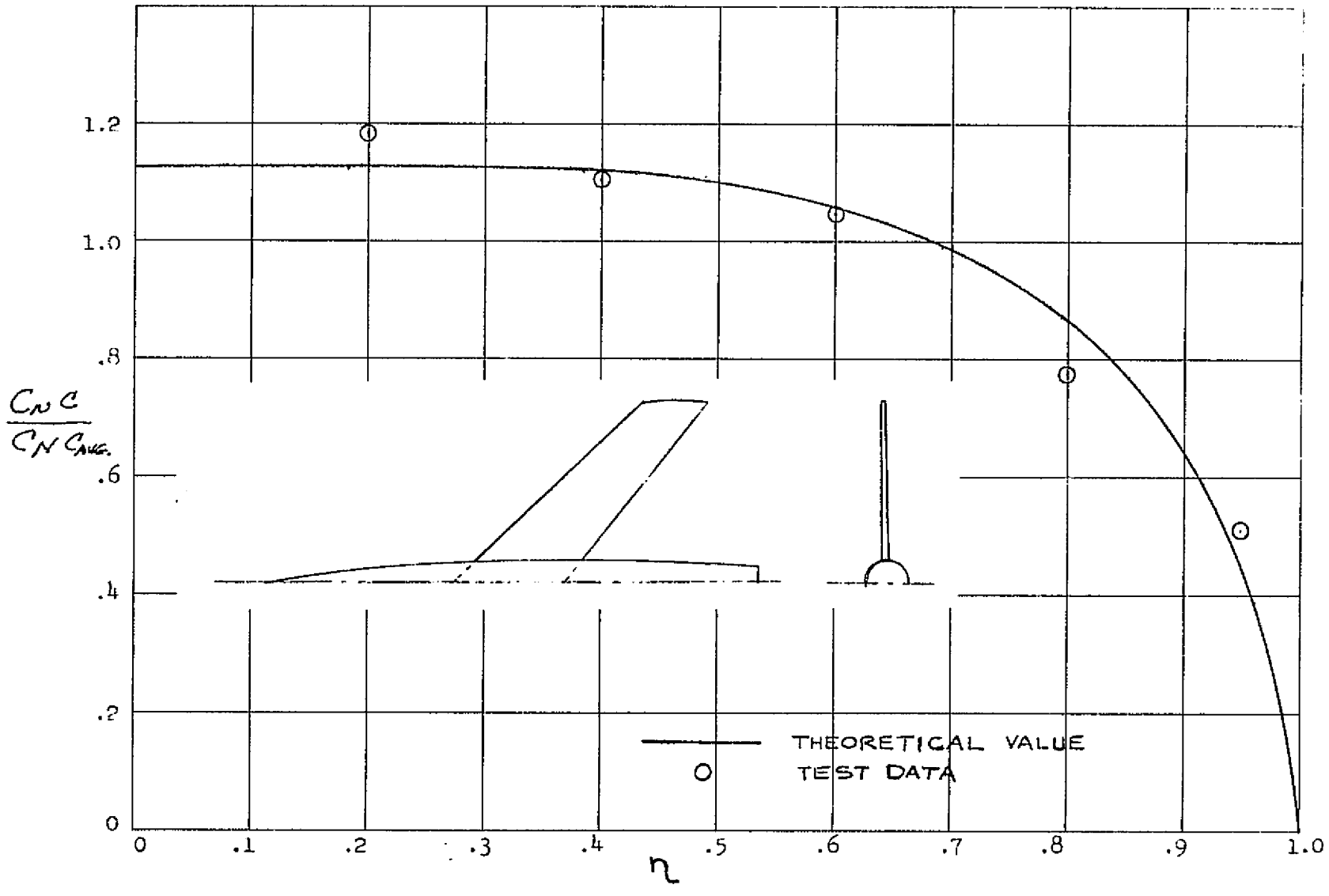

FIGURE 26. WING FUSELAGE SPAN LOAD. $M_\infty = .6$

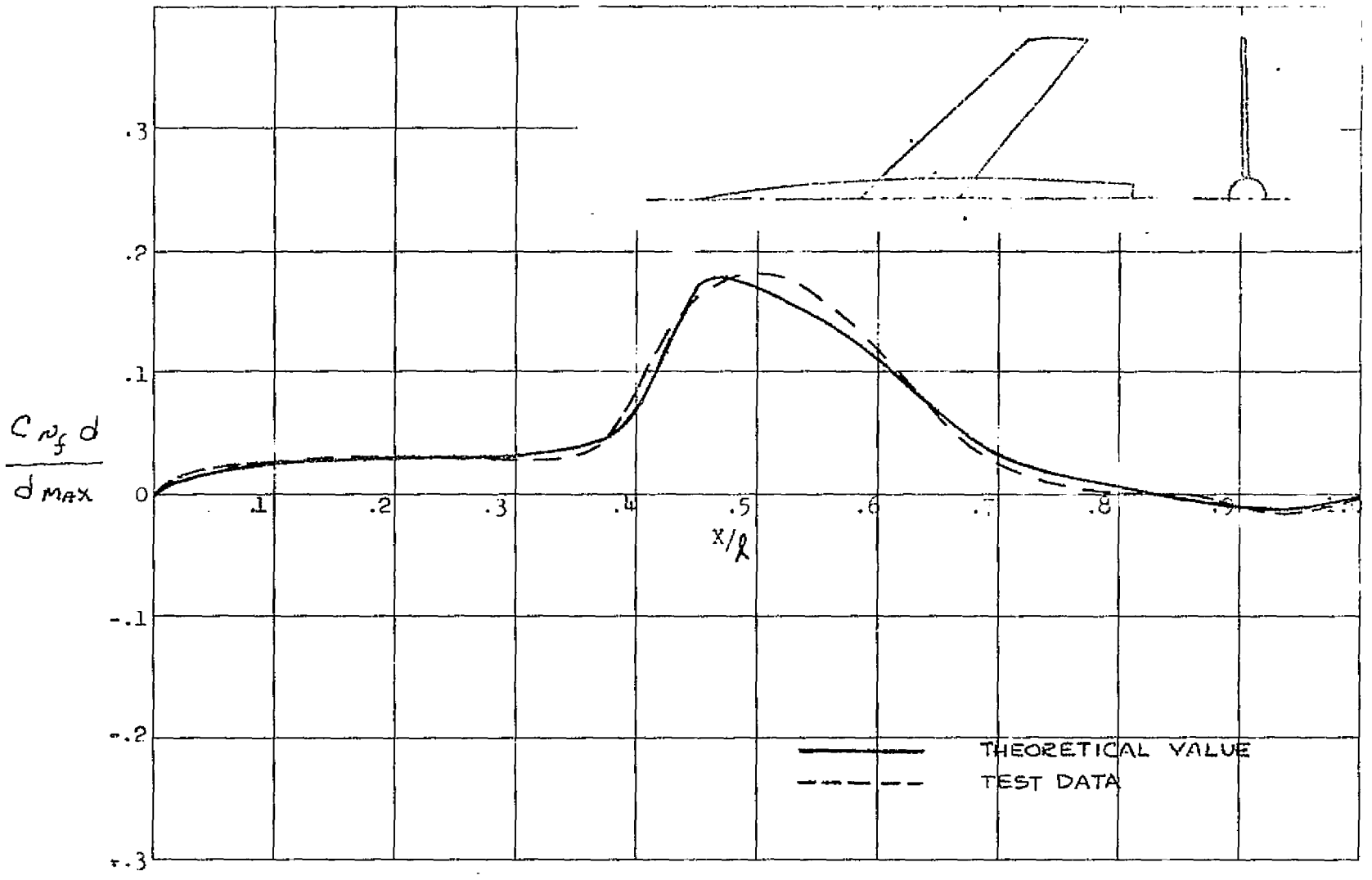

FIGURE 27. LONGITUDINAL LOADING OVER FUSELAGE WITH WING
$M_\infty = .6$, $\alpha = 4$ DEGREES

V/STOL LIFT FAN TRANSPORT

The wing-body and wing-body-fanpod configurations run as Case II are defined in NA-72-17-2.* Comparisons of pressure coefficients at zero and three degrees angle of attack were made for the wing-body, the wing-body-fanpod, and the difference between the wing-body-fanpod and the wing-body.

Figures 28 through 32 show comparisons between data and the program at the 20, 33, 60, 75, and 95 percent semi-span wing stations, at zero degrees angle of attack, for the wing-body configuration. Figures 33 through 37 show analogous comparisons for the three degree angle of attack case.

Figures 38 through 42 and figures 43 through 47 show comparisons between data and the program at the 20, 33, 60, 75, and 95 percent semi-span wing stations for the wing-fuselage-fanpod configuration at zero and three degrees angle of attack, respectively. The 33 and 60 percent semi-span wing stations are just inboard and outboard of the fanpod, respectively.

The comparisons for the upper surface are quite improved over that for the previous program. However, the lower surface comparisons are still not in very good agreement. This difference could be due to either thickness effects of a high wing configuration, which can only be properly accounted for by a surface singularity approach, or due to a wing-fuselage juncture interference problem in the analysis. It is believed to be the former of these two situations, because the problem does not occur in Case I which is a mid-wing configuration.

The increments in the wing pressures due to the fanpod are shown in figures 48 through 52 for the zero degree angle of attack case and in figures 53 through 57 for the three degree angle of attack case. These comparisons are not as good as expected. The three degree angle of attack case is considerably poorer than the zero degree angle of attack case. Also, the comparisons are worse right at the junctures. Both of these situations could be indicating boundary layer effects, since the boundary layer would be thicker at the higher angle of attack and right in the juncture.

* Reference 36

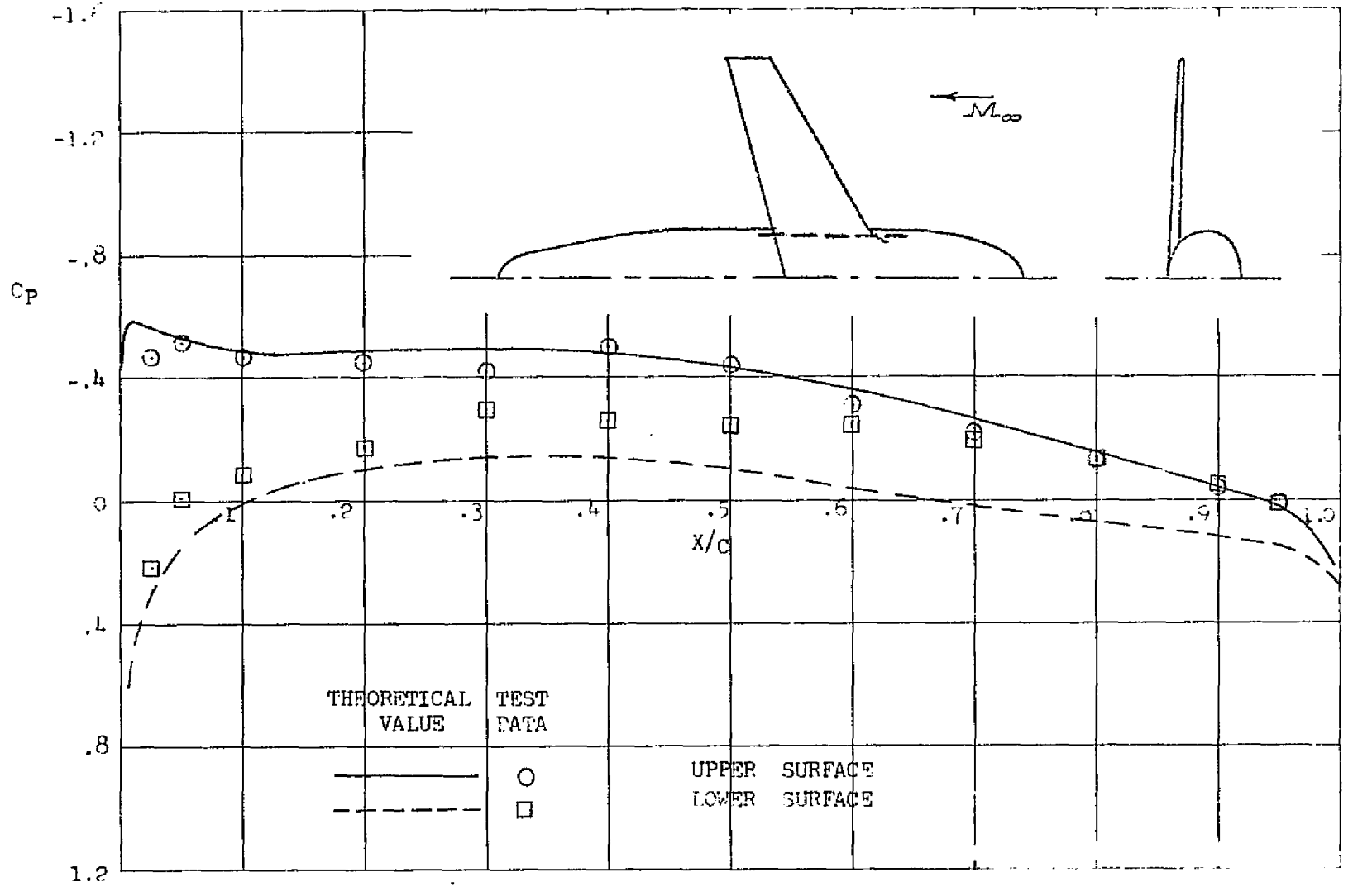

FIGURE 28. CHORDWISE PRESSURE DISTRIBUTION AT THE WING 20 PERCENT SEMI-SPAN STATION. M_∞ = .6, α = 0 DEGREES

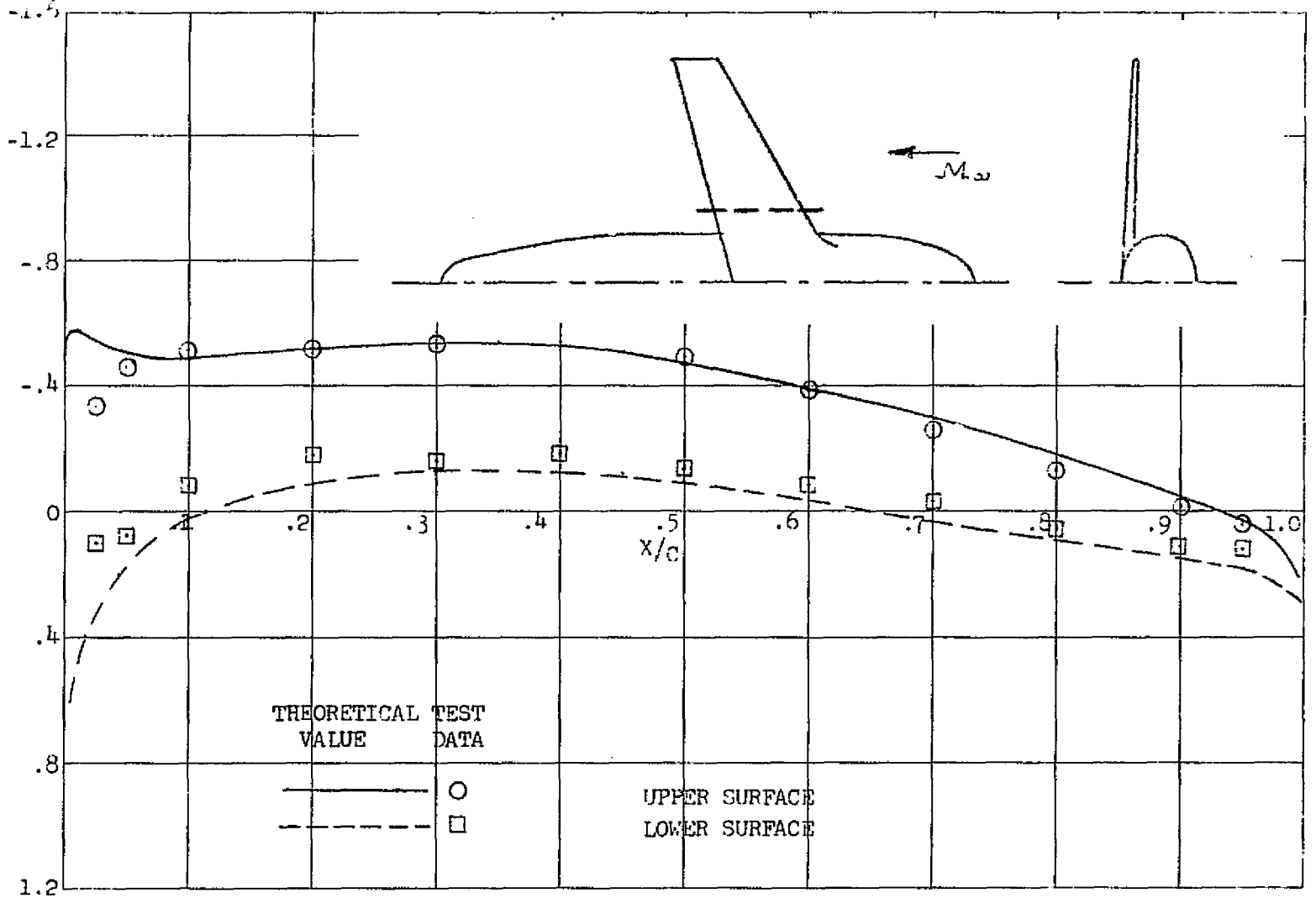

FIGURE 29. CHORDWISE PRESSURE DISTRIBUTION AT THE WING 33 PERCENT SEMI-SPAN STATION. $M_\infty = .6$, $\alpha = 0$ DEGREES

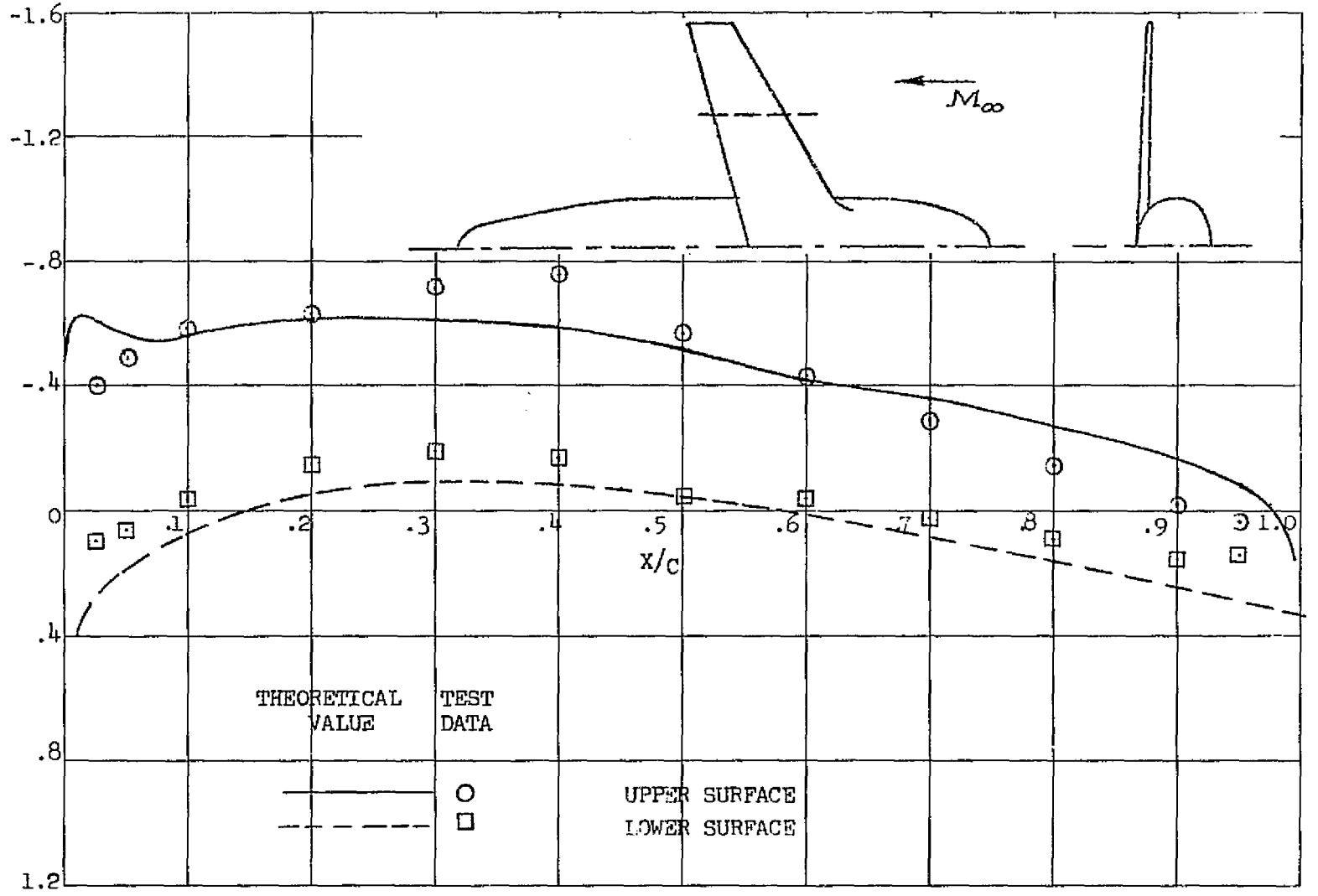

FIGURE 30. CHORDWISE PRESSURE DISTRIBUTION AT THE WING 60 PERCENT SEMI-SPAN STATION. M_∞ = .6, α = 0 DEGREES

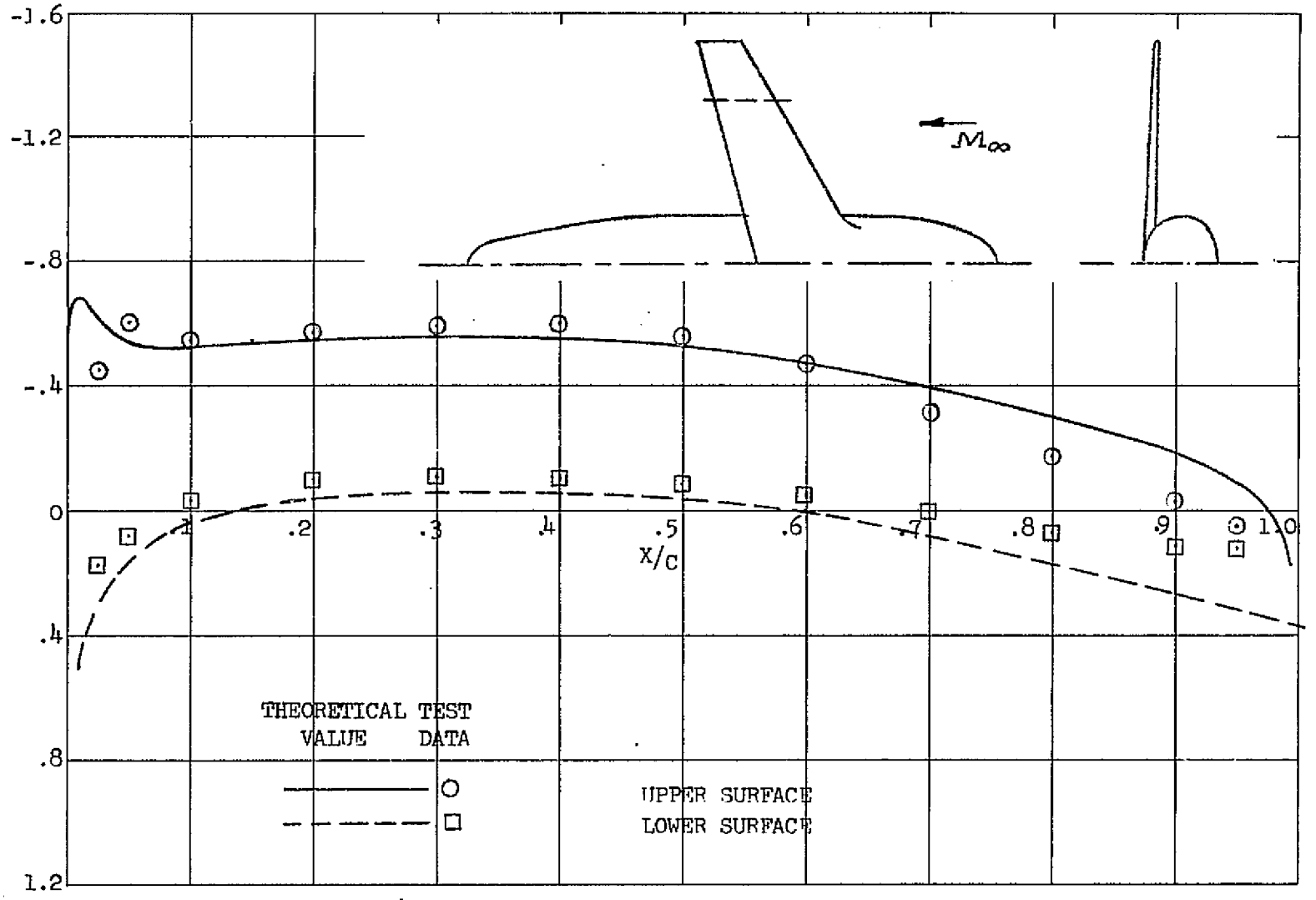

FIGURE 31. CHORDWISE PRESSURE DISTRIBUTION AT THE WING 75 PERCENT SEMI-SPAN STATION. $M_\infty = .6$, $\alpha = 0$ DEGREES

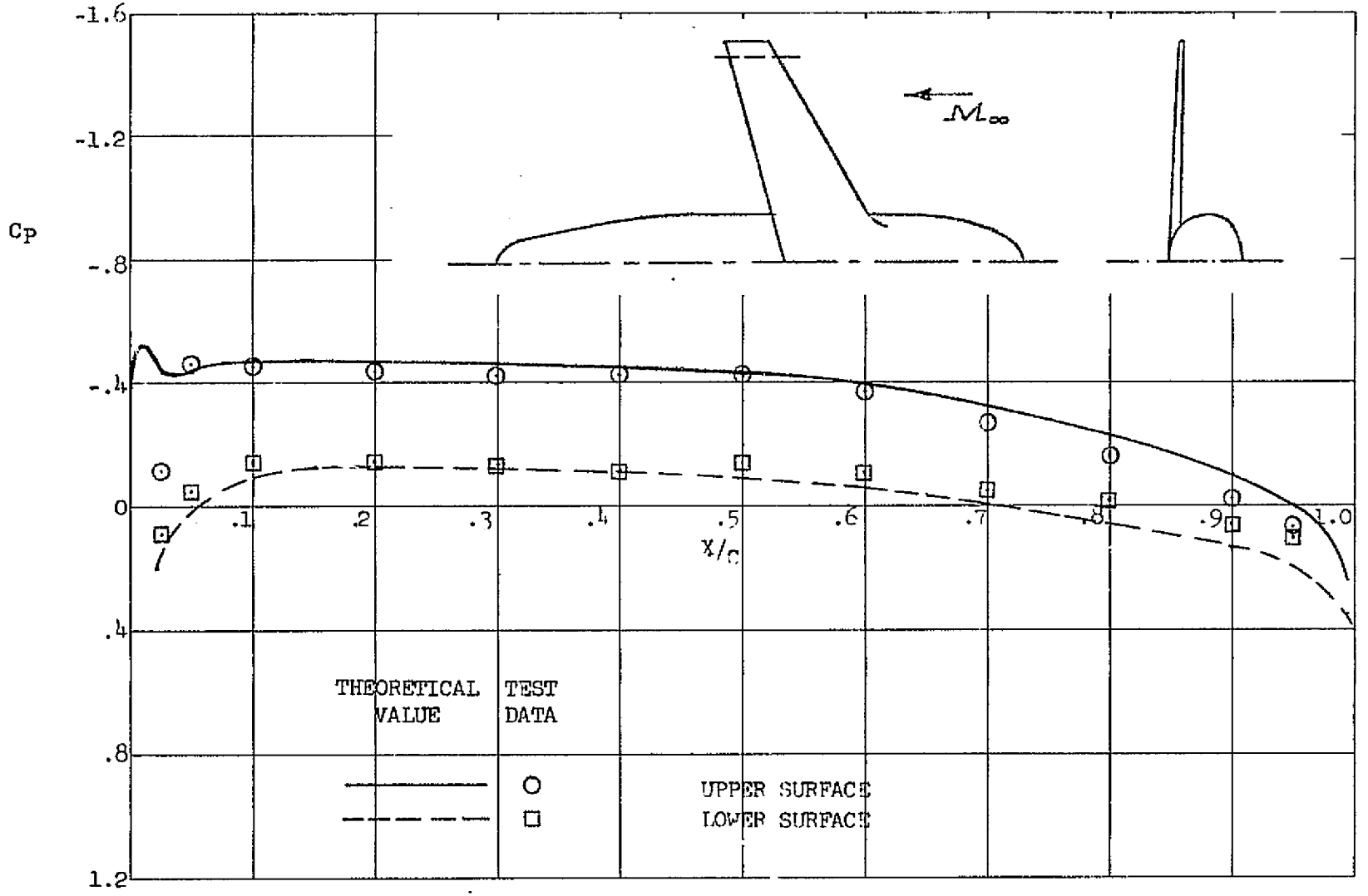

FIGURE 32. CHORDWISE PRESSURE DISTRIBUTION AT THE WING 95 PERCENT SEMI-SPAN STATION. $M_\infty = .6$, $\alpha = 0$ DEGREES

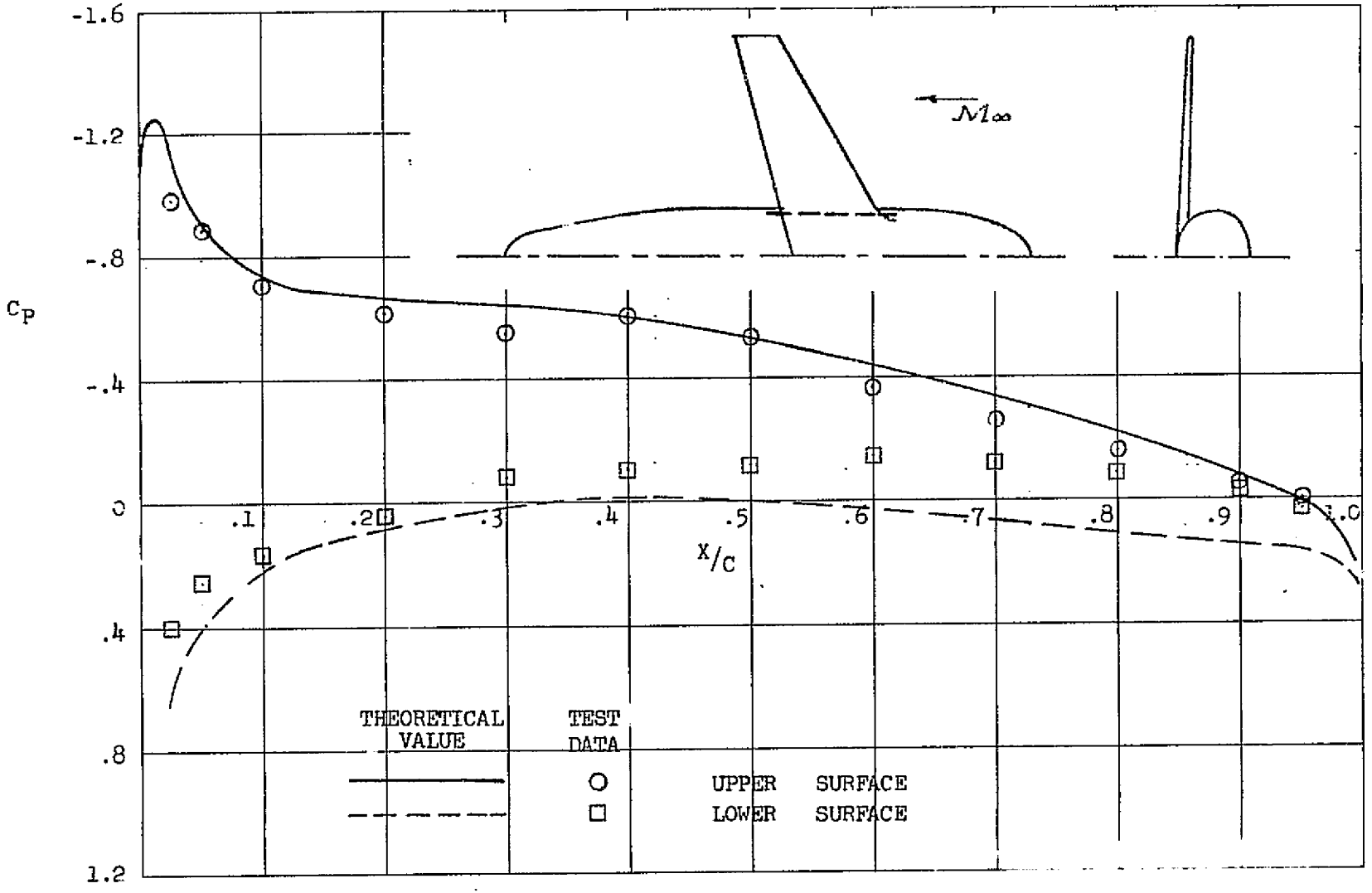

FIGURE 33. CHORDWISE PRESSURE DISTRIBUTION AT THE WING 20 PERCENT SEMI-SPAN STATION. $M_\infty = .6$, $\alpha = 3$ DEGREES

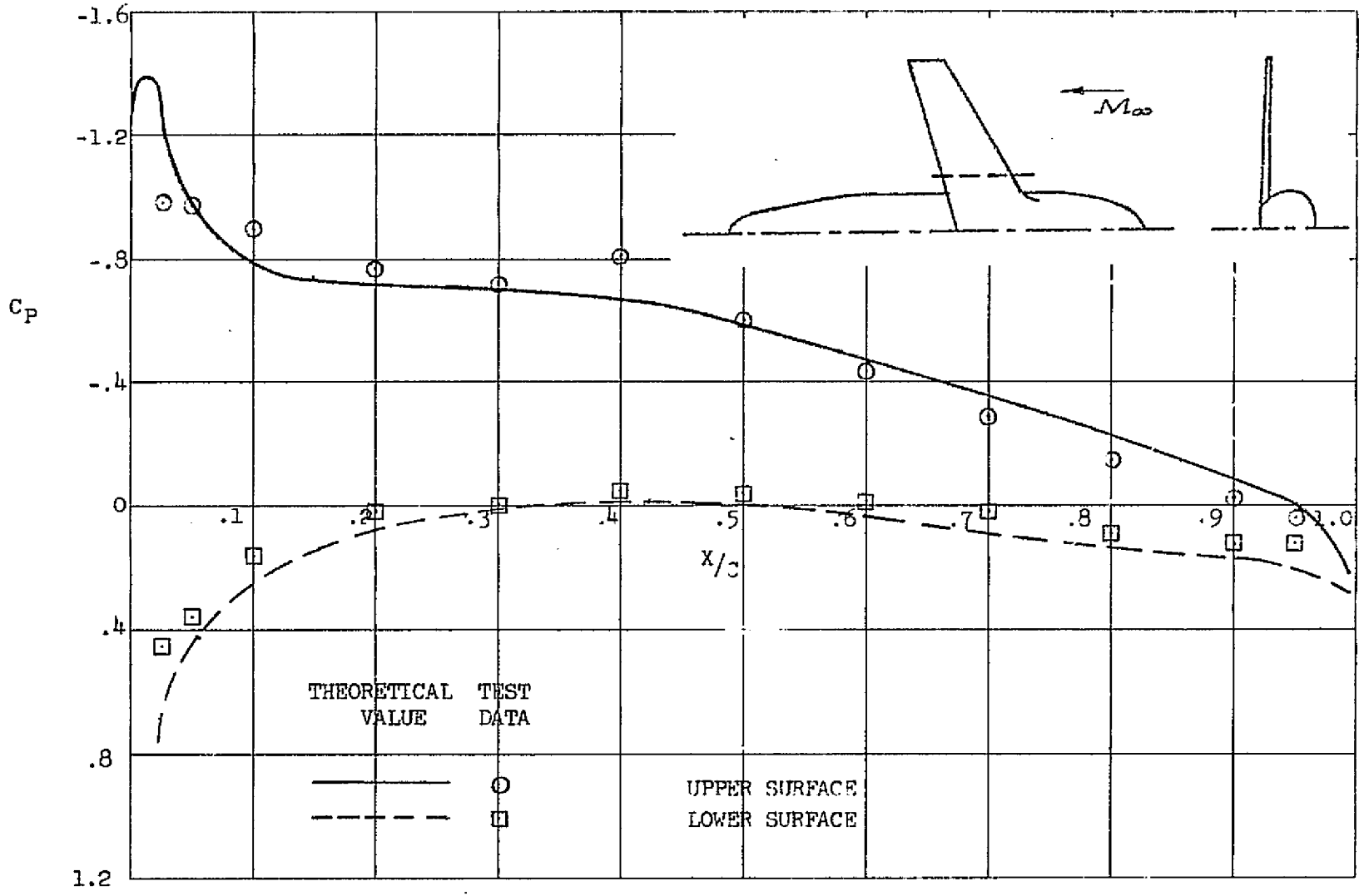

FIGURE 34. CHORDWISE PRESSURE DISTRIBUTION AT THE WING 33 PERCENT SEMI-SPAN STATION. $M_\infty = .6$, $\alpha = 3$ DEGREES

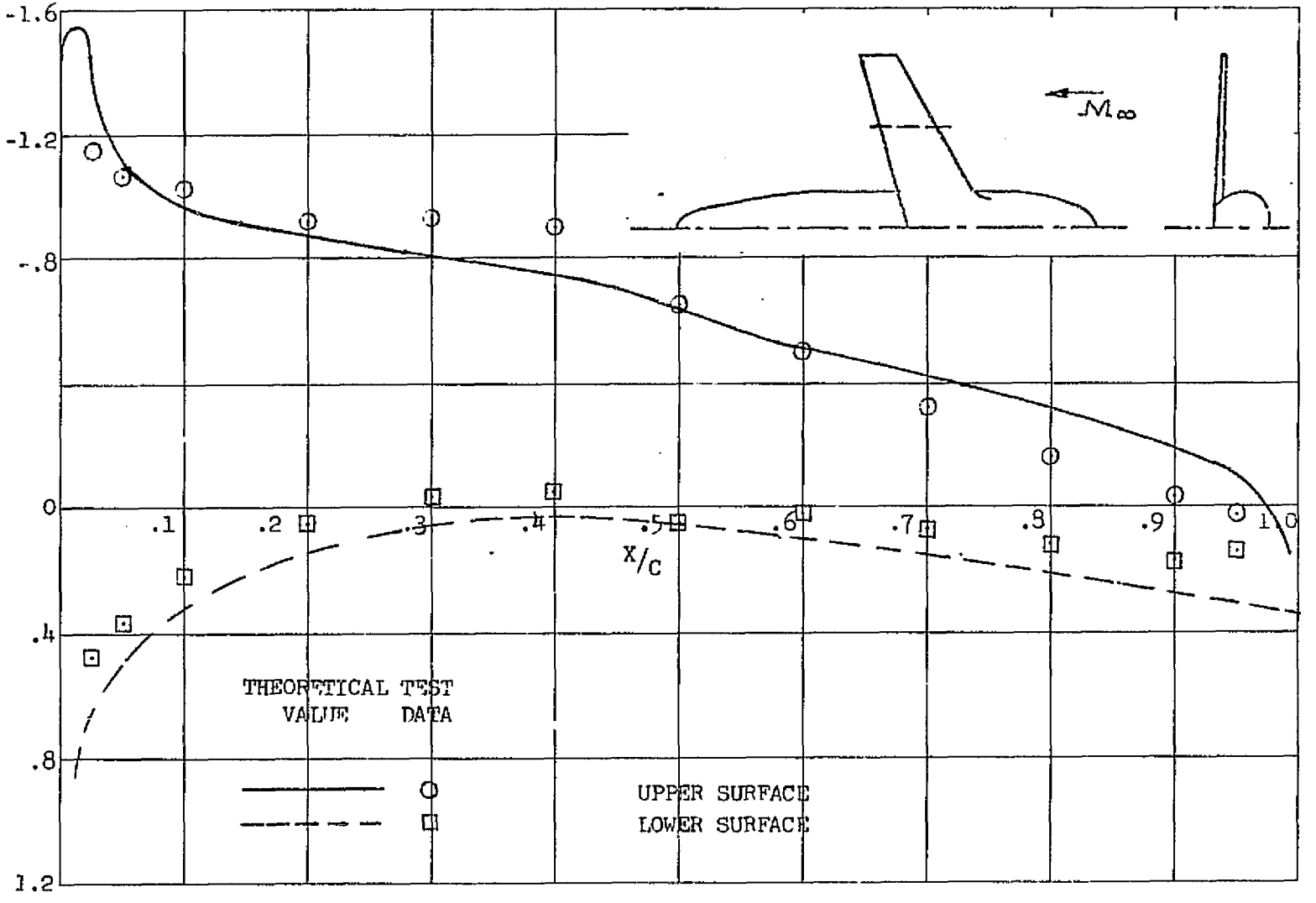

FIGURE 35. CHORDWISE PRESSURE DISTRIBUTION AT THE WING 60 PERCENT SEMI-SPAN STATION. $M_\infty = .6$, $\alpha = 3$ DEGREES

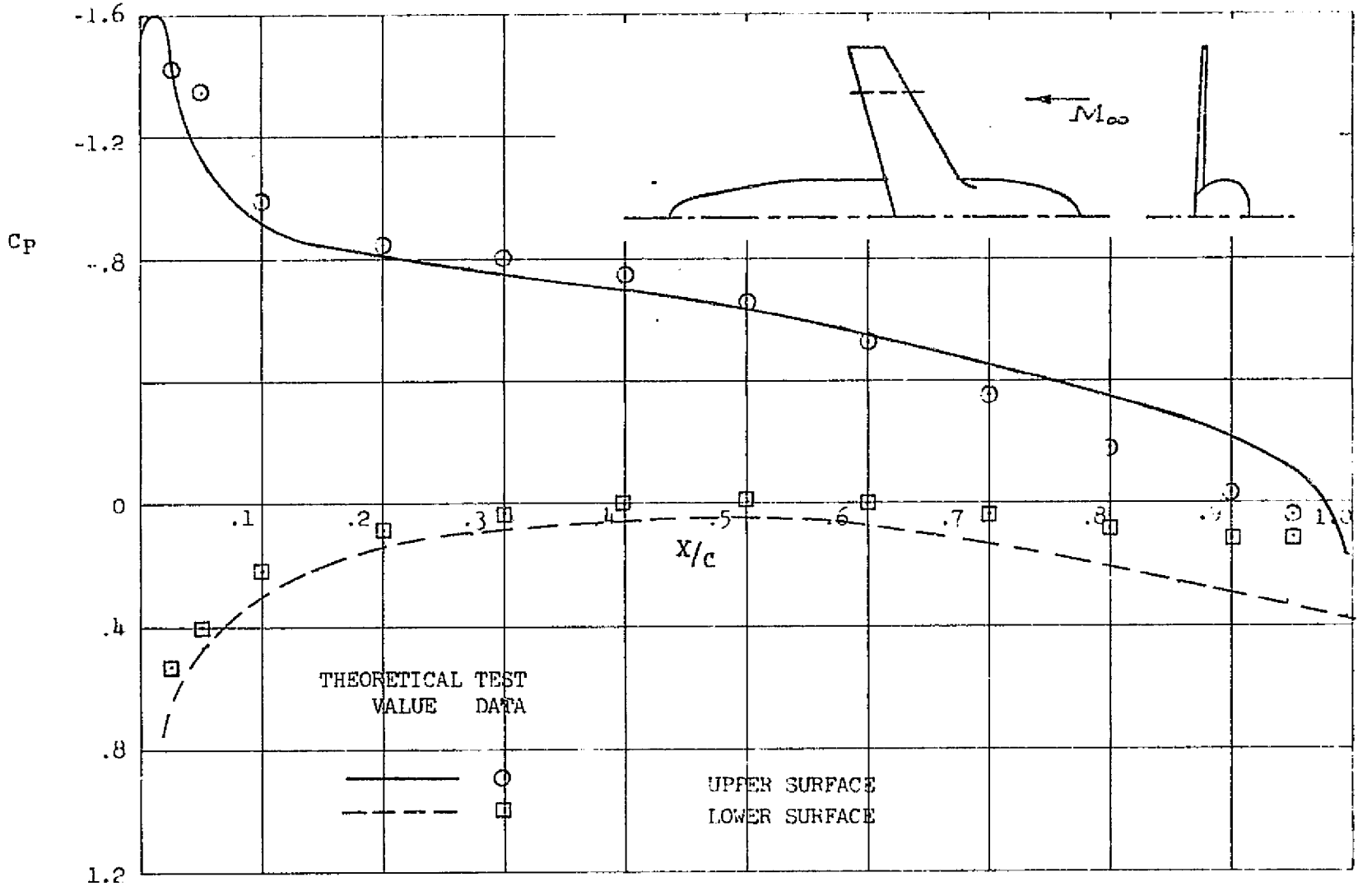

FIGURE 36. CHORDWISE PRESSURE DISTRIBUTION AT THE WING 75 PERCENT SEMI-SPAN STATION. $M_\infty = .6$, $\alpha = 3$ DEGREES

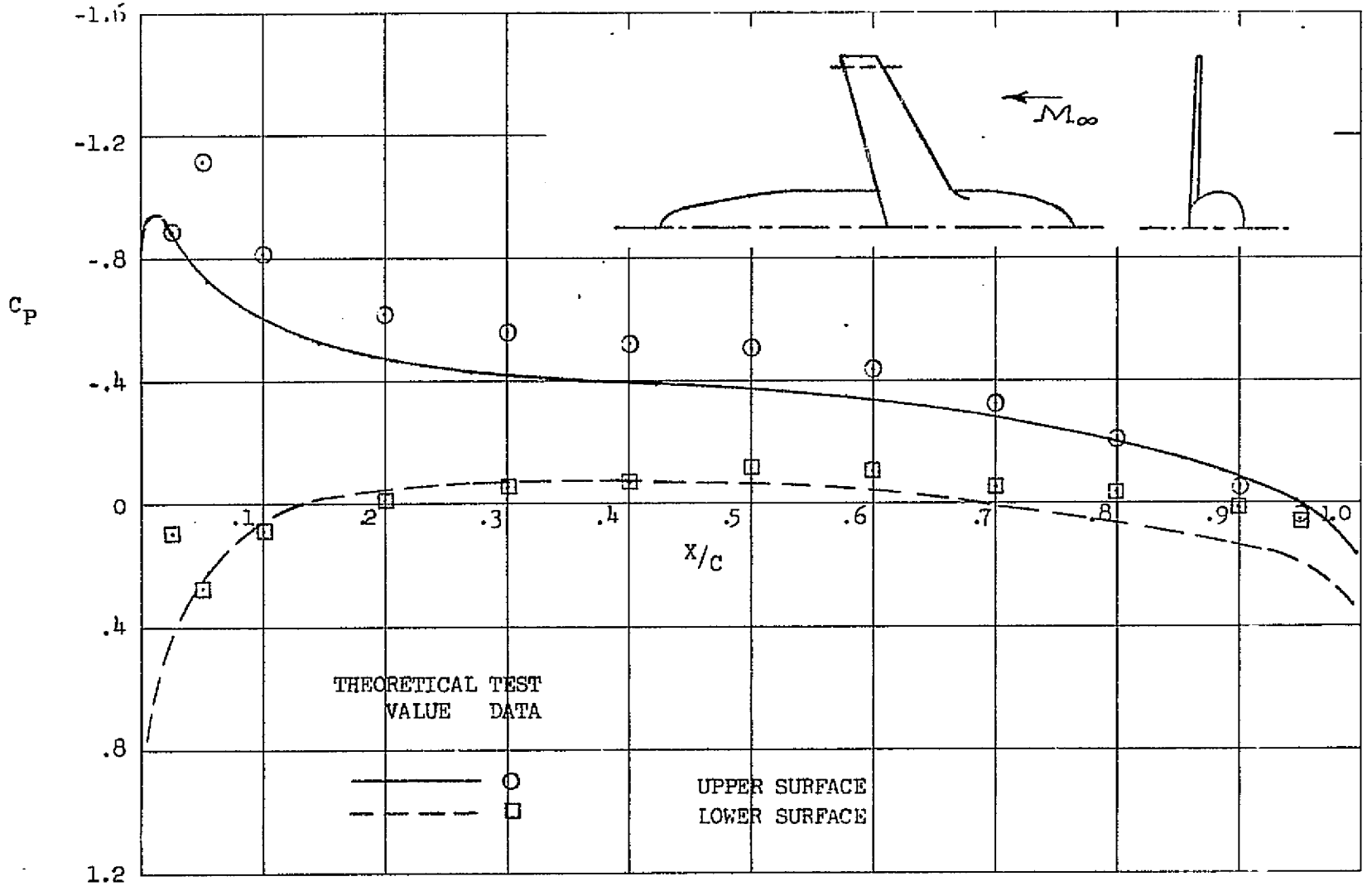

FIGURE 37. CHORDWISE PRESSURE DISTRIBUTION AT THE WING 95 PERCENT SEMI-SPAN STATION. $M_\infty = .6$, $\alpha = 3$ DEGREES

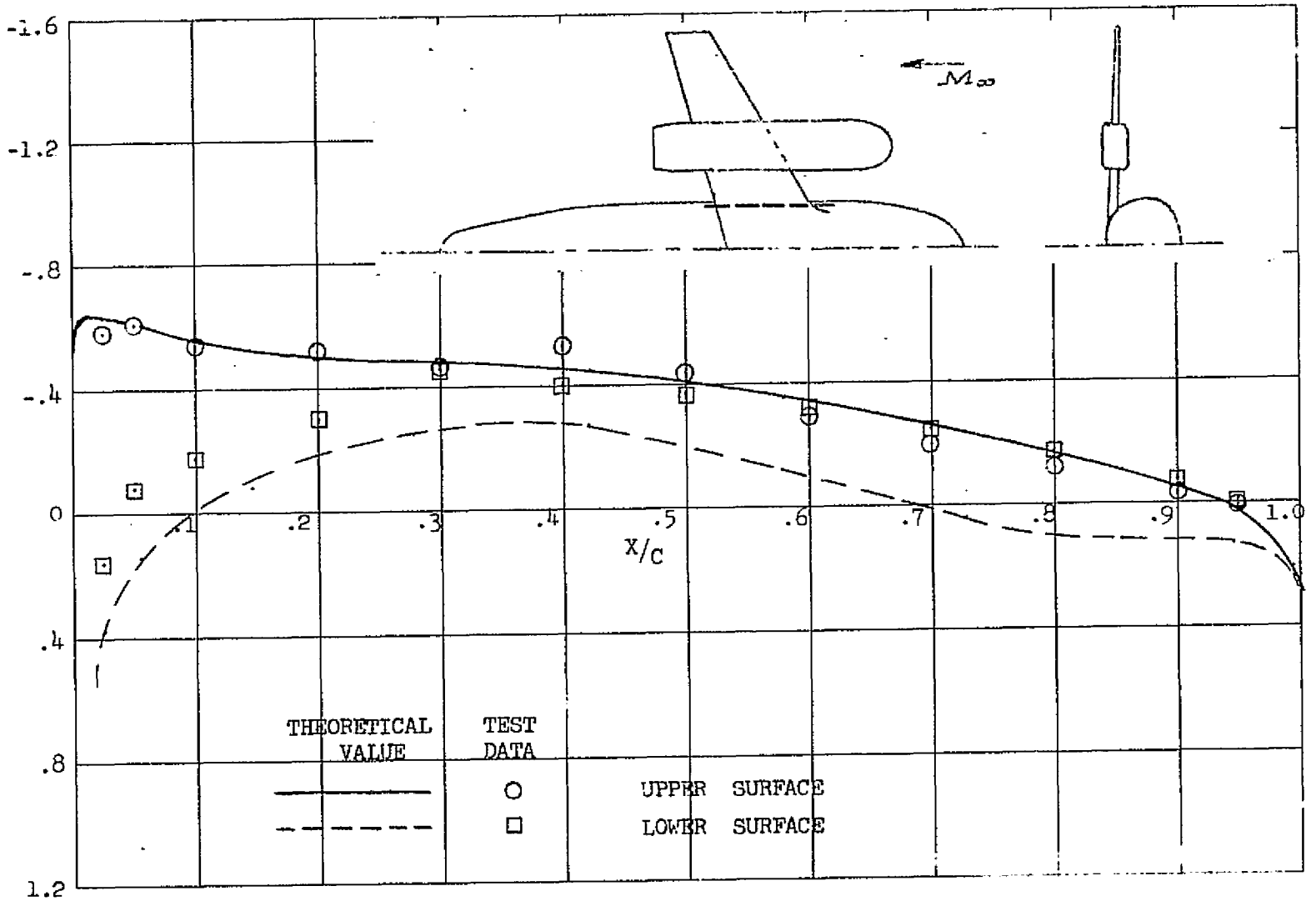

FIGURE 38. CHORDWISE PRESSURE DISTRIBUTION AT THE WING 20 PERCENT SEMI-SPAN STATION. $M_\infty = .6$, $\alpha = 0$ DEGREES

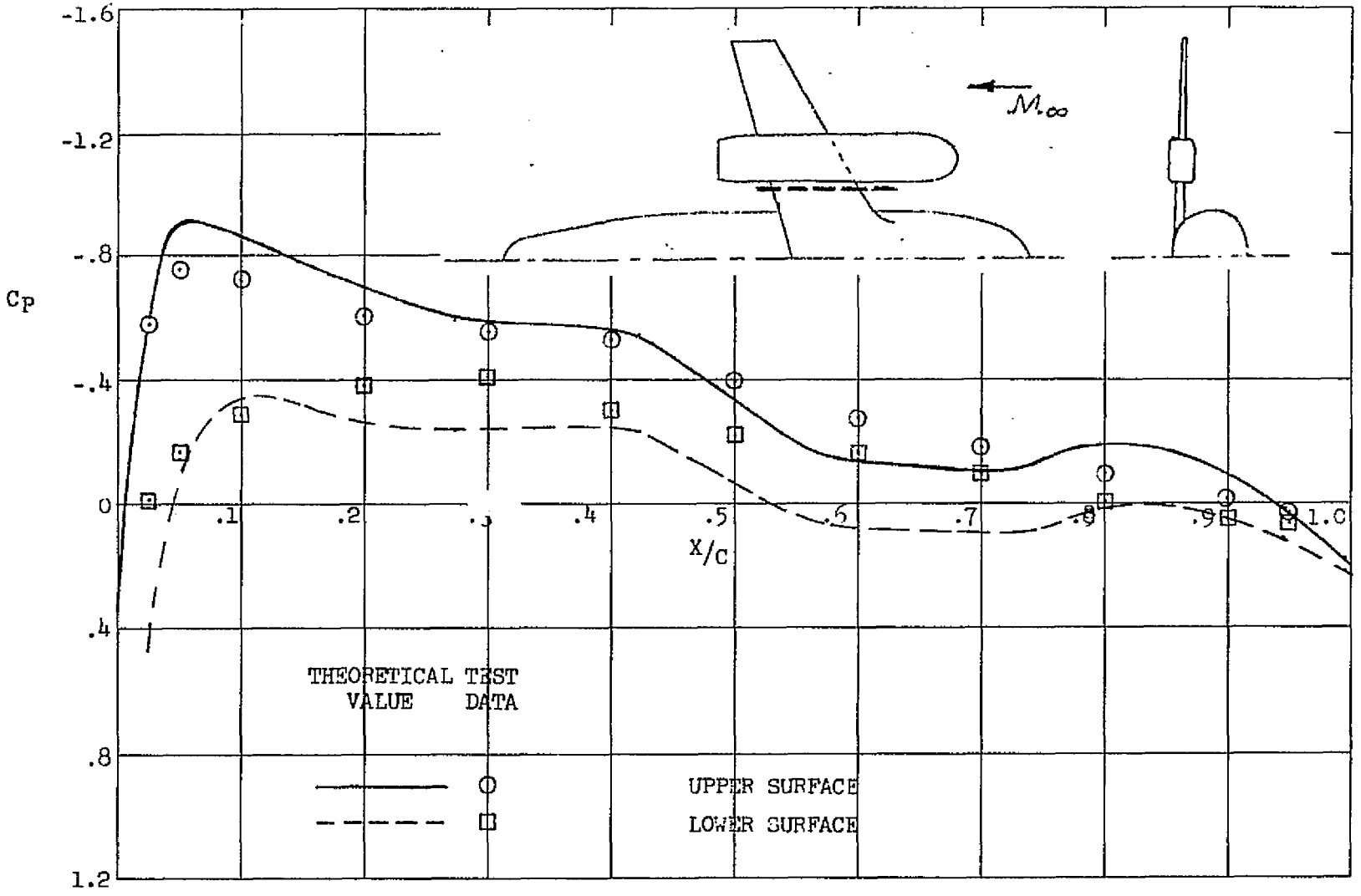

FIGURE 39. CHORDWISE PRESSURE DISTRIBUTION AT THE WING 33 PERCENT SEMI-SPAN STATION. M_∞ = .6, α = 0 DEGREES

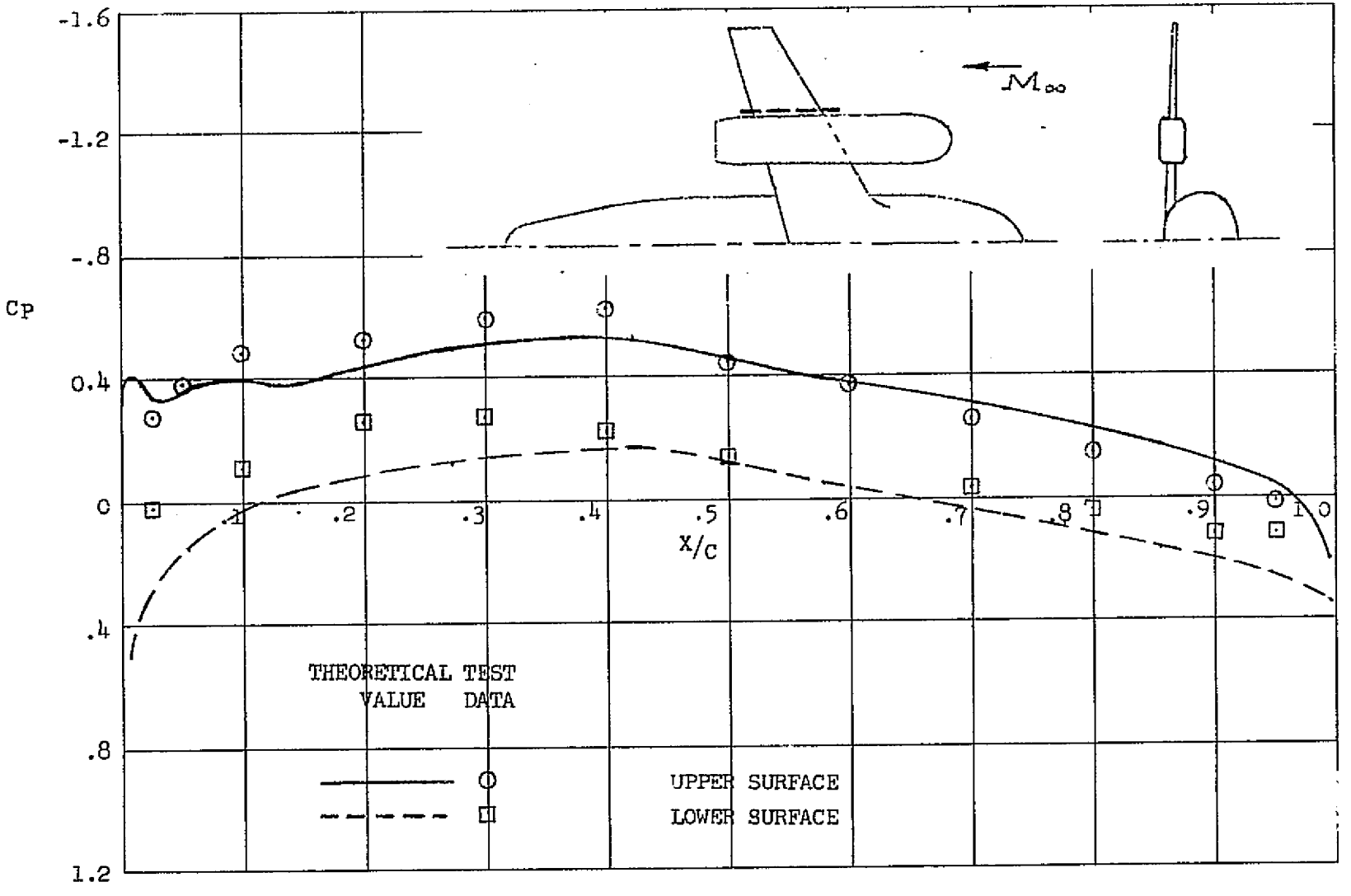

FIGURE 40. CHORDWISE PRESSURE DISTRIBUTION AT THE WING 60 PERCENT SEMI-SPAN STATION. $M_\infty = .6$, $\alpha = 0$ DEGREES

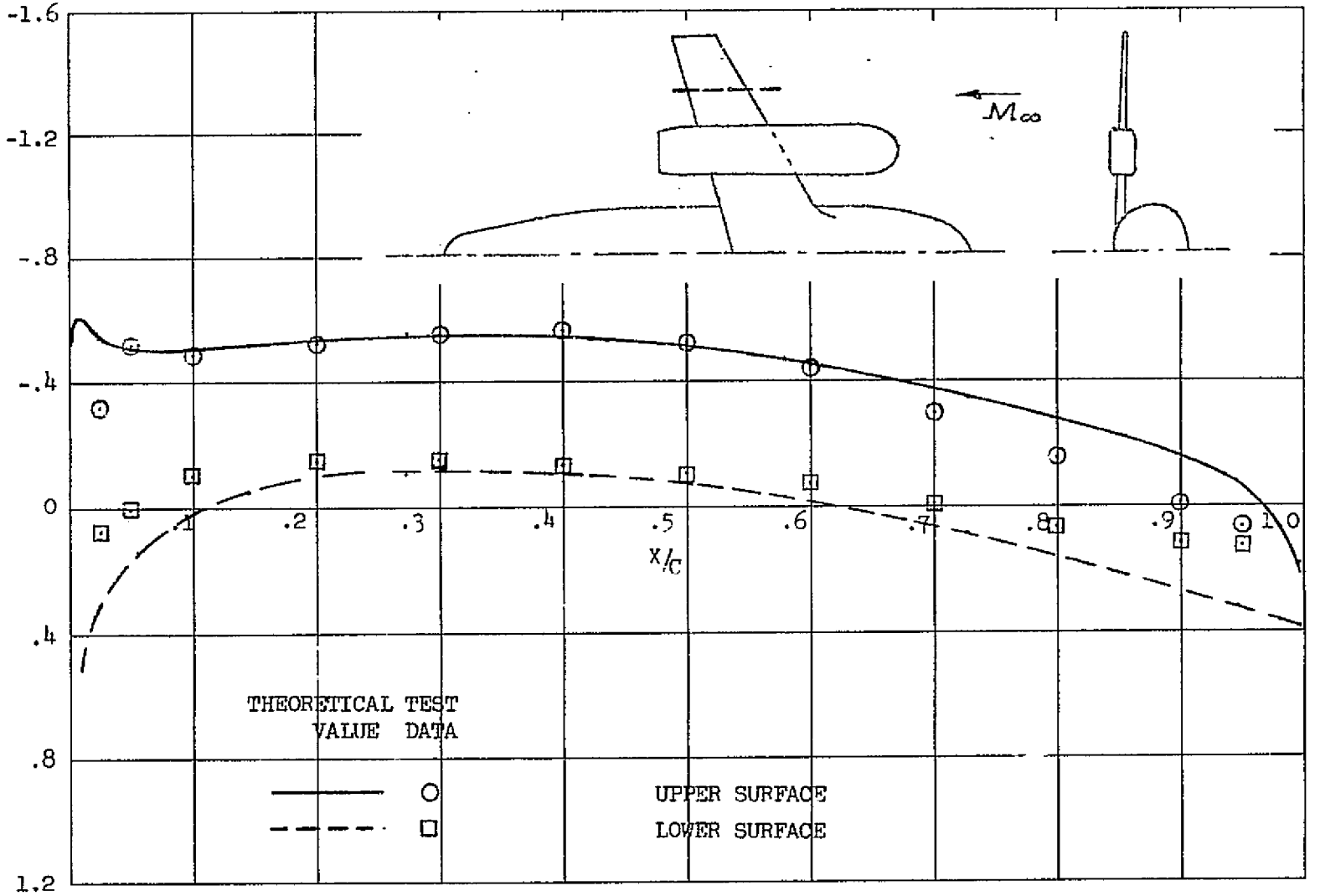

FIGURE 41. CHORDWISE PRESSURE DISTRIBUTION AT THE WING 75 PERCENT SEMI-SPAN STATION. $M_\infty = .6$, $\alpha = 0$ DEGREES

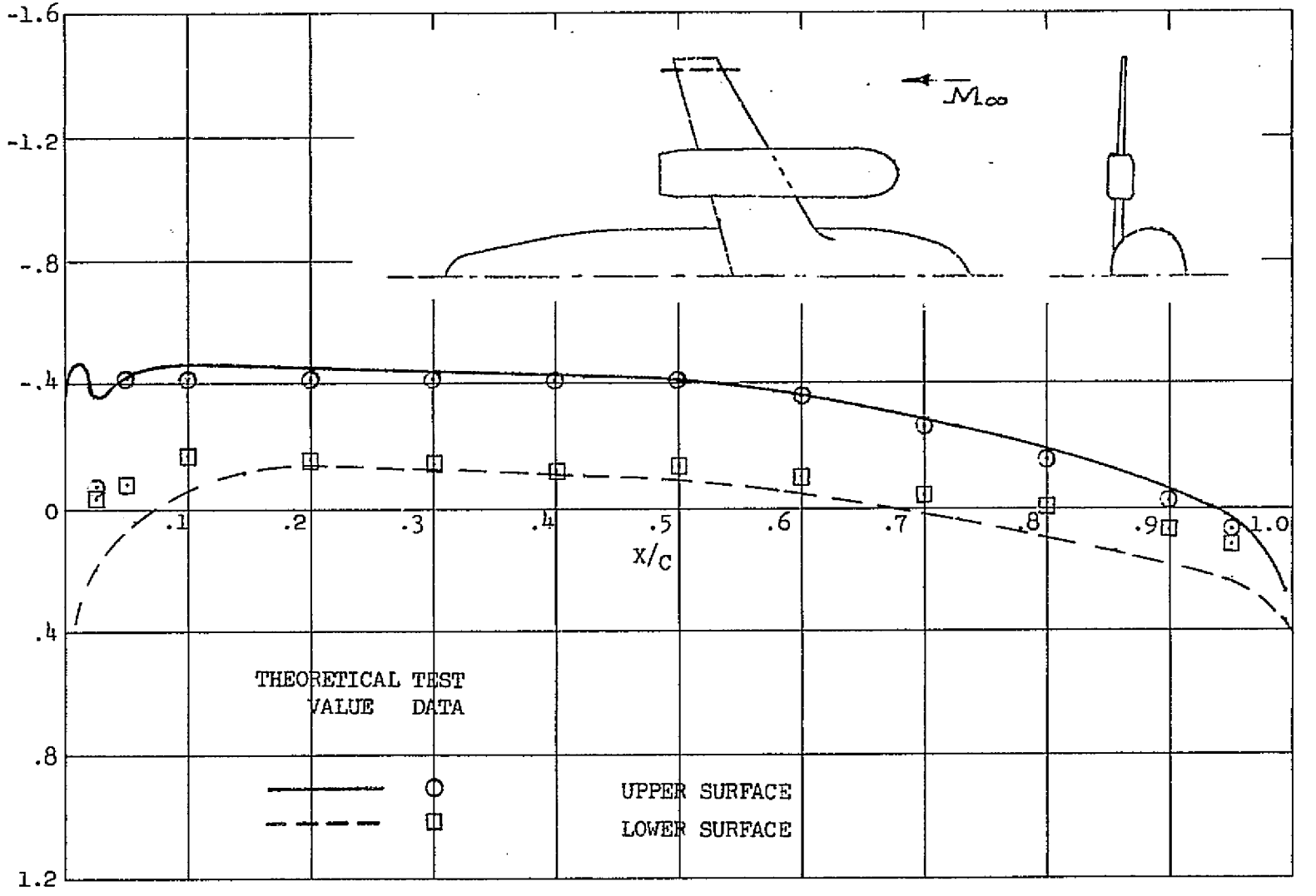

FIGURE 42. CHORDWISE PRESSURE DISTRIBUTION AT THE WING 95 PERCENT SEMI-SPAN STATION. $M_\infty = .6$, $\alpha = 3$ DEGREES

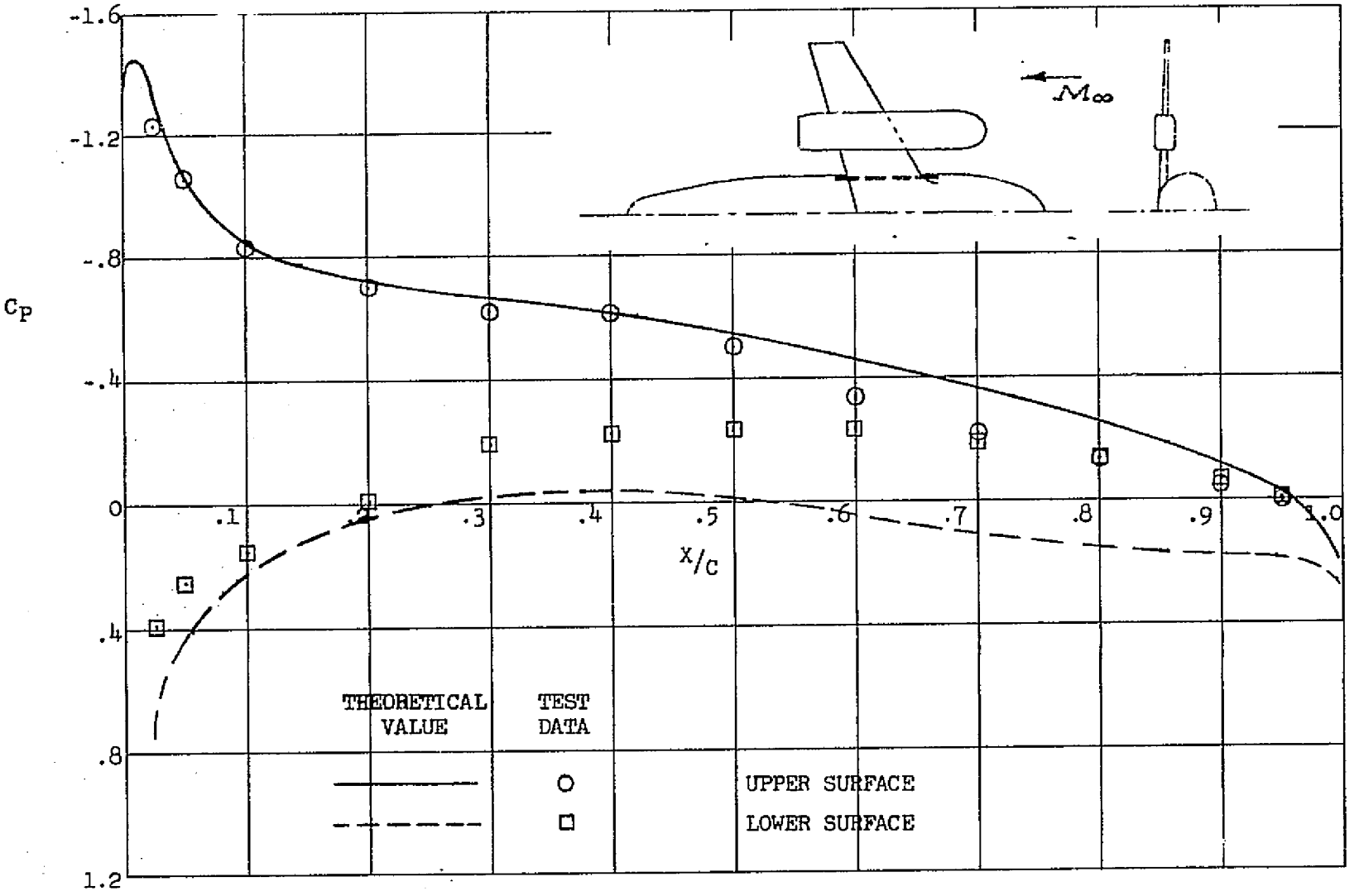

FIGURE 43. CHORDWISE PRESSURE DISTRIBUTION AT THE WING 20 PERCENT SEMI-SPAN STATION. $M_\infty = .6$, $\alpha = 3$ DEGREES

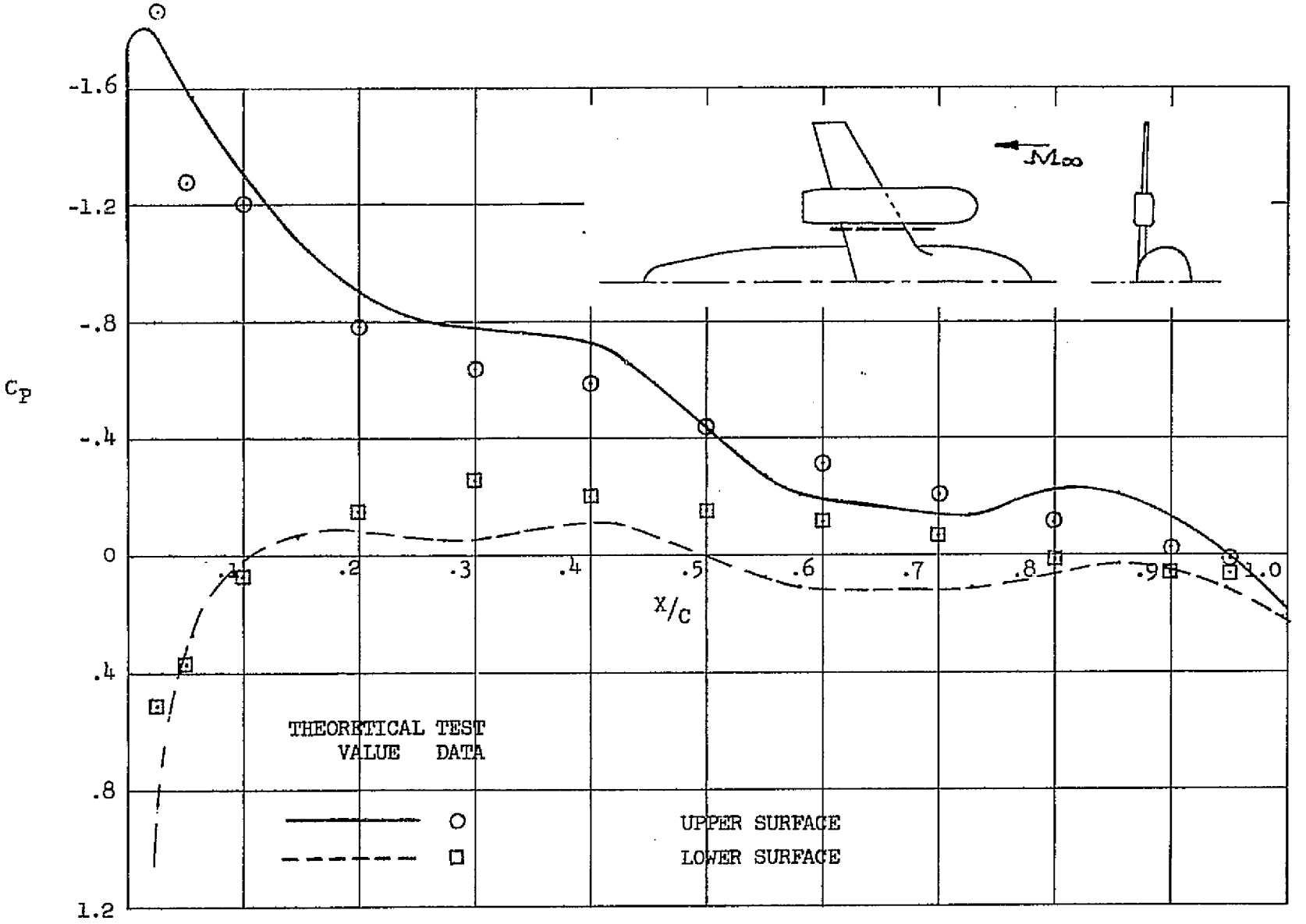

FIGURE 44. CHORDWISE PRESSURE DISTRIBUTION AT THE WING 33 PERCENT SEMI-SPAN STATION. $M_\infty = .6$, $\alpha = 3$ DEGREES

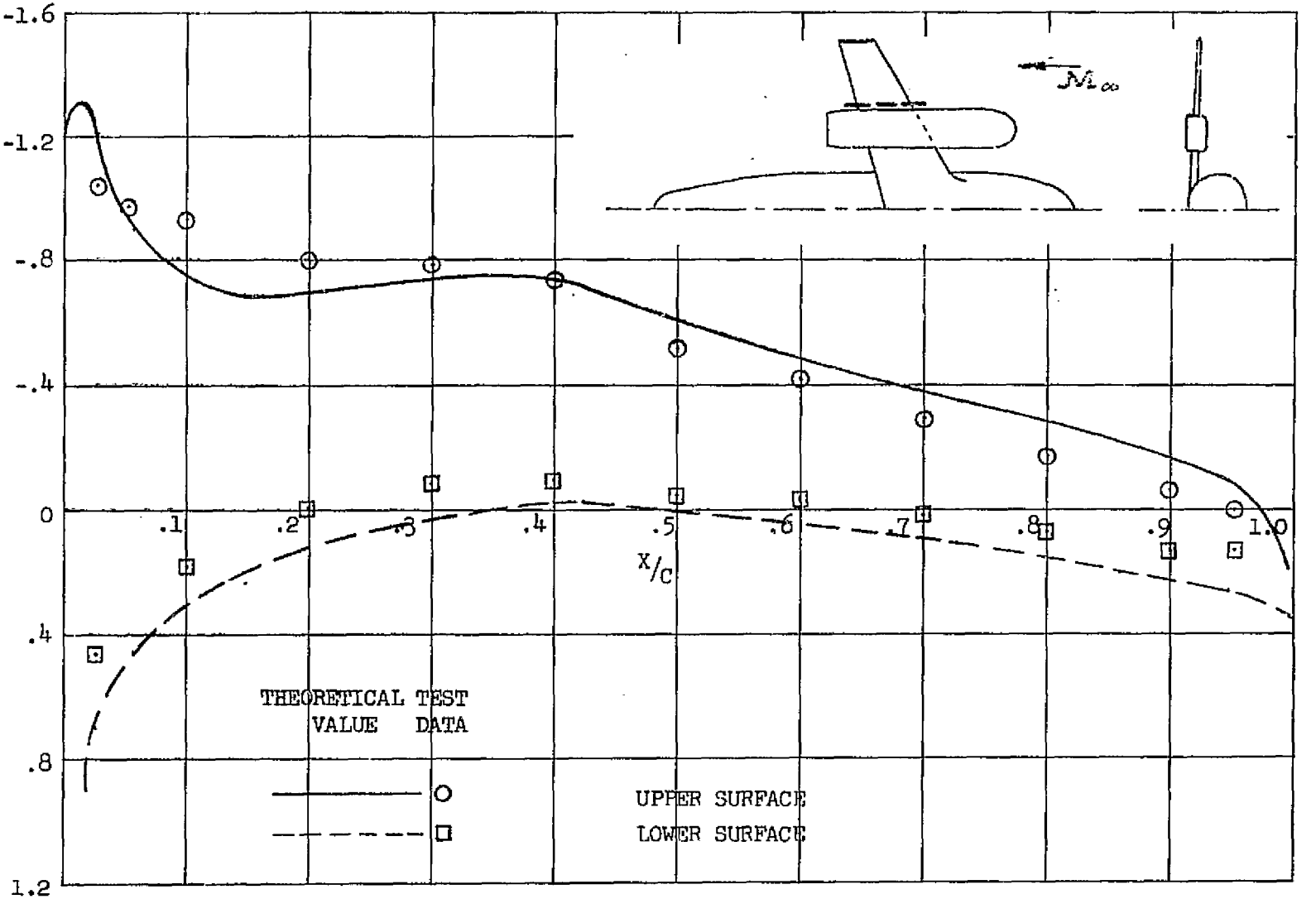

FIGURE 45. CHORDWISE PRESSURE DISTRIBUTION AT THE WING 60 PERCENT SEMI-SPAN STATION. $M_\infty = .6$, $\alpha = 3$ DEGREES

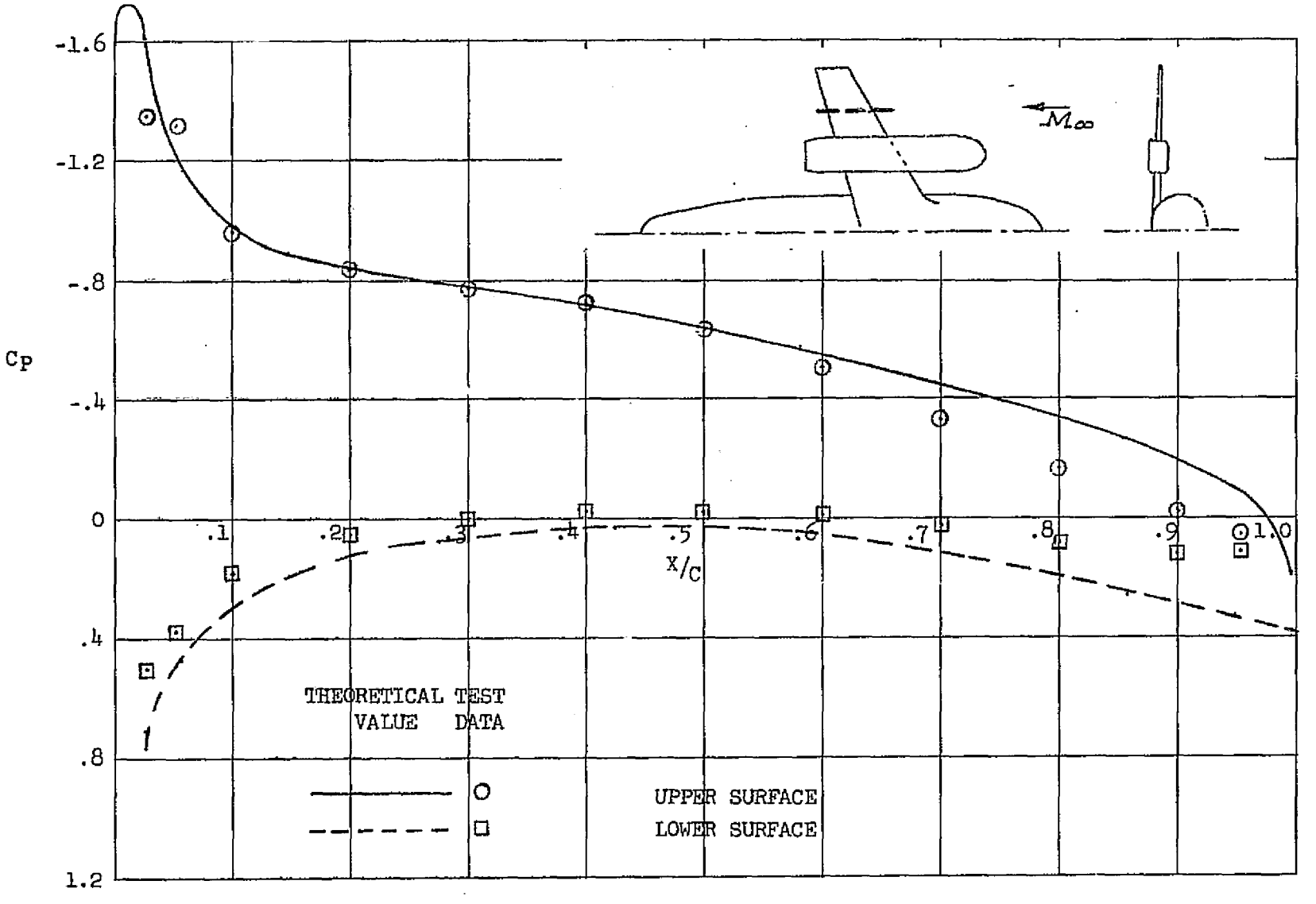

FIGURE 46. CHORDWISE PRESSURE DISTRIBUTION AT THE WING 75 PERCENT SEMI-SPAN STATION. $M_\infty = .6$, $\alpha = 3$ DEGREES

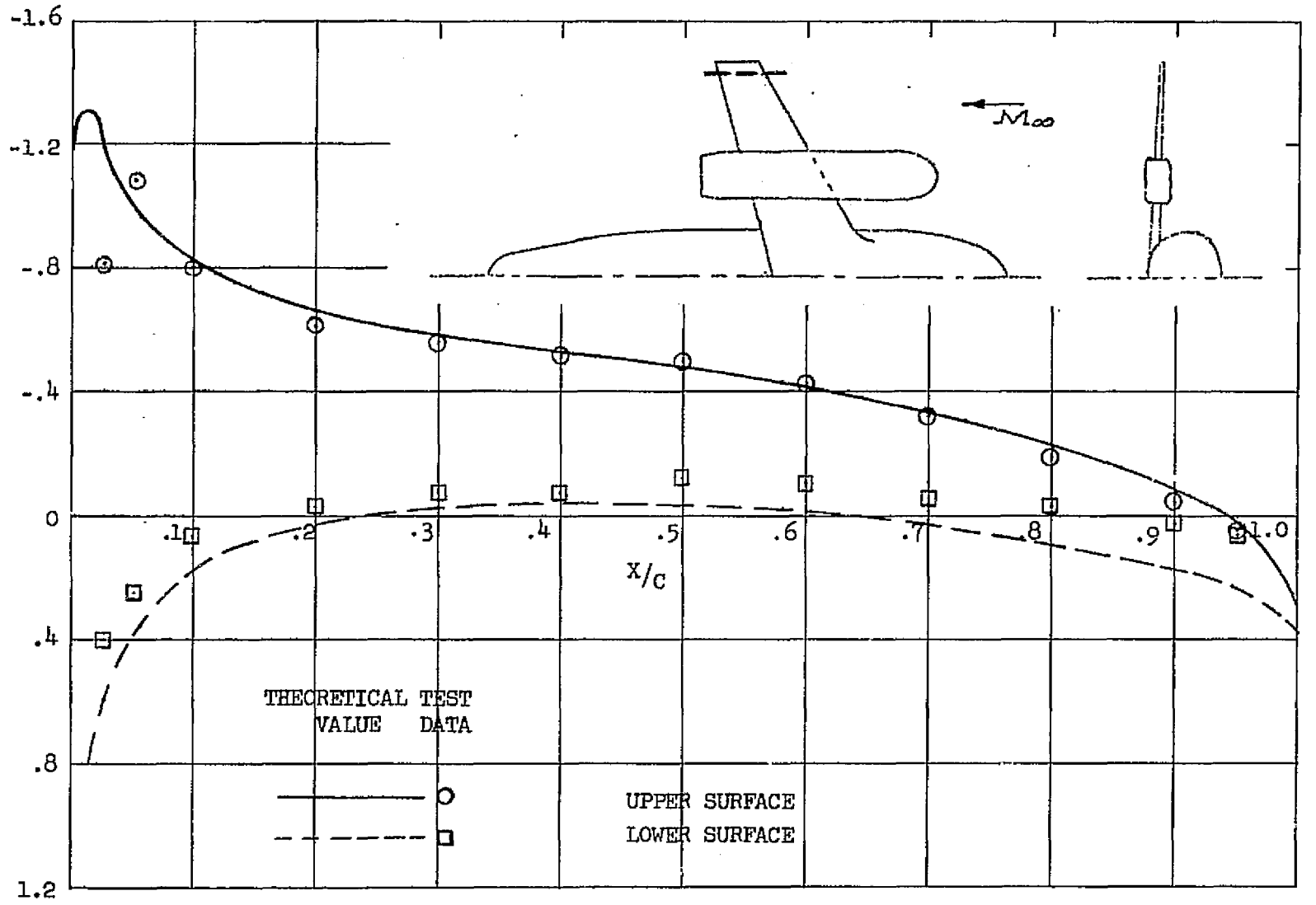

FIGURE 47. CHORDWISE PRESSURE DISTRIBUTION AT THE WING 95 PERCENT SEMI-SPAN STATION. $M_\infty = .6$, $\alpha = 3$ DEGREES

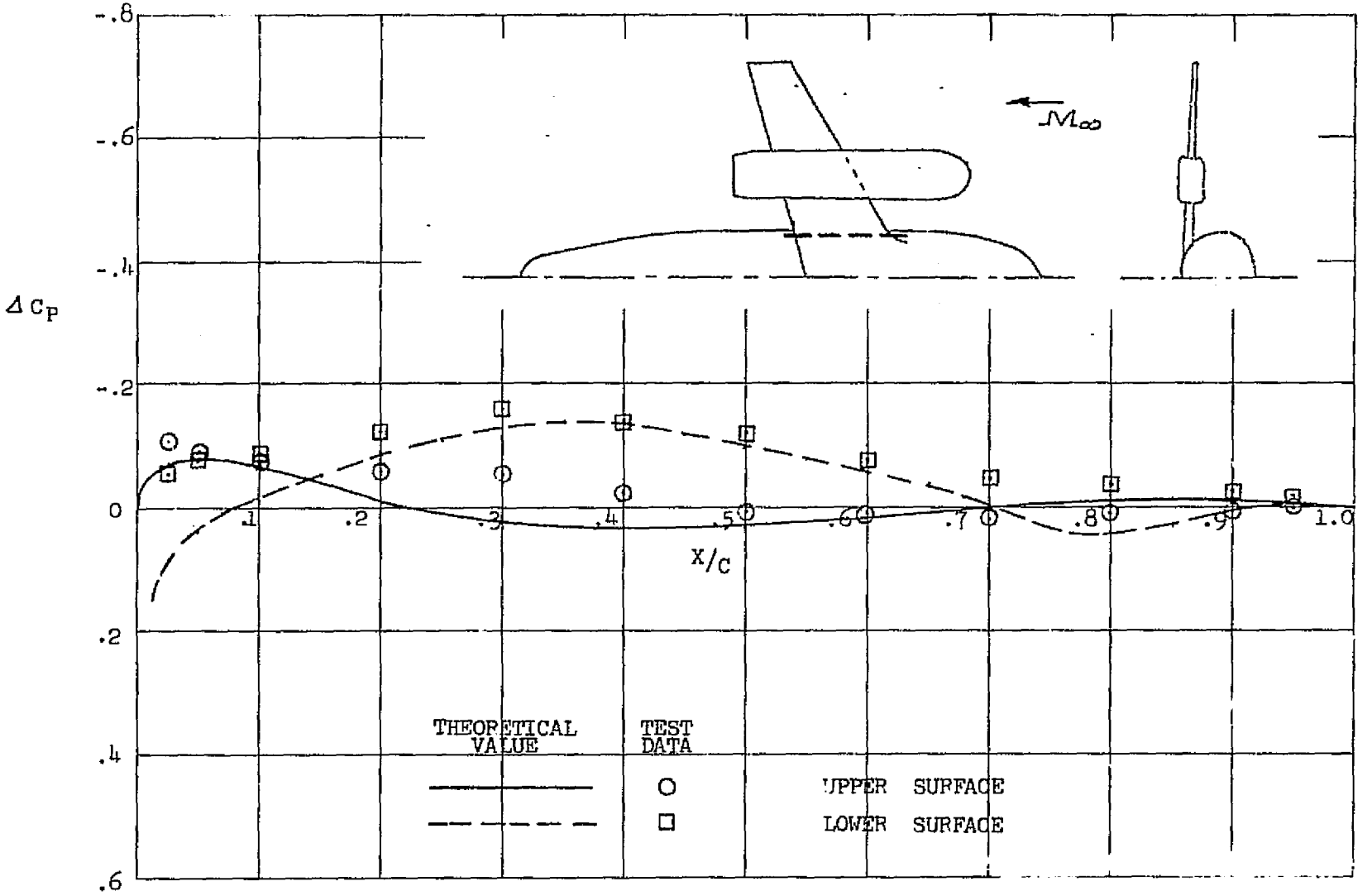

FIGURE 48. PRESSURE INDUCED ON THE WING BY THE FANPOD AT THE WING 20 PERCENT SEMI-SPAN STATION. $M_\infty = .6, \alpha = 0$ DEGREES

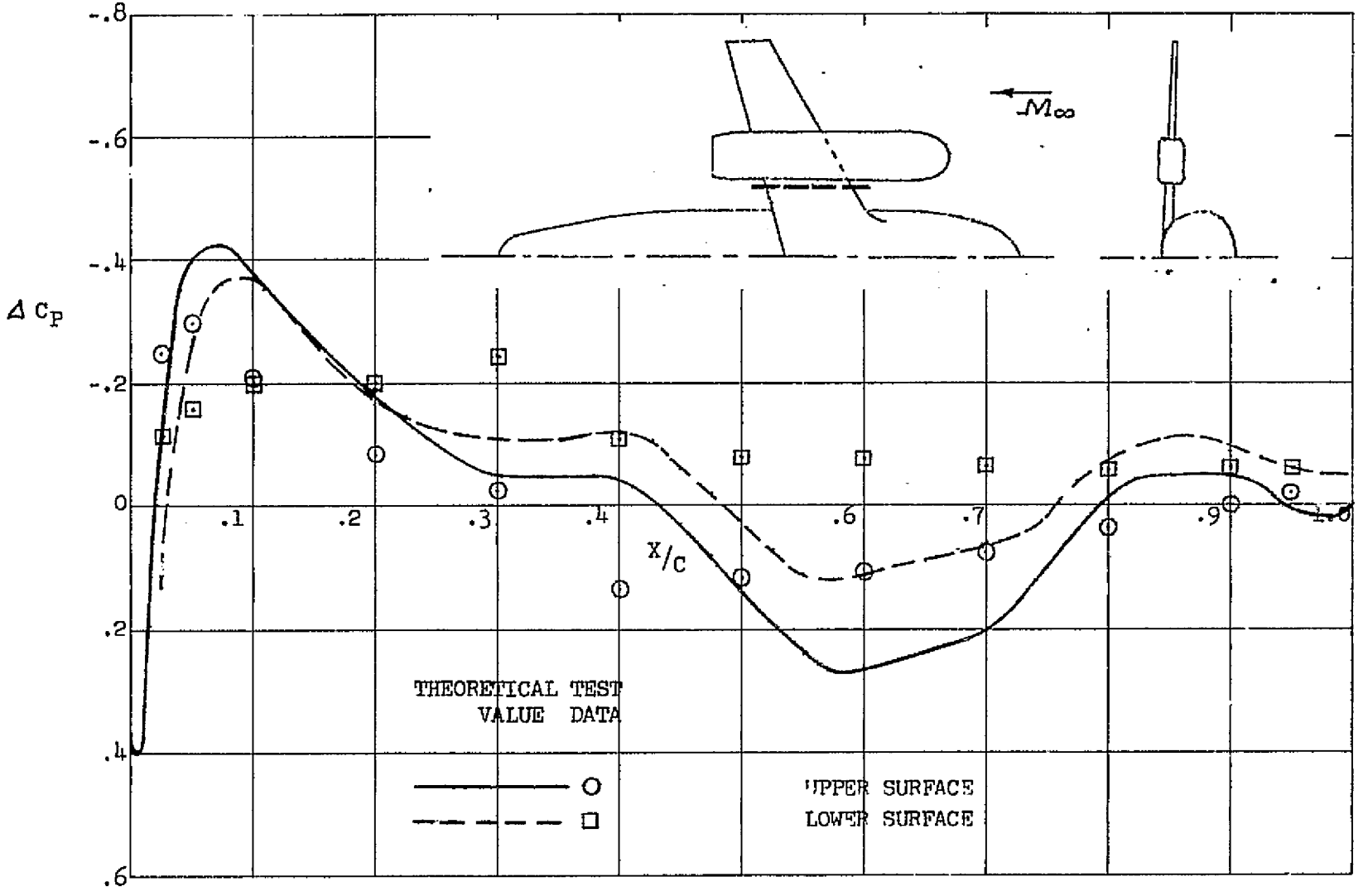

FIGURE 49. PRESSURE INDUCED ON THE WING BY THE FANPOD AT THE WING 33 PERCENT SEMI-SPAN STATION. $M_\infty = .6$, $\alpha = 0$ DEGREES

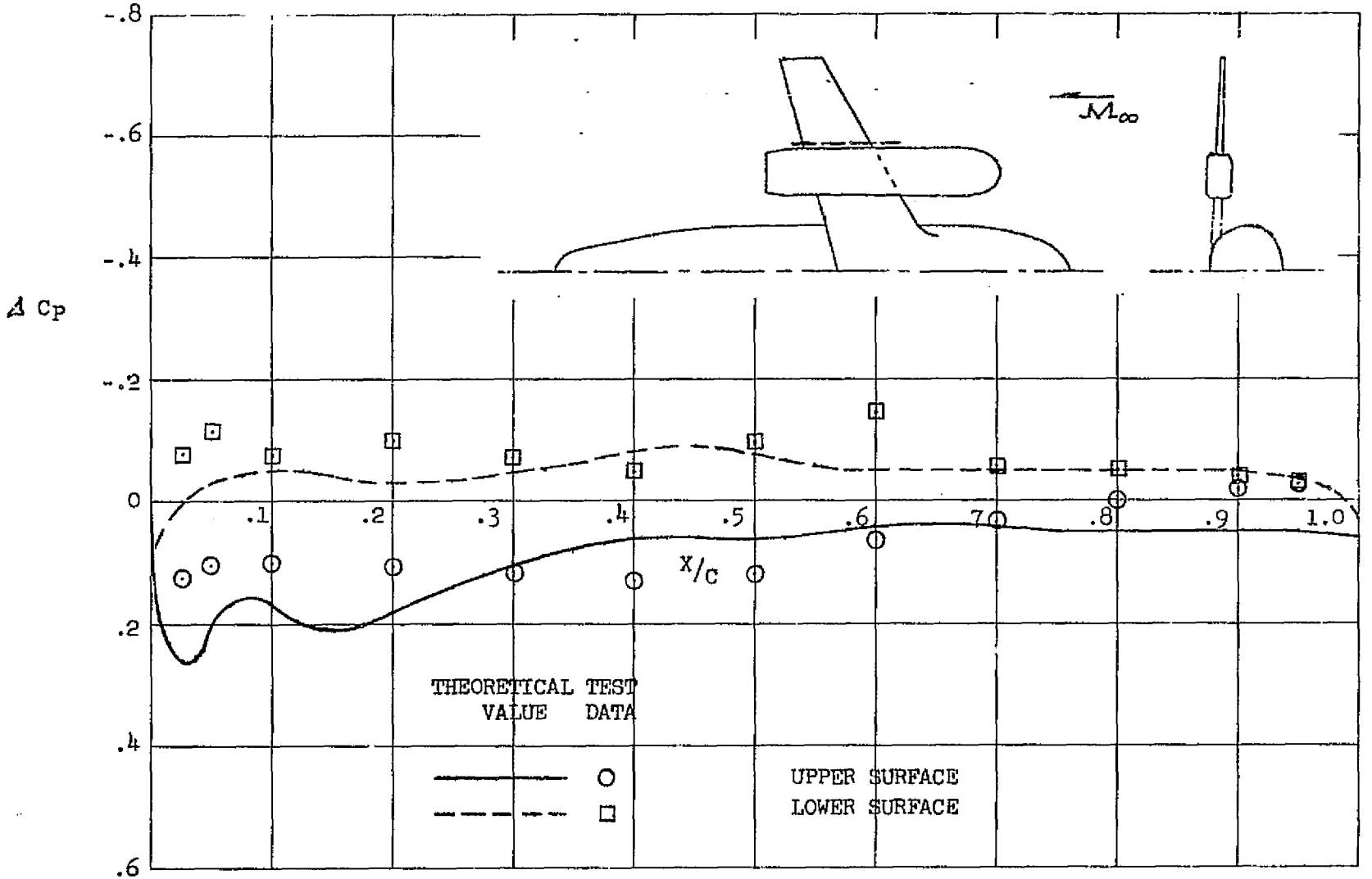

FIGURE 50. PRESSURE INDUCED ON THE WING BY THE FANPOD AT THE WING 60 PERCENT SEMI-SPAN STATION. $M_\infty = .6$, $\alpha = 0$ DEGREES

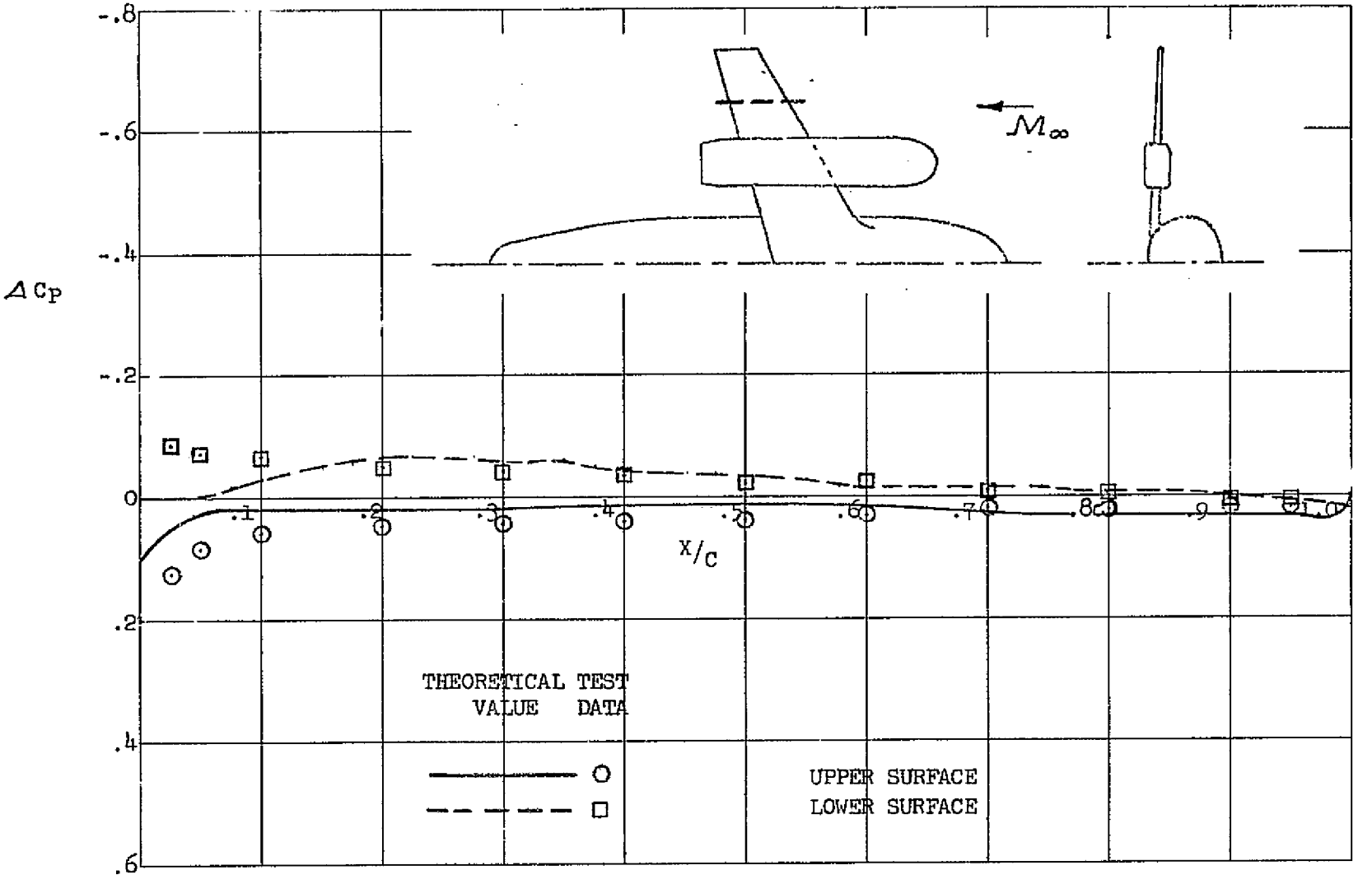

FIGURE 51. PRESSURE INDUCED ON THE WING BY THE FANPOD AT THE WING 75 PERCENT SEMI-SPAN STATION. $M_\infty = .6$ $\alpha = 0$ DEGREES

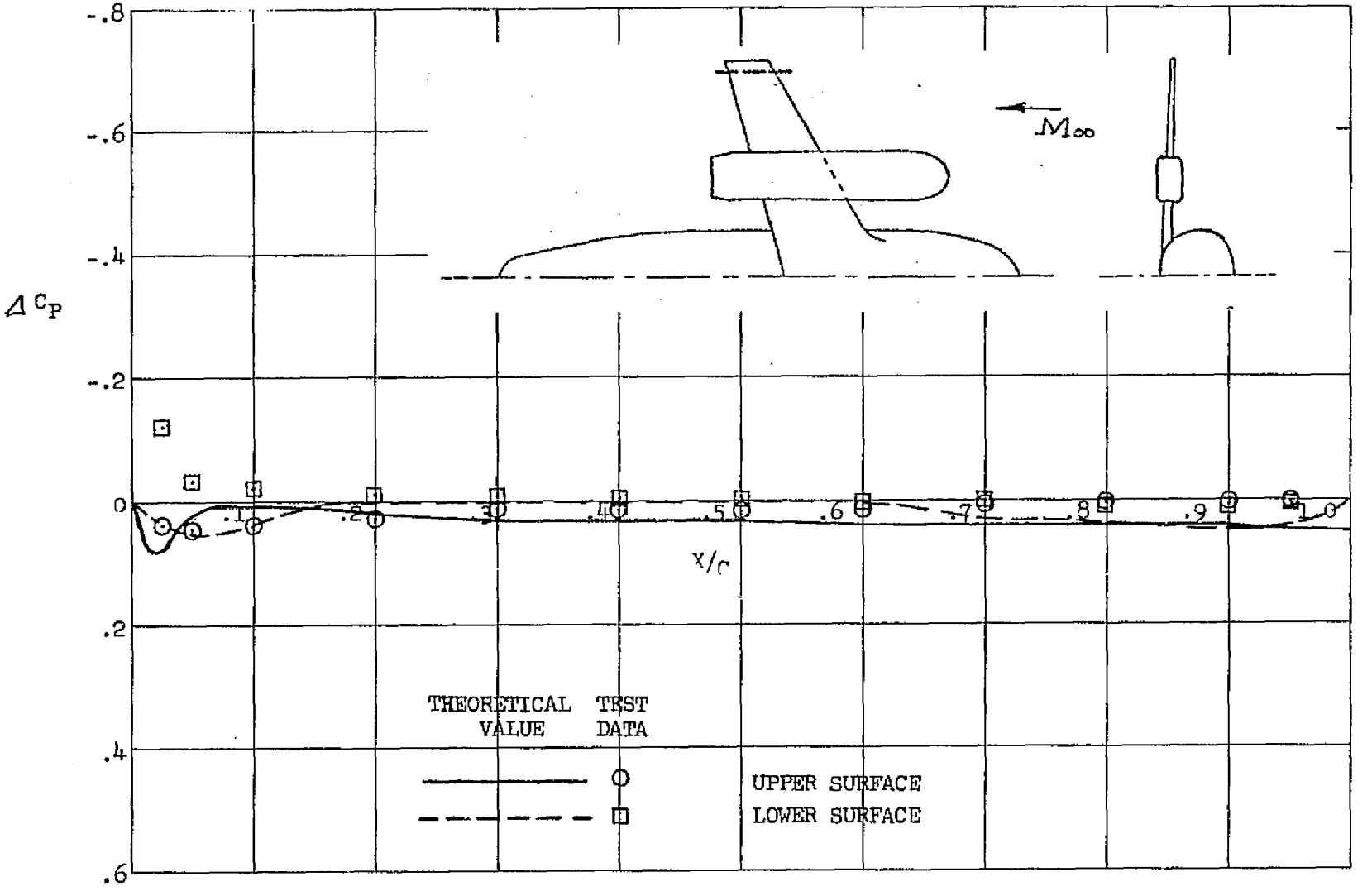

FIGURE 52. PRESSURE INDUCED ON THE WING BY THE FANPOD AT THE WING 95 PERCENT SEMI-SPAN STATION. $M_\infty = .6$, $\alpha = 0$ DEGREES

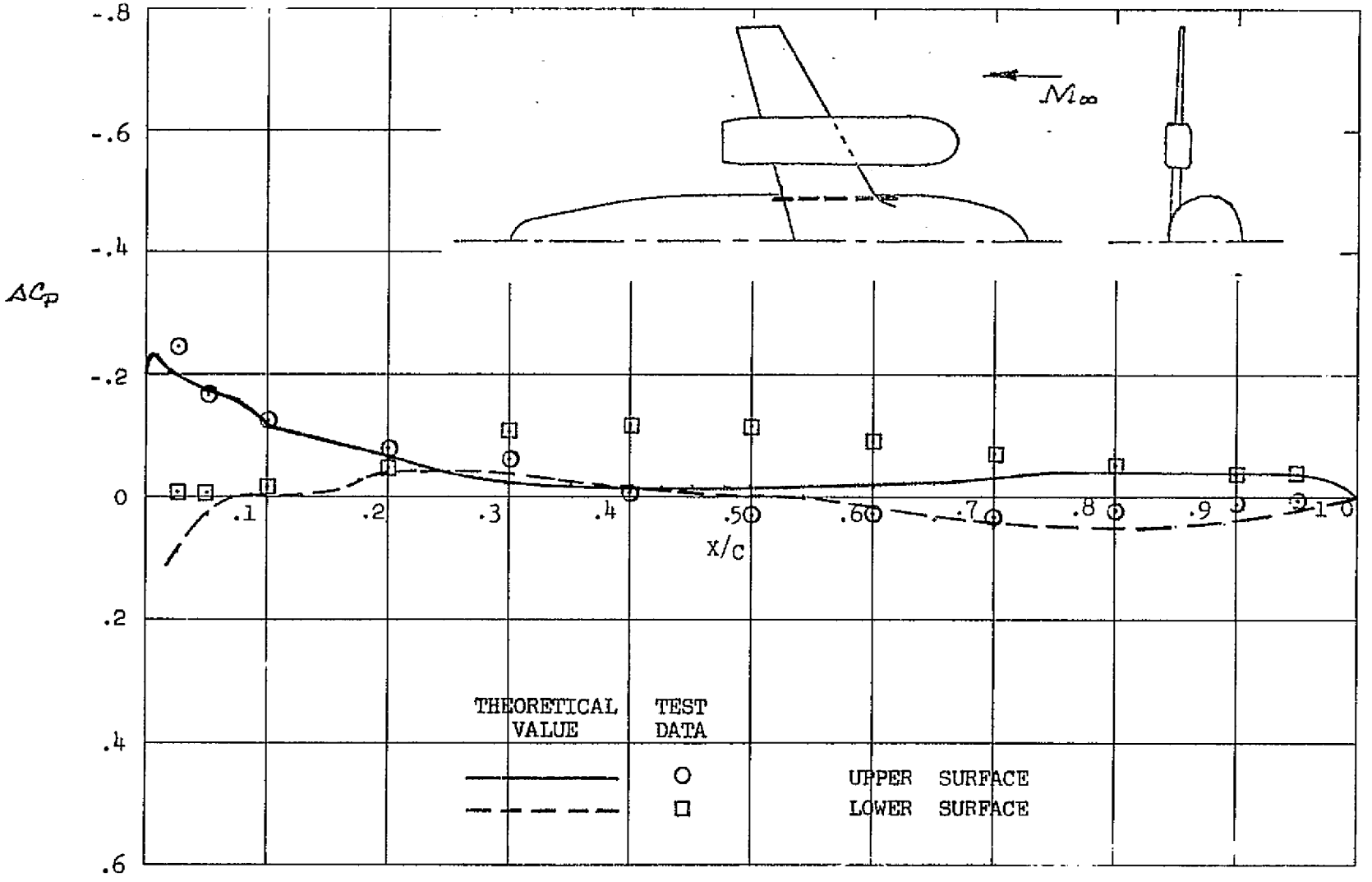

FIGURE 53. PRESSURE INDUCED ON THE WING BY THE FANPOD AT THE WING 20 PERCENT SEMI-SPAN STATION. $M_\infty = .6, \alpha = 3$ DEGREES

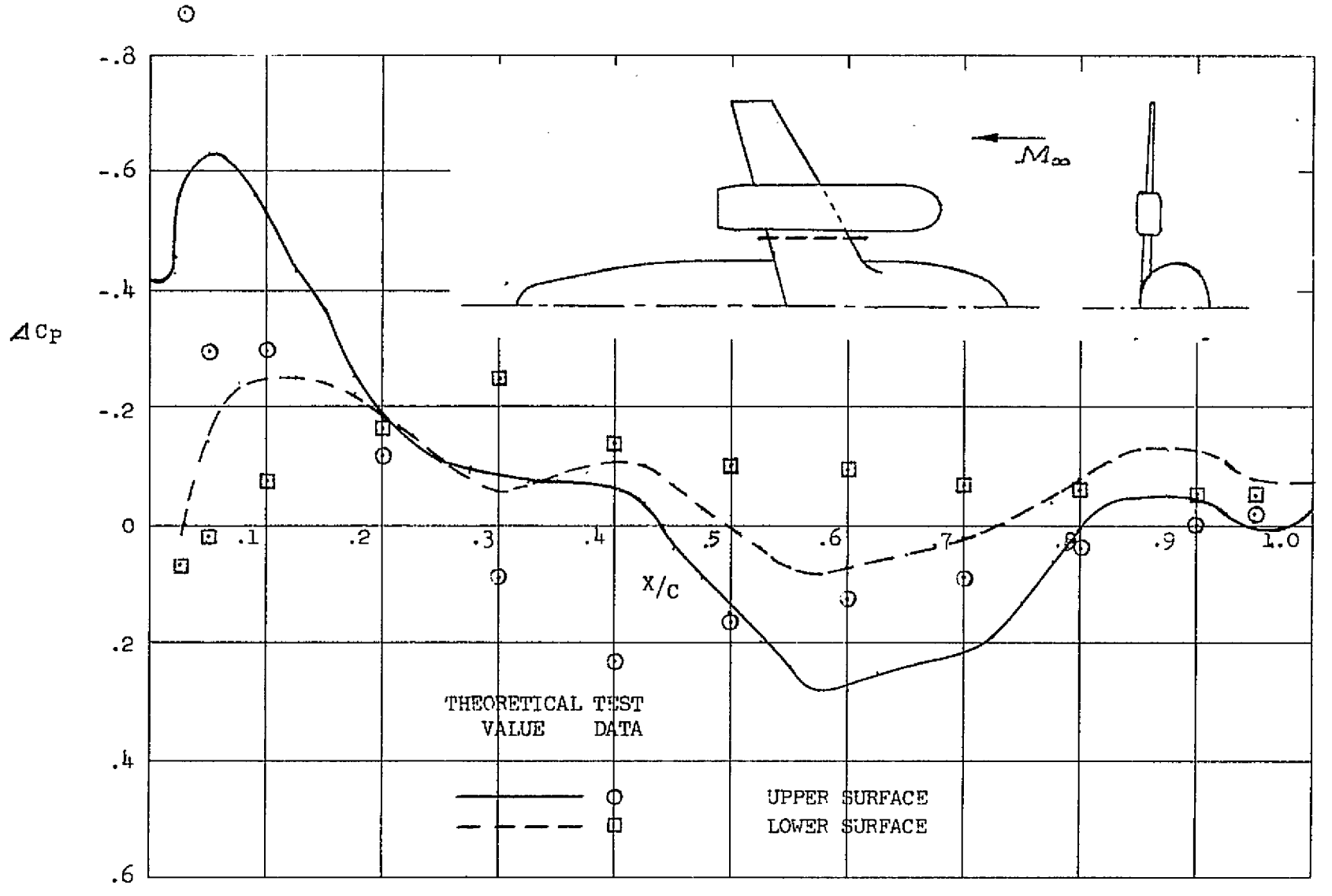

FIGURE 54. PRESSURE INDUCED ON THE WING BY THE FANPOD AT THE WING 33 PERCENT SEMI-SPAN STATION. $M_\infty = .6$, $\alpha = 3$ DEGREES

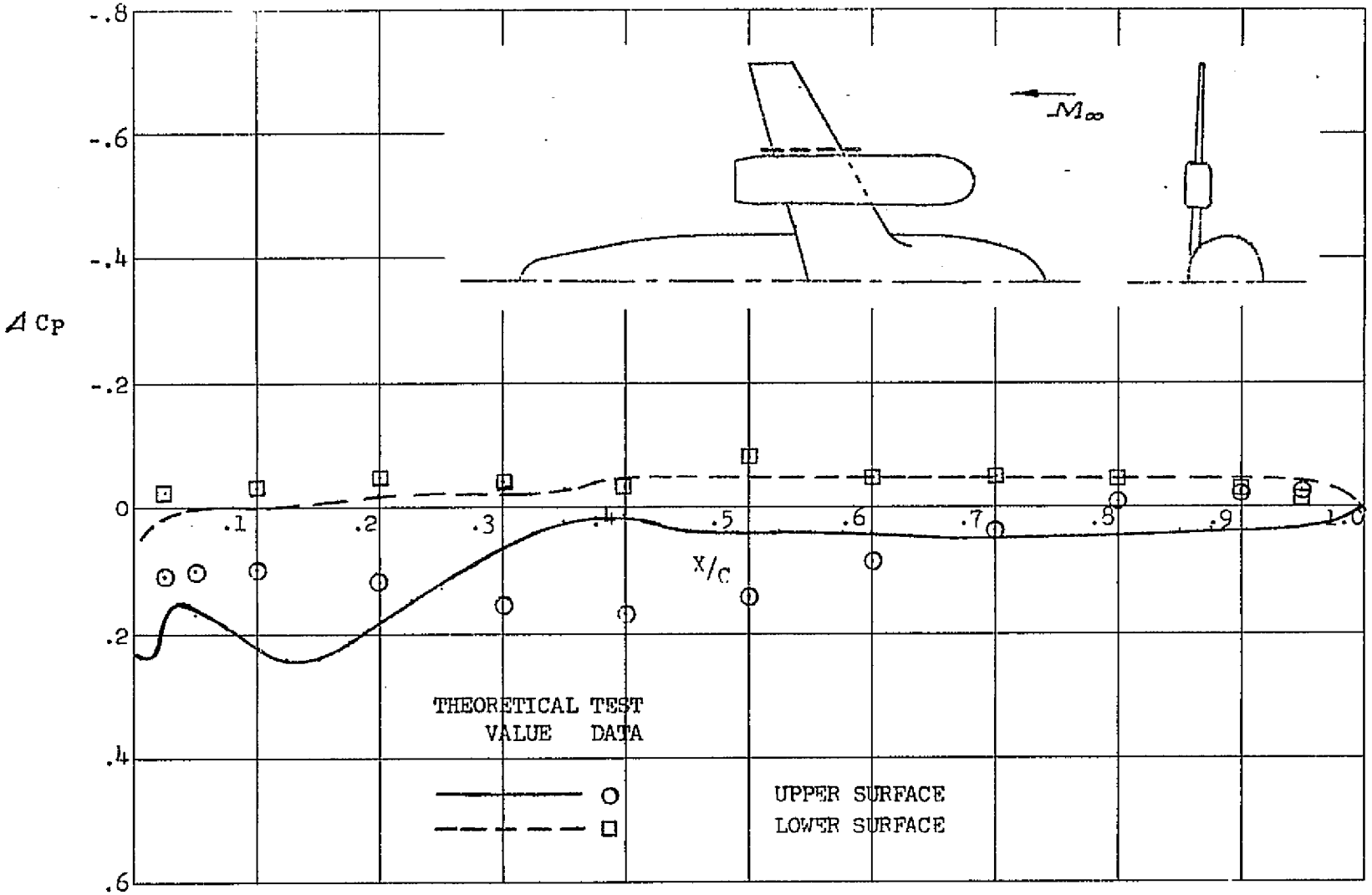

FIGURE 55. PRESSURE INDUCED ON THE WING BY THE FANPOD AT THE WING 60 PERCENT SEMI-SPAN STATION. $M_\infty = .6$, $\alpha = 3$ DEGREES

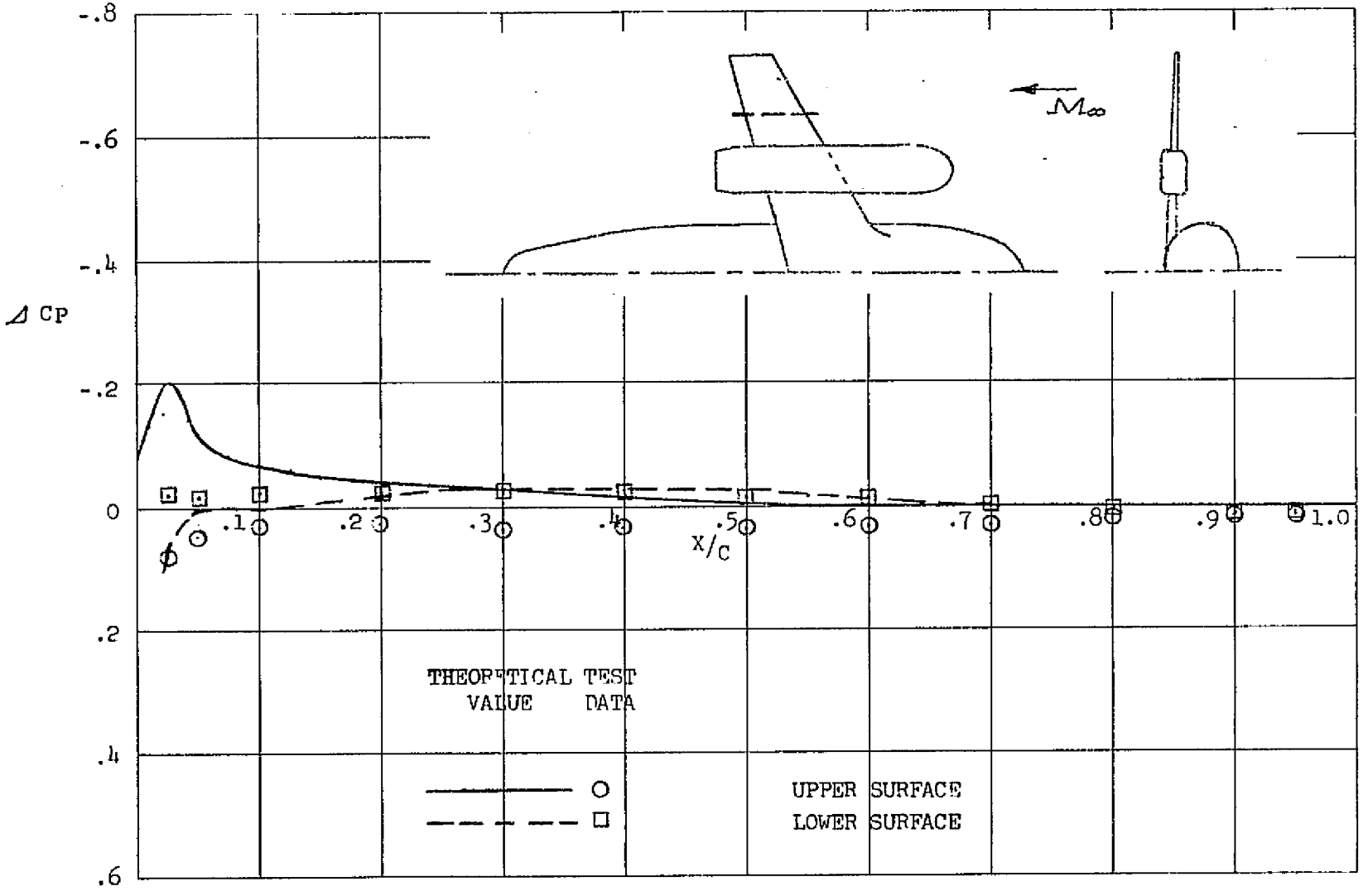

FIGURE 56. PRESSURE INDUCED ON THE WING BY THE FANPOD AT THE WING 75 PERCENT SEMI-SPAN STATION. $M_\infty = .6$, $\alpha = 3$ DEGREES

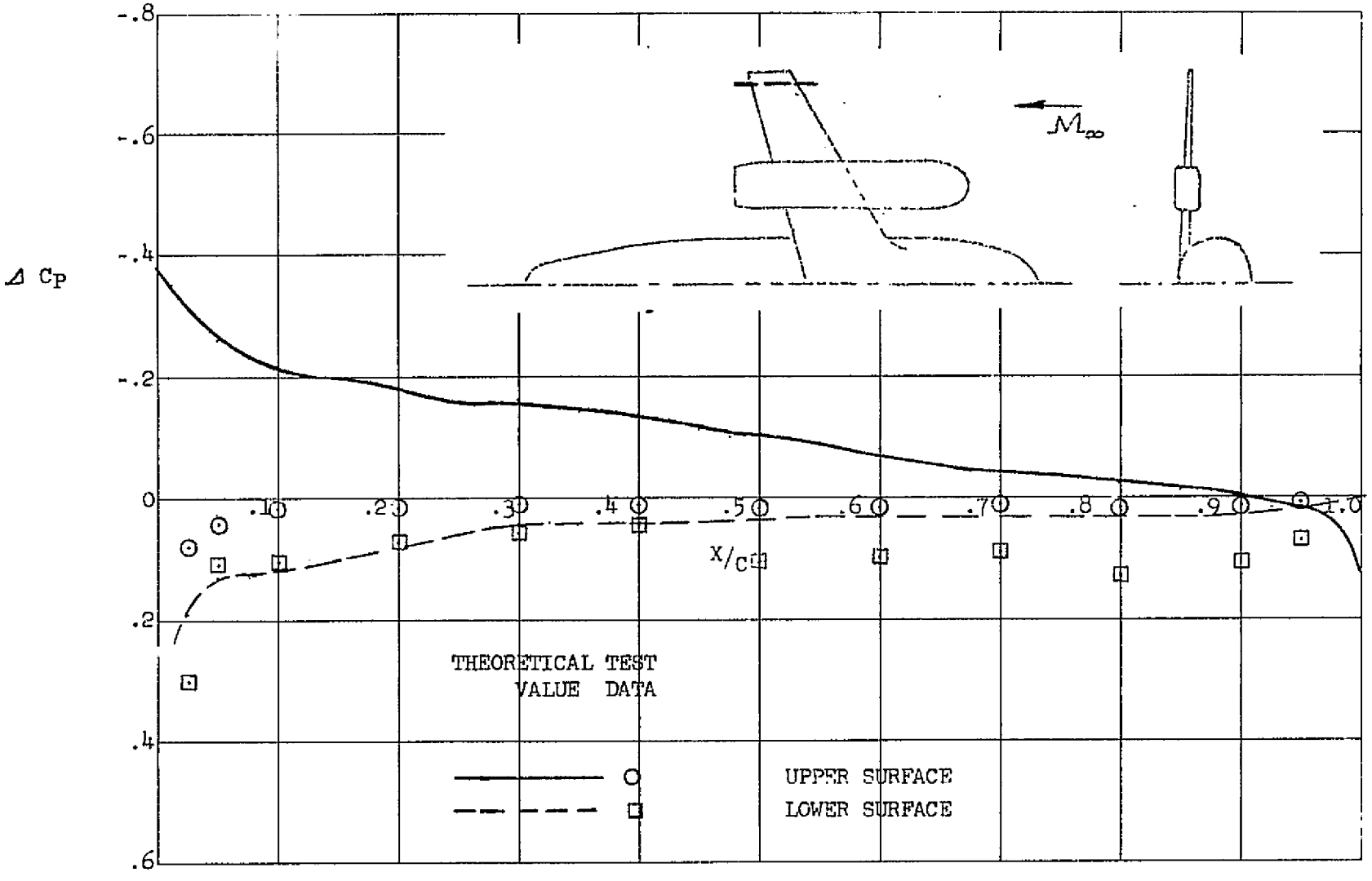

FIGURE 57. PRESSURE INDUCED ON THE WING BY THE FANPOD AT THE WING 95 PERCENT SEMI-SPAN STATION. $M_\infty = .6, \alpha = 3$ DEGREES

APPENDIX A.

NUMERICAL PROCEDURES

Discussions of the prime numerical procedures used within the program are given in this appendix. There are essentially three such procedures; (1) straight line interpolation and extrapolation, (2) controlled deviation interpolation, and (3) Householder's simultaneous equation solution.

For straight line interpolation and extrapolation about two given points (X_1, Y_1) and (X_2, Y_2);

$$Y = \alpha Y_2 + (1-\alpha) Y_1 \tag{1}$$

where

$$\alpha = \frac{X - X_1}{X_2 - X_1} \tag{2}$$

The slope $\frac{dY}{dX}$ for this case is given by;

$$\frac{dY}{dx} = \alpha'(Y_2 - Y_1) \tag{3}$$

where

$$\alpha' = 1/(X_2 - X_1) \tag{4}$$

In the case of the controlled deviation interpolation method (CODIM) parabolae are used to curve fit a set of four given points (X_{N-1}, Y_{N-1}), (X_N, Y_N), (X_{N+1}, Y_{N+1}), and (X_{N+2}, Y_{N+2}) to obtain interpolated Y and $\frac{dY}{dX}$ values for $X_N \le X \le X_{N+1}$. Only that information, relative to this method, which is necessary to judiciously pick input points will be discussed here. A complete derivation is given in reference (20).

One parabola P_1 is fit through (X_{N-1}, Y_{N-1}), (X_N, Y_N), and (X_{N+1}, Y_{N+1}). The other parabola P_2 is fit through (X_N, Y_N), X_{N+1}, Y_{N+1}), and (X_{N+2}, Y_{N+2}). This curve fitting process involves the solution of two sets of simultaneous equations. If,

$$P_1 = A_1 X^2 + B_1 X + C_1 \tag{5}$$

and

$$P_2 = A_2 X^2 + B_2 X + C_2 \tag{6}$$

Then

$$\begin{Bmatrix} A_1 \\ B_1 \\ C_1 \end{Bmatrix} = \begin{bmatrix} X_{N-1}^2 & X_{N-1} & 1 \\ X_N^2 & X_N & 1 \\ X_{N+1}^2 & X_{N+1} & 1 \end{bmatrix}^{-1} \begin{Bmatrix} Y_{N-1} \\ Y_N \\ Y_{N+1} \end{Bmatrix} \tag{7}$$

and

$$\begin{Bmatrix} A_2 \\ B_2 \\ C_2 \end{Bmatrix} = \begin{bmatrix} X_N^2 & X_N & 1 \\ X_{N+1}^2 & X_{N+1} & 1 \\ X_{N+2}^2 & X_{N+2} & 1 \end{bmatrix}^{-1} \begin{Bmatrix} Y_N \\ Y_{N+1} \\ Y_{N+2} \end{Bmatrix} \tag{8}$$

The interpolated values of Y and $\frac{dY}{dX}$ between X_N and X_{N+1} are defined by either P_1, P_2, or a linear combination of P_1 and P_2. The amount of P_1 and P_2 used in the linear combination is determined by comparing both of the parabolae to the straight line.

$$S = \alpha Y_{N+1} + (1-\alpha) Y_N \tag{9}$$

where

$$\alpha = \frac{Y_{N+1} - Y_N}{X_{N+1} - X_N} \tag{10}$$

The parabola which has the least deviation from the straight line is given the greatest weight. The weighting factors E_1 and E_2 are determined as follows;

$$E_1 = |P_1 - S| \tag{11}$$

$$E_2 = |P_2 - S| \tag{12}$$

The weighted expression for Y in the range $X_N \leq X \leq X_{N+1}$ is then;

$$Y = \frac{\alpha E_1 P_2 + (1-\alpha) E_2 P_1}{\alpha E_1 + (1-\alpha) E_2} \tag{13}$$

The derivative $\frac{dY}{dX}$ in the range $X_N \leq X \leq X_{N+1}$ is then;

$$\frac{dY}{dX} = \frac{dN}{dX}/D - N\frac{dD}{dX}/D^2 \qquad \text{FOR } D \neq 0 \tag{14}$$

where

$$N = \alpha E_1 P_2 + (1-\alpha) E_2 P_1 \tag{15}$$

$$D = \alpha E_1 + (1-\alpha) E_2 \tag{16}$$

And then

$$\frac{dN}{dX} = \frac{d\alpha}{dX} E_1 P_2 + \alpha \frac{dE_1}{dX} P_2 + \alpha E_1 \frac{dP_2}{dX} - \frac{d\alpha}{dX} E_2 P_1 + (1-\alpha) \frac{dE_2}{dX} P_1 + E_2 \frac{dP_1}{dX} \tag{17}$$

Therefore;

$$\frac{dD}{dx} = \frac{d\alpha}{dx} E_1 + \alpha \frac{dE_1}{dx} - \frac{d\alpha}{dx} E_2 + (1-\alpha) \frac{dE_2}{dx} \tag{18}$$

$$Y = \begin{cases} P_1 & \text{FOR } x = x_N \\ \dfrac{\alpha E_1 P_2 + (1-\alpha) E_2 P_1}{\alpha E_1 + (1-\alpha) E_2} & \text{FOR } x_N < x < x_{N+1} \\ P_2 & \text{FOR } x = x_{N+1} \end{cases} \tag{19}$$

and

$$\frac{dY}{dx} = \begin{cases} \dfrac{dP_1}{dx} & \text{FOR } x = x_N \\ \dfrac{dn}{dx}/D - n \dfrac{dD}{dx}/D^2 & \text{FOR } x_N < x < x_{N+1} \\ \dfrac{dP_2}{dx} & \text{FOR } x = x_{N+1} \end{cases} \tag{20}$$

In the case of an end interval $X_{N-1} \leq x \leq x_N$; P_1 is set equal to ;

$$P_1 = S + K(P_2 - S) \tag{21}$$

where

$$K = 1 - \frac{|M_1| - |M_2|}{|M_1| + |M_2|} \tag{22}$$

and

$$M_1 = \frac{Y_N - Y_{N-1}}{x_N - x_{N-1}} \tag{23}$$

$$M_2 = \frac{Y_N - Y_{N+1}}{x_N - x_{N+1}} \tag{24}$$

A similar procedure is followed for the other end interval $X_{N+1} \leq x \leq x_{N+2}$

Householder's method for solving simultaneous equations is used in the solution of the aerodynamic influence equations. The method is applicable to both square and rectangular influence matrices. In the case of rectangular matrices it is not necessary to least square the equations first, since Householder's procedure least squares and triangularizes simultaneously. Also, the influence matrix is triangularized by means of orthogonal transformation matrices, which preserve the conditioning of the matrix. The combination of these two advantages, along with a reduction in the number of required computer operations, greatly improves the numerical accuracy and stability of the solution over that of the standard Gaussian reduction method.

A complete, but rather abstract, derivation of the method is given in reference (21). The actual computer subroutine used in the program was developed by L. V. Andrew at NR. The method in the subroutine has been altered from the original to allow the operation on a single row of the matrix at a time. This reduces the required core allocation necessary to triangularize the matrix.

A derivation of the method, developed by the writer, will be given here in order to described the basic philosophy of the method.

If $[A]$ is the rectangular influence matrix, the upper triangle is given by;

$$[R] = [W][A] \tag{25}$$

where $[W]$ is the combined orthogonal transformation matrix used by Householder to triangularize $[A]$.

The relationship between Householder's triangularized matrix (R) and that obtained by Gaussian elimination of the least squared influence matrix $[A]^T[A]$, is

$$[G] = [T][A]^T[A] = [T][R]^T[R] = [D][R] \tag{26}$$

where $[G]$ is the triangular matrix obtained by Gaussian Elimination of $[A]^T[A]$. The matrix $[T]$ is the Gaussian transformation matrix used to triangularized $[A]^T[A]$. And, $[D]$ is a diagonal matrix with the same diagonal as $[R]$. It can be seen from equation (22) that a nonsquare matrix must be least first, before applying the Gaussian transformation $[T]$. Where as, the Householder transformation matrix $[W]$ can be applied directly. The least squared matrix $[A]^T[A]$ is usually more ill-conditioned than $[A]$, and therefore, less accurate results are obtained.

In the Householder method $[W]$ is equal to the product of N+1 individual orthogonal transformation matrices, where n equals the number of unkowns. There are N+1 transformations because the augmented influence matrix, made up of the influence matrix itself plus the boundary condition matrix, added on as the last column, has N+1 columns. Each transformation results in reducing all elements below the diagonal to zero for one column. The columns are reduced from left to right.

The individual transformation matrices $[w]_m$ are defined by;

$$[w]_m = ([I] - 2\{u\}_m \{u\}_m^T) \tag{27}$$

where $[I]$ is a unit diagonal matrix and $[u]_m$ is a column matrix defined by the unit vector $\vec{u}_m = (\vec{a}_m - \alpha_m \vec{v}_m)/\mu_m$. The vector $\vec{a}_m$ is defined by the mth column of $[A]$ where the elements on rows less than m are replaced by zeros. The unit vector $\vec{v}_m$ is defined by a column matrix $[v]_m$ with all zeros except for the mth. row, which is equal to one. The constants α_m and μ_m are defined as,

$$\alpha_m = /\{a_m\}/ \tag{28}$$

$$\mu_m = \sqrt{2\alpha_m(\alpha_m - \vec{v}_m \vec{a}_m)} \tag{29}$$

It can be shown that $[a_m]$ is reduced to $/\{a_m\}/\{v_m\}$ if $\{a_m\}$ is premultiplied by $([I] - 2\{u\}_m\{u\}_m^T)$. Also, that the first m-1 rows of

$$[w_{m-1}][w_{m-2}] \cdots [w_1][A] \tag{30}$$

remain unchanged by the mth transformation. The result after m transformations is then zeros below the diagonal for the first m columns and $/\{a_1\}/, /\{a_2\}/, \cdots, /\{a\}_{m-2}/, /\{a\}_{m-1}/, /\{a\}_m/$ on the diagonal. The elements above the diagonal have been defined by the m preceding transformations and will remain unchanged for the N+1-m remaining transformations.

$$([I] - 2\{u_m\}\{a_m\}^T)\{a_m\} = /\{a_m\}/\{v_m\} \tag{31}$$

$$\vec{u}_m = (\vec{a}_m - \alpha_m \vec{v}_m)/\mu_m \quad \text{or} \quad \{u_m\} = (\{a_m\} - \alpha_m\{v_m\})/\mu_m \tag{32}$$

$$\alpha_m = /\{a_m\}/ \tag{33}$$

and

$$\mu_m = \sqrt{2\alpha_m(\alpha_m - \vec{v}_m \cdot a_m)} \quad \text{or} \quad \mu_m = \sqrt{2\alpha_m(\alpha_m - \{a_m\}^T\{v_m\})} \tag{34}$$

remain to be proved. It is helpful in the derivation of equation (31) if the vector identity

$$|\vec{a}_m|\vec{v} + z(\vec{u}_m \cdot \vec{a}_m)\vec{u}_m = \vec{a}_m \tag{35}$$

is observed from the following vector diagram.

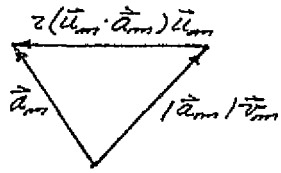

Then from equation (35);

$$|\vec{a}_m|\vec{v}_m + z\vec{u}_m(\vec{u}_m \cdot \vec{a}_m) = \vec{a}_m \tag{36}$$

$$|\vec{a}_m|\vec{v}_m + z\vec{u}_m\vec{u}_m \cdot \vec{a}_m = \vec{a}_m \tag{37}$$

Therefore;

$$|\vec{a}_m|\vec{v}_m = (\hat{e}_m\hat{e}_m - z\vec{u}_m\vec{u}_m)\vec{a}_m \tag{38}$$

where $\hat{e}_m\hat{e}_m$ and $\vec{u}_m\vec{u}_m$ are dyadics. The unit vector $\hat{e}_m$ is in the direction of $\vec{a}_m$.

Equation (38) can then be written in matrix notation as follows;

$$([I] - z\{u\}_m\{u\}_m^T)\{a\}_m = |\{a\}_m|\{v\}_m \tag{39}$$

which is equal to equation (31). In matrix or tensor notation it becomes evident that the dimensions of $\{a\}_m$, $\{v\}_m$, and $\{u\}_m$ are not limited to three.

$$\alpha_m = |\{a_m\}| \tag{40}$$

and

$$\mu_m = z\{a_m\}^T\{a_m\} \tag{41}$$

Then if equation (31) is premultiplied by $\{a_m\}^T$

$$\{a_m\}^T\{a_m\} - 2\{a_m\}^T\{u_m\}\{u_m\}^T\{a_m\} = \lambda\{a_m\}\{a_m\}^T\{v_m\} \tag{42}$$

And substituting α_m and μ_m into equation (42).

$$\alpha_m^2 - \tfrac{1}{2}\mu_m^2 = \alpha_m\{a_m\}^T\{v_m\} \tag{43}$$

or

$$\mu_m = \sqrt{2\alpha_m(\alpha_m - \{a_m\}^T\{v_m\})} \tag{44}$$

In vector notation equation (44) is seen to be equal to;

$$\mu_m = \sqrt{2\alpha_m(\alpha_m - \vec{v}_m\cdot\vec{a}_m)} \tag{45}$$

Also, if equation (44) is substituted back into equation (31)

$$\{a_m\} - \sqrt{2\alpha_m(\alpha_m - \{a_m\}^T\{v_m\})}\,\{a_m\} = \alpha_m\{v_m\} \tag{46}$$

Therefore;

$$\{u_m\} = \frac{\{a_m\} - \alpha_m\{v_m\}}{\sqrt{2\alpha_m(\alpha_m - \{a_m\}^T\{v_m\})}} \tag{47}$$

or in vector notation

$$\vec{u}_m = \frac{\vec{a}_m - \alpha_m\vec{v}_m}{\sqrt{2\alpha_m(\alpha_m - \vec{v}_m\cdot\vec{a}_m)}} \tag{48}$$

APPENDIX B

SKEWED SOURCE INFLUENCE EQUATIONS

FINITE SOURCE LINE

The potential for a finite source line can be obtained from the integral of the potential produced by a distribution of three dimensional sources placed along an axis. An expression for the potential in an incompressible flow field will be derived first, the partial derivatives taken to obtain the perturbation velocity, and then the velocity expressions transformed by the Gothert similarity rule to obtain subcritical compressible velocity expressions. The potential for a three dimensional source is given by:

$$\phi(x_s', y_s', z_s') = -\frac{\sigma}{4\pi}\left[(x_s'-x_s')^2 + (y_s'-y_s')^2 + (z_s'-z_s')^2\right]^{-1/2} \qquad (1)$$

where (x_s', y_s', z_s') and (x_s', y_s', z_s') are the locations of the point being influenced and the source, respectively. The prime indicates the local coordinate frame shown in figure B-1. If a distribution of constant strength sources is placed along the x' axis, the potential of these sources represent that of a finite source line and is given by the following integral expression.

$$\phi(x_s', y_s', z_s') = -\frac{\sigma(x_s')}{4\pi}\int_{-s}^{s} \frac{dx_s'}{\left[(x_s'-x_s')^2 + y_s'^2 + z_s'^2\right]} \qquad (2)$$

where $\sigma(x_s')$ is the source strength per unit length along the x' axis from $x'=-s$ to $x'=s$.

Let $\bar{u} = x_s' - x_s'$ and $\bar{h} = y_s'^2 + z_s'^2$, then for $\bar{h} \neq 0$

$$\phi(x_s', y_s', z_s') = \frac{\sigma(x_s')}{4\pi}\int_{x_s'+s}^{x_s'-s} \frac{d\bar{u}}{\sqrt{\bar{h}^2+\bar{u}^2}}$$

$$= \frac{\sigma(x_s')}{4\pi}\log_e \left/ \frac{(x_s'-s) + \sqrt{(x_s'-s)^2 + y_s'^2 + z_s'^2}}{(x_s'+s) + \sqrt{(x_s'+s)^2 + y_s'^2 + z_s'^2}} \right. \qquad (3)$$

The perturbation velocity u' parallel to and those v' and w' perpendicular to the source line are obtained by taking the partial derivative of equation (3) with respect to x_s', y_s', and z_s', respectively.

$$u' = \frac{\sigma(x_s')}{4\pi}\left\{\frac{1+(x_s'-s)/[(x_s'-s)^2+y_s'^2+z_s'^2]^{1/2}}{(x_s'-s)+[(x_s'-s)^2+y_s'^2+z_s'^2]^{1/2}}\right.$$

$$\left. - \frac{1+(x_s'+s)/[(x_s'+s)^2+y_s'^2+z_s'^2]^{1/2}}{(x_s'+s)+[(x_s'+s)^2+y_s'^2+z_s'^2]^{1/2}}\right\} \tag{4}$$

$$v' = \frac{\sigma(x_s')}{4\pi}\left\{\frac{y_s'/[(x_s'-s)^2+y_s'^2+z_s'^2]^{1/2}}{(x_s'-s)+[(x_s'-s)^2+y_s'^2+z_s'^2]^{1/2}}\right.$$

$$\left. - \frac{y_s'/[(x_s'+s)^2+y_s'^2+z_s'^2]^{1/2}}{(x_s'+s)+[(x_s'+s)^2+y_s'^2+z_s'^2]^{1/2}}\right\} \tag{5}$$

$$w' = \frac{\sigma(x_s')}{4\pi}\left\{\frac{z_s'/[(x_s'-s)^2+y_s'^2+z_s'^2]^{1/2}}{(x_s'-s)+[(x_s'-s)^2+y_s'^2+z_s'^2]^{1/2}}\right.$$

$$\left. - \frac{z_s'/[(x_s'+s)^2+y_s'^2+z_s'^2]^{1/2}}{(x_s'+s)+[(x_s'+s)^2+y_s'^2+z_s'^2]^{1/2}}\right\} \tag{6}$$

The flow produced by a finite source line is axisymmetric, therefore, equations (4), (5), and (6) can be reduced to just two velocity components. The component u^* parallel to and that v^* perpendicular to the source line are then defined by:

$$u^* = \frac{\sigma(x_s')}{4\pi h}(\cos\beta_f - \cos\beta_i) \tag{7}$$

$$v^* = \frac{\sigma(x_s')}{4\pi h}(\sin\beta_f - \sin\beta_i) \tag{8}$$

where β_i and β_f are defined in figure 1.

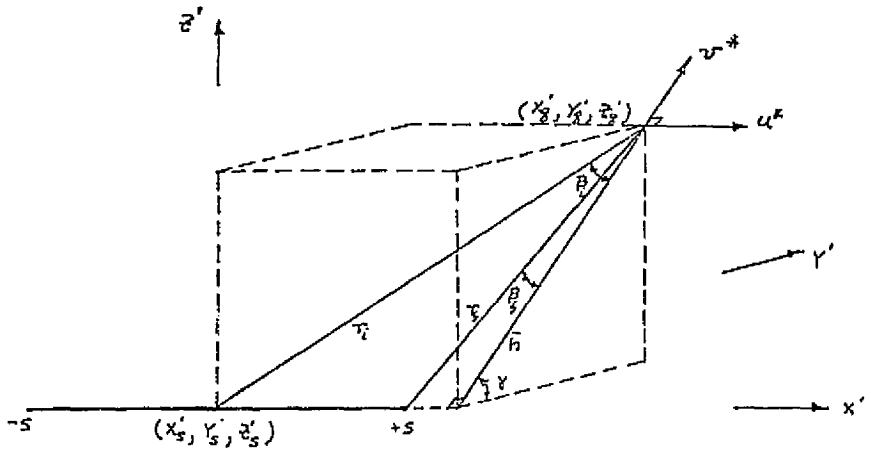

Figure 1. Finite Source Line

Equation (8) is seen to be the same as that derived from the Biot-Savart relation in reference 8 for a finite vortex segment. The influence functions for the velocity v^*, due to a finite source line, and that for the velocity perpendicular to the plane containing r_i and r_f, due to a finite vortex segment, are therefore identical.

CRANKED SOURCE LINE

In general the source lines will be cranked to follow the constant percent chord lines of the wing, as shown in figure 2. Since this is a planar analysis, all of the source lines will lie on the chordal plane. The strength of each source line segment is equal to the integral of the distributed source density over the panel it represents. Each source line segment is divided into two spanwise sections; the inboard or port half denoted by i and the outboard or starboard half denoted by o. If there is a crank in the source line it occurs at the midpoint of the segment. The panels or source line segments are equally spaced in the spanwise direction. In the chordwise direction the lines are placed at equal increments of Θ, where $\Theta = \cos^{-1}(1 - 2x/c)$

The expressions for the velocity induced by a single cranked source segment due to the inboard half (u_i^*, v_i^*) and the outboard half (u_o^*, v_o^*) are obtained directly from equations (7) and (8) and figure 3.

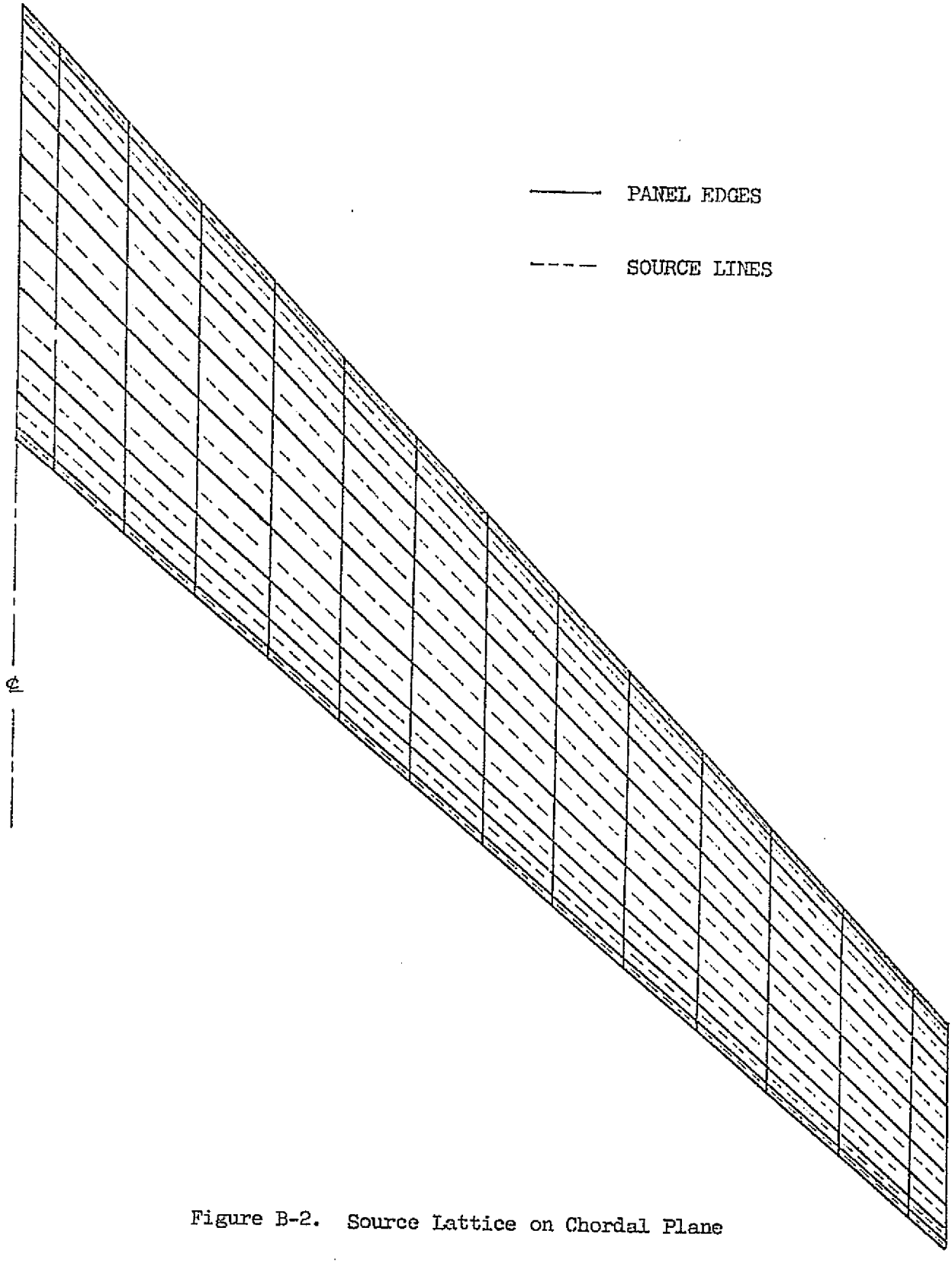

Figure B-2. Source Lattice on Chordal Plane

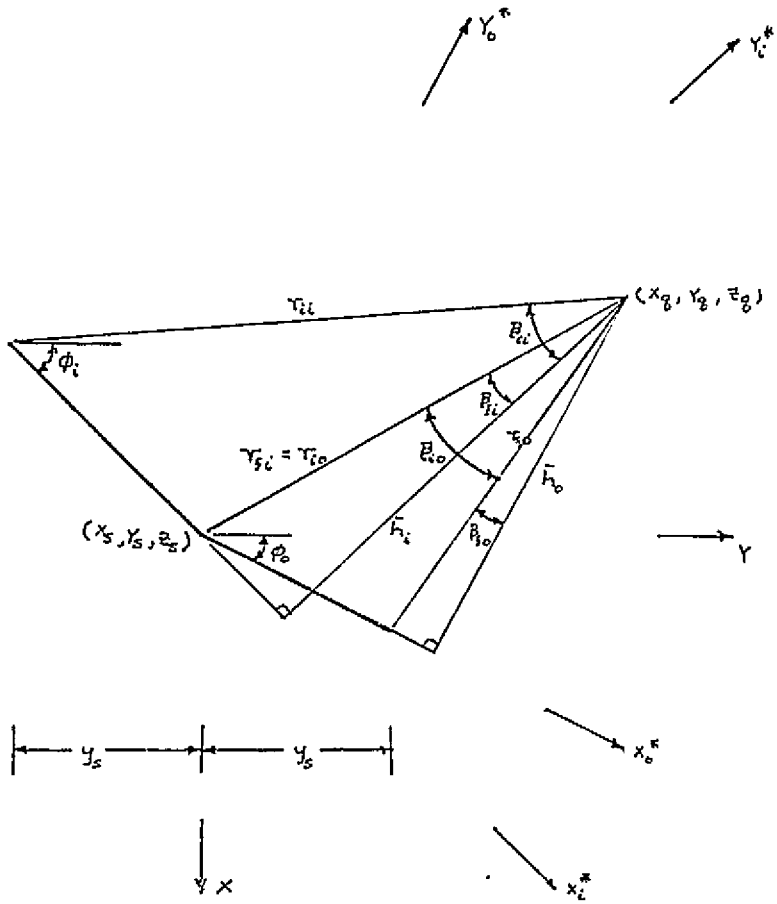

Figure 3. Cranked Source Line Segment

$$u_i^* = \frac{\sigma(x_s, y_s)_i}{4\pi} \left\{ \frac{1}{\sqrt{(x_g - x_s)^2 + (y_g - y_s)^2 + (z_g - z_s)^2}} \right.$$

$$\left. - \frac{1}{\sqrt{[(x_g - x_s) + y_s \tan\phi_i]^2 + [y_g - y_s + y_s]^2 + [z_g - z_s]^2}} \right\} \quad (9)$$

$$w_o^* = \frac{\sigma(x_s, y_s)_o}{4\pi}\left\{\frac{1}{\sqrt{[(x_s - x_s) - y_s \tan\phi_o]^2 + [y_s - y_s + y_s]^2 + [z_s - z_s]^2}}\right.$$

$$\left. - \frac{1}{\sqrt{(x_s - x_s)^2 + (y_s - y_s)^2 + (z_s - z_s)^2}}\right\} \tag{10}$$

Equations (9) and (10) were obtained by noting that Equations (4) and (7) reduce to:

$$w^* = w' = \frac{\sigma(x_s')}{4\pi}\left(\frac{1}{r_s} - \frac{1}{r_i}\right) \tag{11}$$

Also;

$$v_i^* = \frac{\sigma(x_s, y_s)_i}{4\pi} \frac{1}{\sqrt{[(x_s - x_s) - (y_s - y_s)\tan\phi_i]^2 + (z_s - z_s)^2(1 + \tan^2\phi_i)}}\left\{\right.$$

$$\frac{y_s - y_s + (x_s - x_s)\tan\phi_i + y_s(1 + \tan^2\phi_i)}{\sqrt{[(x_s - x_s) + y_s \tan\phi_i]^2 + [y_s - y_s + y_s]^2 + [z_s - z_s]^2}}$$

$$\left. - \frac{y_s - y_s + (x_s - x_s)\tan\phi_i}{\sqrt{(x_s - x_s)^2 + (y_s - y_s)^2 + (z_s - z_s)^2}}\right\} \tag{12}$$

$$v_o^* = \frac{\sigma(x_s, y_s)_o}{4\pi} \frac{1}{\sqrt{[(x_s - x_s) - (y_s - y_s)\tan\phi_o]^2 + (z_s - z_s)^2(1 + \tan^2\phi_o)}}\left\{\right.$$

$$\frac{y_s - y_s + (x_s - x_s)\tan\phi_o}{\sqrt{(x_s - x_s)^2 + (y_s - y_s)^2 + (z_s - z_s)^2}}$$

$$\left. - \frac{y_s - y_s + (x_s - x_s)\tan\phi_o - y_s(1 + \tan^2\phi_o)}{\sqrt{[(x_s - x_s) - y_s \tan\phi_o]^2 + [y_s - y_s - y_s]^2 + [z_s - z_s]^2}}\right\} \tag{13}$$

The following values of $\bar{h}_i$ and $\bar{h}_o$ were substituted into equation (8) to obtain equations (12) and (13).

$$\bar{h}_i = \sqrt{[(X_s - X_s) - (Y_s - Y_s)\tan\phi_i]^2 \cos^2\phi + (Z_s - Z_s)^2} \tag{14}$$

$$\bar{h}_o = \sqrt{[(X_s - X_s) - (Y_s - Y_s)\tan\phi_o]^2 \cos^2\phi_o + (Z_s - Z_s)^2} \tag{15}$$

The velocity components in the prime coordinate frame shown in figure 1 are obtained from the following relations.

$$u' = u^* \tag{16}$$

$$v' = v^* \cos\gamma \tag{17}$$

$$w' = v^* \sin\gamma \tag{18}$$

Therefore;

$$u_i' = u_i^* \tag{19}$$

$$u_o' = u_o^* \tag{20}$$

$$v_i' = \frac{v_i^*[(Y_s - Y_s)\tan\phi_i - (X_s - X_s)]}{\sqrt{[(X_s - X_s) - (Y_s - Y_s)\tan\phi_i]^2 + (Z_s - Z_s)^2(1 + \tan^2\phi_i)}} \tag{21}$$

$$v_o' = \frac{v_o^*[(Y_s - Y_s)\tan\phi_o - (X_s - X_s)]}{\sqrt{[(X_s - X_s) - (Y_s - Y_s)\tan\phi_o]^2 + (Z_s - Z_s)^2(1 + \tan^2\phi_o)}} \tag{22}$$

$$w_i' = \frac{v_i^*(Z_s - Z_s)\sqrt{1 + \tan^2\phi_i}}{\sqrt{[(X_s - X_s) - (Y_s - Y_s)\tan\phi_i]^2 + (Z_s - Z_s)^2(1 + \tan^2\phi_i)}} \tag{23}$$

$$w_o' = \frac{v_o^*(Z_s - Z_s)\sqrt{1 + \tan^2\phi_o}}{\sqrt{[(X_s - X_s) - (Y_s - Y_s)\tan\phi_o]^2 + (Z_s - Z_s)^2(1 + \tan^2\phi_o)}} \tag{24}$$

Then using the following transformation equations the velocity component in the freestream direction u, that in the spanwise direction v, and that perpendicular to the chordal plane w are obtained for a single cranked source line segment

$$u = \frac{u_i' \tan\phi_i - v_i'}{\sqrt{1+\tan^2\phi_i}} + \frac{u_o' \tan\phi_o - v_o'}{\sqrt{1+\tan^2\phi_o}} \tag{25}$$

$$v = \frac{u_i' + v_i' \tan\phi_i}{\sqrt{1+\tan^2\phi_i}} + \frac{u_o' + v_o' \tan\phi_o}{\sqrt{1+\tan^2\phi_o}} \tag{26}$$

$$w = w_i' + w_o' \tag{27}$$

SOURCE STRENGTH

As mentioned above the source strength in a planar analysis is only a function of the local symmetrical airfoil surface gradient. This is due to the fact that sources cannot produce a velocity component perpendicular to the chordal plane at locations other than their own. Also, in order to satisfy continuity the source strength must be equal to the mass flux emitted. Therefore, the local chordwise source density is;

$$\sigma_s(x, y_s) = 2\, w(x, y_s) \tag{28}$$

The discrete source is assumed capable of representing a linearly varying source distribution in the same way that a discrete vortex represents a linearly varying vorticity distribution. Therefore, let $\sigma_s(x, y_s)$ be defined by the first two terms of a Taylor series expansion about the location of the discrete source.

$$\sigma_s(x, y_s) = \sigma_s(x_s, y_s) + (x - x_s)\frac{\partial \sigma_s(x_s, y_s)}{\partial x} \tag{29}$$

Where the subscript s on σ indicates lines of constant source density parallel to the discrete source line.

Also, by equation (28)

$$w(x, y_s) = w(x_s, y_s) + (x - x_s)\frac{\partial w(x_s, y_s)}{\partial x} \tag{30}$$

The discrete source strength $\sigma(x_s, y_s)$ is obtained by integrating equation (29) over the panel in the chordwise direction.

$$\sigma(x_s, y_s) = \int_0^{\ell} \sigma_s(x, y_s)\cos\phi\, dx$$

$$= \int_0^{\ell} \left[\sigma_s(x_s, y_s) + (x - x_s)\frac{\partial \sigma_s(x_s, y_s)}{\partial x}\right]\cos\phi\, dx \tag{31}$$

where $\ell = \frac{\pi c}{2N_c}\sin\theta_s$ is the panel chordwise length and $\theta_s = \cos^{-1}[1 - 2(x_s - x_{LE})/c]$. The $\cos\phi$ term appears due to the fact that the integration is being taken in the chordwise direction rather than perpendicular to the discrete source line.

$$\sigma(x_s, y_s) = \left[\sigma_s(x_s, y_s)\ell + \frac{\ell^2}{2}\frac{\partial \sigma_s(x_s, y_s)}{\partial x} - x_s\ell\frac{\partial \sigma_s(x_s, y_s)}{\partial x}\right]\cos\phi \tag{32}$$

since $x_s = \frac{\ell}{2}$ and $\sigma_s(x_s, y_s) = 2w(x_s, y_s)$;

$$\sigma(x_s, y_s) = \sigma_s(x_s, y_s)\ell\cos\phi = \frac{2w(x_s, y_s)\ell}{\sqrt{1 + \tan^2\phi}} \tag{33}$$

If the source strength is divided by the freestream velocity and the boundary condition for no flow through the airfoil surface $\frac{w}{V_\infty}(x_s, y_s) = \frac{dz}{dx}(x_s, y_s)$ is substituted into equation (33) the following expression for source strength per unit freestream velocity is obtained.

$$\frac{\sigma}{V_\infty}(x_s, y_s) = \frac{2\pi c\sqrt{\left(\frac{x_s - x_{LE}}{c}\right) - \left(\frac{x_s - x_{LE}}{c}\right)^2}}{N_c\sqrt{1 + \tan^2\phi}}\frac{dz}{dx}(x_s, y_s) \tag{34}$$

where N_c equals the number of source lines per chord.

COMPRESSIBLE VELOCITY RATIO EQUATIONS

The final expressions for the compressible perturbation velocity ratios are obtained by transforming the coordinates and perturbation velocities by the Gothert similarity rule and by substituting equations (9), (10), (12), (13), and (34) into equations (19) through (27). Also, the contributions to the velocity ratios at an influence point (X_B, Y_B, Z_B) by all the source line segments at $(X_S, Y_S, Z_S)_{iL}$ are algebraically summed for $i = 1, 2, \cdots, N_i$ and $L = 1, 2, \cdots, N_L$.

$$\frac{u}{V_\infty}(X_B, Y_B, Z_B) = \frac{1}{2N_i y_s \beta^2}\left\{\sum_{L=1}^{N_L}\sum_{i=1}^{N_i} C_L\left[\left(\frac{X_{Si}-X_{LE_i}}{C_L}\right)-\left(\frac{X_{Si}-X_{LE_i}}{C_L}\right)^2\right]^{1/2}\frac{dz}{dx}(X_{S_i}, Y_{S_L})\right.$$

$$\frac{E_{u_0}(\bar{X}_B, \bar{Y}_B, \bar{Z}_B, \bar{X}_{S_i}, \bar{Y}_{S_L})\,T_0(X_{S_i}, Y_{S_L}) - E_{v_0}(\bar{X}_B, \bar{Y}_B, \bar{Z}_B, \bar{X}_{S_i}, \bar{Y}_{S_L})}{P_0^2(X_{S_i}, Y_{S_L})}$$

$$\left.-\frac{E_{u_i}(\bar{X}_B, \bar{Y}_B, \bar{Z}_B, \bar{X}_{S_i}, \bar{Y}_{S_L})\,T_i(X_{S_i}, Y_{S_L}) - E_{v_i}(\bar{X}_B, \bar{Y}_B, \bar{Z}_B, \bar{X}_{S_i}, \bar{Y}_{S_L})}{P_i^2(X_{S_i}, Y_{S_L})}\right]\right\} \tag{35}$$

$$\frac{v}{V_\infty}(X_B, Y_B, Z_B) = \frac{1}{2N_i y_s \beta}\left\{\sum_{L=1}^{N_L}\sum_{i=1}^{N_i} C_L\left[\left(\frac{X_{S_i}-X_{LE_i}}{C_L}\right)-\left(\frac{X_{S_i}-X_{LE_i}}{C_L}\right)^2\right]^{1/2}\frac{dz}{dx}(X_{S_i}, Y_{S_L})\right.$$

$$\frac{E_{v_0}(\bar{X}_B, \bar{Y}_B, \bar{Z}_B, \bar{X}_{S_i}, \bar{Y}_{S_L})\,T_0(X_{S_i}, Y_{S_L}) + E_{u_0}(\bar{X}_B, \bar{Y}_B, \bar{Z}_B, \bar{X}_{S_i}, \bar{Y}_{S_L})}{P_0^2(X_{S_i}, Y_{S_L})}$$

$$\left.-\frac{E_{v_i}(\bar{X}_B, \bar{Y}_B, \bar{Z}_B, \bar{X}_{S_i}, \bar{Y}_{S_L})\,T_i(X_{S_i}, Y_{S_L}) + E_{u_i}(\bar{X}_B, \bar{Y}_B, \bar{Z}_B, \bar{X}_{S_i}, \bar{Y}_{S_L})}{P_i^2(X_{S_i}, Y_{S_L})}\right]\right\} \tag{36}$$

and

$$\frac{w}{V_\infty}(x_g, y_g, z_g) = \frac{1}{2N_i y_s \bar{e}} \left\{ \sum_{i=1}^{N_i} \sum_{i=1}^{N_i} c_i \left[\left(\frac{x_{s_i} - x_{i,t_i}}{c_i} \right) - \left(\frac{x_{s_i} - x_{i,t_i}}{c_i} \right)^2 \right]^{1/2} \frac{dz}{dx}(x_{s_i}, y_{s_i}) \left[\right. \right.$$

$$\left. \left. \frac{E_{w_0}(\bar{x}_g, \bar{y}_g, \bar{z}_g, \bar{x}_{s_i}, \bar{y}_{s_i})}{P_0(x_{s_i}, y_{s_i})} - \frac{E_{w_i}(\bar{x}_g, \bar{y}_g, \bar{z}_g, \bar{x}_{s_i}, \bar{y}_{s_i})}{P_i(x_{s_i}, y_{s_i})} \right] \right\}$$

(37)

where: $\bar{x}_g = x_g/\bar{e}\, y_s$, $\bar{y}_g = y_g/y_s$, $\bar{z}_g = z_g/y_s$, $\bar{x}_{s_i} = x_{s_i}/\bar{e}\, y_s$, $\bar{y}_{s_i} = y_{s_i}/y_s$, $T_i = \frac{1}{\bar{e}} \tan \phi_i$, $T_0 = \frac{1}{\bar{e}} \tan \phi_0$, $P_0 = \left[1 + \left(\frac{\tan \phi_0}{\bar{e}} \right)^2 \right]^{1/2}$, and $P_i = \left[1 + \left(\frac{\tan \phi_i}{\bar{e}} \right)^2 \right]^{1/2}$.

Also; define $\bar{x}_i = \bar{x}_g - \bar{x}_{s_i}$, $\bar{y}_i = \bar{y}_g - \bar{y}_{s_i}$, and $\bar{z} = \bar{z}_g$

Then for $\bar{z}_g \neq 0$

$$E_{w_i}(\bar{x}_g, \bar{y}_g, \bar{z}_g, \bar{x}_{s_i}, \bar{y}_{s_i}) = \frac{1}{\sqrt{(\bar{x}_i + T_{i,t_i})^2 + (\bar{y}_i + 1)^2 + \bar{z}^2}}$$

$$- \frac{1}{\sqrt{\bar{x}_i^2 + \bar{y}_i^2 + \bar{z}^2}}$$

(38)

$$E_{u_0}(\bar{X}_g, \bar{Y}_g, \bar{z}_g, \bar{X}_{s_i}, \bar{Y}_{s_i}) = \frac{1}{\sqrt{(\bar{X}_i - \bar{r}_{o_{ik}})^2 + (\bar{Y}_k - 1)^2 + \bar{z}^2}}$$

$$- \frac{1}{\sqrt{\bar{X}_i^2 + \bar{Y}_k^2 + \bar{z}^2}} \qquad (39)$$

$$E_{u_i}(\bar{X}_g, \bar{Y}_g, \bar{z}_g, \bar{X}_{s_i}, \bar{Y}_{s_i}) = \frac{(\bar{X}_i - \bar{Y}_k \bar{r}_{ik})(\bar{Y}_k + \bar{X}_i \bar{r}_{ik}) + (\bar{X}_i - \bar{Y}_k \bar{r}_{ik}) \bar{r}_{ik}^2}{[(\bar{X}_i - \bar{Y}_k \bar{r}_{ik})^2 + \bar{z}^2 \bar{r}_{ik}^2] \sqrt{(\bar{X}_i + \bar{r}_{ik})^2 + (\bar{Y}_k + 1)^2 + \bar{z}^2}}$$

$$+ \frac{(\bar{Y}_k + \bar{X}_i \bar{r}_{ik}) \bar{r}_{ik}^2 \bar{z}^2}{(\bar{X}_i - \bar{Y}_k \bar{r}_{ik})[(\bar{X}_i - \bar{Y}_k \bar{r}_{ik})^2 + \bar{z}^2 \bar{r}_{ik}^2] \sqrt{\bar{X}_i^2 + \bar{Y}_k^2 + \bar{z}^2}}$$

$$- \frac{\bar{Y}_k + \bar{X}_i \bar{r}_{ik}}{(\bar{X}_i - \bar{Y}_k \bar{r}_{ik}) \sqrt{\bar{X}_i^2 + \bar{Y}_k^2 + \bar{z}^2}} \qquad (40)$$

$$E_{v_0}(\bar{X}_g, \bar{Y}_g, \bar{z}_g, \bar{X}_{s_i}, \bar{Y}_{s_i}) = \frac{(\bar{X}_i - \bar{Y}_k \bar{r}_{ik})(\bar{Y}_k + \bar{X}_i \bar{r}_{ik}) - (\bar{X}_i - \bar{Y}_k \bar{r}_{ik}) \bar{r}_{ik}^2}{[(\bar{X}_i - \bar{Y}_k \bar{r}_{ik})^2 + \bar{z}^2 \bar{r}_{ik}^2] \sqrt{(\bar{X}_i - \bar{r}_{ik})^2 + (\bar{Y}_k - 1)^2 + \bar{z}^2}}$$

$$+ \frac{(\bar{Y}_k + \bar{X}_i \bar{r}_{ik}) \bar{r}_{ik}^2 \bar{z}^2}{(\bar{X}_i - \bar{Y}_k \bar{r}_{ik})[(\bar{X}_i - \bar{Y}_k \bar{r}_{ik})^2 + \bar{z}^2 \bar{r}_{ik}^2] \sqrt{\bar{X}_i^2 + \bar{Y}_k^2 + \bar{z}^2}}$$

$$- \frac{\bar{Y}_k + \bar{X}_i \bar{r}_{ik}}{(\bar{X}_i - \bar{Y}_k \bar{r}_{ik}) \sqrt{\bar{X}_i^2 + \bar{Y}_k^2 + \bar{z}^2}} \qquad (41)$$

$$E_{w_i}(\bar{X}_g, \bar{Y}_g, \bar{z}_g, \bar{X}_{s_i}, \bar{Y}_{s_i}) = -\frac{\bar{z}\,\bar{r}_{i_{ik}}\,(\bar{Y}_i + \bar{x}_i\bar{r}_{i_{ik}}) + \bar{z}\,\bar{r}_{i_{ik}}^3}{[(\bar{x}_i - \bar{Y}_i\bar{r}_{i_{ik}})^2 + \bar{z}^2\bar{r}_{i_{ik}}^2]\sqrt{(\bar{x}_i + \bar{r}_{i_{ik}})^2 + (\bar{Y}_i + 1)^2 + \bar{z}^2}}$$

$$-\frac{(\bar{Y}_i + \bar{x}_i\bar{r}_{i_{ik}})\,\bar{r}_{i_{ik}}^3\,\bar{z}^3}{(\bar{x}_i - \bar{Y}_i\bar{r}_{i_{ik}})[(\bar{x}_i - \bar{Y}_i\bar{r}_{i_{ik}})^2 + \bar{z}^2\bar{r}_{i_{ik}}^2]\sqrt{\bar{x}_i^2 + \bar{Y}_i^2 + \bar{z}^2}}$$

$$+\frac{\bar{z}(\bar{Y}_i + x_i\bar{r}_{i_{ik}})\,\bar{r}_{i_{ik}}}{(\bar{x}_i - \bar{Y}_i\bar{r}_{i_{ik}})^2\sqrt{\bar{x}_i^2 + \bar{Y}_i^2 + \bar{z}^2}} \qquad (42)$$

$$E_{w_o}(\bar{X}_g, \bar{Y}_g, \bar{z}_g, \bar{X}_{s_i}, \bar{Y}_{s_i}) = -\frac{\bar{z}\,\bar{r}_{o_{ik}}\,(\bar{Y}_i + \bar{x}_i\bar{r}_{o_{ik}}) - \bar{z}\,\bar{r}_{o_{ik}}^3}{[(\bar{x}_i - \bar{Y}_i\bar{r}_{o_{ik}})^2 + \bar{z}^2\bar{r}_{o_{ik}}^2]\sqrt{(\bar{x}_i - \bar{r}_{o_{ik}})^2 + (\bar{Y}_i - 1)^2 + \bar{z}^2}}$$

$$-\frac{(\bar{Y}_i + \bar{x}_i\bar{r}_{o_{ik}})\,\bar{r}_{o_{ik}}^3\,\bar{z}^3}{(\bar{x}_i - \bar{Y}_i\bar{r}_{o_{ik}})[(\bar{x}_i - \bar{Y}_i\bar{r}_{o_{ik}})^2 + \bar{z}^2\bar{r}_{o_{ik}}^2]\sqrt{\bar{x}_i^2 + \bar{Y}_i^2 + \bar{z}^2}}$$

$$+\frac{\bar{z}\,(\bar{Y}_i + \bar{x}_i\bar{r}_{o_{ik}})\,\bar{r}_{o_{ik}}}{(\bar{x}_i - \bar{Y}_i\bar{r}_{o_{ik}})\sqrt{\bar{x}_i^2 + \bar{Y}_i^2 + \bar{z}^2}} \qquad (43)$$

As discussed in reference 2 the form of the influence equations (40) through (43) are such that $\bar{z}_g$ cannot be set equal to zero to obtain the flow on the surface of the wing without losing a substantial portion of the solution. This problem is due to the singular nature of these equations. Equations (42) and (43) will not be discussed further here since $\frac{w}{V_\infty}(x_g, y_g, 0) = \frac{\partial \bar{z}}{\partial x}(x_g, y_g, 0)$.

The first and third terms of equations (40) and (41) cause no special problem as $\bar{z}_g \to 0$. However, the second terms in these equations do contribute nonzero finite values to $\frac{u}{V_\infty}(x_g, y_g, 0)$ and $\frac{w}{V_\infty}(x_g, y_g, 0)$ at the tips and at span stations where kinks or cranks occur in the source lines. It is suggested in reference 2 that the influence equations be integrated in the freestream direction before letting $\bar{z}_g \to 0$. This integration was discussed in detail in reference 2 for the semi-infinite sheared source lines with $y_g = y_{s_\ell} = 0$. The same procedure used there to account for kink, crank, and tip effects when $\bar{z}_g = 0$ will also be used here.

If equations (38) through (41) are specialized to the case of $\bar{z}_g = 0$ and the second terms in equations (40) and (41) are replaced by expressions derived in references 2 and 6 , the following expressions are obtained for $E_{u_i}(\bar{x}_g, \bar{y}_g, 0, \bar{x}_{s_i}, \bar{y}_{s_\ell})$, $E_{u_o}(\bar{x}_g, \bar{y}_g, 0, \bar{x}_{s_i}, \bar{y}_{s_\ell})$, $E_{w_i}(\bar{x}_g, \bar{y}_g, 0, \bar{x}_{s_i}, \bar{y}_{s_\ell})$, and $E_{w_o}(\bar{x}_g, \bar{y}_g, 0, \bar{x}_{s_i}, \bar{y}_{s_\ell})$.

$$E_{u_i}(\bar{x}_g, \bar{y}_g, 0, \bar{x}_{s_i}, \bar{y}_{s_\ell}) = \frac{1}{\sqrt{(\bar{x}_i + \bar{r}_{i_\ell})^2 + (\bar{y}_\ell + 1)^2}} - \frac{1}{\sqrt{\bar{x}_i^2 + \bar{y}_\ell^2}} \tag{44}$$

$$E_{u_o}(\bar{x}_g, \bar{y}_g, 0, \bar{x}_{s_i}, \bar{y}_{s_\ell}) = \frac{1}{\sqrt{(\bar{x}_i - \bar{r}_{o_\ell})^2 + (\bar{y}_\ell - 1)^2}} - \frac{1}{\sqrt{\bar{x}_i^2 + \bar{y}_\ell^2}} \tag{45}$$

$$E_{w_i}(\bar{x}_g, \bar{y}_g, 0, \bar{x}_{s_i}, \bar{y}_{s_\ell}) = \frac{1}{(\bar{x}_i - \bar{y}_\ell \bar{r}_{i_\ell})} \left\{ \frac{(\bar{y}_\ell + \bar{x}_i \bar{r}_{i_\ell}) + \bar{r}_{i_\ell}^2}{\sqrt{(\bar{x}_i + \bar{r}_{i_\ell})^2 + (\bar{y}_\ell + 1)^2}} - \frac{(\bar{y}_\ell + \bar{x}_i \bar{r}_{i_\ell})}{\sqrt{\bar{x}_i^2 + \bar{y}_\ell^2}} \right\}$$

$$+ \frac{M_\infty \bar{r}_{i_\ell} y_g (.068 C_\ell - .122 |\beta y_g \bar{y}_\ell|) \log_e \left| \frac{\bar{r}_{i_\ell} + \bar{r}_{i_\ell}}{\bar{r}_{i_\ell} - \bar{r}_{i_\ell}} \right|}{2\pi C_\ell \sqrt{\left(\frac{x_g - x_{s_i}}{C_\ell}\right) - \left(\frac{x_{s_i} - x_{s_{i_\ell}}}{C_\ell}\right)^2} \left[.068 C_\ell + |\beta y_g \bar{y}_\ell| \right]} \tag{46}$$

$$E_{v_0}(\bar{X}_\ell, \bar{Y}_\ell, 0, \bar{X}_{s_\ell}, \bar{Y}_{s_\ell}) = \frac{1}{(\bar{X}_\ell - \bar{Y}_\ell T_{\ell_\ell})} \left\{ \frac{(\bar{Y}_\ell + \bar{X}_\ell T_{\ell_\ell}) - B_{\ell_\ell}^2}{\sqrt{(\bar{X}_\ell - T_{\ell_\ell})^2 + (\bar{Y}_\ell - 1)^2}} - \frac{(\bar{Y}_\ell + \bar{X}_\ell T_{\ell_\ell})}{\sqrt{\bar{X}_\ell^2 + \bar{Y}_\ell^2}} \right\}$$

$$+ \frac{M_i B_{\ell_\ell} y_\ell (.068\, C_\ell - .122 |B y_\ell \bar{Y}_\ell|) \log \left| \frac{B_{\ell_\ell} + T_{\ell_\ell}}{B_{\ell_\ell} - T_{\ell_\ell}} \right|}{2\pi C_\ell \sqrt{\left(\frac{X_{3_\ell} - X_{LE_\ell}}{C_\ell}\right) - \left(\frac{X_{3_\ell} - X_{LE_\ell}}{C_\ell}\right)} \left[.068\, C_\ell + |B y_\ell \bar{Y}_\ell| \right]}$$

(47)

The third terms in equations (46) and (47) are only evaluated when $|B y_\ell \bar{X}_\ell| \leq .557\, C_\ell$, when $i = j$, where j is the number of the panel aft of the leading edge on which the velocity is being computed, and when ℓ is at a span station where a break in a source line occurs. When these conditions are not all met the third terms are set equal to zero.

The expressions for the velocity components given in equations (35), (36), and (37) can be represented by the product of source influence matrices and the source strengths.

$$\left\{ \frac{u}{V_\infty} \right\} = \frac{1}{B^2} \left[\quad S_x \quad \right] \left\{ \frac{\sigma}{V_\infty} \right\} \tag{48}$$

$$\left\{ \frac{v}{V_\infty} \right\} = \frac{1}{B^2} \left[\quad S_y \quad \right] \left\{ \frac{\sigma}{V_\infty} \right\} \tag{49}$$

and

$$\left\{ \frac{w}{V_\infty} \right\} = \frac{1}{B^2} \left[\quad S_z \quad \right] \left\{ \frac{\sigma}{V_\infty} \right\} \tag{50}$$

where the elements of S_x , S_y , and S_z are computed from

$$S_x = \frac{1}{4\pi y_s}\left\{\left[\frac{E_{u_0}\tau_0 - E_{v_0}}{r_0}\right] - \left[\frac{E_{u_i}\tau_i - E_{v_i}}{r_i}\right]\right\} \tag{51}$$

$$S_y = \frac{1}{4\pi y_s}\left\{\left[\frac{E_{v_0}\tau_0 + E_{u_0}}{r_0}\right] - \left[\frac{E_{v_i}\tau_i + E_{u_i}}{r_i}\right]\right\} \tag{52}$$

and

$$S_z = \frac{1}{4\pi y_s}\left\{E_{w_0} - E_{w_i}\right\} \tag{53}$$

APPENDIX C

SKEWED VORTEX INFLUENCE EQUATIONS

The velocity induced by a skewed vortex in the plane of the wing can be derived from the Biot-Savart law. The expressions for the velocity relative to the wing coordinate frame will be derived for the incompressible case first and then modified by means of the Goethert transformation to account for compressibility. For the general skewed planar vortex shown in figure C-1 the total velocity $\vec{q}$ induced at point Q is the vector sum of the velocity induced by the four vortex segments $\infty A'$, $A'V$, VA, AND $A\infty$.

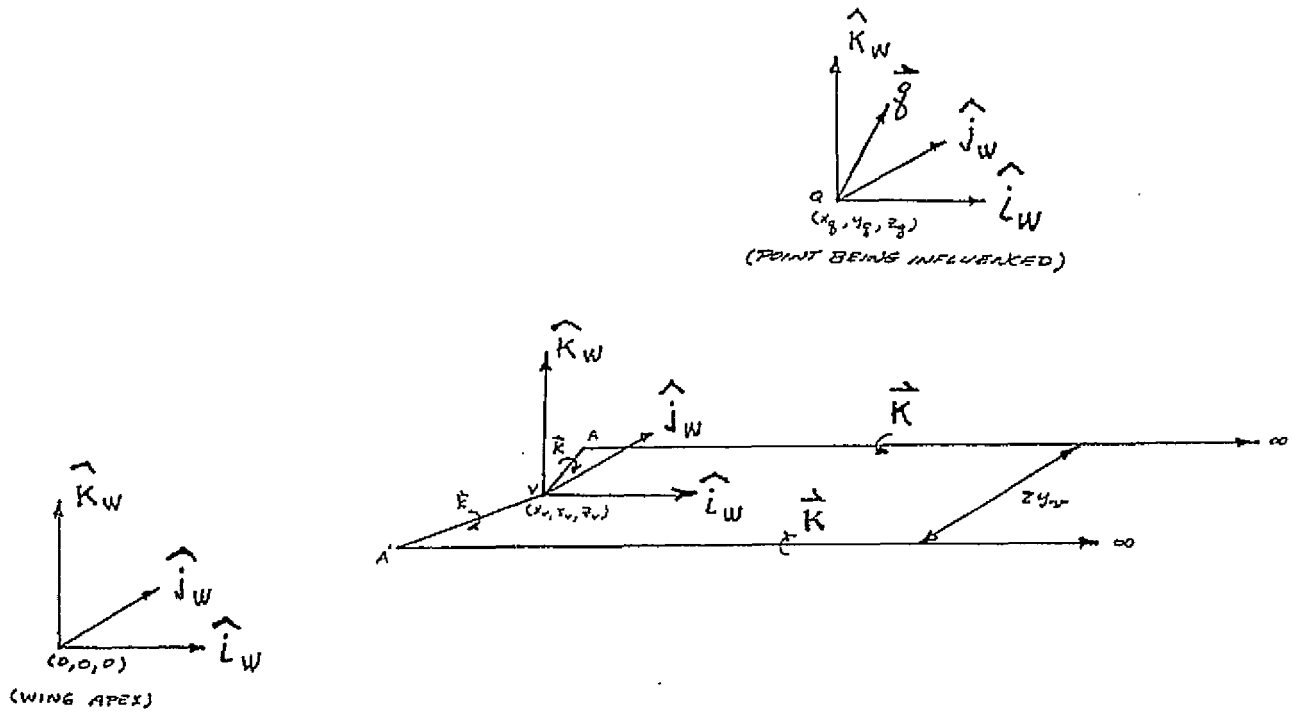

Figure C-1. Skewed Planar Vortex

The Biot-Savart law is given by the following expression:

$$|\vec{q}| = \frac{K}{4\pi|\vec{h}|}\oint \sin\varepsilon \, de \qquad (1)$$

where $|\vec{h}|$ is the perpendicular distance from the vortex segment to the point Q, and ε is the angle between the vortex segment and the line from the point Q to the increment of vortex segment being integrated. The integral is evaluated around the complete closed path ∞ A' V A ∞. The direction of the induced velocity is given by the following unit vector.

$$\hat{\nu} = \frac{\vec{k} \times \vec{h}}{|\vec{k} \times \vec{h}|} \tag{2}$$

The contribution from segment ∞A' is derived as follows.

$$\vec{q}_{\infty A'} = \frac{K}{4\pi \sqrt{(y^* + y_w)^2 + z^{*2}}} \left[\cos(0) - \cos(180 - \infty A'\Phi)\right] \hat{\nu}(\infty A'\Phi) \tag{3}$$

where

$$\begin{aligned} x^* &= x_B - x_V \\ y^* &= y_B - y_V \\ z^* &= z_B - z_V \end{aligned} \tag{4}$$

since

$\cos(0) = 1$

$$\cos(180 - \infty A'\Phi) = -\cos(\infty A'\Phi) = -\frac{x^* + y_w \tan\phi_L}{\left[(x^* + y_w \tan\phi_L)^2 + (y^* + y_w)^2 + z^{*2}\right]^{1/2}}$$

where ϕ_L is the sweep of the port side of the skewed vortex.

and

$$\hat{\nu}(\infty A'\Phi) = \left\{\frac{z^*}{\sqrt{(y^* + y_w)^2 + z^{*2}}}\right\} - \left\{\frac{y^* + y_w}{\sqrt{(y^* + y_w)^2 + z^{*2}}}\right\} \hat{k}_w$$

then:

$$\vec{q}_{\infty A'} = \frac{K}{4\pi\left[(y^* + y_w)^2 + z^{*2}\right]} \left\{\frac{x^* + y_w \tan\phi_L}{\left[(x^* + y_w \tan\phi_L)^2 + (y^* + y_w)^2 + z^{*2}\right]^{1/2}} + 1\right\} \left\{z^* \hat{j}_w - (y^* + y_V)\hat{k}_w\right\} \tag{5}$$

The contribution from segment A'V is determined similarly.

$$\vec{g}_{A'V} = \frac{K(\tan^2\phi_i + 1)^{1/2}}{4\pi\left[(x^* - y^*\tan\phi_i)^2 + z^{*2}(\tan^2\phi_i + 1)\right]^{1/2}}\left[\cos(\theta A'V) - \cos(180 - \theta VA')\right]\hat{n}(\theta A'V) \tag{6}$$

where

$$\cos(\theta A'V) = \frac{y^* + \cdots + (x^* + y_w\tan\phi_i)\tan\phi_i}{\left[\tan^2\phi_i + 1\right]^{1/2}\left[(x^* + y_w\tan\phi_i)^2 + (y^* + y_w)^2 + z^{*2}\right]^{1/2}}$$

$$\cos(180 - \theta VA') = \frac{y^* + x^*\tan\phi_i}{\left[\tan^2\phi_i + 1\right]^{1/2}\left[x^{*2} + y^{*2} + z^{*2}\right]^{1/2}}$$

and

$$\hat{n}(\theta A'V) = \frac{1}{\left[(x^* - y^*\tan\phi_i)^2 + z^{*2}(\tan^2\phi_i + 1)\right]^{1/2}}\left\{z^*\hat{\imath}_w - z^*\tan\phi_i\,\hat{\jmath}_w - (x^* - y^*\tan\phi_i)\hat{k}_w\right\}$$

therefore;

$$\vec{q}_{A'V} = \frac{K}{4\pi\left[(x^*-y^*\tan\phi_i)^2+z^{*2}(\tan^2\phi_i+1)\right]}\left\{\frac{y^*+x^*\tan\phi_i+y_w(1+\tan^2\phi_i)}{\left[(x^*+y_w\tan\phi_i)^2+(y^*+y_w)^2+z^{*2}\right]^{1/2}}\right.$$

$$\left.-\frac{y^*+x^*\tan\phi_i}{\left[x^{*2}+y^{*2}+z^{*2}\right]^{1/2}}\right\}\left\{z^*\hat{\ell}_w - z^*\tan\phi_i\,\hat{j}_w - (x^*-y^*\tan\phi_i)\hat{k}_w\right\} \qquad (7)$$

The expression for the contribution from segment VA is analogous to that of A'V. The angle ϕ_o is the sweep of the starboard portion of the skewed vortex.

$$\vec{q}_{VA} = \frac{K}{4\pi\left[(x^*-y^*\tan\phi_o)^2+z^{*2}(\tan^2\phi_o+1)\right]}\left\{\frac{y^*+x^*\tan\phi_o}{\left[x^{*2}+y^{*2}+z^{*2}\right]^{1/2}}\right.$$

$$\left.-\frac{y^*+x^*\tan\phi_o-y_w(1+\tan^2\phi_o)}{\left[(x^*-y_w\tan\phi_o)^2+(y^*-y_w)^2+z^{*2}\right]^{1/2}}\right\}\left\{z^*\hat{\ell}_w - z^*\tan\phi_o\,\hat{j}_w - (x^*-y^*\tan\phi_o)\hat{k}\right\} \qquad (8)$$

The velocity induced by the semi-infinite trailing vortex $A\infty$ is analogous to that of $\infty A'$. Therefore;

$$\vec{q}_{A\infty} = \frac{K}{4\pi\left[(y^*-y_r)^2+z^{*2}\right]}\left\{\frac{x^*-y_r\tan\phi_0}{\left[(x^*-y_r\tan\phi_0)^2+(y^*-y_r)^2+z^{*2}\right]^{1/2}}+1\right\}\left\{-z^*j_w+(y^*-y_r)\hat{k}\right\} \quad (9)$$

If the Goethert transformation is made and the coordinates nondimensionalized in terms of the semi-width of the skewed vortex, the following expressions for the nondimensional induced velocity ratios are obtained.

$$\frac{u_r}{V_\infty} = \frac{(K/V_\infty)E_u}{4\pi y_r z} \quad , \quad \frac{v_r}{V_\infty} = \frac{(K/V_\infty)E_v}{4\pi y_r z} \quad , \text{ AND } \quad \frac{w_r}{V_\infty} = \frac{(K/V_\infty)E_w}{4\pi y_r z} \qquad (10)$$

where

$$E_u = z'\left[\frac{(I_2+I_3)}{R_3^2} + \frac{(I_4+I_5)}{R_5^2}\right]$$

$$E_v = z'\left[\frac{(I_1+1)}{R_1^2} - \frac{(I_6+1)}{R_6^2} - \frac{(I_2+I_3)\tan\phi_{ii}}{R_3^2} - \frac{(I_4+I_5)\tan\phi_{oi}}{R_5^2}\right] \qquad (11)$$

$$E_w = \left[\frac{(y'-1)(I_6+1)}{R_6^2} - \frac{(y'+1)(I_1+1)}{R_1^2} - \frac{(x'-y'\tan\phi_{ii})(I_2+I_3)}{R_3^2}\right.$$

$$\left. - \frac{(x'-y'\tan\phi_{oi})(I_4+I_5)}{R_5^2}\right]$$

and

$$R_1^2 = [(y'+1)^2 + z'^2]$$

$$R_2^2 = [(x'-y'\tan\phi_{ii})^2 + z'^2(\tan^2\phi_{ii}+1)]$$

$$R_3^2 = [(x'-y'\tan\phi_{oi})^2 + z'^2(\tan^2\phi_{oi}+1)]$$

$$R_4^2 = [(y'-1)^2 + z'^2]$$

$$I_1 = \frac{x' + \tan\phi_{ii}}{[(x'+\tan\phi_{ii})^2+(y'+1)^2+z'^2]^{1/2}}$$

$$I_2 = \frac{y' + x'\tan\phi_{ii} + (1+\tan^2\phi_{ii})}{[(x'+\tan\phi_{ii})^2+(y'+1)^2+z'^2]^{1/2}}$$

$$I_3 = \frac{y' + x'\tan\phi_{ii}}{[x'^2+y'^2+z'^2]^{1/2}} \qquad (12)$$

$$I_4 = \frac{y' + x'\tan\phi_{oi}}{[x'^2+y'^2+z'^2]^{1/2}}$$

$$I_5 = -\frac{y' + x'\tan\phi_{oi} - (1+\tan^2\phi_{oi})}{[(x'-\tan\phi_{oi})^2+(y'-1)^2+z'^2]^{1/2}}$$

$$I_6 = \frac{x' - \tan\phi_{oi}}{[(x'-\tan\phi_{oi})^2+(y'-1)^2+z'^2]^{1/2}}$$

The nondimensional coordinates (x', Y', Z') are defined as follows.

$$x' = \frac{x_s - x_v}{\beta\, y_r} \quad , \quad y' = \frac{y_s - y_v}{y_r} \quad , \quad z' = \frac{z_s - z_v}{y_r} \tag{13}$$

$$\tan\phi_{ii} = \frac{1}{\beta}\tan\phi_i \quad , \text{ AND } \quad \tan\phi_{oi} = \frac{1}{\beta}\tan\phi_o$$

The equations for the velocity ratios can be simplified for the following conditions.

1) if R_2^2 or R_3^2 equal zero, then the terms in which these quantities appear can be neglected.

2) if $\phi_{ii} = \phi_{oi}$ then the third and fourth terms of E_v and E_w can be replaced by

$$-\frac{(I_2 + I_5)\tan\phi}{R^2} \quad \text{IN} \quad E_v$$

and

$$-\frac{(I_5 + I_2)(x' - y'\tan\phi)}{R^2} \quad \text{IN} \quad E_w$$

where $\phi = \phi_{ii} = \phi_{oi}$ and $R^2 = R_2^2 = R_3^2$

It should be noted that the condition $\phi_{ii} = \phi_{oi}$ is satisfied at every span station except where there is a discontinuity in the rate of change of leading or trailing sweep.

The equations can be specialized to that used in near planar lifting surface theory. In that case Z' is assumed small enough that only the upwash is considered in the determination of the wing vorticity. The influence function E_W then becomes:

$$E_W = \frac{1}{y'-1}\left\{\frac{x'-\tan\phi_{oi}}{\left[(x'-\tan\phi_{oi})^2+(y'-1)^2\right]^{1/2}}+1\right\} - \frac{1}{y'+1}\left\{\frac{x'+\tan\phi_{ii}}{\left[(x'+\tan\phi_{ii})^2+(y'+1)^2\right]^{1/2}}+1\right\}$$

$$-\frac{1}{(x'-y'\tan\phi_{ii})}\left\{\frac{y'+x'\tan\phi_{ii}+(1+\tan^2\phi_{ii})}{\left[(x'+\tan\phi_{ii})^2+(y'+1)^2\right]^{1/2}}-\frac{y'+x'\tan\phi_{ii}}{\left[x'^2+y'^2\right]^{1/2}}\right\} \qquad (14)$$

$$-\frac{1}{(x'-y'\tan\phi_{oi})}\left\{\frac{y'+x'\tan\phi_{oi}}{\left[x'^2+y'^2\right]^{1/2}}-\frac{y'+x'\tan\phi_{oi}-(1+\tan^2\phi_{oi})}{\left[(x'-\tan\phi_{oi})^2+(y'-1)^2\right]^{1/2}}\right\}$$

The third and fourth terms in E_W can be neglected when $(x' - y' \tan \phi_{ii})$ or $(x' - y' \tan \phi_{oi})$ equal zero respectively. Also, when $\phi_{ii} = \phi_{oi}$ the third and fourth terms can be replaced by:

$$-\frac{1}{(x'-y'\tan\phi)}\left\{\frac{y'+x'\tan\phi+(1+\tan^2\phi)}{\left[(x'+\tan\phi)^2+(y'+1)^2\right]^{1/2}}-\frac{y'+x'\tan\phi-(1+\tan^2\phi)}{\left[(x'-\tan\phi)^2+(y'-1)^2\right]^{1/2}}\right\}$$

where $\phi = \phi_{ii} = \phi_{oi}$

The components of velocity induced by the skewed vortices can be written as the product of vortex influence matrices and the vortex strengths.

$$\left\{\frac{u}{V_\infty}\right\} = \left[\quad A_x \quad\right]\left\{\frac{K}{V_\infty}\right\} \tag{15}$$

$$\left\{\frac{v}{V_\infty}\right\} = \left[\quad A_y \quad\right]\left\{\frac{K}{V_\infty}\right\} \tag{16}$$

and

$$\left\{\frac{w}{V_\infty}\right\} = \left[\quad A_z \quad\right]\left\{\frac{K}{V_\infty}\right\} \tag{17}$$

where the elements of A_x , A_y , and A_z are computed from

$$A_x = \frac{E_u}{4\pi y_r^2} \tag{18}$$

$$A_y = \frac{E_v}{4\pi y_r^2} \tag{19}$$

and

$$A_z = \frac{E_w}{4\pi y_r^2} \tag{20}$$

Appendix D

QUADRILATERAL VORTEX INFLUENCE EQUATIONS

The Biot-Savart law can be used to calculate the influence of a finite vortex segment on a point in three-dimensional space. The incremental change in induced velocity at a point in space due to an incremental change in length of a finite vortex is given by the following expression.

$$dq = \frac{K \cos \phi \quad d\phi}{4\pi h} \tag{1}$$

where;

K = Vortex strength

h = Perpendicular distance from the vortex segment to the point in space.

ϕ = Angle between the line formed by h and a line from the field point to a point on the vortex segment.

q = Velocity induced by the finite vortex segment perpendicular to the plane formed by h and the vortex segment.

A vector expression for $\vec{q}$ can be determined from figure (D-1):

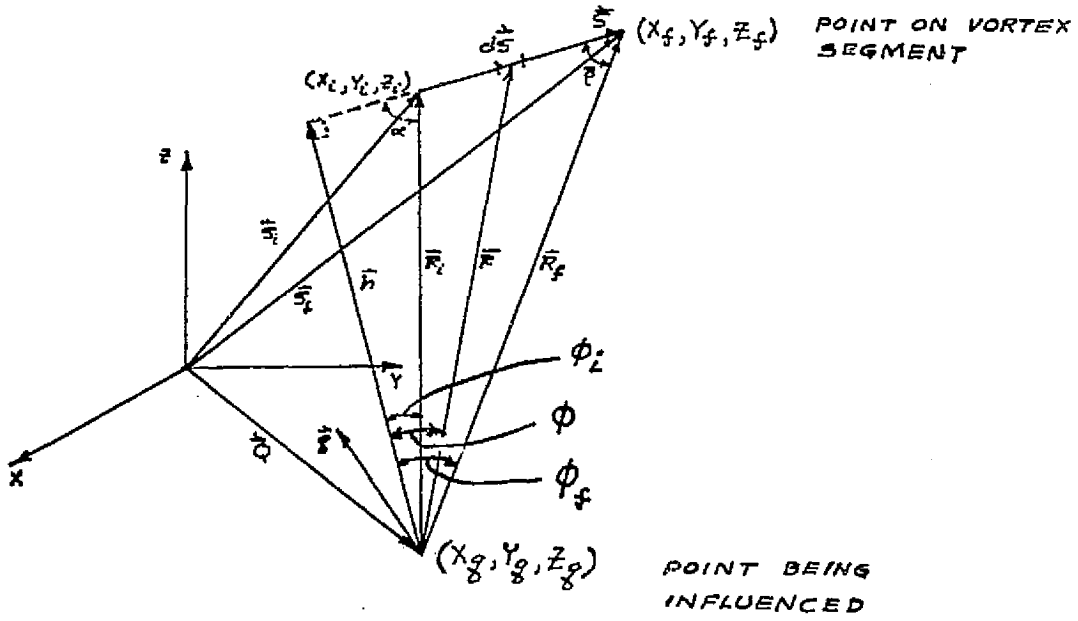

Figure D-1. Velocity Induced by Finite Vortex Segment

The magnitude of the velocity $\vec{q}$ induced at (x_3 , y_3 , z_3) by the vortex segment $\vec{s}$ is given by the following equation after equation (1) has been integrated from ϕ_i to ϕ_f .

$$|\vec{q}| = \frac{K}{4\pi h}(\cos\beta - \cos\alpha) \tag{2}$$

where

$$\cos\beta = \frac{\vec{s}\cdot\vec{r}_f}{|s||r_f|}$$

$$\cos\alpha = \frac{\vec{s}\cdot\vec{r}_i}{|s||r_i|}$$

The vector $\vec{h}$ is determined such that it satisfies the conditions of being perpendicular to $\vec{s}$ and equal to the vector sum $\vec{h} = \vec{r}_f - a\vec{s}$ where "a" defines the length of $\vec{h}$.

Since;

$$\vec{h} = \vec{r}_f - a\vec{s} \tag{3}$$

and

$$\vec{h}\cdot\vec{s} = 0 \tag{4}$$

then

$$\vec{h}\cdot\vec{s} = \vec{r}_f\cdot\vec{s} - a\vec{s}\cdot\vec{s} = 0 \tag{5}$$

therefore;

$$a = \frac{\vec{r}_f\cdot\vec{s}}{\vec{s}\cdot\vec{s}} \tag{6}$$

After substituting "a" into equation (3), $\bar{h}$ is defined as;

$$\vec{h} = \vec{r_q} - \frac{\vec{r_q} \cdot \vec{s}}{\vec{s} \cdot \vec{s}} \vec{s} \tag{7}$$

Also, a unit vector $\hat{g}$ in the direction of $\vec{g}$ is seen to be equal to;

$$\hat{g} = \frac{\vec{r_q} \times \vec{s}}{|\vec{r_q} \times \vec{s}|} \tag{8}$$

The magnitude and direction of $\vec{g}$ are then expressed in terms of the coordinates of the control point (x_q , y_q , z_q) and the end points of the vortex segment (x_i , y_i , z_i) and (x_f , y_f , z_f). If $\hat{i}$, $\hat{j}$ and $\hat{k}$ are defined as unit vectors in the x , y , and z directions respectively, then;

$$\vec{s} = \vec{s_f} - \vec{s_i} = (x_f - x_i)\hat{i} + \beta^2(y_f - y_i)\hat{j} + \beta^2(z_f - z_i)\hat{k}$$

$$\vec{r_i} = \vec{s_i} - \vec{q} = (x_i - x_q)\hat{i} + \beta^2(y_i - y_q)\hat{j} + \beta^2(z_i - z_q)\hat{k} \tag{9}$$

and

$$\vec{r_f} = \vec{s_f} - \vec{q} = (x_f - x_q)\hat{i} + \beta^2(y_f - y_q)\hat{j} + \beta^2(z_f - z_q)\hat{k} \tag{10}$$

The value of "a" is then expressed as;

$$a = \frac{\vec{r_f} \cdot \vec{s}}{\vec{s} \cdot \vec{s}} = \frac{(x_f - x_q)(x_f - x_i) + \beta^2(y_f - y_q)(y_f - y_i) + \beta^2(z_f - z_q)(z_f - z_i)}{(x_f - x_i)^2 + \beta^2(y_f - y_i)^2 + \beta^2(z_f - z_i)^2} \tag{11}$$

and the components of $\bar{h}$ by,

$$h_x = (x_f - x_g) - \left[\frac{(x_f - x_g)(x_f - x_i) + (Y_f - Y_g)(Y_f - Y_i)\beta^2 + (z_f - z_g)(z_f - z_i)\beta^2}{(x_f - x_i)^2 + (Y_f - Y_i)^2\beta^2 + (z_f - z_i)^2\beta^2}\right](x_f - x_i)$$

$$h_Y = (Y_f - Y_g) - \left[\frac{(x_f - x_g)(x_f - x_i) + (Y_f - Y_g)(Y_f - Y_i)\beta^2 + (z_f - z_g)(z_f - z_i)\beta^2}{(x_f - x_i)^2 + \beta^2(Y_f - Y_i)^2 + (z_f - z_i)^2\beta^2}\right] \tag{12}$$

$$h_z = (z_f - z_g) - \left[\frac{(x_f - x_g)(x_f - x_i) + \beta^2(Y_f - Y_g)(Y_f - Y_i) + \beta^2(z_f - z_g)(z_f - z_i)}{(x_f - x_i)^2 + \beta^2(Y_f - Y_i)^2 + \beta^2(z_f - z_i)^2}\right](z_f - z_i)$$

The magnitude of $\bar{g}$ is found by substituting $h = |\bar{h}| = \sqrt{h_x^2 + h_y^2 + h_z^2}$ and the following expressions for $\cos\alpha$ and $\cos\beta$ into equation (2).

$$\cos\alpha = \frac{(x_f - x_i)(x_i - x_g) + \beta^2(Y_f - Y_i)(Y_i - Y_g) + \beta^2(z_f - z_i)(z_i - z_g)}{\sqrt{(x_f - x_i)^2 + \beta^2(Y_f - Y_i)^2 + \beta^2(z_f - z_i)^2}\sqrt{(x_i - x_g)^2 + \beta^2(Y_i - Y_g)^2 + \beta^2(z_i - z_g)^2}}$$

$$\cos\beta = \frac{(x_f - x_i)(x_f - x_g) + \beta^2(Y_f - Y_i)(Y_f - Y_g) + \beta^2(z_f - z_i)(z_f - z_g)}{\sqrt{(x_f - x_i)^2 + \beta^2(Y_f - Y_i)^2 + \beta^2(z_f - z_i)^2}\sqrt{(x_f - x_g)^2 + \beta^2(Y_f - Y_g)^2 + \beta^2(z_f - z_g)^2}} \tag{13}$$

The components of the vector $\bar{g}$ are then given by the multiplication of the components of equation (8) by $|\bar{g}|$.

$$g_x = \frac{|\bar{g}|[(Y_f - Y_g)(z_f - z_i) - (z_f - z_g)(Y_f - Y_i)]\beta^2}{|\bar{r} \times \bar{s}|}$$

$$g_Y = \frac{|\bar{g}|[(x_f - x_i)(z_f - z_g) - (z_f - z_i)(x_f - x_g)]\beta^2}{|\bar{r} \times \bar{s}|} \tag{14}$$

$$g_z = \frac{|\bar{g}|[(x_f - x_g)(Y_f - Y_i) - (Y_f - Y_g)(x_f - x_i)]\beta^2}{|\bar{r} \times \bar{s}|}$$

where

$$|\vec{R}\times\vec{S}| = \{[(Y_f - Y_g)(Z_f - Z_i) - (Z_f - Z_g)(Y_f - Y_i)]^2$$

$$+[(X_f - X_i)(Z_f - Z_g) - (Z_f - Z_i)(X_f - X_g)]^2$$

$$+[(X_f - X_g)(Y_f - Y_i) - (Y_f - Y_g)(X_f - X_i)]^2\}^{1/2} \qquad (15)$$

The velocity induced at a control point by a vortex segment is then given by equation (14). Since a curved vortex can be represented by a number of straight segments, this equation can be used to compute the induced flow produced by a vortex of arbitrary shape.

The components of velocity induced by a quadrilateral vortex can be written as ratios computed by the product of influence matrices and the vortex strengths.

$$\left\{\frac{u}{V_\infty}\right\} = \left[\ A_x\ \right]\left\{\frac{K}{V_\infty}\right\} \qquad (16)$$

$$\left\{\frac{v}{V_\infty}\right\} = \left[\ A_y\ \right]\left\{\frac{K}{V_\infty}\right\} \qquad (17)$$

and

$$\left\{\frac{w}{V_\infty}\right\} = \left[\ A_z\ \right]\left\{\frac{K}{V_\infty}\right\} \qquad (18)$$

where the elements of A_x , A_y , and A_z , are computed from the following equations.

$$A_x = \sum \frac{R^2[\cos\beta - \cos\alpha][(Y_f - Y_g)(Z_f - Z_i) - (Z_f - Z_g)(Y_f - Y_i)]}{4\pi|\vec{h}||\vec{R}\times\vec{S}|} \qquad (19)$$

$$A_y = \sum \frac{R[\cos\beta - \cos\alpha][(X_f - X_i)(Z_f - Z_g) - (Z_f - Z_i)(X_f - X_g)]}{4\pi|\vec{h}||\vec{R}\times\vec{S}|} \qquad (20)$$

and

$$A_z = \sum \frac{\vec{z}[\cos\vec{z} - \cos\alpha]\pi(x_f - x_g)(Y_f - Y_i) - (Y_f - Y_g)(x_f - x_i)]}{4\pi|\vec{h}||\vec{e}\times\vec{s}|} \qquad (21)$$

The Σ sign indicates that the contributions from all of the sides of the quadrilateral vortex are summed.

Appendix E

SOURCE FRUSTUM INFLUENCE EQUATIONS

The flow through nacelle is represented by a distribution of source frustums on the surface of the nacelle. The expressions for the velocity induced by a source frustum are given in reference 22. If the nacelle is defined by a series of points (XI_i , $YI_i = \beta YI_i$), and these points represent the ends of the frustums, then the midpoints of the frustums are given by;

$$XZ_i = \frac{XI_{i+1} + XI_i}{2} \tag{1}$$

$$YZ_i = \frac{YI_{i+1} + YI_i}{2} \tag{2}$$

The surface lengths of the frustums are defined by;

$$\Delta S_i = \left[(XI_{i+1} - XI_i)^2 + (YI_{i+1} - YI_i)^2 \right]^{1/2} \tag{3}$$

and the X_N component of the vector normal to the frustum surface is given by;

$$N_{X_N} = - \frac{YI_{i+1} - YI_i}{\Delta S_i} = - \sin \alpha_{N_i} \tag{4}$$

The Y_N component of the frustum normal vector is given by;

$$N_{Y_N} = \frac{XI_{i+1} - XI_i}{\Delta S_i} = \cos \alpha_{N_i} \tag{5}$$

If the points being influenced are denoted by (XZ_i, YZ_i), then the velocity ratios induced by a frustum of unit strength at (XZ_j, YZ_j) in the X_N and Y_N directions are given by;

$$\left(\frac{V_{X_N}}{V_\infty} \right)_{ij} = - 4 \int_0^{\Delta S_j} F_{ij} \, dS_j \tag{6}$$

and

$$\left(\frac{V_{rw}}{V_\infty}\right)_{ij} = -2\int_0^{\Delta S_j} E_{ij}\, dS_j \tag{7}$$

respectively.

Where, from reference 22;

$$E_{ij} = \frac{1}{(YZ_i - Y_j)^2 + (XZ_i - X_j)^2}\ \frac{Y_j (XZ_i - X_j) E(K_{ij})}{\left[(YZ_i + Y_j)^2 + (XZ_i - X_j)^2\right]^{1/2}} \tag{8}$$

and

$$E_{Zij} = \frac{Y_j}{YZ_j\left[(YZ_i + Y_j)^2 + (XZ_i - X_j)^2\right]^{1/2}}\left[K(K_{ij}) + E(K_{ij})\ \frac{YZ_i^2 - Y_j - (XZ_i - X_j)^2}{(XZ_i - Y_j)^2 + (XZ_i - X_j)^2}\right] \tag{9}$$

Also where;

$$X_j = X1_j + S_j \cos\alpha_{Nj} \tag{10}$$

$$Y_j = Y1_j + S_j \sin\alpha_{Nj} \tag{11}$$

and S_j is the surface distance measured from $(X1_j, Y1_j)$ along the j^{th} frustum. $K(K_{ij})$ and $E(K_{ij})$ are complete elliptic integrals of the first and second kind, respectively. Where,

$$K_{ij} = \left[\frac{4(Y_j)(YZ_i)}{(YZ_i + Y_j)^2 + (XZ_i - X_j)^2}\right]^{1/2} \tag{12}$$

For the special case where (XZ_i, YZ_i) and (XZ_j, YZ_j) are the same point;

$$\left(\frac{V_{Zii}}{V_\infty}\right)_{ii} = 2\pi \sin\alpha_{Ni} + \sin\alpha_{Ni}\cos\alpha_{Ni}\left[2S_i + \left(\frac{13}{6} + \ln\frac{S_i}{8} + \sin^2\alpha_{Ni}\right)\frac{S_i^2}{12}\right] \tag{13}$$

and

$$\left(\frac{V_{YN}}{V_\infty}\right)_{ii} = -2\pi\cos\alpha_{N_i} + 2\left(\sin^2\alpha_{N_i} + \ln\frac{s_i}{8}\right)s_i$$

$$-\left(3 + 3\ln\frac{s_i}{8} - 3\sin^2\alpha_{N_i} - 2\sin^4\alpha_{N_i}\right)\frac{s_i^3}{24} \tag{14}$$

where $s_i = \frac{\Delta s_i}{2 Yz_i} \leq .08$

for $s_i > .08$, set $s_i = .08$ and use;

$$\left(\frac{V_{YN}}{V_\infty}\right)_{ii} = -2\pi\cos\alpha_{N_i} + 2\left(\sin^2\alpha_{N_i} + \ln\frac{s_i}{8}\right)s_i$$

$$-\left(3 + 3\ln\frac{s_i}{8} - 3\sin^2\alpha_{N_i} - 2\sin^4\alpha_{N_i}\right)\frac{s_i^3}{24}$$

$$-2\int_0^{uL} F_{ii}\,ds_i - 2\int_{LL}^{\Delta s_i} F_{ii}\,ds_i \tag{15}$$

and

$$\left(\frac{V_{XN}}{V_\infty}\right)_{ii} = -2\pi\sin\alpha_{N_i} + \sin\alpha_{N_i}\cos\alpha_{N_i}\left[2s_i + \left(\frac{13}{6} + \ln\frac{s_i}{8} + \sin^2\alpha_{N_i}\right)\frac{s_i^3}{12}\right]$$

$$-4\int_0^{uL} F_{ij}\,ds_i - 4\int_{LL}^{\Delta s_i} F_{ii}\,ds_i \tag{16}$$

where

$$ds_i = \frac{\Delta s_i/2 - .08 Yz_i}{32}$$

$$uL = \frac{\Delta s_i}{2} - .08 Yz_i$$

$$LL = \frac{\Delta s_i}{2} + .08 Yz_i$$

The velocity ratios in the X_N and Y_N directions are then given by:

$$\left\{\frac{u}{V_\infty}\right\} = \left[\ S_x\ \right]\left\{\frac{q}{V_\infty}\right\} \tag{17}$$

and

$$\left\{\frac{v}{V_\infty}\right\} = \left[\ S_y\ \right]\left\{\frac{q}{V_\infty}\right\} \tag{18}$$

where the elements of S_x and S_y are;

$$S_x = \frac{V_{x_N}}{V_\infty} \tag{19}$$

and

$$S_y = \frac{V_{y_N}}{V_\infty} \tag{20}$$

APPENDIX F

WING AND PYLON VORTICITY SERIES

A modified double Fourier series suitable for representing the loading component of vorticity over a thin wing in subsonic flow will be derived in this section. The series will be general enough to represent the loading over a wing of arbitrary planform, twist and camber, and with leading and trailing edge flaps. The boundary conditions of zero net load at the wing tips and trailing edge are satisfied by all the terms in the series.

A series applicable to wings with continuous spanwise variations of leading and trailing edge sweeps and chordwise variations of mean camber line slopes was first developed by Blenk (12). The series was derived by combining the expression for the spanwise variation of circulation developed by Betz (13) with the expression for the chordwise variation of vorticity developed by Birnbaum (14). The expressions by Betz and Birnbaum were derived by means of thin wing section and lifting line theory, respectively.

The general expression derived here will be developed in the same way as that by Blenk. An expression such as Blenk's will be derived first and then modified to represent planforms of arbitrary shape and wings with leading and trailing edge flaps. Even though the expression will be derived for a thin wing in a uniform flow it will be applicable to a wing-pylon-fanpod-nacelle combination if the induced flow from the fanpod and nacelle is smooth and continuous and if the coefficients in the series are determined such that the boundary conditions over the wing, pylon, fanpod, and nacelle are satisfied simultaneously.

In thin airfoil theory, where the camber is assumed small enough to replace the singularities on the mean camber surface by singularities in a reference plane, the velocity induced by a chordwise distribution of vorticity $\gamma(x)$ is given by the following expression.

$$V_i(x_0) = -\frac{1}{2\pi}\int_{L.E.}^{T.E.} \frac{\gamma(x)\,dx}{x_0 - x} \qquad (1)$$

Where x is measured from the leading edge and x_0 is the location of the point being influenced. To satisfy the boundary condition of zero net flow through the mean camber surface of the airfoil, the sum of the normal components of velocity due to the freestream and the distribution of vorticity is set equal to zero. The following constraint equation results.

$$V_i(x_0) + V_\infty\left(\alpha - \frac{dz}{dx}\right) = 0 \qquad (2)$$

where α is the airfoil angle of attack and $\frac{dz}{dx}$ is the slope of the mean camber surface. Substituting (1) into (2) gives;

$$\frac{1}{2\pi}\int_0^c \frac{\gamma(x)\,dx}{x_0 - x} = V_\infty\left(\alpha - \frac{dz}{dx}\right)_0 \tag{3}$$

This equation can be transformed into polar coordinates using;

$$x = \frac{c}{2}(1-\cos\theta)$$

to obtain

$$\frac{1}{2\pi}\int_0^\pi \frac{\gamma(\theta)\sin\theta\,d\theta}{\cos\theta - \cos\theta_0} = V_\infty\left(\alpha - \frac{dz}{dx}\right)_0 \tag{4}$$

and solved for $\gamma(\theta)$. The flat plate solution is already known from the Joukowski transformation of the flow over a rotating circular cylinder such that the Kutta condition is satisfied. This solution is given by;

$$\gamma_1(\theta) = 2V_\infty A_0 \cot\theta/2 \tag{5}$$

where A_0 is a constant. It can be shown that A_0 not only equals α for a flat plate but also equals α in the case of an airfoil with camber which is symmetrical about $x = \frac{c}{2}$.

In general the distribution of vorticity over a cambered airfoil is a combination of a term such as in equation (5) and an infinite series which can account for any arbitrary deviation in vorticity about the $\cot\theta/2$ term. A series which satisfies the Kutta condition and when combined with the $\cot\theta/2$ term is sufficient to represent the vorticity over any cambered airfoil is the following infinite series.

$$\gamma_2(\theta) = 2V_\infty \sum_{N=1}^{\infty} A_N \sin N\theta \tag{6}$$

If equation (6) is substituted into equation (1)

$$\frac{1}{\pi}\int_0^\pi \frac{\sin\theta \sum_{N=1}^{\infty} A_N \sin N\theta}{\cos\theta - \cos\theta_0}\,d\theta = \frac{V_i}{V_\infty}(\theta_0) \tag{7}$$

and integrated the following expression for $\frac{V_i}{V_\infty}(\theta_0)$ is obtained.

$$\frac{V_i}{V_\infty}(\theta_0) = \sum_{N=1}^{\infty} A_N \cos N\theta \tag{8}$$

Since equation (6) and equation (8) are Fourier conjugates, equation (7) can be inverted to obtain a general integral expression for $\gamma_2(\theta)$ in terms of any arbitrary $\frac{V_i}{V_\infty}(\theta_0)$ which satisfies equation (8).

$$\gamma_2(\theta) = \frac{2V_\infty}{\pi}\int_0^{\pi} \frac{\frac{V_i}{V_\infty}(\theta_0)\sin\theta}{\cos\theta - \cos\theta_0}\, d\theta_0 \tag{9}$$

This expression can be used to reduce the requirement of an infinite series, to represent the vorticity over airfoils with discontinuous free-stream slopes such as in the case of leading or trailing edge flaps, to that of a finite series. This is done by representing the net pressures due to a smooth camber and angle of attack by a combination of $\gamma_1(\theta)$ and a finite form of $\gamma_2(\theta)$ such that;

$$\gamma(\theta) = \gamma_1(\theta) + \gamma_2(\theta) = 2V_\infty\left[A_0 \cot\theta/2 + \sum_{N=1}^{N_0-1} A_N \sin N\theta\right] \tag{10}$$

then adding to this expression additional terms evaluated from equation (9) for distributions associated with leading and trailing edge flaps. It should be noted that both $\gamma_1(\theta)$ and $\gamma_2(\theta)$ are needed to represent smooth cambers which are nonsymmetric about $x = c/2$, even if α equals zero. This is because the antisymmetric sine terms in equation (10) contribute to the value of A_0. For the same reason both $\gamma_1(\theta)$ and $\gamma_2(\theta)$ along with the additional terms from equation (9) must in general be used to represent either leading or trailing edge flap deflections.

The relation between the sine terms, α, and A_0 is derived in reference (15) and repeated below

$$A_0 = \alpha - \sum_{m=1}^{(N_0-2)\le 2m\le(N_0-1)} \frac{A_{2m}}{4m^2-1} \tag{11}$$

This relation demonstrates the dependence between the terms in equation (10). This dependence could cause the influence matrix, eventually to be inverted to solve for the coefficients A_0 and A_N, to be illconditioned. In the limit as $N \to \infty$ it can be shown that $\cot\theta/2 = \sum_{n=1}^{\infty} \sin n\cdot\theta$ for $0<\theta<\pi$ which would make the influence matrix singular. This can be avoided if the influence is considered over the complete range $0 \le \theta \le \pi$ as done by Wagner (15).

Due to the finite nature of the series in equation (10) and the convenience to be derived from its use, equation (10) and its modification to account for flaps will be used here. It is thought that the above mentioned problems can be minimized by judicious selection of the points where the boundary conditions are to be satisfied.

The special chordwise terms needed to account for trailing edge flaps can be derived by setting $\frac{v_i}{V_\infty}(\theta_0) = 0$ for $0 \le \theta_0 < \theta_f$ and $\frac{v_i}{V_\infty}(\theta_0) = \delta_f$ for $\theta_f \le \theta_0 \le \pi$ in equation (9) and integrating over the chord. Where θ_f is the trailing edge flap hinge location and δ_f the deflection

$$\gamma_f(\theta) = \frac{2V_\infty}{\pi} \int_{\theta_f}^{\pi} \frac{\delta_f \sin\theta}{\cos\theta - \cos\theta_0} \, d\theta_0 \tag{12}$$

$$= \frac{2V_\infty}{\pi} \delta_f \left[\log_e \left| \frac{\sin\frac{1}{2}(\theta - \theta_0)}{\sin\frac{1}{2}(\theta + \theta_0)} \right| \right]_{\theta_f}^{\pi}$$

$$\gamma_f(\theta) = \frac{2V_\infty \delta_f}{\pi} \log_e \left| \frac{\sin\frac{1}{2}(\theta + \theta_f)}{\sin\frac{1}{2}(\theta - \theta_f)} \right| \tag{13}$$

A similar expression can be obtained for leading edge flaps by setting $\frac{v_i}{V_\infty} = -\delta_k$ for $0 \le \theta_0 \le \theta_k$ and $\frac{v_i}{V_\infty} = 0$ for $\theta_k < \theta_0 \le \pi$, where θ_k is the leading edge flap hinge location and δ_k the deflection. After evaluating equation (9) the following expression is obtained.

$$\gamma_k(\theta) = \frac{2V_\infty \delta_k}{\pi} \log_e \left| \frac{\sin\frac{1}{2}(\theta + \theta_k)}{\sin\frac{1}{2}(\theta - \theta_k)} \right| \tag{14}$$

The subscript k is used to indicate a leading edge flap or droop, both can equally well be represented by equation (14).

All the expressions derived thus far have been for a two-dimensional airfoil. A set of representative spanwise functions, to represent the spanwise variation of circulation over a lifting line, will be derived at this point. These functions will then be combined with the chordwise terms to represent the variation of the loading component of vorticity over a finite lifting surface.

In lifting line theory the induced velocity due to the spanwise variation of circulation is given by the following expression.

$$w(y) = \frac{1}{4\pi}\int_{-b/2}^{b/2} \frac{(d\Gamma/dy_1)}{y - y_1}\, dy_1 \tag{15}$$

This expression can be transformed into polar coordinates by letting $y = \frac{b}{2}\eta$, where $\eta = \cos\phi$.

$$w(\phi) = \frac{1}{2\pi b}\int_0^{\pi} \frac{(d\Gamma/d\phi_1)}{\cos\phi_1 - \cos\phi}\, d\phi_1 \tag{16}$$

A series which satisfied the boundary condition of zero circulation at the wing tips and is sufficiently general to represent any spanwise variation of circulation is the following sine series.

$$\Gamma(\phi_1) = 2bV_\infty \sum_{n=1}^{\infty} B_n \sin n\phi_1 \tag{17}$$

If equation (16) is multiplied through by $\sin\phi$ and equation (17) substituted in for $\Gamma(\phi_1)$ the following convenient integral equation is obtained.

$$\frac{w}{V_\infty}(\phi)\sin\phi = \frac{1}{\pi}\int_0^{\pi} \frac{\sin\phi \frac{d}{d\phi_1}\left[\frac{\Gamma(\phi_1)}{2V_\infty b}\right]}{\cos\phi_1 - \cos\phi}\, d\phi_1 \tag{18}$$

since:

$$\frac{d}{d\phi_1}\left(\frac{\Gamma(\phi_1)}{2V_\infty b}\right) = \sum_{n=1}^{\infty} n B_n \cos n\phi_1 \tag{19}$$

and that after substituting equation (19) into equation (18) and integrating it is observed that $\frac{d}{d\phi_1}\left(\Gamma(\phi_1)/2V_\infty b\right)$ and $\frac{w}{V_\infty}(\phi)\sin\phi$ are Fourier conjugates.

$$\frac{w}{V_\infty}(\phi)\sin\phi = \frac{1}{\pi}\int_0^{\pi} \frac{\sin\phi \sum_{n=1}^{\infty} n B_n \cos n\phi_1}{\cos\phi_1 - \cos\phi} = \sum_{n=1}^{\infty} n B_n \sin n\phi \tag{20}$$

It is also observed from equation (20) that

$$\frac{w}{V_\infty}(\phi) = \sum_{n=1}^{\infty} \frac{nB_n \sin n\phi}{\sin\phi} = C_0 + \sum_{n=1}^{\infty} C_n \cos n\phi \tag{21}$$

which demonstrates that equation (17) is sufficient to represent any spanwise variation of twist.

Since $\frac{d}{d\phi}\left(\Gamma(\phi)/2bV_\infty\right)$ and $\frac{w}{V_\infty}(\phi)\sin\phi$ are Fourier conjugates, equation (18) can be inverted and a general integral equation obtained for calculating the spanwise variation of circulation due to discontinuous rates of change of induced velocity such as obtained when the spanwise variation of leading or trailing edge sweep is discontinuous or partial span flaps are deflected on the leading or trailing edge. When these special spanwise expressions for circulation are added to equation (17), the infinite series in that equation can be reduced to a finite number of terms.

When equation (18) is inverted the following integral equation is obtained.

$$\frac{d}{d\phi}\left(\frac{\Gamma(\phi)}{2bV_\infty}\right) = -\frac{1}{\pi}\int_0^\pi \frac{\sin\phi\left[\frac{w}{V_\infty}(\phi_1)\sin\phi_1\right]}{\cos\phi_1 - \cos\phi}\, d\phi_1 \tag{22}$$

This equation is then integrated with respect to ϕ to obtain a general relation for calculating the spanwise variation of circulation due to any arbitrary induced downwash distribution.

$$\frac{\Gamma}{2bV_\infty}(\phi) = -\frac{1}{\pi}\int_0^\pi \frac{w}{V_\infty}(\phi_1)\sin\phi_1 \log_e \left|\frac{\sin\frac{1}{2}(\phi_1+\phi)}{\sin\frac{1}{2}(\phi_1-\phi)}\right| d\phi_1 \tag{23}$$

The type of downwash distribution due to leading and trailing edge flaps is known, however, it is not obvious what type of downwash is produced by breaks in the leading or trailing edge. This can be determined by computing the variation in downwash, over the planform of interest, produced by a vorticity distribution which would produce a constant downwash over a high aspect ratio elliptic wing. Any variation in downwash, relative to the constant distribution on an elliptic wing, can be associated with the difference in planform shape between the wing being analyzed and the elliptic wing. In this way the extent and shape of the downwash discontinuities due to the breaks in the leading and trailing edge can be studied. It is only necessary to account for the discontinuities in the downwash distributions by means of the special spanwise functions because the smooth variations in the downwash will be accounted for by equation (17).

The special spanwise functions necessary to account for these discontinuities are then variations of circulation which will produce downwash distributions with the same shape as the discontinuous variations found using the above procedure. It has been determined that if the discontinuous deviations are represented by polygonal downwash distributions, that the variations of circulation due to these downwash distribution calculated from equation (23), do an acceptable job of accounting for breaks in the leading or trailing edge. Even though the discontinuities are of a logarithmic type, the polygonal downwash distributions are acceptable due to the presence of the other terms in equation (17). Also, it is felt that the use of the more simple polygonal functions is justifiable because of the eventual representation of the vorticity by a finite number of discrete vortices.

These polygonal downwash functions can be built up by superimposing two basic types of distributions. These basic distributions produce variation of circulation which will be called "M" or Multhopp functions, named after Multhopp, who first derived the functions, and "P" functions because of the polygonal nature of the downwash produced by them. The special functions necessary to account for flaps, leading edge droops, and ailerons can also be built up by different combinations of the Multhopp functions.

The Multhopp functions are associated with an induced downwash ratio $\frac{w}{V_\infty}(\eta)$ which is zero for $-1 \le \eta < \eta^*$ and unity for $\eta^* \le \eta \le 1$. Substituting this downwash distribution into equation (23) and integrating by parts the following integral relation is obtained.

$$\left(\frac{\Gamma(\phi)}{2bV_\infty}\right)_{M_x} = \frac{1}{\pi}\left\{\cos\phi^* \log_e\left|\frac{\sin\frac{1}{2}(\phi^*-\phi)}{\sin\frac{1}{2}(\phi^*+\phi)}\right| + \int_0^{\phi^*}\frac{\sin\phi\cos\phi_1}{\cos\phi_1-\cos\phi}\,d\phi_1\right\} \tag{24}$$

The integral;

$$\int_0^{\phi^*}\frac{\sin\phi\cos\phi_1}{\cos\phi_1-\cos\phi}\,d\phi_1 = \frac{1}{2}\int_0^{\phi^*}\cos\phi_1\left[\cot\tfrac{1}{2}(\phi_1+\phi)-\cot\tfrac{1}{2}(\phi_1-\phi)\right]d\phi_1 \tag{25}$$

which when evaluated gives

$$\int_0^{\phi^*}\frac{\sin\phi\cos\phi_1}{\cos\phi_1-\cos\phi}\,d\phi_1 = \cos\phi\log_e\left|\frac{\sin\frac{1}{2}(\phi^*+\phi)}{\sin\frac{1}{2}(\phi^*-\phi)}\right| + \phi^*\sin\phi \tag{26}$$

Therefore;

$$\left(\frac{\Gamma(\phi)}{2bV_\infty}\right) = \frac{1}{\pi}\left\{(\cos\phi^*-\cos\phi)\log_e\left|\frac{\sin\frac{1}{2}(\phi^*-\phi)}{\sin\frac{1}{2}(\phi^*+\phi)}\right| + \phi^*\sin\phi\right\} \tag{27}$$

Another type of Multhopp function necessary to build up symmetric and antisymmetric loading functions is one in which the ratio $\frac{w}{V_\infty}(\eta)$ is equal to one for $-1 \le \eta \le \eta^*$ and equal to zero for $\eta^* < \eta \le 1$. For this downwash distribution the spanwise variation of circulation is best calculated by transforming the coordinates such that;

$$\phi' = \phi - 180 \tag{28}$$

Then equation (23) becomes;

$$\left(\frac{\Gamma(\phi')}{2bV_\infty}\right)_{M_2} = -\frac{1}{\pi}\int_0^{\phi^*} \sin\phi_1' \log_e \left|\frac{\sin\frac{1}{2}(\phi_1' - \phi')}{\sin\frac{1}{2}(\phi_1' + \phi')}\right| d\phi_1' \tag{29}$$

$$= \frac{1}{\pi}\left\{\cos\phi^* \log_e \left|\frac{\sin\frac{1}{2}(\phi^* - \phi')}{\sin\frac{1}{2}(\phi^* + \phi')}\right| + \int_0^{\phi^*} \frac{\sin\phi' \cos\phi_1'}{\cos\phi_1' - \cos\phi'}\, d\phi_1'\right\} \tag{30}$$

Since equation (30) is identical in form to equation (24), the following result can be obtained in the same way as equation (27).

$$\left(\frac{\Gamma(\phi')}{2bV_\infty}\right)_{M_2} = \frac{1}{\pi}\left\{(\cos\phi^* - \cos\phi')\log_e \left|\frac{\sin\frac{1}{2}(\phi^* - \phi')}{\sin\frac{1}{2}(\phi^* + \phi')}\right| + \phi^* \sin\phi'\right\} \tag{31}$$

Then after substituting equation (28) into equation (31) the following expression for the port wing panel is obtained.

$$\left(\frac{\Gamma(\phi)}{2bV_\infty}\right)_{M_2} = \frac{1}{\pi}\left\{(\cos\phi^* + \cos\phi)\log_e \left|\frac{\cos\frac{1}{2}(\phi^* + \phi)}{\cos\frac{1}{2}(\phi^* - \phi)}\right| + \phi^* \sin\phi\right\} \tag{32}$$

A symmetrical and an antisymmetrical Multhopp function can be formed by superimposing equation (27) and equation (32). The symmetrical function will be used when the wing contour is symmetrical about the plane of pitch and the airplane is rotated in this plane. The antisymmetric function is used when the ailerons are deflected and the airplane is in a rolling maneuver. The symmetric Multhopp function is;

$$M(\phi,\phi^*)_S = \frac{1}{\pi}\left\{(\cos\phi^* - \cos\phi)\log_e\left|\frac{\sin\frac{1}{2}(\phi^*-\phi)}{\sin\frac{1}{2}(\phi^*+\phi)}\right| + (\cos\phi^* + \cos\phi)\log_e\left|\frac{\cos\frac{1}{2}(\phi^*+\phi)}{\cos\frac{1}{2}(\phi^*-\phi)}\right| + 2\phi^*\sin\phi\right\} \tag{33}$$

The antisymmetric Multhopp function is as follows.

$$M(\phi,\phi^*)_{AS} = \frac{1}{\pi}\left\{(\cos\phi^* - \cos\phi)\log_e\left|\frac{\sin\frac{1}{2}(\phi^*-\phi)}{\sin\frac{1}{2}(\phi^*+\phi)}\right| - (\cos\phi^* + \cos\phi)\log_e\left|\frac{\cos\frac{1}{2}(\phi^*+\phi)}{\cos\frac{1}{2}(\phi^*-\phi)}\right|\right\} \tag{34}$$

The "P" function is associated with a downwash distribution which is zero for $-1 \le \eta \le \eta^*$ and varies linearly from zero to unity for $\eta^* < \eta \le 1$. For this distribution equation (23) becomes;

$$\left(\frac{\Gamma(\phi)}{2bV_\infty}\right)_{P_{TE}} = -\frac{1}{\pi}\int_0^{\phi^*}\left(\frac{\cos\phi_1 - \cos\phi^*}{1-\cos\phi^*}\right)\sin\phi_1\log_e\left|\frac{\sin\frac{1}{2}(\phi_1-\phi)}{\sin\frac{1}{2}(\phi_1+\phi)}\right|d\phi_1 \tag{35}$$

After integrating by parts;

$$\left(\frac{\Gamma(\phi)}{2bV_\infty}\right)_{P_{TE}} = \frac{\cos\phi^*}{\pi(1-\cos\phi^*)}\left\{(\cos\phi - \cos\phi^*)\log_e\left|\frac{\sin\frac{1}{2}(\phi^*-\phi)}{\sin\frac{1}{2}(\phi^*+\phi)}\right| - \phi^*\sin\phi\right\} - \frac{1}{\pi(1-\cos\phi^*)}\int_0^{\phi^*}\cos\phi_1\sin\phi_1\log_e\left|\frac{\sin\frac{1}{2}(\phi_1-\phi)}{\sin\frac{1}{2}(\phi_1+\phi)}\right|d\phi_1 \tag{36}$$

The integral;

$$\int_0^{\phi^*} \cos\phi_1 \sin\phi_1 \log_e \left| \frac{\sin\frac{1}{2}(\phi_1 - \phi)}{\sin\frac{1}{2}(\phi_1 + \phi)} \right| d\phi_1 = \frac{1}{4}\cos 2\phi^* \log_e \left| \frac{\sin\frac{1}{2}(\phi^* + \phi)}{\sin\frac{1}{2}(\phi^* - \phi)} \right|$$

$$+ \frac{1}{8}\left\{ \int_0^{\phi^*} \cos 2\phi_1 \cot\tfrac{1}{2}(\phi_1 - \phi)\, d\phi_1 \right.$$

$$\left. - \int_0^{\phi^*} \cos 2\phi_1 \cot\tfrac{1}{2}(\phi_1 + \phi)\, d\phi_1 \right\} \qquad (37)$$

where,

$$\int_0^{\phi^*} \cos 2\phi_1 \cot\tfrac{1}{2}(\phi_1 - \phi)\, d\phi_1 - \int_0^{\phi^*} \cos 2\phi_1 \cot\tfrac{1}{2}(\phi_1 + \phi)\, d\phi_1 = 2\cos 2\phi \log_e \left| \frac{\sin\frac{1}{2}(\phi^* - \phi)}{\sin\frac{1}{2}(\phi^* + \phi)} \right|$$

$$- 4\sin\phi^* \sin\phi - 2\phi^* \sin 2\phi \qquad (38)$$

therefore;

$$\left(\frac{\Pi(\phi)}{2bV_\infty}\right)_{P_2} = -\frac{1}{2\pi(1 - \cos\phi^*)} \left\{ (\cos\phi^* - \cos\phi)^2 \log_e \left| \frac{\sin\frac{1}{2}(\phi^* - \phi)}{\sin\frac{1}{2}(\phi^* + \phi)} \right| \right.$$

$$\left. + (2\phi^* \cos\phi^* - \sin\phi^*) \sin\phi - \tfrac{1}{2}\phi^* \sin 2\phi \right\} \qquad (39)$$

Then similarly the "P" function associated with the port wing panel is derived by making the same coordinate transformation as used in the Multhopp function.

Let $\phi' = 180 - \phi$, then;

$$\left(\frac{\Pi(\phi')}{2bV_\infty}\right)_{P_2} = -\frac{1}{\pi} \int_0^{\phi^*} \left(\frac{\cos\phi_1' - \cos\phi^*}{1 - \cos\phi^*} \right) \sin\phi_1' \log_e \left| \frac{\sin\frac{1}{2}(\phi_1' - \phi)}{\sin\frac{1}{2}(\phi_1' + \phi)} \right| d\phi_1' \qquad (40)$$

Since equation (40) is identical in form to equation (35) its integral is of the same form as equation (39).

$$\left(\frac{\Gamma(\phi')}{2bV_\infty}\right)_{R_1} = -\frac{1}{2\pi(1-\cos\phi^*)}\left\{(\cos\phi^*-\cos\phi')^2 \log_e\left|\frac{\sin\frac{1}{2}(\phi^*-\phi')}{\sin\frac{1}{2}(\phi^*+\phi')}\right|\right.$$

$$\left.+(2\phi^*\cos\phi^*-\sin\phi^*)\sin\phi'-\tfrac{1}{2}\phi^*\sin 2\phi'\right\} \qquad (41)$$

After substituting $\phi' = 180 - \phi$ into equation (41) the following expression is obtained

$$\left(\frac{\Gamma(\phi)}{2bV_\infty}\right)_{R_1} = -\frac{1}{2\pi(1-\cos\phi^*)}\left\{(\cos\phi^*+\cos\phi)^2 \log_e\left|\frac{\cos\frac{1}{2}(\phi^*+\phi)}{\cos\frac{1}{2}(\phi^*-\phi)}\right|\right.$$

$$\left.+(2\phi^*\cos\phi^*-\sin\phi^*)\sin\phi\right\} \qquad (42)$$

As in the case of the Multhopp functions a symmetric and an antisymmetric "P" function can be formed from equation (39) and equation (42).

The symmetric "P" function is formed by adding equations (39) and (42).

$$P(\phi,\phi^*)_S = -\frac{1}{2\pi(1-\cos\phi^*)}\left\{(\cos\phi^*-\cos\phi)^2 \log_e\left|\frac{\sin\frac{1}{2}(\phi^*-\phi)}{\sin\frac{1}{2}(\phi^*+\phi)}\right|\right.$$

$$+(\cos\phi^*+\cos\phi)^2 \log_e\left|\frac{\cos\frac{1}{2}(\phi^*+\phi)}{\cos\frac{1}{2}(\phi^*-\phi)}\right|$$

$$\left.+(4\phi^*\cos\phi^*-2\sin\phi^*)\sin\phi\right\} \qquad (43)$$

The antisymmetric "P" function is then obtained by subtracting equation (42) from equation (39).

$$P(\phi,\phi^*)_{AS} = \frac{-1}{2\pi(1-\cos\phi^*)}\left\{(\cos\phi^*-\cos\phi)^2 \log_e \left|\frac{\sin\frac{1}{2}(\phi^*-\phi)}{\sin\frac{1}{2}(\phi^*+\phi)}\right| \right.$$

$$-(\cos\phi^*+\cos\phi)^2 \log_e \left|\frac{\cos\frac{1}{2}(\phi^*+\phi)}{\cos\frac{1}{2}(\phi^*-\phi)}\right|$$

$$\left. -\phi^* \sin 2\phi \right\} \qquad (44)$$

The spanwise variation of vorticity necessary to represent polygonal downwash distributions are then built up by the superposition of the $M(\phi,\phi^*)$ and $P(\phi,\phi^*)$ functions. The proportion of each used depends on the location of the break in the lifting line η_b and the ranges R_i and R_o over which the downwash is affected. The range varies with the degree of discontinuity in the sweep angle of each lifting line. In general, the change in sweep angle is not the same on the leading and trailing edges, in which case R_i and R_o becomes functions of x/c. However, the special functions are calculated for constant values of R_i and R_o with the assumption that any variation with x/c can be compensated for by the other terms in equation (17). This appears to be a safe assumption since the range has been observed to vary only slightly about the value $.05\frac{b}{2}$. The actual plot of the induced downwash can be obtained from the elements of the influence matrix.

The special functions which must be added to equation (17) to account for discontinuities in the variation of leading and trailing edge sweep are given by the following relations.

For $\eta_b = 0$

$$P(\phi) = M(\phi,\tfrac{\pi}{2}) - \frac{1}{R_o}P(\phi,\tfrac{\pi}{2}) + \frac{1-R_o}{R_o}P(\phi,\cos^{-1}R_o) \qquad (45)$$

For $0 < |\eta_b| < R_i$

$$P(\phi) = (1 - \eta_b/R_i) M(\phi, \tfrac{\pi}{2}) + \frac{1}{R_i} P(\phi, \tfrac{\pi}{2})$$

$$- \left[\frac{(R_i + R_o)(1 - \eta_b)}{R_i R_o}\right] P(\phi, \phi_b)$$

$$+ \left[\frac{R_i + R_o}{R_i R_o} - \frac{1}{R_i}\right]\left[1 - R_o - \eta_b\right] P(\phi, \cos^{-1}(\eta_b + R_o)) \qquad (46)$$

For $R_i \le |\eta_b| \le (1 - R_o)$

$$P(\phi) = (1 - \eta_b + R_i)(1/R_i) P(\phi, \cos^{-1}(\eta_b - R_i))$$

$$- \left[\frac{R_o + R_i}{R_o R_i}\right]\left[1 - \eta_b\right] P(\phi, \phi_b)$$

$$+ (1 - \eta_b - R_o)(1/R_o) P(\phi, \cos^{-1}(\eta_b + R_o)) \qquad (47)$$

For $(1 - R_o) \le |\eta_b| < 1$

$$P(\phi) = (1 - \eta_b + R_i)(1/R_i) P(\phi, \cos^{-1}(\eta_b - R_i))$$

$$- \left[1 + (1 - \eta_b)/R_i\right] P(\phi, \phi_b) \qquad (48)$$

These same relations are used for both symmetric and antisymmetric loadings. The only difference being the use of $M(\phi, \phi^*)_S$ and $P(\phi, \phi^*)_S$ for the symmetric loading and $M(\phi, \phi^*)_{AS}$ and $P(\phi, \phi^*)_{AS}$ for antisymmetric loading. Also, equation (45) is always zero for the antisymmetric loading.

The special spanwise functions for flaps, leading edge droop and ailerons are similarly developed. The function added to equation (17), in addition to the above relations, for flaps and leading edge droop is as follows:

$$P(\phi) = M(\phi, \phi_i) - M(\phi, \phi_o) \qquad (49)$$

ϕ_i and ϕ_o are the inboard and outboard spanwise locations where the partial span flap begins and ends, respectively. For ailerons, the special spanwise function is the same as equation (49) except that the antisymmetric Multhopp functions are used instead of the symmetric. One special function should be used for each flap or leading edge droop for which ϕ_i and ϕ_o are different.

At this point all the necessary expressions needed to represent both chordwise and spanwise variations in the loading component of vorticity have been derived. The expressions have been derived from lifting line and two dimensional thin airfoil theory. However, they can be combined to represent the vorticity over a lifting surface since their shape is representative of the type of vorticity expected over a lifting surface. The amount of each function is determined by satisfying the boundary condition of no flow through the mean camber surfaces of the wing at a series of points, called control points. In the case of a lifting surface, however, the velocity induced by the vorticity is computed using three dimensional influence functions instead of the two dimensional functions used in the derivation of the loading expressions. These three dimensional influence functions are derived in Appendix C.

The combined general expression for the vorticity over a thin lifting surface is then obtained by merging equations (10), (13), and (14) with equation (17) and the appropriate versions of equations (45), (46), (47), (48), or (49). After transforming the spanwise coordinate back to η the following expression is obtained.

$$\gamma(\theta,\eta) = \frac{4bV_\infty}{c}\left\{F_0 \cot\theta/2 + \sum_{N=1}^{N_u-3} F_N \sin N\theta \right.$$

$$+F_j \log_e \left|\frac{\sin\frac{1}{2}(\theta+\theta_i)}{\sin\frac{1}{2}(\theta-\theta_i)}\right| \qquad (50)$$

$$\left. +F_k \log_e \left|\frac{\sin\frac{1}{2}(\theta+\theta_o)}{\sin\frac{1}{2}(\theta-\theta_o)}\right| \right\}$$

where, for a symmetric span load;

$$F_0 = \sqrt{1-\eta^2} \sum_{N=1}^{N_N - P_N} a_{0N}\,\eta^{2(N-1)} + \sum_{N=(N_N-P_N+1)}^{N_N} a_{0N}\,P_N(\eta)$$

$$F_N = \sqrt{1-\eta^2} \sum_{N=1}^{N_N - P_N} a_{NN}\,\eta^{2(N-1)} + \sum_{N=(N_N-P_N+1)}^{N_N} a_{NN}\,P_N(\eta)$$

$$F_K = \sqrt{1-\eta^2} \sum_{N=1}^{N_N - P_N} a_{KN}\,\eta^{2(N-1)} + \sum_{N=(N_N-P_N+1)}^{N_N} a_{KN}\,P_N(\eta)$$

$$F_f = \sqrt{1-\eta^2} \sum_{N=1}^{N_N - P_N} a_{fN}\,\eta^{2(N-1)} + \sum_{N=(N_N-P_N+1)}^{N_N} a_{fN}\,P_N(\eta) \qquad (51)$$

and where N_N equals the total number of span loads, P_N equals the number of special span functions needed to account for breaks in the leading or trailing edge and for flaps and leading edge droop and where the $P_N(\eta)$'s are the special spanwise functions. The coefficients a_{0N}, a_{NN}, a_{fN}, and a_{KN} are the unknown's to be computed such that the boundary conditions are satisfied.

If the loading on the wing is antisymmetric change the power on η from $2(N-1)$ to $2N-1$ and use antisymmetric P functions.

Since the pylon does not utilize a spanwise series or have flaps, the vorticity is defined by a chordwise series only of the following type at each span station.

$$\gamma(\theta,\eta) = \frac{4bV_\infty}{c}\left\{F_0 \cot\theta/2 + \sum_{N=1}^{N_N-1} F_N \sin N\theta\right\} \qquad (52)$$

In this case F_0 and F_N are the unknown coefficients to be determine by the solution of the influence equations.

APPENDIX G

WING AND PYLON VORTEX STRENGTHS

The expression for the vorticity over a lifting surface is given in Appendix F by equation (50). The unknown coefficients of the vorticity series are determined such that the boundary conditions of no flow through the surface of the complete configuration are satisfied. This is done by setting up and solving a set of simultaneous aerodynamic influence equations which represent these boundary conditions. In order to set up these influence equations it is necessary to sum up the velocity induced at a series of points by the vorticity. This summing process is in general the integration of the product of the vorticity and an influence function over the entire lifting surface for each of the boundary points.

In order to eliminate this analytical integration the continuous vorticity distribution is replaced by a grid of constant strength vortices as shown in figure 4. This is in essence a numerical integration scheme which does an excellent job of representing the induced velocities with a minimum of numerical computation. The technique of representing the vorticity over a lifting surface by constant strength vortices was used by Falkner in reference 16 . Falkner utilized horseshoe vortices and obtained good results for wings of low or moderate sweep. However, the number of vortices required increases for wings of higher sweep and eventually the representation becomes unacceptable. This is because the bound segment of the horseshoe vortex is perpendicular to the freestream rather than along a line of constant vorticity. Since lines of constant vorticity tend to lie along lines of constant percent chord, the so-called bound portion of the horseshoe vortex has been skewed to lie along constant percent chord lines in this analysis. This procedure should also produce a better representation of broken leading and trailing edge planforms.

It can be shown that discrete vortices produce the same downwash, at points half way between the vortices, as a continuous distribution of vorticity represented by small linearly varying distributions over regions equal in length to the distance between the discrete vortices. Since any distribution of vorticity can be represented by a set of linearly varying regions, the number of which depends on the rate of change of the gradient along the distribution, it is reasonable to use discrete vortices to compute the induced velocity produced by a continuous variation of vorticity.

If the arbitrary vorticity distribution, as shown in figure G-1 , is represented by both linearly varying vorticity distributions and by discrete vortices the following expressions for downwash at a boundary point midway between the vortices are obtained.

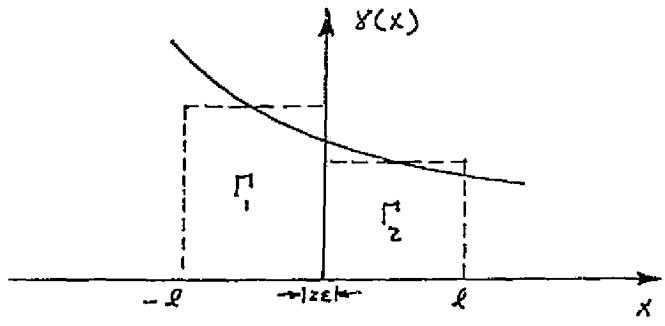

Figure G-1. Vorticity Distribution

The downwash induced at x = 0 by two dimensional discrete vortices at $x = -\frac{\ell}{2}$ and $x = \frac{\ell}{2}$ equal in strength to Γ_1 and Γ_2, respectively, is given by;

$$\frac{w}{V_\infty}(0) = \frac{1}{2\pi V_\infty}\left\{\frac{2\Gamma_1}{\ell} - \frac{2\Gamma_2}{\ell}\right\} = \frac{\Gamma_1 - \Gamma_2}{\pi V_\infty \ell} \tag{1}$$

If the continuous vorticity over the intervals $-\ell \le x \le 0$ and $0 \le x \le \ell$ is represented by Taylor series expansions about $x = -\ell/2$ and $x = \ell/2$ respectively, then

$$\gamma(x) = \gamma(-\tfrac{\ell}{2}) + (x + \tfrac{\ell}{2})\,\gamma'(-\tfrac{\ell}{2}) + \cdots \qquad -\ell \le x \le 0$$

$$\gamma(x) = \gamma(\tfrac{\ell}{2}) + (x - \tfrac{\ell}{2})\,\gamma'(\tfrac{\ell}{2}) + \cdots \qquad 0 \le x \le \ell \tag{2}$$

If these series are truncated after the first two terms, the vorticity is represented by two linear functions which produce the following downwash at x = 0.

$$\frac{w}{V_\infty}(0) = \lim_{\varepsilon \to 0} \frac{-1}{2\pi V_\infty}\left\{\int_{-\ell}^{-\varepsilon} \frac{\left[\gamma(-\frac{\ell}{2}) + (x + \frac{\ell}{2})\,\gamma'(-\frac{\ell}{2})\right]}{x}\,dx\right.$$

$$\left. + \int_{\varepsilon}^{\ell} \frac{\left[\gamma(\frac{\ell}{2}) + (x - \frac{\ell}{2})\,\gamma'(\frac{\ell}{2})\right]}{x}\,dx\right\} \tag{3}$$

$$\frac{w}{v_0}(0) = -\frac{1}{2\pi v_0} \lim_{\varepsilon \to 0} \left\{ \left[\gamma\left(-\tfrac{\ell}{2}\right) - \gamma\left(\tfrac{\ell}{2}\right) + \tfrac{\ell}{2}\gamma'\left(-\tfrac{\ell}{2}\right) + \tfrac{\ell}{2}\gamma'\left(\tfrac{\ell}{2}\right) \right] \log_e \frac{\varepsilon}{\ell} \right.$$

$$\left. + \left[\gamma'\left(-\tfrac{\ell}{2}\right) + \gamma'\left(\tfrac{\ell}{2}\right) \right] \ell - \left[\gamma'\left(\tfrac{\ell}{2}\right) + \gamma'\left(\tfrac{\ell}{2}\right) \right] \varepsilon \right\} \qquad (4)$$

since;

$$\Gamma_1 = \int_{-\ell}^{0} \left[\gamma\left(-\tfrac{\ell}{2}\right) + \left(x + \tfrac{\ell}{2}\right)\gamma'\left(-\tfrac{\ell}{2}\right) \right] dx = \left[\gamma\left(-\tfrac{\ell}{2}\right) + \tfrac{\ell}{2}\gamma'\left(-\tfrac{\ell}{2}\right) \right] \ell - \gamma'\left(-\tfrac{\ell}{2}\right)\frac{\ell^2}{2}$$

(5)

$$\Gamma_1 = \gamma\left(-\tfrac{\ell}{2}\right)\ell$$

and

$$\Gamma_2 = \int_{0}^{\ell} \left[\gamma\left(\tfrac{\ell}{2}\right) + \left(x - \tfrac{\ell}{2}\right)\gamma'\left(\tfrac{\ell}{2}\right) \right] dx = \left[\gamma\left(\tfrac{\ell}{2}\right) - \tfrac{\ell}{2}\gamma'\left(\tfrac{\ell}{2}\right) \right] \ell + \gamma'\left(\tfrac{\ell}{2}\right)\frac{\ell^2}{2}$$

(6)

$$\Gamma_2 = \gamma\left(\tfrac{\ell}{2}\right)\ell$$

Therefore, after solving equation (2) for $\gamma'\left(-\frac{\ell}{2}\right)$ and $\gamma'\left(\frac{\ell}{2}\right)$ at x = 0 and substituting into equation (4);

$$\frac{w}{v_0}(0) = \frac{-1}{2\pi v_0} \lim_{\varepsilon \to 0} \left\{ \left[\gamma\left(-\tfrac{\ell}{2}\right) - \gamma\left(\tfrac{\ell}{2}\right) + \gamma(0) - \gamma\left(-\tfrac{\ell}{2}\right) - \gamma(0) + \gamma\left(\tfrac{\ell}{2}\right) \right] \log_e \frac{\varepsilon}{\ell} \right.$$

$$+ 2\left[\gamma(0) - \gamma\left(-\tfrac{\ell}{2}\right) - \gamma(0) + \gamma\left(\tfrac{\ell}{2}\right) \right]$$

(7)

$$\left. - \left[\gamma'\left(-\tfrac{\ell}{2}\right) + \gamma'\left(\tfrac{\ell}{2}\right) \right] \varepsilon \right\}$$

Then in taking the limit, it is observed that;

$$\frac{w}{V_\infty}(0) = \frac{1}{\pi V_\infty}\left[\gamma(-\tfrac{\ell}{2}) - \gamma(\tfrac{\ell}{2})\right] \tag{8}$$

Therefore; from equations (5) and (6);

$$\frac{w}{V_\infty}(0) = \frac{\Gamma_1 - \Gamma_2}{\pi V_\infty \ell} \tag{9}$$

which is the same result obtained from the discrete vortices.

Even though this argument and others to follow in this section are based on the two dimensional specialized Biot-Savart relations it can be shown that there is no loss of generality and that the above conclusion and the relations between the chordwise variation of discrete vortex strength and the continuous distribution of vorticity, represented by those vortices, are valid for finite vortex segments and vortex grids such as shown in figure 4. More general expressions which give the induced velocity due to skewed vortices of finite length can be derived from downwash relations given in Appendix C. Using these relations the downwash produced by the bound portions of the discrete skewed vortices, at a point mid-way between them, is given by;

$$\frac{w}{V_\infty}(0) = -\frac{1}{4\pi V_\infty}\left\{\Gamma_1\left[E_{w_1}(-\tfrac{\ell}{2}) + E_{w_0}(-\tfrac{\ell}{2})\right] + \Gamma_2\left[E_{w_1}(\tfrac{\ell}{2}) + E_{w_0}(\tfrac{\ell}{2})\right]\right\} \tag{10}$$

where

$$E_{w_1} = \frac{s(\tan^2\phi_1 + 1) + x\tan\phi_1}{x\left[(s\tan\phi_1 - x)^2 + s^2\right]^{1/2}} + \frac{\tan\phi_1}{|x|} \tag{11}$$

$$E_{w_0} = \frac{s(\tan^2\phi_0 + 1) + x\tan\phi_0}{x\left[(s\tan\phi_0 + x)^2 + s^2\right]^{1/2}} - \frac{\tan\phi_0}{|x|} \tag{12}$$

Where s is half the y distance between the ends of the bound vortices. The sweep angles of the port and starboard portions of the bound vortices are represented by ϕ_1 and ϕ_0, respectively.

For a continuous distribution of vorticity the downwash at x = 0 is given by the principle value of the following integral.

$$\frac{w}{V_\infty}(0) = -\frac{1}{4\pi V_\infty}\int_{-l}^{l} \gamma(x)\left[E_{w_i} + E_{w_0}\right] dx \tag{13}$$

where the variation in sweep of the vorticity is represented by a Taylor series expansion about x = 0, which is truncated after the first two terms. Therefore;

$$\tau_i(x) = \tau_i(0) + x\,\tau_i'(0) = \tau_i + x\,\tau_i' \tag{14}$$

and

$$\tau_0(x) = \tau_0(0) + x\,\tau_0'(0) = \tau_0 + x\,\tau_0' \tag{15}$$

where

$$\tau_i = \tan\phi_i(0) \qquad \text{AND} \qquad \tau_0 = \tan\phi_0(0)$$

After substituting equations (14) and (15) into equations (11) and (12) the following influence functions are obtained.

$$) = \frac{P_i\tau_i' x + (2P_i + 1)\tau_i}{\sqrt{(P_i x + 5\tau_i)^2 + 5^2}} + \frac{5 S_i'^2}{x\sqrt{(P_i x + 5\tau_i)^2 + 5^2}} + \frac{\tau_i}{|x|} + \frac{\tau_i' x}{|x|} \tag{16}$$

$$E_{w_0}(x) = \frac{P_0\tau_0' x + (2P_0 - 1)\tau_0}{\sqrt{(P_0 x + 5\tau_0)^2 + 5^2}} + \frac{5 S_0'^2}{x\sqrt{(P_0 x + 5\tau_0)^2 + 5^2}} - \frac{\tau_0}{|x|} - \frac{\tau_0' x}{|x|} \tag{17}$$

where $P_i = 5\tau_i' - 1$, $P_0 = 5\tau_0' + 1$, $S_i' = \sec\phi_i(0)$, AND $S_0 = \sec\phi_0(0)$

If equations (16) and (17) are substituted into equation (13) the following integrals are obtained.

$$\frac{w}{V_\infty}(0) = -\frac{\bar{P}}{4\pi V_\infty}\int_{-\ell}^{0}\gamma(0)\left\{\frac{P_i T_i' x + (2P_i+1)T_i}{\sqrt{(P_i x + s T_i)^2 + s^2}} + \frac{P_0 T_0' x + (2P_0-1)T_0}{\sqrt{(P_0 x + s T_0)^2 + s^2}}\right.$$

$$\left. + \frac{s S_i'^2}{x\sqrt{(P_i x + s T_i)^2 + s^2}} + \frac{s S_0'^2}{x\sqrt{(P_0 x + s T_0)^2 + s^2}}\right\} dx - \frac{\bar{P}}{4\pi V_\infty}\int_{-\ell}^{0}\gamma(0)\left\{-\frac{T_i}{x}\right.$$

$$\left. + \frac{T_0}{x} - T_i' + T_0'\right\} dx - \frac{\bar{P}}{4\pi V_\infty}\int_{0}^{\ell}\gamma(0)\left\{\frac{T_i}{x} - x + T_i' - T_0'\right\} dx$$

$$-\frac{\bar{P}}{4\pi V_\infty}\int_{-\ell}^{0}\left\{\frac{2}{\ell}\gamma(0)x - \frac{2}{\ell}\gamma(-\tfrac{\ell}{2})x\right\}\left\{\frac{P_i T_i' x + (2P_i+1)T_i}{\sqrt{(P_i x + s T_i)^2 + s^2}} + \frac{P_0 T_0' x + (2P_0-1)T_0}{\sqrt{(P_0 x + s T_0)^2 + s^2}}\right.$$

$$\left. + \frac{s S_i'^2}{x\sqrt{(P_i x + s T_i)^2 + s^2}} + \frac{s S_0'^2}{x\sqrt{(P_0 x + s T_0)^2 + s^2}} - \frac{T_i}{x} + \frac{T_0}{x} - T_i' + T_0'\right\} dx$$

$$-\frac{\bar{P}}{4\pi V_\infty}\int_{0}^{\ell}\left\{-\frac{2}{\ell}\gamma(0)x + \frac{2}{\ell}\gamma(\tfrac{\ell}{2})x\right\}\left\{\frac{P_i T_i' x + (2P_i+1)T_i}{\sqrt{(P_i x + s T_i)^2 + s^2}} + \frac{P_0 T_0' x + (2P_0-1)T_0}{\sqrt{(P_0 x + s T_0)^2 + s^2}}\right.$$

$$\left. + \frac{s S_i'^2}{x\sqrt{(P_i x + s T_i)^2 + s^2}} + \frac{s S_0'^2}{x\sqrt{(P_0 x + s T_0)^2 + s^2}} + \frac{T_i}{x} - \frac{T_0}{x}\right.$$

$$\left. + T_i' + T_0'\right\} dx \qquad (18)$$

where $\bar{P}$ means to take the principle value of the integral.

The integrals in equation (18) are evaluated as follows;

$$I_{i_1} = \bar{P}\int_{-l}^{l} \frac{\gamma(0) P_i T_i' x\, dx}{\sqrt{(P_i x + s T_i)^2 + s^2}} = \frac{\gamma(0) T_i'}{P_i}\left\{ \sqrt{(P_i l + s T_i)^2 + s^2} \right.$$

$$\left. - \sqrt{(P_i l - s T_i)^2 + s^2} - s T_i \log_e \left| \frac{(P_i l + s T_i) + \sqrt{(P_i l + s T_i)^2 + s^2}}{-(P_i l - s T_i) + \sqrt{(P_i l - s T_i)^2 + s^2}} \right| \right.$$

$$I_{o_1} = \bar{P}\int_{-l}^{l} \frac{\gamma(0) P_o T_o' x\, dx}{\sqrt{(P_o x + s T_o)^2 + s^2}} = \frac{\gamma(0) T_o'}{P_o}\left\{ \sqrt{(P_o l + s T_o)^2 + s^2} \right.$$

$$\left. - \sqrt{(P_o l - s T_o)^2 + s^2} - s T_o \log_e \left| \frac{(P_o l + s T_o) + \sqrt{(P_o l + s T_o)^2 + s^2}}{-(P_o l - s T_o) + \sqrt{(P_o l - s T_o)^2 + s^2}} \right| \right.$$

$$I_{i_2} = \bar{P}\int_{-l}^{l} \frac{\gamma(0)(2P_i + 1) T_i\, dx}{\sqrt{(P_i x + s T_i)^2 + s^2}} = \frac{\gamma(0)(2P_i + 1) T_i}{P_i} \log_e \left| \frac{(P_i l + s T_i) + \sqrt{(P_i l + s T_i)^2 + s^2}}{-(P_i l - s T_i) + \sqrt{(P_i l - s T_i)^2 + s^2}} \right|$$

$$I_{o_2} = \bar{P}\int_{-l}^{l} \frac{\gamma(0)(2P_o - 1) T_o}{\sqrt{(P_o x + s T_o)^2 + s^2}} dx = \frac{\gamma(0)(2P_o - 1) T_o}{P_o} \log_e \left| \frac{(P_o l + s T_o) + \sqrt{(P_o l + s T_o)^2 + s^2}}{-(P_o l - s T_o) + \sqrt{(P_o l - s T_o)^2 + s^2}} \right|$$

$$I_{i_3} = \bar{P}\int_{-l}^{l} \frac{\gamma(0) s P_i^2\, dx}{x\sqrt{(P_i x + s T_i)^2 + s^2}} = \gamma(0) s P_i^2 \left\{ \lim_{\varepsilon \to 0} \int_{-l}^{-\varepsilon} \frac{dx}{x\sqrt{(P_i x + s T_i)^2 + s^2}} \right.$$

$$\left. + \lim_{\varepsilon \to 0} \int_{\varepsilon}^{l} \frac{dx}{x\sqrt{(P_i x + s T_i)^2 + s^2}} \right\}$$

$$I_{i_3} = -\gamma(0)\, S_i' \log_e \left| \frac{s S_i^2 + T_i' P_i' l + S_i' \sqrt{(P_i' l + s T_i')^2 + s^2}}{s S_i^2 - T_i' P_i' l + S_i' \sqrt{(P_i' l - s T_i')^2 + s^2}} \right|$$

$$I_{o_3} = -\gamma(0)\, S_o' \log_e \left| \frac{s S_o^2 + T_o' P_o' l + S_o' \sqrt{(P_o' l + s T_o')^2 + s^2}}{s S_o^2 - T_o' P_o' l + S_o' \sqrt{(P_o' l - s T_o')^2 + s^2}} \right|$$

$$I_{i_4} = -\gamma(0)\, T_i' \int_{-l}^{0} dx + \gamma(0)\, T_i' \int_{0}^{l} dx = 0$$

$$I_{o_4} = \gamma(0)\, T_o' \int_{-l}^{0} dx - \gamma(0)\, T_o' \int_{0}^{l} dx = 0$$

The integrals;

$$I_{i_5} = -\gamma(0)\, T_i' \lim_{\varepsilon \to 0} \int_{-l}^{-\varepsilon} \frac{dx}{x} + \gamma(0) T_i' \lim_{\varepsilon \to 0} \int_{\varepsilon}^{l} \frac{dx}{x} = 2\gamma(0)\, T_i' \lim_{\varepsilon \to 0} \log_e \left| \frac{l}{\varepsilon} \right|$$

and

$$I_{05} = \gamma(0)\tau_0 \lim_{\epsilon \to 0} \int_{-1}^{-\epsilon} \frac{dx}{x} - \gamma(0)\tau_0 \lim_{\epsilon \to 0} \int_{\epsilon}^{1} \frac{dx}{x} = 2\gamma(0)\tau_0 \lim_{\epsilon \to 0} \log_e \left|\frac{\epsilon}{1}\right|$$

go logarithmically to infinity as $\epsilon \to 0$. This is a consequence of evaluating the downwash at a break in a line of constant vorticity. If the more complete planar influence equation, equation (11) of Appendix C, is used in equation (10) an additional term is obtained in the limit as $\epsilon \to 0$. This limit is difficult to obtain because of I_{i5} and I_{05}, however, it was noted in reference 17 that if the downwash were computed at a point on the surface of the airfoil instead of in the X = 0 plane, that the downwash at Y = 0 due to the break in the constant vorticity line would be approximately proportional to the vorticity at that point. It was further noted that the downwash was not sensitive to the thickness ratio of the airfoil section. A more complete study of the downwash at breaks in the vorticity lines will be made, using equation (11) of Appendix C, at some time in the future. The results noted in reference 17 are not obvious when equation (11) is used due to the complex nature of the integrals involved. These integrals may have to be evaluated numerically as in reference 17.

From a physical point of view there is no reason to assume that the lines of constant vorticity will be discontinuous at any point on the wing except possibly at the leading edge of span stations where the sweep is discontinuous. It is therefore a result of not knowing the shape of the constant vorticity lines a priori, and the necessity of assuming shapes before they can be determined, which results in the singular integrals I_{i5} and I_{05}. The actual shape of the vortex lines used becomes less important as the size of the vortex grid decreases and there is no reason to assume that a set of pressures, for which lines of constant vorticity are aligned with the assumed vortex lines, cannot be converged to after a certain number of iterations. For these reasons the exact behavior of the integrals I_{i5} and I_{05} in the limit, as $(X,Y,Z) \to (0,0,0)$ is only of academic interest at points other than the leading edge.

The complete integral in equation (18) will be evaluated here except for I_{i5} and I_{05}, which will be replaced by the values determined numerically in reference 17. However, the comparison between downwash computed at (0,0,0) by integrating the continuous vorticity times the continuous influence function and that obtained by numerically summing the downwash induced by equivalent discrete vortices will be limited to the case where the lines of constant vorticity are continuous. For this case $\phi_i = \phi_0 = 0$ and therefore $I_{i5} + I_{05} = 0$.

Now continuing with the evaluation of the integrals of equation (18).

$$I_{i_6} = \bar{P}\int_{-l}^{0}\left\{\frac{2}{l}\gamma(0)x - \frac{2}{l}\gamma(-\tfrac{l}{2})x\right\}\left\{\frac{P_i T_i' x + (2P_i+1)T_i}{\sqrt{(P_i x + S T_i)^2 + S^2}}\right\}dx$$

$$= \left\{\gamma(0) - \gamma(-\tfrac{l}{2})\right\}\left\{\frac{T_i}{P_i^2 l}\left[-3S^2 T_i S_i' + (P_i l + 3ST_i)\sqrt{(P_i l - ST_i)^2 + S^2}\right.\right.$$

$$\left. + S^2(2T_i^2 - 1)\log_e\left|\frac{S(T_i + S_i')}{-(P_i l - ST_i) + \sqrt{(P_i l - ST_i)^2 + S^2}}\right|\right] + \frac{2(2P_i+1)T_i}{P_i^2 l}\left[S S_i'\right.$$

$$\left.\left. - \sqrt{(P_i l - ST_i)^2 + S^2} + S T_i \log_e\left|\frac{-(P_i l - ST_i) + \sqrt{(P_i l - ST_i)^2 + S^2}}{S(T_i + S_i')}\right|\right]\right\}$$

$$I_{o_6} = \bar{P}\int_{-l}^{0}\left\{\frac{2}{l}\gamma(0)x - \frac{2}{l}\gamma(-\tfrac{l}{2})x\right\}\left\{\frac{P_o T_o' x + (2P_o - 1)T_o}{\sqrt{(P_o x + S T_o)^2 + S^2}}\right\}dx$$

$$= \left\{\gamma(0) - \gamma(-\tfrac{l}{2})\right\}\left\{\frac{T_o'}{P_o^2 l}\left[-3S^2 T_o S_o' + (P_o l + 3ST_o)\sqrt{(P_o l - ST_o)^2 + S^2}\right.\right.$$

$$\left. + S^2(2T_o^2 - 1)\log_e\left|\frac{S(T_o + S_o')}{-(P_o l - ST_o) + \sqrt{(P_o l - ST_o)^2 + S^2}}\right|\right] + \frac{2(2P_o - 1)T_o}{P_o^2 l}\left[S S_o'\right.$$

$$\left.\left. - \sqrt{(P_o l - ST_o)^2 + S^2} + S T_o \log_e\left|\frac{-(P_o l - ST_o) + \sqrt{(P_o l - ST_o)^2 + S^2}}{S(T_o + S_o')}\right|\right]\right\}$$

$$I_{i_7} = \bar{P}\int_{-l}^{0}\left\{\frac{2}{l}\gamma(0)x - \frac{2}{l}\gamma(-\tfrac{l}{2})x\right\}\left\{\frac{S S_i'^2}{x\sqrt{(P_i x + S T_i)^2 + S^2}}\right\}dx$$

$$= \frac{2 S S_i'^2}{P_i l}\left\{\gamma(0) - \gamma(-\tfrac{l}{2})\right\}\left\{\log_e\left|\frac{S(T_i + S_i')}{-(P_i l - ST_i) + \sqrt{(P_i l - ST_i)^2 + S^2}}\right|\right\}$$

$$I_{oq} = \bar{P} \int_{-\ell}^{0} \left\{ \frac{2}{\ell} \gamma(0) x - \frac{2}{\ell} \gamma(-\tfrac{\ell}{2}) x \right\} \left\{ \frac{s\, S_o'^2}{x \sqrt{(P_o x + s T_o)^2 + s^2}} \right\} dx$$

$$= \frac{2 s S_o'^2}{P_o \ell} \left\{ \gamma(0) - \gamma(-\tfrac{\ell}{2}) \right\} \left\{ \log_e \left| \frac{s(T_o + S_o')}{-(P_o \ell - s T_o) + \sqrt{(P_o \ell - s T_o)^2 + s^2}} \right| \right\}$$

$$I_{iB} = -\int_{-\ell}^{0} \left\{ \frac{2}{\ell} \gamma(0) x - \frac{2}{\ell} \gamma(-\tfrac{\ell}{2}) x \right\} \left\{ \frac{T_i}{x} + T_i' \right\} dx$$

$$= -2 \left\{ \gamma(0) - \gamma(-\tfrac{\ell}{2}) \right\} \left\{ T_i - \frac{\ell}{2} T_i' \right\}$$

$$I_{oB} = \int_{-\ell}^{0} \left\{ \frac{2}{\ell} \gamma(0) x - \frac{2}{\ell} \gamma(-\tfrac{\ell}{2}) x \right\} \left\{ \frac{T_o}{x} + T_o' \right\} dx$$

$$= 2 \left\{ \gamma(0) - \gamma(-\tfrac{\ell}{2}) \right\} \left\{ T_o - \frac{\ell}{2} T_o' \right\}$$

$$I_{iq} = \bar{P} \int_{0}^{\ell} \left\{ -\frac{2}{\ell} \gamma(0) x + \frac{2}{\ell} \gamma(\tfrac{\ell}{2}, x) \right\} \left\{ \frac{P_i T_i' x + (2P_i + 1) T_i}{\sqrt{(P_i x + s T_i)^2 + s^2}} \right\} dx$$

$$= \left\{ -\gamma(0) + \gamma(\tfrac{\ell}{2}) \right\} \left\{ \frac{T_i'}{P_i^2 \ell} \left[3 s^2 T_i S_i' + (P_i \ell - 3 s T_i) \sqrt{(P_i \ell + s T_i)^2 + s^2} \right. \right.$$

$$\left. + s^2 (2 T_i^2 - 1) \log_e \left| \frac{(P_i \ell + s T_i) + \sqrt{(P_i \ell + s T_i)^2 + s^2}}{s(T_i + S_i')} \right| \right] + \frac{2(2P_i + 1) T_i}{P_i^2 \ell} \left[-s S_i' \right.$$

$$\left. \left. + \sqrt{(P_i \ell + s T_i)^2 + s^2} + s T_i \log_e \left| \frac{s(T_i + S_i')}{(P_i \ell + s T_i) + \sqrt{(P_i \ell + s T_i)^2 + s^2}} \right| \right] \right\}$$

$$I_{0_9} = \bar{P}\int_0^{\ell}\left\{-\frac{2}{\ell}\gamma(0)x + \frac{2}{\ell}\gamma\left(\frac{\ell}{2}\right)x\right\}\left\{\frac{P_0 T_0' x + (2P_0 - 1)\,T_0}{\sqrt{(P_0 x + 5T_0)^2 + 5^2}}\right\}dx$$

$$= \left\{-\gamma(0) + \gamma\left(\frac{\ell}{2}\right)\right\}\left\{\frac{T_0'}{P_0^2\ell}\left[3S^2 T_0 S_0' + (P_0\ell - 3ST_0)\sqrt{(P_0\ell + 5T_0)^2 + S^2}\right.\right.$$

$$\left. + S^2(2T_0^2 - 1)\,\text{LOG}_e\left/\frac{(P_0\ell + 5T_0) + \sqrt{(P_0\ell + 5T_0)^2 + S^2}}{S(T_0 + S_0')}\right/\right] + \frac{2(2P_0 - 1)\,T_0}{P_0^2\ell}\left[-5S_i'\right.$$

$$\left. + \sqrt{(P_0\ell + 5T_0)^2 + S^2} + 5T_0\,\text{LOG}_e\left/\frac{S(T_0 + S_0')}{(P_0\ell + 5T_0) + \sqrt{(P_0\ell + 5T_0)^2 + S^2}}\right/\right]\right\}$$

$$I_{i_{10}} = \bar{P}\int_0^{\ell}\left\{-\frac{2}{\ell}\gamma(0)x + \frac{2}{\ell}\gamma\left(\frac{\ell}{2}\right)x\right\}\left\{\frac{S S_i'^2}{x\sqrt{(P_i x + 5T_i)^2 + S^2}}\right\}dx$$

$$= \frac{2SS_i'^2}{P_i\ell}\left\{-\gamma(0) + \gamma\left(\frac{\ell}{2}\right)\right\}\text{LOG}_e\left/\frac{(P_i\ell + 5T_i) + \sqrt{(P_i\ell + 5T_i)^2 + S^2}}{S(T_i + S_i')}\right/$$

$$I_{0_{10}} = \bar{P}\int_0^{\ell}\left\{-\frac{2}{\ell}\gamma(0)x + \frac{2}{\ell}\gamma\left(\frac{\ell}{2}\right)x\right\}\left\{\frac{S S_0'^2}{x\sqrt{(P_0 x + 5T_0)^2 + S^2}}\right\}dx$$

$$= \frac{2SS_0'^2}{P_0\ell}\left\{-\gamma(0) + \gamma\left(\frac{\ell}{2}\right)\right\}\text{LOG}_e\left/\frac{(P_0\ell + 5T_0) + \sqrt{(P_0\ell + 5T_0)^2 + S^2}}{S(T_0 + S_0')}\right/$$

$$\int_0^{\ell}\left\{-\frac{2}{\ell}\gamma(0)x + \frac{2}{\ell}\gamma\left(\frac{\ell}{2}\right)x\right\}\left\{\frac{T_i}{x} + T_i'\right\}dx$$

$$= 2\left\{-\gamma(0) + \gamma\left(\frac{\ell}{2}\right)\right\}\left\{\frac{T_i}{x} + T_i'\right\}dx$$

$$I_{0_{11}} = -\int_0^{\ell}\left\{-\frac{2}{\ell}\gamma(0)x + \frac{2}{\ell}\gamma\left(\frac{\ell}{2}\right)x\right\}\left\{\frac{T_0}{x} + T_0'\right\}dx$$

$$= -2\left\{-\gamma(0) + \gamma\left(\frac{\ell}{2}\right)\right\}\left\{T_0 - \frac{\ell}{2}T_0'\right\}$$

When the integrals associated with the downwash due to the vorticity on the inboard side of the continuous vorticity patch are substituted back into equation (18) the following downwash expression is obtained.

$$\frac{w}{V_\infty}(0)_i = -\frac{1}{4\pi V_\infty}\left[\frac{1}{R_i}\left\{\gamma\left(\tfrac{l}{2}\right)T_i' - \frac{T_i(R_i-1)}{R_i l}\left[\gamma(0)-\gamma\left(\tfrac{l}{2}\right)\right]\right\}\sqrt{(R_i l+sT_i)^2+s^2}\right.$$

$$-\frac{1}{R_i}\left\{\gamma\left(-\tfrac{l}{2}\right)T_i' + \frac{T_i(R_i-1)}{R_i l}\left[\gamma(0)-\gamma\left(-\tfrac{l}{2}\right)\right]\sqrt{(R_i l-sT_i)^2+s^2}\right.$$

$$+\frac{s(R_i-1)}{R_i^2 l}\left[2\gamma(0)-\gamma\left(-\tfrac{l}{2}\right)-\gamma\left(\tfrac{l}{2}\right)\right]\log_e\left|s(S_i'+T_i)\right|$$

$$-\gamma(0)S_i'\log_e\left|\frac{sS_i'^2+T_iR_il+S_i'\sqrt{(R_il+sT_i)^2+s^2}}{sS_i'^2-T_iR_il+S_i'\sqrt{(R_il-sT_i)^2+s^2}}\right|$$

$$-\frac{1}{R_i}\left\{\gamma(0)T_i(3R_i+1)+\frac{s(R_i-1)}{R_i l}\left[\gamma(0)-\gamma\left(-\tfrac{l}{2}\right)\right]\right\}\log_e\left|-(R_il-sT_i)+\sqrt{(R_il-sT_i)^2+s^2}\right|$$

$$+\frac{1}{R_i}\left\{\gamma(0)T_i(3R_i+1)-\frac{s(R_i-1)}{R_i l}\left[\gamma(0)-\gamma\left(\tfrac{l}{2}\right)\right]\right\}\log_e\left|(R_il+sT_i)+\sqrt{(R_il+sT_i)^2+s^2}\right|$$

$$+\frac{T_isS_i(R_i-1)}{R_i^2 l}\left[2\gamma(0)-\gamma\left(-\tfrac{l}{2}\right)-\gamma\left(\tfrac{l}{2}\right)\right]-2\left[2\gamma(0)-\gamma\left(-\tfrac{l}{2}\right)-\gamma\left(\tfrac{l}{2}\right)\right]\left[T_i-\tfrac{l}{2}T_i'\right]$$

$$\left.+\pi T_iS_i'\gamma(0)\right] \qquad (19)$$

Where I_{i5} has been replaced with $\pi T_i S_i' \gamma(0)$ from reference 17.

An expression similar to equation (19) can be given for the downwash due to the starboard side.

$$\frac{w}{V_\infty}(0)_o = -\frac{1}{4\pi V_\infty}\left[\frac{1}{R_o}\left\{\gamma\left(\frac{\ell}{2}\right)T_o' - \frac{T_o(R_o+1)}{R_o\ell}\left[\gamma(0)-\gamma\left(\frac{\ell}{2}\right)\right]\right\}\sqrt{(R_o\ell+sT_o)^2+s^2}\right.$$

$$-\frac{1}{R_o}\left\{\gamma\left(-\frac{\ell}{2}\right)T_o' + \frac{T_o(R_o+1)}{R_o\ell}\left[\gamma(0)-\gamma\left(-\frac{\ell}{2}\right)\right]\right\}\sqrt{(R_o\ell-sT_o)^2+s^2}$$

$$+\frac{s(R_o+1)}{R_o^2\ell}\left[2\gamma(0)-\gamma\left(-\frac{\ell}{2}\right)-\gamma\left(\frac{\ell}{2}\right)\right]\log_e\left|s(T_o+S_o')\right|$$

$$-\gamma(0)S_o'\log_e\left|\frac{sS_o'^2+T_oR_o\ell+S_o'\sqrt{(R_o\ell+sT_o)^2+s^2}}{sS_o'^2-T_oR_o\ell+S_o'\sqrt{(R_o\ell-sT_o)^2+s^2}}\right|$$

$$-\frac{1}{R_o}\left\{\gamma(0)T_o(3R_o-1)+\frac{s(R_o+1)}{R_o\ell}\left[\gamma(0)-\gamma\left(-\frac{\ell}{2}\right)\right]\log_e\left|-(R_o\ell-sT_o)+\sqrt{(R_o\ell-sT_o)+s^2}\right|\right\}$$

$$+\frac{1}{R_o}\left\{\gamma(0)T_o(3R_o-1)-\frac{s(R_o+1)}{R_o\ell}\left[\gamma(0)-\gamma\left(\frac{\ell}{2}\right)\right]\log_e\left|(R_o\ell+sT_o)+\sqrt{(R_o\ell+sT_o)+s^2}\right|\right\}$$

$$+\frac{T_osS_o(R_o+1)}{R_o^2\ell}\left[2\gamma(0)-\gamma\left(-\frac{\ell}{2}\right)-\gamma\left(\frac{\ell}{2}\right)\right]+2\left\{2\gamma(0)-\gamma\left(-\frac{\ell}{2}\right)-\gamma\left(\frac{\ell}{2}\right)\right\}\left\{T_o-\frac{\ell}{2}T_o'\right\}$$

$$\left.-\pi T_oS_o'\gamma(0)\right] \qquad (20)$$

Equations (19) and (20) when added represent the total downwash at x = 0 due to a distribution of vorticity, where the sweep of the constant vorticity lines vary with x. The span of the vorticity lines is arbitrary in length and can be varied to determine the effect of grid aspect ratio on the ability of discrete vortices to represent the downwash of continuous vorticity distributions. Also, the sweep of the port and starboard portions of the vorticity patch can be varied independently to represent a kink or crank in the wing planform. Therefore, the ability of discrete vortices to represent breaks in the leading and trailing edges can also be checked with these expressions.

In order to obtain the effects of grid aspect ratio and vortex sweep on the accuracy of the induced downwash calculation, when the continuous vorticity is represented by a grid of discrete skewed vortices, equations (11), (12), (19), and (20) will be specialized to the case where $T_i = T_o = 0$, $T_{\bar{i}} = T_{\bar{o}} = T$, and the vortex grid aspect ratio $2s/\ell$ is finite. The downwash at $x = 0$ due to two finite skewed vortices at $x = -\frac{\ell}{2}$ and at $x = \frac{\ell}{2}$ is obtained from equations (10), (11), and (12).

$$\frac{w}{V_\infty}(0) = \frac{K_1 - K_2}{2\pi V_\infty \ell}\left\{\frac{S'^2 + \xi T}{\sqrt{(\xi+T)^2+1}} + \frac{S'^2 - \xi T}{\sqrt{(\xi-T)^2+1}}\right\} \tag{21}$$

Where $S' = \sec.\phi$, $T = \tan\phi$, $\xi = \ell/2s$ and K_1 and K_2 are the strengths of the discrete vortices at $x = -\ell/2$ and $x = \ell/2$ respectively.

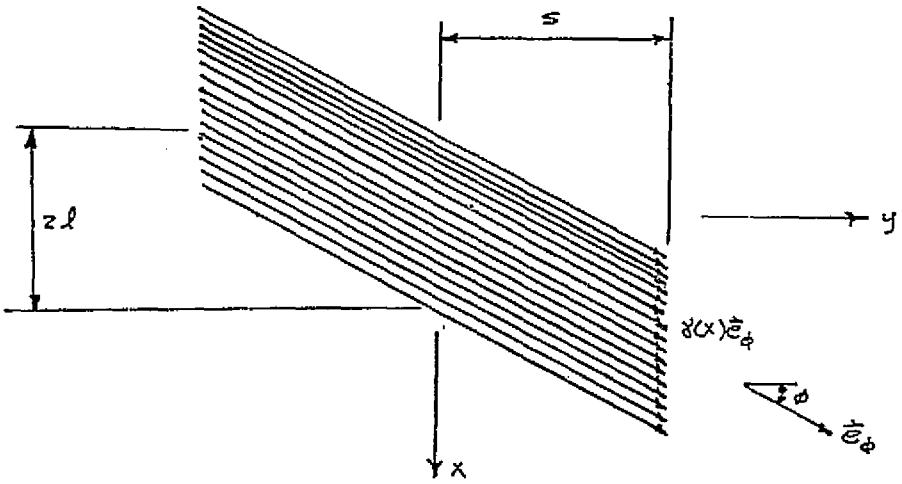

Figure G-2. Skewed Vorticity

If K_1 and K_2 are the absolute values of $\vec{K}_1$ and $\vec{K}_2$, respectively, where

$$\vec{K}_1 = \int_{-\ell}^{0} \gamma(x)\,\hat{e}_\phi\,dx = \gamma(-\tfrac{\ell}{2})\,\ell\,\hat{e}_\phi \quad \text{and} \quad \vec{K}_2 = \int_{0}^{\ell} \gamma(x)\,\hat{e}_\phi\,dx = \gamma(\tfrac{\ell}{2})\,\ell\,\hat{e}_\phi \tag{22}$$

Then;

$$\frac{w}{V_\infty}(0) = \frac{\gamma(-\frac{\ell}{2}) - \gamma(\frac{\ell}{2})}{2\pi V_\infty}\left\{\frac{S'^2 + \xi T}{\sqrt{(\xi+T)^2+1}} + \frac{S'^2 - \xi T}{\sqrt{(\xi-T)^2+1}}\right\} \tag{23}$$

Also, from equations (13), (19), and (20) the downwash at x = 0 due to the continuous distribution of vorticity $\gamma(x)$ from $x = -\ell$ to $x = \ell$ is given by;

$$\frac{w}{V_\infty}(0) = \frac{\gamma(-\frac{\ell}{2}) - \gamma(\frac{\ell}{2})}{4\pi V_\infty \xi} \left\{ \log_e \left| \frac{(2\xi+T) + \sqrt{(2\xi+T)^2+1}}{-(2\xi-T) + \sqrt{(2\xi-T)^2+1}} \right| + T \left[\sqrt{(2\xi+T)^2+1} - \sqrt{(2\xi-T)^2+1} \right] \right\} \tag{24}$$

It is interesting to note that the downwash induced at x = 0 due to two infinite skewed vortices, one at $x = -\ell/2$ and the other at $x = \ell/2$, and that induced at x = 0 due to a continuous distribution of infinite skewed vorticity are equal. This is observed in the limit as $\xi \to 0$ in equations (23) and (24).

For $\xi = 0$ the downwash ratio at x = 0 due to equation (23) is,

$$\frac{w}{V_\infty}(0) = \frac{\gamma(-\frac{\ell}{2}) - \gamma(\frac{\ell}{2})}{\pi V_\infty \cos\phi} \tag{25}$$

and due to equation (24)

$$\frac{w}{V_\infty}(0) = \frac{\gamma(-\frac{\ell}{2}) - \gamma(\frac{\ell}{2})}{4\pi V_\infty} \lim_{\xi \to 0} \left\{ \frac{\frac{\partial}{\partial \xi} \log_e \left| (2\xi+T) + \sqrt{(2\xi+T)^2+1} \right|}{\frac{\partial \xi}{\partial \xi}} \right.$$

$$- \frac{\frac{\partial}{\partial \xi} \log_e \left| -(2\xi-T) + \sqrt{(2\xi-T)^2+1} \right|}{\frac{\partial \xi}{\partial \xi}}$$

$$\left. + T \frac{\frac{\partial}{\partial \xi} \left[\sqrt{(2\xi+T)^2+1} - \sqrt{(2\xi-T)^2+1} \right]}{\frac{\partial \xi}{\partial \xi}} \right\} \tag{26}$$

$$\frac{w}{V_\infty}(0) = \frac{\gamma(-\frac{\ell}{2}) - \gamma(\frac{\ell}{2})}{4\pi V_\infty} \lim_{\xi \to 0} \left\{ \frac{2(2\xi+\tau)\tau}{\sqrt{(2\xi+\tau)^2+1}} - \frac{2(2\xi-\tau)\tau}{\sqrt{(2\xi-\tau)^2+1}} \right.$$

$$+ \frac{2 + 2(2\xi+\tau)/\sqrt{(2\xi+\tau)^2+1}}{(2\xi+\tau) + \sqrt{(2\xi+\tau)^2+1}}$$

$$\left. - \frac{-2 + 2(2\xi-\tau)/\sqrt{(2\xi-\tau)^2+1}}{-(2\xi-\tau) + \sqrt{(2\xi-\tau)^2+1}} \right\} \tag{27}$$

$$\frac{w}{V_\infty}(0) = \frac{\gamma(-\frac{\ell}{2}) - \gamma(\frac{\ell}{2})}{\pi V_\infty \cos\phi} \tag{28}$$

which is the same as equation (25). It is also noted that for $\phi = 0$ both equations (25) and (28) reduce to that obtained for the two dimensional case in equations (1) and (9).

Another interesting observation which can be made from equations (19) and (20) is that the downwash is independent of the vorticity, at the downwash point, when the lines of constant vorticity are continuous. For the case in which the lines of constant vorticity are not continuous, the additional downwash is seen to be proportional to the vorticity at the downwash point.

The ratio of equation (23) to equation (24) is shown in figure G-3 as a function of grid aspect ratio for two sweeps. It is evident from this figure that the simpler infinite aspect ratio expressions can be used to determine the strengths of the discrete vortices used to represent the continuous distribution of vorticity. These vortex strengths will be determined such that the same downwash is obtained at points midway between each vortex and the same circulation developed at each span station, when the discrete vortices are used, as would be obtained by analytically integrating the influence of the continuous vorticity.

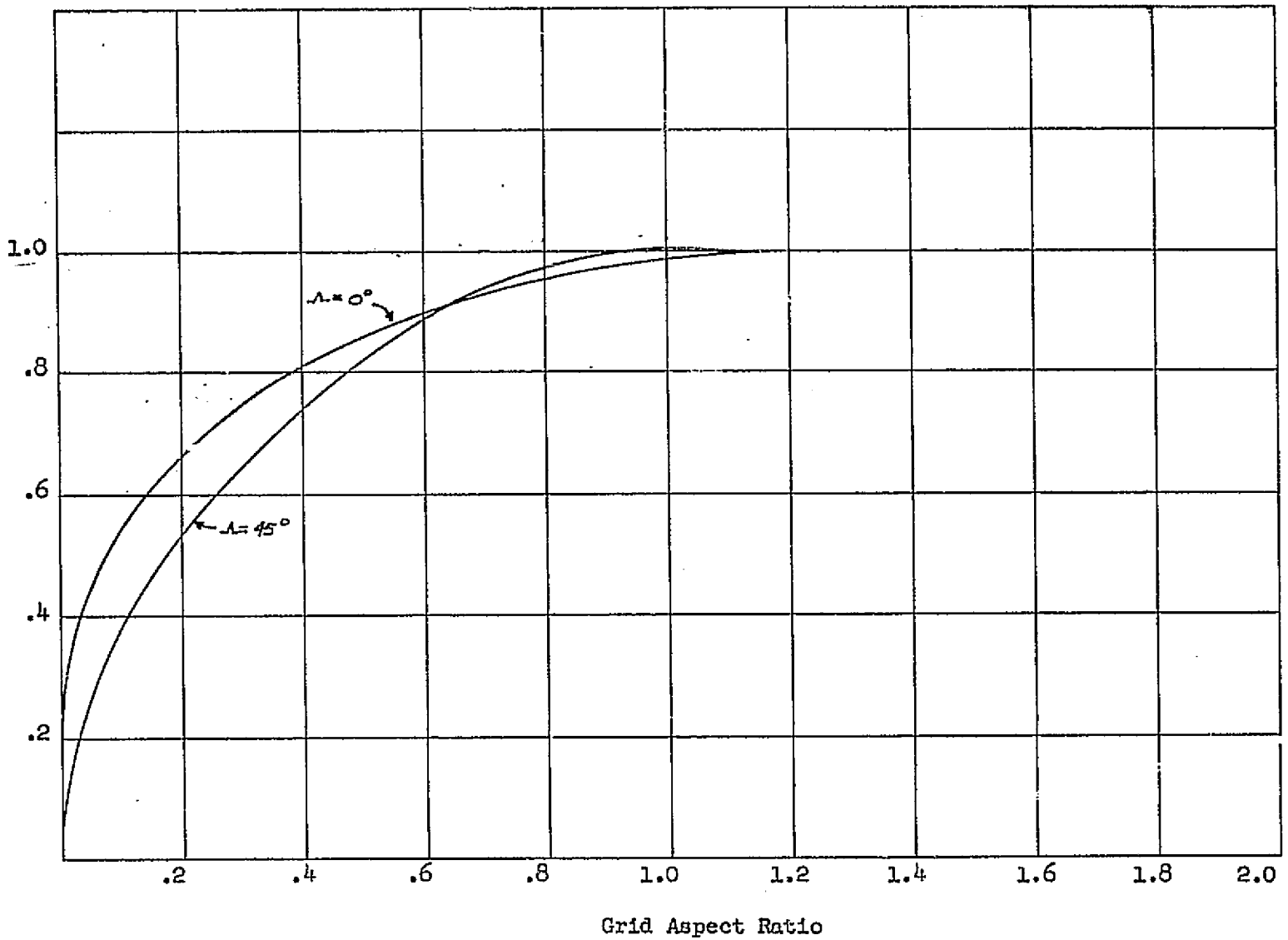

Figure G-3. Comparison of Downwash due to Discrete Vortices and Continuous Vorticity as a Function of Grid Aspect Ratio

If s is allowed to approach infinity in equations (11) and (12), influence functions for an infinite aspect ratio grid are obtained.

$$E_{w_i} = \frac{1}{\cos\phi_i}\left\{\frac{\sin\phi_i}{|x_j - x_i|} - \frac{1}{(x_j - x_i)}\right\} \tag{29}$$

$$E_{w_0} = -\frac{1}{\cos\phi_0}\left\{\frac{\sin\phi_0}{|x_j - x_i|} + \frac{1}{(x_j - x_i)}\right\} \tag{30}$$

The downwash at X_j due to a vortex K_i at X_i is then given by;

$$\frac{w}{V_\infty}(x_j)_i = \frac{K_i}{4\pi V_\infty}\left\{\frac{1}{\cos\phi_{ii}}\left[\frac{1}{(x_j - x_i)} - \frac{\sin\phi_{ii}}{|x_j - x_i|}\right]\right.$$

$$\left. + \frac{1}{\cos\phi_{0i}}\left[\frac{1}{(x_j - x_i)} + \frac{\sin\phi_{0i}}{|x_j - x_i|}\right]\right\} \tag{31}$$

The downwash at X_j due to the distribution of vorticity $\gamma(x)$ between $x_i - \varepsilon$ and $x_i + \varepsilon$ is similarly given by;

$$\frac{w}{V}(x_j)_i = \frac{1}{4\pi V_\infty}\int_{x_i-\varepsilon}^{x_i+\varepsilon}\gamma(x)\left\{\frac{1}{\cos\phi_{ii}}\left[\frac{1}{(x_j - x)} - \frac{\sin\phi_{ii}}{|x_j - x|}\right]\right. \tag{32}$$

$$\left. + \frac{1}{\cos\phi_{0i}}\left[\frac{1}{(x_j - x)} + \frac{\sin\phi_{0i}}{|x_j - x|}\right]\right\} dx$$

where $\varepsilon = \dfrac{x_{i+1} - x_i}{2}$

The vortex grid is shown schematically in figure G-4.

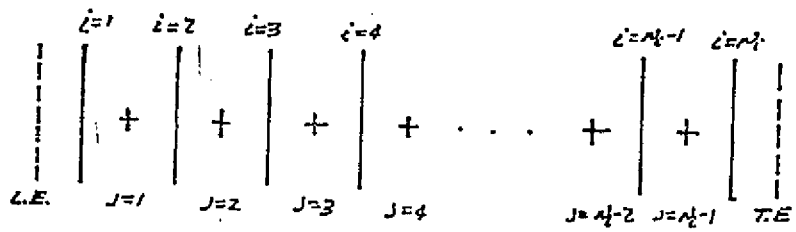

Figure G-4. Schematic of Vortex Grid

Equations (31) and (32) are then summed over the chord to obtain the total downwash at each j point. The discrete vortex pattern produces the following total downwash at any j point.

$$\frac{w}{V_\infty}(x_j) = \frac{1}{4\pi V_\infty}\left\{\sum_{i=1}^{j}\left[\frac{K_i(1-\sin\phi_{ii})}{(x_j-x_i)\cos\phi_{ii}} + \frac{K_i(1+\sin\phi_{oi})}{(x_j-x_i)\cos\phi_{oi}}\right]\right.$$

$$\left. + \sum_{i=j+1}^{N_i}\left[\frac{K_i(1+\sin\phi_{ii})}{(x_j-x_i)\cos\phi_{ii}} + \frac{K_i(1-\sin\phi_{oi})}{(x_j-x_i)\cos\phi_{oi}}\right]\right\} \tag{33}$$

A similar expression can be obtained for the total downwash at any j point due to the continuous vorticity distribution.

$$\frac{w}{V_\infty}(x_j) = \frac{1}{4\pi V_\infty}\left\{\sum_{i=1}^{j}\int_{\frac{1}{2}(3x_i - x_{i+1})}^{\frac{1}{2}(x_i + x_{i+1})}\left[\frac{\gamma(x)(1-\sin\phi_{ii})}{(x_j-x)\cos\phi_{ii}} + \frac{\gamma(x)(1+\sin\phi_{oi})}{(x_j-x)\cos\phi_{oi}}\right]dx\right.$$

$$\left. + \sum_{i=j+1}^{N_i}\int_{\frac{1}{2}(3x_i - x_{i+1})}^{\frac{1}{2}(x_i + x_{i+1})}\left[\frac{\gamma(x)(1+\sin\phi_{ii})}{(x_j-x)\cos\phi_{ii}} + \frac{\gamma(x)(1-\sin\phi_{oi})}{(x_j-x)\cos\phi_{oi}}\right]dx\right\} \tag{34}$$

If the sweep of the lines of constant vorticity are held constant over each of the grid panels, then;

$$\frac{w}{V_\infty}(x_j) = \frac{1}{4\pi V_\infty}\left\{\sum_{i=1}^{j}\left[\frac{1-\sin\phi_{ii}}{\cos\phi_{ii}} + \frac{1+\sin\phi_{oi}}{\cos\phi_{oi}}\right]\int_{\frac{1}{2}(3x_i - x_{i+1})}^{\frac{1}{2}(x_i + x_{i+1})}\frac{\gamma(x)\,dx}{x_j - x}\right.$$

$$\left. + \sum_{i=j+1}^{N_i}\left[\frac{1+\sin\phi_{ii}}{\cos\phi_{ii}} + \frac{1-\sin\phi_{oi}}{\cos\phi_{oi}}\right]\int_{\frac{1}{2}(3x_i - x_{i+1})}^{\frac{1}{2}(x_i + x_{i+1})}\frac{\gamma(x)\,dx}{x_j - x}\right\} \tag{35}$$

Equation (33) can be put into a similar form as follows.

$$\frac{w}{V_\infty}(x_j) = \frac{1}{4\pi V_\infty}\left\{\sum_{i=1}^{j}\left[\frac{1-\sin\phi_{ii}}{\cos\phi_{ii}} + \frac{1+\sin\phi_{oi}}{\cos\phi_{oi}}\right]\frac{K_i}{x_j - x_i}\right.$$

$$\left. + \sum_{i=j+1}^{N_i}\left[\frac{1+\sin\phi_{ii}}{\cos\phi_{ii}} + \frac{1-\sin\phi_{oi}}{\cos\phi_{oi}}\right]\frac{K_i}{x_j - x_i}\right\} \qquad (36)$$

The vorticity $\gamma(x)$ is defined in equation (50) of Appendix A.

$$\gamma(\theta,\eta) = \frac{4bV_\infty}{c}\left\{F_0 \cot\frac{\theta}{2} + \sum_{N=1}^{N_0-3} F_N \sin N\theta\right.$$

$$+ F_f \log_e\left|\frac{\sin\frac{1}{2}(\theta+\theta_f)}{\sin\frac{1}{2}(\theta-\theta_f)}\right| \qquad (37)$$

$$\left. + F_k \log_e\left|\frac{\sin\frac{1}{2}(\theta+\theta_k)}{\sin\frac{1}{2}(\theta-\theta_k)}\right|\right\}$$

where $\theta = \cos^{-1}(1-\frac{2x}{c})$

Therefore; $\gamma(x)$ is a linear combination of N_L load shapes.

$$\gamma(x) = \gamma_0(x) + \gamma_f(x) + \gamma_k(x) + \sum_{N=1}^{N_0-3}\gamma_N(x) \qquad (38)$$

There will be one set of K_i's for each of these load shapes, therefore;

$$K_i = K_{0i} + K_{fi} + K_{ki} + \sum_{N=1}^{N_0-3} K_{Ni} \qquad (39)$$

It is these $N_u \times N_i$ values of K which must be determined such that the downwash and section circulation are the same for both the discrete and continuous loadings. Equations (35) and (36) will supply $(N_i - 1) \times N_u$ equations. An additional N_u equations can be developed from the condition that the section circulations due to the discrete and continuous loadings agree.

The total section circulation per freestream velocity for the discrete vortices is;

$$\Gamma/V_\infty = \sum_{i=1}^{N_i} K_i/V_\infty \tag{40}$$

The corresponding circulation ratio for the continuous loadings is;

$$\Gamma/V_\infty = 2b\pi\left[E_0 + \tfrac{1}{2}E_1 + E_2 \sin\theta_f + E_3 \sin\theta_k\right] \tag{41}$$

where θ_k and θ_f are the leading and trailing edge flap hinge locations respectively.

After substituting equation (38) into equation (35) and equation (39) into equation (36) the following equations are obtained respectively.

$$\left[\frac{w}{V_\infty}(x_j)\right]_{1 \times N_u} = \frac{1}{4\pi V_\infty}\left[\ \Phi_i\ \right]_{1 \times N_i}\left[\overline{E}_{0i}, \overline{E}_{1i}, \overline{E}_{2i}, \cdots, \overline{E}_{(N_u-3)i}, \overline{E}_{3i}, E_{ki}\right]_{N_i \times N_u} \tag{42}$$

$$\left[\frac{w}{V_\infty}(x_j)\right]_{1 \times N_u} = \frac{1}{4\pi V_\infty}\left[\ \Phi_i\ \right]_{1 \times N_i}\left[E'_{0i}, E'_{1i}, E'_{2i}, \cdots, E'_{(N_u-3)}, E'_{3i}, E'_{ki}\right]_{N_i \times N_u} \tag{43}$$

where

$$\Phi_i = \left[\frac{1-\sin\phi_{ii}}{\cos\phi_{ii}} + \frac{1+\sin\phi_{oi}}{\cos\phi_{oi}} \right] \qquad 1 \le i \le j$$

$$\Phi_i = \left[\frac{1+\sin\phi_{ii}}{\cos\phi_{ii}} + \frac{1-\sin\phi_{oi}}{\cos\phi_{oi}} \right] \qquad j < i \le N_i$$

$$\bar{E}_{Ni} = \int_{\frac{1}{2}(3x_i - x_{i+1})}^{\frac{1}{2}(x_i - x_{i+1})} \frac{\gamma_N(x)\,dx}{x_j - x} = \bar{E}_{Ni}(x_j, x_i) \qquad N = 0, 1, 2, \cdots, N_i - 3$$

$$\bar{E}_{fi} = \int_{\frac{1}{2}(3x_i - x_{i+1})}^{\frac{1}{2}(x_i - x_{i+1})} \frac{\gamma_f(x)\,dx}{x_j - x} = \bar{E}_{fi}(x_j, x_i)$$

$$\bar{E}_{ki} = \int_{\frac{1}{2}(3x_i - x_{i+1})}^{\frac{1}{2}(x_i - x_{i+1})} \frac{\gamma_k(x)\,dx}{x_j - x} = \bar{E}_{ki}(x_j, x_i)$$

$$E'_{Ni} = \frac{K_{Ni}}{x_j - x_i} = E'_{Ni}(x_j, x_i)$$

$$E'_{fi} = \frac{K_{fi}}{x_j - x_i} = E'_{fi}(x_j, x_i)$$

$$E'_{ki} = \frac{K_{ki}}{x_j - x_i} = E'_{ki}(x_j, x_i)$$

Since the elements of the matrix $[\bar{\phi}_i]$ are independent, equation (42) and equation (43) are equal at the j points provided $\bar{E}(x_j, x_i) = E'(x_j, x_i)$ for all of the chordwise load shapes.

Also, since the functions $\bar{E}(x_j, x_i)$ obtained for each value of i are independent, then $\bar{E}(x_j, x_i) = E'(x_j, x_i)$ for all chordwise load shapes if;

$$\left[\frac{w}{V_\infty}(x_j)_0, \frac{w}{V_\infty}(x_j)_1, \cdots, \frac{w}{V_\infty}(x_j)_{N_u-3}, \frac{w}{V_\infty}(x_j)_f, \frac{w}{V_\infty}(x_j)_\alpha\right]$$

$$= \frac{1}{4\pi V_\infty}\left[\frac{1}{x_j - x_i}\right]_{(N_i-1)\times N_i}\left[K_{0i}, K_{1i}, K_{2i}, \cdots, K_{(N_u-3)i}, K_{fi}, K_{\alpha i}\right]_{N_i \times N_u}$$

$$= \frac{1}{4\pi V_\infty}\left[\sum_{i=1}^{N_i}\bar{E}_{0i}, \sum_{i=1}^{N_i}\bar{E}_{1i}, \sum_{i=1}^{N_i}\bar{E}_{2i}, \cdots, \sum_{i=1}^{N_i}\bar{E}_{(N_u-3)i}, \sum_{i=1}^{N_i}\bar{E}_{fi}, \sum_{i=1}^{N_i}\bar{E}_{\alpha i}\right] \qquad (44)$$

The matrix equation (44) represents $N_i \times N_u$ unknowns and $(N_i-1)\times N_i$ independent equations. An additional N_u equations are obtained from equations (39), (40), and (41).

$$\left[1, 1, \cdots, 1\right]_{1\times N_i}\left[K_{0i}, K_{1i}, K_{2i}, \cdots, K_{(N_u-3)i}, K_{fi}, K_{\alpha i}\right]_{N_i \times N_u}$$

$$= 2b\pi\left[F_0, \tfrac{1}{2}F_1, 0, \cdots, 0, F_f \sin\theta_f, F_\alpha \sin\theta_\alpha\right]_{1\times N_u} \qquad (45)$$

Expressions for $\sum_{i=1}^{N_i} \bar{E}_{Ni}$, $\sum_{i=1}^{N_i} \bar{E}_{fi}$ and $\sum_{i=1}^{N_i} \bar{E}_{ki}$ are then evaluated as follows.

$$\sum_{i=1}^{N_i} \bar{E}_{0i} = \int_0^c \frac{\gamma_0(x)}{x_j - x_i}\,dx = \frac{4bV_0}{c} \int_0^\pi \frac{E_0 \cot\theta/2 \sin\theta\, d\theta}{\cos\theta - \cos\theta_j}$$

$$= \frac{4bV_0 E_0}{c}\left[\int_0^\pi \frac{d\theta}{\cos\theta - \cos\theta_j} + \int_0^\pi \frac{\cos\theta\, d\theta}{\cos\theta - \cos\theta_j}\right]$$

$$= \frac{4\pi V_0 b E_0}{c} \tag{46}$$

$$\sum_{i=1}^{N_i} \bar{E}_{Ni} = \int_0^c \frac{\gamma_N(x)\,dx}{x_j - x_i} = \frac{4bV_0}{c} \sum_{N=1}^{N_0-3} E_N \int_0^\pi \frac{\sin N\theta \sin\theta\, d\theta}{\cos\theta - \cos\theta_j}$$

$$= \frac{2bV_0}{c} \sum_{N=1}^{N_0-3} E_N \left\{\int_0^\pi \frac{\cos(N-1)\theta\, d\theta}{\cos\theta - \cos\theta_j} - \int_0^\pi \frac{\cos(N+1)\theta\, d\theta}{\cos\theta - \cos\theta_j}\right\}$$

$$= \frac{2\pi V_0 b}{c} \sum_{N=1}^{N_0-3} E_N \left[\frac{\sin(N-1)\theta_j}{\sin\theta_j} - \frac{\sin(N+1)\theta_j}{\sin\theta_j}\right]$$

$$= -\frac{4\pi V_0 b}{c} \sum_{N=1}^{N_0-3} E_N \cos N\theta_j \tag{47}$$

$$\sum_{i=1}^{N_i} \bar{E}_{fi} = \int_0^c \frac{\gamma_f(x)\,dx}{x_j - x} = \frac{4bV_0}{c} \int_0^\pi \frac{E_f \log_e \left|\sin\frac{1}{2}(\theta+\theta_j)\right| / \left|\sin\frac{1}{2}(\theta-\theta_j)\right| \sin\theta\, d\theta}{\cos\theta - \cos\theta_j}$$

since;

$$\sum_{N=1}^{\infty}\left[\frac{\cos N(\theta-\theta_i)}{N}-\frac{\cos N(\theta+\theta_i)}{N}\right]=\log_e\left|\frac{\sin\frac{1}{2}(\theta+\theta_i)}{\sin\frac{1}{2}(\theta-\theta_i)}\right|$$

$$\sum_{i=1}^{N_i}E_{fi}=\frac{4bV_0F_z}{c}\sum_{N=1}^{\infty}\frac{1}{N}\left[\int_0^{\pi}\frac{\cos N(\theta-\theta_i)}{\cos\theta-\cos\theta_j}\sin\theta\,d\theta\right.$$

$$\left.-\int_0^{\pi}\frac{\cos N(\theta+\theta_i)}{\cos\theta-\cos\theta_j}\sin\theta\,d\theta\right]$$

$$=\frac{8bV_0F_z}{c}\sum_{N=1}^{\infty}\frac{\sin N\theta_i}{N}\int_0^{\pi}\frac{\sin N\theta\sin\theta}{\cos\theta-\cos\theta_j}\,d\theta$$

$$=\frac{4bV_0F_z}{c}\sum_{N=1}^{\infty}\frac{\sin N\theta_i}{N}\left[\int_0^{\pi}\frac{\cos(N-1)\theta}{\cos\theta-\cos\theta_j}\,d\theta\right.$$

$$\left.-\int_0^{\pi}\frac{\cos(N+1)\theta}{\cos\theta-\cos\theta_j}\,d\theta\right]$$

$$=\frac{4\pi V_0bF_z}{c}\sum_{N=1}^{\infty}\frac{\sin N\theta_i}{N}\left[\frac{\sin(N-1)\theta_j-\sin(N+1)\theta_j}{\sin\theta_j}\right]$$

$$=-\frac{8\pi V_0bF_z}{c}\sum_{N=1}^{\infty}\frac{\sin N\theta_i\cos N\theta_j}{N}$$

$$=-\frac{4\pi V_0bF_z}{c}\sum_{N=1}^{\infty}\left[\frac{\sin N(\theta_i+\theta_j)}{N}+\frac{\sin N(\theta_i-\theta_j)}{N}\right]$$

since;

$$\sum_{N=1}^{\infty} \frac{\sin N\theta}{N} = \frac{1}{2}(\pi - \theta) \qquad \text{FOR} \quad 0 < \theta < 2\pi$$

then,

$$\sum_{i=1}^{N_i} \bar{E}_{fi} = -\frac{2\pi V_0 b F_f}{c} \left\{ [\pi - (\theta_f + \theta_j)] + [\pi - (\theta_f - \theta_j)] \right\}$$

where $0 < (\theta_f + \theta_j) < 2\pi$ AND $0 < (\theta_f - \theta_j) < 2\pi$

Therefore;

$$\sum_{i=1}^{N_i} \bar{E}_{fi} = -\frac{4\pi V_0 b F_f (\pi - \theta_f)}{c} \qquad \text{FOR } 0 \le \theta < \theta_f \tag{48}$$

and

$$\sum_{i=1}^{N_i} \bar{E}_{fi} = \frac{4\pi V_0 b F_f \theta_f}{c} \qquad \text{FOR } \theta_f \le \theta \le \pi \tag{49}$$

Similarly;

$$\sum_{i=1}^{N_i} \bar{E}_{ki} = -\frac{2\pi V_0 b F_k}{c} \left\{ [\pi - (\theta_k + \theta_j)] + [\pi - (\theta_k - \theta_j)] \right\}$$

where again $0 < (\theta_k + \theta_j) < 2\pi$ AND $0 < (\theta_k - \theta_j) < 2\pi$

Therefore;

$$\sum_{i=1}^{N_i} \bar{E}_{ki} = -\frac{4\pi V_0 b F_k (\pi - \theta_k)}{c_1} \qquad \text{FOR } 0 \le \theta \le \theta_k \tag{50}$$

and

$$\sum_{i=1}^{N_i} \bar{E}_{ki} = \frac{4\pi V_0 b F_k \theta_k}{c} \qquad \text{FOR } \theta_k < \theta \le \pi \tag{51}$$

After substituting equations (46), (47), (48), (49), (50), and (51) into equations (44) and (45) the following set of simultaneous equations is obtained from which the discrete vortex strengths K_{oi} , K_{Ni} , K_{fi} , and K_{ki} can be determined.

$$\begin{bmatrix} \dfrac{1}{\left[\left(\frac{x}{c}\right)_j - \left(\frac{x}{c}\right)_i\right]} \\ \hline 1, 1, \cdots, 1 \end{bmatrix}_{N_c \times N_c} \begin{bmatrix} K'_{o1}/V_\infty, K'_{11}/V_\infty, \cdots, K'_{(N_c-3)1}/V_\infty, K'_{f1}/V_\infty, K'_{k1}/V_\infty \\ K'_{o2}/V_\infty, K'_{12}/V_\infty, \cdots, K'_{(N_c-3)2}/V_\infty, K'_{f2}/V_\infty, K'_{k2}/V_\infty \\ \vdots \quad \vdots \quad \cdots \quad \vdots \quad \vdots \\ K'_{oN_c}/V_\infty, K'_{1N_c}/V_\infty, \cdots, K'_{(N_c-3)N_c}/V_\infty, K'_{fN_c}/V_\infty, K'_{kN_c}/V_\infty \end{bmatrix}_{N_c \times N_u}$$

$$= \begin{bmatrix} 1, -\cos\theta_j, -\cos 2\theta_j, \cdots, -\cos(N_c-3)\theta_j, -(\pi-\theta_f), -(\pi-\theta_k) \\ 1, -\cos\theta_j, -\cos 2\theta_j, \cdots, -\cos(N_c-3)\theta_j, -(\pi-\theta_f), -(\pi-\theta_k) \\ \cdots \\ 1, -\cos\theta_j, -\cos 2\theta_j, \cdots, -\cos(N_c-3)\theta_j, -(\pi-\theta_f), (\pi-\theta_k) \\ \hline 1/2, 1/4, 0, \cdots, 0, \sin\theta_f/2, \sin\theta_k/2 \end{bmatrix} \qquad (52)$$

Note, in equation (52) the N_c-1 column is $-(\pi-\theta_j)$ for $0 \le \theta_j < \theta_f$ and θ_f for $\theta_f \le \theta_j \le \pi$.

Also, the N_u column is $-(\pi-\theta_k)$ for $0 \le \theta_j \le \theta_k$ and zero for $\theta_k < \theta_j \le \pi$. In equation (52)

$$K'_{oi}/V_\infty = K_{oi}/4\pi b V_\infty F_o \quad , \quad K'_{Ni}/V_\infty = K_{Ni}/4\pi b V_\infty F_N \; , \quad K'_{fi}/V_\infty = K_{fi}/4\pi b V_\infty F_f \; ,$$

$$\text{AND} \quad K'_{ki}/V_\infty = K_{ki}/4\pi b V_\infty F_k$$

Equation (52) is solved for the K'/V_∞'s by premultiplying both sides by;

$$\begin{bmatrix} \dfrac{1}{\left[\left(\frac{x}{c}\right)_j - \left(\frac{x}{c}\right)_i\right]} \\ \hline 1, 1, \cdots, 1 \end{bmatrix}^{-1}$$

The discrete vortex strengths are then given by;

$$K(\theta_i,\eta) = 4\pi b V_\infty \Big\{ \sqrt{1-\eta^2} \sum_{N=1}^{N_W-P_W} \Big[(K'_{0i}/V_\infty) a_{0N} + (K'_{1i}/V_\infty) a_{1N} + (K'_{2i}/V_\infty) a_{2N} + \sum_{N=1}^{N_W-3} (K'_{Ni}/V_\infty) a_{NN} \Big] \eta^{2(N-1)} + \sum_{W=(N_W-P_W+1)}^{N_W} \Big[(K'_{0i}/V_\infty) a_{0N} + (K'_{1i}/V_\infty) a_{1N} + (K'_{2i}/V_\infty) a_{2N} + \sum_{N=1}^{N_W-3} (K'_{Ni}/V_\infty) a_{NN} \Big] P_N(\eta) \Big\} \tag{53}$$

Equation (53) is for symmetric span loadings, if the span load is antisymmetric the exponent $2(N-1)$ is replaced by $2N-1$ and the special span functions $P_N(\eta)$ are computed such that they are antisymmetric.

Since the pylon does not utilize a spanwise vorticity series and does not have flaps, the discrete pylon vortex strengths are given by;

$$K(\theta_i,\eta) = 4\pi b V_\infty \Big\{ (K'_{0i}/V_\infty) F_0 + \sum_{N=1}^{N_W-1} (K'_{Ni}/V_\infty) F_N \Big\} \tag{54}$$

where F_0 and F_N become the unknown coefficients to be determined from the solution of the influence equations.

Appendix H

FUSELAGE AND FANPOD VORTEX STRENGTHS

The perturbation velocity due to the fanpod is represented by a vortex grid on the fuselage surface. This grid is made up of a number of closed circuits of constant vortex strength which are in turn represented by a number of constant strength vortex segments. The velocity induced by each of these constant strength vortices, at a point on or off the fanpod surface, is given by the algebraic sum of the velocity induced by each of the segments making up the closed circuit. The velocity induced by each of the segments is given by expressions derived in Appendix D. The closed circuit can be of any shape, and can overlap in any arbitrary manner without changing the total induced velocity at a point due to the vorticity distribution being represented. It can be shown that there is a linear relationship between the influence matrices of two different grid mappings.

There is however, numerical advantages to one mapping over another. It is for this reason that a quadrilateral vortex grid with the smallest possible grid size is chosen. It can be shown that the influence of a quadrilateral vortex tends to damp out at a rate proportional to $(\frac{\Delta}{r})^2$ where Δ is the vortex dimension parallel to $\vec{r}$ and $r = |\vec{r}|$ is the distance between the point being influenced and the centroid of the vortex. Therefore; the smaller Δ is, the smaller the area being influenced by each vortex and the smaller the number of vortices which need be considered as contributing a significant amount of induced flow at each influence point. This fact can be used to reduce the computing time per case by limiting the vortices for which a contribution is computed to those for which $(\frac{\Delta}{r})^2$ is larger than some prescribed value. The vortices for which $(\frac{\Delta}{r})^2$ is smaller than that value should contribute such a small amount that no discernible change in the influence matrix is made, if their contribution is neglected. It is therefore advantageous to use a grid pattern for which the grid elements are nearly square and as small as possible. This is obviously not the case for the standard horseshoe vortex which trails to infinity behind either the wing, pylon or fanpod.

Another method for reducing the computer time per case is to constrain the strengths of the quadrilateral vortices such that the amount of each constraint function, rather than the strength of each vortex, becomes the unknowns in the problem. In this way the number of unknowns can be drastically reduced, thereby reducing computer time. The constraint functions, which in this case are vorticity distributions, must be representative of the type of spatial variation expected of the vorticity over the fanpod, and must be a series for which end conditions, such as those at the nose and the base, are satisfied. The series must also be such that as the number of terms are increased the boundary condition of no flow through the surface of the wing and the fanpod is better satisfied, in a least square sense.

These vorticity functions can be continuous provided the surface gradients are continuous. It will be assumed at this point that the surface gradients along meridian lines of the fanpod to be analyzed will be either continuous or that special vorticity functions will be added as part of the program input to account for any surface discontinuities. Under these conditions the following modified Fourier series is sufficient to represent the longitudinal variation of vorticity over arbitrary, but smooth, fanpod surfaces.

$$\gamma(\phi,\Theta) = V_\infty \left[F_1(\Theta)\left(\frac{1+\cos\phi}{\sin\phi}\right) + F_2(\Theta)\left(\frac{1-\cos\phi}{\sin\phi}\right) + \sum_{N=1}^{N_{H_F}} F_{2(N+1)}(\Theta)\sin N\phi \right.$$

$$\left. + \sum_{N=1}^{N_{H_F}} F_{2(N+1)}(\Theta)\cos\phi + \sum_{W=2(N_{V_F}+1)+1}^{N_{H_F}} F_W(\Theta)\, P_W(\phi) \right] \qquad (1)$$

where

$$\phi = \cos^{-1}(1 - 2\,x_c/c_F)$$

This series was used because of its general nature and its ability to represent the vorticity over both blunt and sharp ended bodies. One set of "F" values is determined for each of the Θ roll angles. That is, the vorticity is only constrained in the longitudinal direction since the nature of the vorticity in the lateral direction is more uncertain due to the presence of the wing and pylon.

The first and second terms represent the vorticity over a pointed nose and tail respectively. These terms are identical to that used to represent the vorticity over a flat plate at angle of attack. The sine and cosine series is sufficient to represent the variation of vorticity due to continuous longitudinal variations of cross sectional shape. The last term in equation (1) is a set of special functions which can be input to the program to account for variation in vorticity due to discontinuous variations of cross sectional shape or any other condition for which the standard terms are incapable of representing. The sine and cosine series should be sufficient for most shapes provided enough terms are used. The special functions can, however, reduce the requirement for a large number of Fourier terms and thereby reduce computer time. These special terms can be computed from either slender body theory or from axisymmetric body theory such as used in the Douglas-Neumann program of reference 22.

Not all the terms need be used for every body shape, however, if more terms are used than necessary the answer will be unaffected, since a least squared solution is obtained for the influence equations. Computing time, however, can be saved by judiciously picking only those terms necessary to satisfy the boundary conditions.

The type of solution can also be altered by using only certain types of terms. For instance, if it is desired to obtain a solution for which the flow leaves the body tangent to the surface, at the edge of the base, such as is usually the case in a viscous flow for bodies at small angles of attack, rather than a solution for which the flow will negotiate the sharp base edge and continue down the base to a rear stagnation point, then only those terms for which the vorticity goes to zero at the base edge should be used. Forcing the flow to leave the body surface tangentially is similar to the Kutta condition used to define the amount of circulation around an airfoil. The reasons for such a constraint are purely empirical in nature and will only represent the physical nature of the flow at certain angles of attack. At large angles of attack the flow would be expected to leave the surface on the leeward side at some unknown forward longitudinal station.

The strength of the discrete vortex Γ_i used to represent the vorticity over an incremental distance l_i along a meridian line on the fanpod surface is equal to the integral of the vorticity over the distance l_i.

Then Γ_i can be written in matrix notation from equation (1);

$$\{\Gamma_i(\theta)\} = V_\infty \left[\; l_i(\theta) \;\right] \left[\; \phi \;\right] \left\{ F_i(\theta) \right\} \tag{2}$$

where

$$[\phi] = \begin{bmatrix} \frac{1+\cos\phi_1}{\sin\phi_1}, & \frac{1-\cos\phi_1}{\sin\phi_1}, & \cdots & \sin\phi_1, \sin 2\phi_1, \cdots, \text{ETC.} \\ \vdots & \vdots & \vdots & \vdots \\ \frac{1+\cos\phi_{N_i}}{\sin\phi_{N_i}}, & \frac{1-\cos\phi_{N_i}}{\sin\phi_{N_i}}, & \cdots & \sin\phi_{N_i}, \sin 2\phi_{N_i}, \cdots, \text{ETC.} \end{bmatrix}$$

and N_i is the number of discrete vortices on the fanpod in the chordwise direction.

It should be noted that there is one equation; such as equation (2), for each roll angle. The discrete horseshoe type vortex strengths Γ can be transformed into a set of equivalent quadrilateral vortex strengths by means of the following expression.

$$\{K_i(\theta)\} = \left[\; R \;\right] \left\{ \Gamma_i(\theta) \right\} \tag{3}$$

where

$$[R] = \begin{bmatrix} 1 & 0 & 0 & 0 & 0 & \cdots & 0 \\ 1 & 1 & 0 & 0 & 0 & \cdots & 0 \\ 1 & 1 & 1 & 0 & 0 & \cdots & 0 \\ \vdots & \vdots & \vdots & & & & \\ 1 & 1 & 1 & 1 & 1 & \cdots & 1 \end{bmatrix}$$

The relationship between the horseshoe and quadrilateral vortex systems is best illustrated by the following schematic of the vortex grid at a given lateral Θ station.

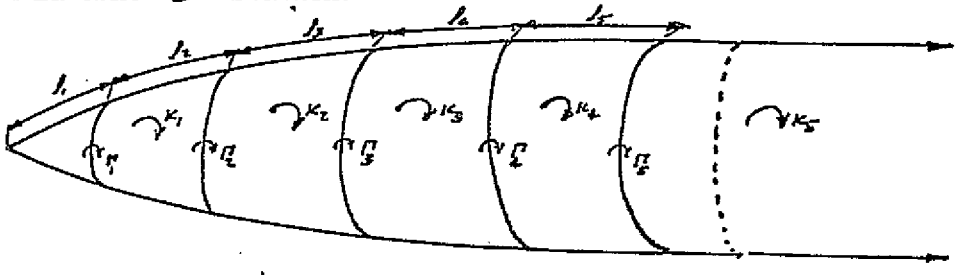

The quadrilateral vortex strengths are then written as a function of the unknown vorticity function coefficients $F(\Theta)$ by substituting equation (2) into equation (3).

$$\left\{K_i(\Theta)\right\} = V_\infty \left[R \right]\left[l_i(\Theta) \right]\left[\Phi \right]\left\{F_p(\Theta)\right\} \tag{4}$$

Since there is one equation, such as equation (4), for each roll angle Θ the matrix equation for $0 < \Theta < 360$ is given by;

$$\begin{Bmatrix} \left\{\frac{K_i}{V_\infty}\right\}_{\Theta_1} \\ \left\{\frac{K_i}{V_\infty}\right\}_{\Theta_2} \\ \vdots \\ \left\{\frac{K_i}{V_\infty}\right\}_{\Theta_{NB}} \end{Bmatrix} = \begin{bmatrix} \left[R L \Phi \right]_{\Theta_1} & & & \\ & \left[R L \Phi \right]_{\Theta_2} & & \\ & & \ddots & \\ & & & \left[R L \Phi \right]_{\Theta_{NB}} \end{bmatrix} \begin{Bmatrix} \left\{F_p(\Theta_1)\right\} \\ \left\{F_p(\Theta_2)\right\} \\ \vdots \\ \left\{F_p(\Theta_{NB})\right\} \end{Bmatrix} \tag{5}$$

where

$$\left[R L \Phi \right] = \left[R \right]\left[l_i \right]\left[\Phi \right] \tag{6}$$

APPENDIX I

CROSS FLOW DUE TO LIFT

The cross flow due to lift is a combination of that due to the chordwise component of bound vorticity along constant percent chord lines and that due to the trailing vorticity. The spanwise component of bound vorticity is given by equation (50) of Appendix F.

$$\gamma_b = \frac{4bV_\infty}{c}\left\{F_0 \cot\theta/2 + \sum_{N=1}^{N_u-3} F_N \sin N\theta + F_f \log_e\left|\frac{\sin\frac{1}{2}(\theta+\theta_f)}{\sin\frac{1}{2}(\theta-\theta_f)}\right| + F_k \log_e\left|\frac{\sin\frac{1}{2}(\theta+\theta_k)}{\sin\frac{1}{2}(\theta-\theta_k)}\right|\right\} \tag{1}$$

The trailing vorticity is given by;

$$\gamma_t = \frac{\partial}{\partial\eta}\int_0^\theta \frac{c}{b}\gamma_b \sin\theta\, d\theta \tag{2}$$

where $\eta = \frac{2y}{b}$ and $\theta = \cos^{-1}(1-\frac{2x}{c})$

therefore; the cross flow due to lift is then given by;

$$\frac{w_t}{V_\infty} = 2\int_0^\theta \frac{\partial}{\partial\eta}\left\{F_0 \cot\theta/2 + \sum_{N=1}^{N_u-3} F_N \sin N\theta + F_f \log_e\left|\frac{\sin\frac{1}{2}(\theta+\theta_f)}{\sin\frac{1}{2}(\theta-\theta_f)}\right| + F_k \log_e\left|\frac{\sin\frac{1}{2}(\theta+\theta_k)}{\sin\frac{1}{2}(\theta-\theta_k)}\right|\right\}\sin\theta\, d\theta - \frac{2b}{c}\left\{F_0 \cot\theta/2 + \sum_{N=1}^{N_u-3} F_N \sin N\theta + F_f \log_e\left|\frac{\sin\frac{1}{2}(\theta+\theta_f)}{\sin\frac{1}{2}(\theta-\theta_f)}\right| + F_k \log_e\left|\frac{\sin\frac{1}{2}(\theta+\theta_k)}{\sin\frac{1}{2}(\theta-\theta_k)}\right|\right\}\tan\phi \tag{3}$$

where ϕ is the local sweep of the constant percent chord line.

The spanwise functions f_0, f_w, f_t, and f_a for the wing are defined in Appendix F. Their derivatives are given below.

$$\frac{dF_0}{d\eta} = -\frac{\eta}{\sqrt{1-\eta^2}} \sum_{w=1}^{N_w-P_w} a_{0w}\,\eta^{2(w-1)} + \sqrt{1-\eta^2} \sum_{w=2}^{N_w-P_w} 2(w-1)\,a_{0w}\,\eta^{2w-3} + \sum_{w=(N_w-P_w+1)}^{N_w} a_{0w}\,\frac{dP_w(\eta)}{d\eta} \tag{4}$$

$$\frac{dF_w}{d\eta} = -\frac{\eta}{\sqrt{1-\eta^2}} \sum_{w=1}^{N_w-P_w} a_{ww}\,\eta^{2(w-1)} + \sqrt{1-\eta^2} \sum_{w=2}^{N_w-P_w} 2(w-1)\,a_{ww}\,\eta^{2w-3} + \sum_{w=(N_w-P_w+1)}^{N_w} a_{ww}\,\frac{dP_w(\eta)}{d\eta} \tag{5}$$

$$\frac{dF_t}{d\eta} = -\frac{\eta}{\sqrt{1-\eta^2}} \sum_{w=1}^{N_w-P_w} a_{tw}\,\eta^{2(w-1)} + \sqrt{1-\eta^2} \sum_{w=2}^{N_w-P_w} 2(w-1)\,a_{tw}\,\eta^{2w-3} + \sum_{w=(N_w-P_w+1)}^{N_w} a_{tw}\,\frac{dP_w(\eta)}{d\eta} \tag{6}$$

and

$$\frac{dF_a}{d\eta} = -\frac{\eta}{\sqrt{1-\eta^2}} \sum_{w=1}^{N_w-P_w} a_{aw}\,\eta^{2(w-1)} + \sqrt{1-\eta^2} \sum_{w=2}^{N_w-P_w} 2(w-1)\,a_{aw}\,\eta^{2w-3} + \sum_{w=(N_w-P_w+1)}^{N_w} a_{aw}\,\frac{dP_w(\eta)}{d\eta} \tag{7}$$

The derivatives of the $P_w(\eta)$ functions for breaks in the leading or trailing edges are obtained from the following relations.

For $\eta_b = 0$

$$\frac{\partial P_w(\eta)}{\partial \eta} = \frac{\partial M(\eta,0)}{\partial \eta} - \frac{1}{R_0}\frac{\partial P(\eta,0)}{\partial \eta} + \frac{1-R_0}{R_0}\frac{\partial P(\eta,R_0)}{\partial \eta} \tag{8}$$

For $0 < |\eta_b| < R_i$

$$\frac{\partial P_w(\eta)}{\partial \eta} = (1-\eta_b/R_i)\frac{\partial M(\eta,0)}{\partial \eta} + \frac{1}{R_i}\frac{\partial P(\eta,0)}{\partial \eta}$$

$$-\left[\frac{(R_i+R_0)(1-\eta_b)}{R_i R_0}\right]\frac{\partial P(\eta,\eta_b)}{\partial \eta} \tag{9}$$

$$+\left[\frac{R_i+R_0}{R_i R_0} - \frac{1}{R_i}\right]\left[1-R_0-\eta_b\right]\frac{\partial P(\eta,\eta_b+R_0)}{\partial \eta}$$

For $R_i \le |\eta_b| \le (1-R_0)$

$$\frac{\partial P_w(\eta)}{\partial \eta} = (1-\eta_b+R_i)(1/R_i)\frac{\partial P(\eta,\eta_b-R_i)}{\partial \eta}$$

$$-\left[\frac{R_0+R_i}{R_0 R_i}\right]\left[1-\eta_b\right]\frac{\partial P(\eta,\eta_b)}{\partial \eta}$$

$$+(1-\eta_b-R_0)(1/R_0)\frac{\partial P(\eta,\eta_b+R_0)}{\partial \eta} \tag{10}$$

and for $(1-R_0) < |\eta_b| < 1$

$$\frac{\partial P_w(\eta)}{\partial \eta} = (1-\eta_b+R_i)(1/R_i)\frac{\partial P(\eta,\eta_b-R_i)}{\partial \eta}$$

$$-\left[1+(1-\eta_b)/R_i\right]\frac{\partial P(\eta,\eta_b)}{\partial \eta} \tag{11}$$

Also, the derivative of $P_w(\eta)$ for partial span leading and trailing edge flaps.

$$\frac{\partial P_w(\eta)}{\partial \eta} = \frac{\partial M(\eta, \eta_i)}{\partial \eta} - \frac{\partial M(\eta, \eta_o)}{\partial \eta} \tag{12}$$

where η_b , η_i , and η_o are the span stations where the break in the leading or trailing edge occurs, where the partial span flap begins inboard, and where the partial span flap ends outboard, respectively. The derivatives $\partial M(\eta,\eta^*)/\partial \eta$ and $\partial P(\eta,\eta^*)/\partial \eta$ used in equations (8) through (12) are derived below. The variable η^* is a dummy variable. Since $M(\phi,\phi^*)_s$ defined in equation (33) of Appendix A, is given as;

$$M(\phi,\phi^*)_s = \frac{1}{\pi}\left\{(\cos\phi^* - \cos\phi)\log_e\left|\frac{\sin\frac{1}{2}(\phi^* - \phi)}{\sin\frac{1}{2}(\phi^* + \phi)}\right| + (\cos\phi^* + \cos\phi)\log_e\left|\frac{\cos\frac{1}{2}(\phi^* + \phi)}{\cos\frac{1}{2}(\phi^* - \phi)}\right| + 2\phi^*\sin\phi\right\} \tag{13}$$

where $\phi = \cos^{-1}\eta$ and $\phi^* = \cos^{-1}\eta^*$

$$\frac{\partial M(\phi,\phi^*)_s}{\partial \phi} = -\frac{1}{2\pi}\left\{(\cos\phi^* - \cos\phi)\left[\cot\tfrac{1}{2}(\phi^* - \phi) + \cot\tfrac{1}{2}(\phi^* + \phi)\right]\right.$$

$$+ (\cos\phi^* + \cos\phi)\left[\tan\tfrac{1}{2}(\phi^* - \phi) + \tan\tfrac{1}{2}(\phi^* + \phi)\right]$$

$$\left. + 2\sin\phi\left[\log_e\left|\frac{\sin\frac{1}{2}(\phi^* + \phi)}{\sin\frac{1}{2}(\phi^* - \phi)}\right| + \log_e\left|\frac{\cos\frac{1}{2}(\phi^* + \phi)}{\cos\frac{1}{2}(\phi^* - \phi)}\right|\right] - 4\phi^*\cos\phi\right\} \tag{14}$$

then;

$$\frac{\partial M(\phi,\phi^*)}{\partial \eta} = \frac{1}{2\pi\sin\phi}\left\{\frac{(\cos\phi^* - \cos\phi)\sin\phi^*}{\sin\frac{1}{2}(\phi^* - \phi)\sin\frac{1}{2}(\phi^* + \phi)}\right.$$

$$\left. + \frac{(\cos\phi^* + \cos\phi)\sin\phi}{\cos\frac{1}{2}(\phi^* - \phi)\cos\frac{1}{2}(\phi^* + \phi)} + 2\sin\phi\log_e\left|\frac{\sin(\phi^* + \phi)}{\sin(\phi^* - \phi)}\right| - 4\phi^*\cos\phi\right\} \tag{15}$$

$$\frac{\partial M(\phi,\phi^*)_s}{\partial \eta} = \frac{1}{\pi}\left\{\log_e\left|\frac{\sin(\phi^*+\phi)}{\sin(\phi^*-\phi)}\right| - 2\phi^*\cot\phi\right\} \tag{16}$$

or

$$\frac{\partial M(\eta,\eta^*)_s}{\partial \eta} = \frac{1}{\pi}\left\{\log_e\left|\frac{\eta^*\sqrt{1-\eta^2}+\eta\sqrt{1-\eta^{*2}}}{\eta^*\sqrt{1-\eta^2}-\eta\sqrt{1-\eta^{*2}}}\right| - \frac{2\eta}{\sqrt{1-\eta^2}}\tan^{-1}\frac{\sqrt{1-\eta^{*2}}}{\eta^*}\right\} \tag{17}$$

The expression for $P(\phi,\phi^*)_s$ is given as equation (43) of Appendix A.

$$P(\phi,\phi^*)_s = \frac{-1}{2\pi(1-\cos\phi^*)}\left\{(\cos\phi^*-\cos\phi)^2\log_e\left|\frac{\sin\frac{1}{2}(\phi^*-\phi)}{\sin\frac{1}{2}(\phi^*+\phi)}\right|\right.$$

$$+(\cos\phi^*+\cos\phi)^2\log_e\left|\frac{\cos\frac{1}{2}(\phi^*+\phi)}{\cos\frac{1}{2}(\phi^*-\phi)}\right|$$

$$\left.+(4\phi^*\cos\phi^*-2\sin\phi^*)\sin\phi\right\} \tag{18}$$

$$\frac{\partial P(\phi,\phi^*)_s}{\partial \phi} = \frac{1}{2\pi(1-\cos\phi^*)}\left\{2\cos\phi^*\sin\phi\log_e\left|\frac{\sin(\phi^*+\phi)}{\sin(\phi^*-\phi)}\right|\right.$$

$$+\sin^2\phi\log_e\left|\frac{\sin\phi^*-\sin\phi}{\sin\phi^*+\sin\phi}\right|$$

$$\left.+4(\sin\phi^*-\phi^*\cos\phi^*)\cos\phi\right\} \tag{19}$$

$$\frac{\partial P(\phi,\phi^*)_s}{\partial \eta} = \frac{1}{\pi(1-\cos\phi^*)}\left\{\cos\phi^* \log_e\left|\frac{\sin(\phi^*-\phi)}{\sin(\phi^*+\phi)}\right| + \cos\phi \log_e\left|\frac{\sin\phi^*+\sin\phi}{\sin\phi^*-\sin\phi}\right| + 2(\phi^*\cos\phi^*-\sin\phi^*)\cot\phi\right\} \tag{20}$$

or

$$\frac{\partial P(\eta,\eta^*)}{\partial \eta} = \frac{1}{\pi(1-\eta^*)}\left\{\eta^* \log_e\left|\frac{\eta^*\sqrt{1-\eta^2}-\eta\sqrt{1-\eta^{*2}}}{\eta^*\sqrt{1-\eta^2}+\eta\sqrt{1-\eta^{*2}}}\right| + \eta \log_e\left|\frac{\sqrt{1-\eta^{*2}}+\sqrt{1-\eta^2}}{\sqrt{1-\eta^{*2}}-\sqrt{1-\eta^2}}\right| + 2\left[\eta^* \tan^{-1}\left(\frac{\sqrt{1-\eta^{*2}}}{\eta^*}\right)-\sqrt{1-\eta^{*2}}\right]\frac{\eta}{\sqrt{1-\eta^2}}\right\} \tag{21}$$

Due to the singular nature of equation (21) special attention must be given to the case when $\eta=\eta^*$. Returning to equation (20) and determining $\partial P(\phi,\phi^*)/\partial\eta$ in the limit as $\phi \to \phi^*$.

$$\frac{\partial P(\phi^*,\phi^*)}{\partial \eta} = \lim_{\varepsilon\to 0} \frac{1}{\pi(1-\cos\phi^*)}\left\{\cos\phi^* \log_e\left|\frac{\sin(\phi^*-\phi^*-\varepsilon)}{\sin(\phi^*+\phi^*+\varepsilon)}\right| + \cos(\phi^*+\varepsilon)\log_e\left|\frac{\sin\phi^*+\sin(\phi^*+\varepsilon)}{\sin\phi^*-\sin(\phi^*+\varepsilon)}\right| + 2(\phi^*\cos\phi^*-\sin\phi^*)\cot(\phi^*+\varepsilon)\right\} \tag{22}$$

$$\frac{\partial P(\phi^*,\phi^*)}{\partial \eta} = \frac{1}{\pi(1-\cos\phi^*)}\Big\{-\cos\phi^*\log_e|\sin 2\phi^*|$$

$$+2(\phi^*\cos\phi^*-\sin\phi^*)\cot\phi^* + \lim_{\varepsilon\to 0}\Big[\cos\phi^*\log_e|\sin\varepsilon|$$

$$+\cos\phi^*\cos\varepsilon\log_e\Big|\frac{2\cos^2\frac{1}{2}\varepsilon+\cot\phi^*\sin\varepsilon}{2\sin^2\frac{1}{2}\varepsilon-\cot\phi^*\sin\varepsilon}\Big|$$

$$+\sin\phi^*\sin\varepsilon\log_e\Big|\frac{2\sin^2\frac{1}{2}\varepsilon-\cot\phi^*\sin\varepsilon}{2\cos^2\frac{1}{2}\varepsilon+\cot\phi^*\sin\varepsilon}\Big|\Big]\Big\} \qquad (23)$$

Let $\varepsilon = 2\delta$

then;

$$\frac{\partial P(\phi^*,\phi^*)}{\partial \eta} = \frac{1}{\pi(1-\cos\phi^*)}\Big\{-\cos\phi^*\log_e|\sin 2\phi^*|$$

$$+2(\phi^*\cos\phi^*-\sin\phi^*)\cot\phi^* \qquad (24)$$

$$+\lim_{\delta\to 0}\Big[\cos\phi^*\log_e|\sin 2\delta|$$

$$+\cos\phi^*\cos 2\delta\log_e\Big|\frac{2\cos^2\delta+\cot\phi^*\sin 2\delta}{2\cos^2\delta-\cot\phi^*\sin 2\delta}\Big|$$

$$-\cos\phi^*\cos 2\delta\log_e\Big|\frac{2\sin^2\delta-\cot\phi^*\sin 2\delta}{2\sin^2\delta+\cot\phi^*\sin 2\delta}\Big|\Big]\Big\}$$

$$\frac{\partial P(\phi^*,\phi^*)}{\partial \eta} = \frac{1}{\pi(1-\cos\phi^*)}\Big\{-\cos\phi^* \log_e/\sin^2\phi^*/ + 2(\phi^*\cos\phi^* - \sin\phi^*)\cot\phi^*$$

$$+ \lim_{\delta\to 0}\Big[\cos\phi^* \log_e/\sin 2\delta/$$

$$+ \cos\phi^*\cos 2\delta \log_e/2\cos^2\delta + \cot\phi^*\sin 2\delta/$$

$$- \cos\phi^*\cos 2\delta \log_e/\tan\delta - \cos\phi^*/$$

$$- \cos\phi^*\cos 2\delta \log_e/\sin 2\delta/\Big]\Big\} \tag{25}$$

$$\frac{\partial P(\phi^*,\phi^*)}{\partial \eta} = \frac{1}{\pi(1-\cos\phi^*)}\Big\{-\cos\phi^* \log_e/\cos^2\phi^*/$$

$$+ 2(\phi^*\cos\phi^* - \sin\phi^*)\cot\phi^*\Big\} \tag{26}$$

$$\frac{\partial P(\eta^*,\eta^*)}{\partial \eta} = \frac{1}{\pi(1-\eta^*)}\Big\{-\eta^* \log_e \eta^{*2}$$

$$+ 2\Big[\eta^* \tan^{-1}\Big(\frac{\sqrt{1-\eta^{*2}}}{\eta^*}\Big) - \sqrt{1-\eta^{*2}}\Big]\frac{\eta}{\sqrt{1-\eta^{*2}}}\Big\} \tag{27}$$

The integration with respect to Θ in equation (3) is completed as follows;

$$\int_0^\Theta \frac{\partial F_\bullet}{\partial \eta}\cot\Theta/2 \sin\theta\, d\theta = \int_0^\Theta \frac{\partial F_\bullet}{\partial \eta}(1+\cos\theta)\, d\theta$$

$$= \frac{\partial F_\bullet}{\partial \eta}(\theta + \sin\theta) \tag{28}$$

$$\sum_{N=1}^{N_U-3} \int_0^{\theta} \frac{\partial F_N}{\partial \eta} \sin N\theta \sin\theta \, d\theta = \sum_{N=1}^{N_U-3} \frac{\partial F_N}{\partial \eta} \int_0^{\theta} \sin N\theta \sin\theta \, d\theta$$

$$= \frac{\partial F_1}{\partial \eta} \int_0^{\theta} \sin^2\theta \, d\theta + \sum_{N=2}^{N_U-3} \frac{\partial F_N}{\partial \eta} \int_0^{\theta} \sin N\theta \sin\theta \, d\theta$$

$$\sum_{N=1}^{N_U-3} \int_0^{\theta} \frac{\partial F_N}{\partial \eta} \sin N\theta \sin\theta \, d\theta = \frac{\partial F_1}{\partial \eta} \left(\frac{\theta}{2} - \frac{1}{4}\sin 2\theta\right)$$

$$+ \sum_{N=2}^{N_U-3} \frac{\partial F_N}{\partial \eta} \left[\frac{\sin(N-1)\theta}{2(N-1)} - \frac{\sin(N+1)\theta}{2(N+1)}\right] \qquad (29)$$

$$\int_0^{\theta} \frac{\partial F_1}{\partial \eta} \log_e \left|\frac{\sin\frac{1}{2}(\theta+\theta_1)}{\sin\frac{1}{2}(\theta-\theta_1)}\right| \sin\theta \, d\theta = \frac{\partial F_1}{\partial \eta} \left\{\cos\theta \log_e \left|\frac{\sin\frac{1}{2}(\theta-\theta_1)}{\sin\frac{1}{2}(\theta+\theta_1)}\right|\right|_0^{\theta}$$

$$+ \int_0^{\theta} \frac{\sin\theta_1 \cos\theta \, d\theta}{\cos\theta - \cos\theta_1} \Bigg\}$$

IF $\theta < \theta_1$

$$\int_0^{\theta} \frac{\partial F_1}{\partial \eta} \log_e \left|\frac{\sin\frac{1}{2}(\theta+\theta_1)}{\sin\frac{1}{2}(\theta-\theta_1)}\right| \sin\theta \, d\theta = \frac{\partial F_1}{\partial \eta} \left\{(\cos\theta - \cos\theta_1) \log_e \left|\frac{\sin\frac{1}{2}(\theta+\theta_1)}{\sin\frac{1}{2}(\theta-\theta_1)}\right|\right.$$

$$\left. + \theta \sin\theta_1 \right\} \qquad (30)$$

IF $\theta > \theta_1$

$$\int_0^{\theta} \frac{\partial F_1}{\partial \eta} \log_e \left|\frac{\sin\frac{1}{2}(\theta+\theta_1)}{\sin\frac{1}{2}(\theta-\theta_1)}\right| \sin\theta \, d\theta = \frac{\partial F_1}{\partial \eta} \lim_{\varepsilon \to 0} \int_0^{\theta_1-\varepsilon} \log_e \left|\frac{\sin\frac{1}{2}(\theta+\theta_1)}{\sin\frac{1}{2}(\theta-\theta_1)}\right| \sin\theta \, d\theta$$

$$+ \frac{\partial F_1}{\partial \eta} \lim_{\varepsilon \to 0} \int_{\theta_1+\varepsilon}^{\theta} \log_e \left|\frac{\sin\frac{1}{2}(\theta+\theta_1)}{\sin\frac{1}{2}(\theta-\theta_1)}\right| \sin\theta \, d\theta$$

$$\int_0^{\theta} \frac{\partial F_i}{\partial \eta} \log_e \left| \frac{\sin\frac{1}{2}(\theta+\theta_i)}{\sin\frac{1}{2}(\theta-\theta_i)} \right| \sin\theta \, d\theta = \frac{\partial F_i}{\partial \eta} \lim_{\varepsilon \to 0} \left\{ \left[\cos(\theta_i-\varepsilon)-\cos\theta_i\right] \log_e \left| \frac{\sin\frac{1}{2}(\theta_i-\varepsilon-\theta_i)}{\sin\frac{1}{2}(\theta_i-\varepsilon+\theta_i)} \right| \right.$$

$$+(\theta_i-\varepsilon)\sin\theta_i - \left[\cos(\theta_i-\varepsilon)-\cos\theta_i\right] \log_e \left| \frac{\sin\frac{1}{2}(\theta_i-\varepsilon-\theta_i)}{\sin\frac{1}{2}(\theta_i+\varepsilon+\theta_i)} \right|$$

$$-(\theta_i+\varepsilon)\sin\theta_i + \left[\cos\theta-\cos\theta_i\right] \log_e \left| \frac{\sin\frac{1}{2}(\theta-\theta_i)}{\sin\frac{1}{2}(\theta+\theta_i)} \right|$$

$$\left. +\theta\sin\theta_i \right\}$$

$$= \frac{\partial F_i}{\partial \eta} \left\{ (\cos\theta-\cos\theta_i) \log_e \left| \frac{\sin\frac{1}{2}(\theta-\theta_i)}{\sin\frac{1}{2}(\theta+\theta_i)} \right| \right.$$

$$\left. +\theta\sin\theta_i \right\} \qquad (31)$$

and similarly;

$$\int_0^{\theta} \frac{\partial F_k}{\partial \eta} \log_e \left| \frac{\sin\frac{1}{2}(\theta+\theta_k)}{\sin\frac{1}{2}(\theta-\theta_k)} \right| \sin\theta \, d\theta = \frac{\partial F_k}{\partial \eta} \left\{ (\cos\theta-\cos\theta_k) \log_e \left| \frac{\sin\frac{1}{2}(\theta-\theta_k)}{\sin\frac{1}{2}(\theta+\theta_k)} \right| \right.$$

$$\left. +\theta\sin\theta_k \right\} \qquad (32)$$

Therefore; equation (3) becomes

$$\frac{v_t}{V_\infty} = \left(\frac{v_t}{V_\infty}\right)_{N=0} + \left(\frac{v_t}{V_\infty}\right)_{N=1,2,\cdots,N_0-3,\,f,\,k} \tag{33}$$

where

$$\left(\frac{v_t}{V_\infty}\right)_{N=0} = 2\frac{dF_0}{d\eta}(\sin\theta+\theta) - \frac{2k}{c}F_0\cot\theta/2\left[\tan\phi^*_{L.E.} + (\tan\phi^*_{T.E.} - \tan\phi^*_{L.E.})(1-\cos\theta)\right] \tag{34}$$

and

$$\left(\frac{v_t}{V_\infty}\right)_{N=1,2,\cdots,N_0-3,\,f,\,k} = 2\left\{\frac{dF_1}{d\eta}\left(\frac{\theta}{2} - \frac{1}{4}\sin 2\theta\right) + \sum_{N=2}^{N_0-3}\frac{dF_N}{d\eta}\left[\frac{\sin(N-1)\theta}{2(N-1)} - \frac{\sin(N+1)\theta}{2(N+1)}\right]\right.$$

$$+\frac{dF_f}{d\eta}\left[(\cos\theta-\cos\theta_f)\log_e\left|\frac{\sin\frac{1}{2}(\theta-\theta_f)}{\sin\frac{1}{2}(\theta+\theta_f)}\right| + \theta\sin\theta_f\right]$$

$$+\frac{dF_k}{d\eta}\left[(\cos\theta-\cos\theta_k)\log_e\left|\frac{\sin\frac{1}{2}(\theta-\theta_k)}{\sin\frac{1}{2}(\theta+\theta_k)}\right| + \theta\sin\theta_k\right]$$

$$-\frac{2k}{c}\left\{\sum_{N=1}^{N_0-3}F_N\sin N\theta + F_f\log_e\left|\frac{\sin\frac{1}{2}(\theta+\theta_f)}{\sin\frac{1}{2}(\theta-\theta_f)}\right|\right.$$

$$\left.\left.+F_k\log_e\left|\frac{\sin\frac{1}{2}(\theta+\theta_k)}{\sin\frac{1}{2}(\theta-\theta_k)}\right|\right\}\left\{\tan\phi^*_{L.E.} + \frac{1}{2}(\tan\phi^*_{T.E.} - \tan\phi^*_{L.E.})(1-\cos\theta)\right\} \tag{35}$$

where $\tan\phi^*_{L.E.}$ and $\tan\phi^*_{T.E.}$ are the values of $\tan\phi^*$ at the leading and trailing edge, respectively.

The equation for $\tan \phi^*$ was obtained from reference 6. In reference 6 the effect of leading and trailing edge breaks on the local isobars is given by the following expression for the local sweep of the isobars.

$$\tan \phi^* = \frac{\left\{\cos^2(\lambda_b - \Lambda_m) - \cos^2 \Lambda_m \cos^2\left[\lambda_b \left(\frac{\phi_i + \phi_o}{2}\right)_b\right]\right\}^{1/2}}{\cos \Lambda_m \cos\left[\lambda_b \left(\frac{\phi_i + \phi_o}{2}\right)_b\right]} \tag{36}$$

where

$$\lambda_b = \sqrt{1 + \left[2\pi \frac{\tan \Lambda_m}{\Lambda_m}\left(\frac{y - y_b}{c_b}\right)\right]^2} - 2\pi \frac{\tan \Lambda_m}{\Lambda_m} \left|\frac{y - y_b}{c_b}\right| \tag{37}$$

The subscript b indicates values at a break in either the leading or trailing edge. Also, ϕ_i and ϕ_o are the sweeps of the constant percent chord lines on the port and starboard sides of the break, respectively. The angle Λ_m is the value of sweep to which the isobar line converges as the effect of the break station dies in the spanwise direction. If a span station is influenced by more than one break station the effect is obtained by interpolation.

APPENDIX J

INDUCED DRAG

The vortex drag arises from the momentum transported away from an arbitrary lifting system by the trailing vortices and is given (25) by the integral equation

$$D_v = \frac{\rho}{2} \int_{-\infty}^{\infty}\int_{-\infty}^{\infty} (\beta^2 \phi_x^2 + \phi_y^2 + \phi_z^2)\, dy\, dz \tag{1}$$

This result is usually simplified by allowing the control surface to recede indefinitely far behind the object. That is, a so called Trefftz plane analysis is performed.

For this condition $\phi_x = 0$ and

$$D_v\Big|_{x\to\infty} = \frac{\rho}{2} \int_{-\infty}^{\infty}\int_{-\infty}^{\infty} (\phi_y^2 + \phi_z^2)\, dy\, dz \tag{2}$$

For a plane potential wake, this latter result can be transformed (25) and (26) by the use of Green's theorem to

$$D_v = -\frac{\rho}{4\pi} \int_{-\frac{b}{2}}^{\frac{b}{2}}\int_{-\frac{b}{2}}^{\frac{b}{2}} \frac{d\Gamma}{dy}(y)\, \frac{d\Gamma}{dy_1}(y_1)\, \log|y - y_1|\, dy\, dy_1 \tag{3}$$

This result is cast here into the following form by use of a change of variable $\eta = (y + \frac{b}{2})/b$ for numerical purposes

$$\frac{D_v}{\rho b} = \frac{1}{-8\pi} \int_0^1\int_0^1 \frac{d}{d\eta}\left(\frac{\ell}{g}(\eta)\right) \frac{d}{d\eta_1}\left(\frac{\ell}{g}(\eta_1)\right) \log|\eta - \eta_1|\, d\eta\, d\eta_1 \tag{4}$$

Solution of integrals of the type

$$I = -\frac{1}{2\pi} \int_0^1\int_0^1 f''(\xi)\, f''(\xi_1)\, \log|\xi - \xi_1|\, d\xi\, d\xi_1 \tag{5}$$

with a numerically given function $f(\eta)$, $f'(\eta)$ continuous on the interval $(0, 1)$, and $f'(0) = f'(1) = 0$ have been studied by Ementon (27) and (28) using Fournier series analyses in conjunction with the condition that the integral I be a minimum in order to eliminate numerical induced inaccuracies.

The result for the current problem is

$$\frac{D_v}{\beta} = \frac{I}{4} \tag{6}$$

$$I = \frac{4}{\pi} f^2(1) + \pi \sum_{i=1}^{i=N} \sum_{j=1}^{N} c_i c_j \tilde{P}_{ij} \tag{7}$$

$$c_i = f(\eta_i) - f(1)\mu_i \tag{8}$$

$$f(\eta_i) = \int_0^{\eta_i} \frac{J}{\beta}(\eta)\, d\eta \tag{9}$$

$$\mu_i = \frac{1}{\pi}\left[\cos^{-1}(1-2\eta_i) - 2(1-2\eta_i)\sqrt{\eta_i(1-\eta_i)}\right] \tag{10}$$

$$\eta_i = \frac{i}{N+1} \qquad 1 \le i \le N \tag{11}$$

$$[\tilde{P}_{ij}] = [P_{ij}]^{-1} \tag{12}$$

$$P_{ij} = -\frac{(\eta_i - \eta_j)^2}{2} \log\left[\frac{\eta_i + \eta_j - 2\eta_i\eta_j + 2\sqrt{\eta_i\eta_j(1-\eta_i)(1-\eta_j)}}{\eta_i + \eta_j - 2\eta_i\eta_j - 2\sqrt{\eta_i\eta_j(1-\eta_i)(1-\eta_j)}}\right] \tag{13}$$

$$+ 2(\eta_i + \eta_j - 2\eta_i\eta_j)\sqrt{\eta_i\eta_j(1-\eta_i)(1-\eta_j)}$$

APPENDIX K

SKIN FRICTION DRAG

Several well established semiempirical techniques for the evaluation of laminar and turbulent flat plate skin friction at incompressible and compressible speeds are used to develop a subroutine to estimate the viscous drag of advanced aircraft using a component buildup approach. Specified or flat plate natural transition point calculation options are provided for in conjunction with a matching of the momentum thickness to link the two boundary layer states. For the turbulent condition, the increase in drag due to distributed surface roughness is treated using uniformly distributed sand grain results. Component thickness effects are approximated using experimental data correlations for two-dimensional airfoil sections and bodies of revolution.

Considerations such as separation, component interference, and discrete protuberances (e.g. antennas, drains, aft facing steps, etc.) must be accounted for separately if present or judged to be significant.

In the following, a discussion is presented for a single component evaluation in order to simplify writing of the equations and eliminate multiple subscripting. The total result is obtained by a surface area weighted summation of the various component analyses.

LAMINAR/TRANSITION

A specified and flat plate natural transition option are provided in the program. The principal function of the calculation is to provide the conditions required to initialize the turbulent solution. In particular, the transition point length and momentum thickness Reynolds numbers are required.

SPECIFIED

$$R_{x_{TRAN}} = R \cdot \frac{X_{TRAN}}{L} \cdot L \tag{1}$$

$$R\theta_{TRAN} = .664\sqrt{R_{x_{TRAN}} C^*} \tag{2}$$

where

$$C^* = \frac{\mu^*}{\mu_\infty} \frac{T_\infty}{T^*} \tag{3}$$

$$\frac{T_\infty}{T^*} = 1 + .72\left(\frac{T_r}{T_\infty} - 1\right) \tag{4}$$

$$\gamma = \sqrt{P_r} = .851 \tag{5}$$

$$\mu = 2.270 \times 10^{-8} \frac{T^{3/2}}{T + 198.6} \tag{6}$$

This solution is based on the laminar Blasius result (29, chapter VII) in conjunction with Eckert's (30) compressibility transformation. This option permits an assessment of the reduction in skin friction drag if laminar flow can be maintained for the specified extent. It does not establish the likelihood that such a condition will be realized in practice or to what extent with the following exception.

FLAT PLATE NATURAL

$$R_{\theta_{TRAN}} = R_{\theta_{INST}} + \Delta R_\theta \tag{7}$$

$$R_{\theta_{INST}} = 163 \tag{8}$$

$$\Delta R_\theta = f_1(\Pi) \tag{9}$$

$$R_{x_{TRAN}} = (R_{\theta_{TRAN}} / .664)^2 / C^* \tag{10}$$

SMOOTH

$$R_{x_{TRAN}} = f_2(R_k)\, R_{x_{TRAN_{SMOOTH}}} \tag{11}$$

$$R_{\theta_{TRAN}} = .664 \sqrt{R_{x_{TRAN}} \cdot C^*} \tag{12}$$

ROUGH ($K_S > 70$)

These techniques have been taken from Schlicting (29, chapters XVI and XVII). The functions of f_1 and f_2 which relate the effect of freestream turbulence intensity as the difference between the transition and critical Reynolds number and the effect of roughness on smooth flat plate transition are figures 16.21 and a flat plate normalized version of 17.28, respectively.

The flat plate natural transition option is an oversimplified description of what actually takes place as a result of the neglect of pressure gradient and three dimensional crossflow vorticity effects.

TURBULENT

A smooth and distributed rough surface option have been provided in the analysis. In either case, the solution is initialized by matching the momentum thickness at the transition point produced by the laminar/transition solution. That is, an effective origin (commonly referred to as a virtual origin) is established for the turbulent analysis.

SMOOTH

$$C_F R_{\Delta X} = 2 R_{\Theta_{TRAN}} \tag{13}$$

$$R_{\Delta X} = C_F R_{\Delta X} / C_F \; ; \; C_F \text{ FROM EQ. 18 FOR KNOWN } C_F R_{\Delta X} \tag{14}$$

$$\Delta X = R_{\Delta X} / R \tag{15}$$

$$l = L - X_{TRAN} + \Delta X \tag{16}$$

$$R_l = R \cdot l \tag{17}$$

$$\frac{.242 (\sin^{-1}\alpha + \sin^{-1}\beta)}{\left(\frac{\gamma-1}{2} M_\infty^2 C_F'\right)^{1/2}} = \log_{10} C_F' R_l - w \log_{10} T_T/T_\infty \tag{18}$$

$$C_F = \frac{2\Theta_{X\to\infty}}{L} = \frac{2\Theta_{TE}}{l}\frac{l}{L} = C_F'\frac{l}{L} \tag{19}$$

where

$$X_{TRAN} = R_{X_{TRAN}} / R \tag{20}$$

$$\alpha = (2A^2 - B) / \sqrt{B^2 + 4A^2} \tag{21}$$

$$\beta = B / \sqrt{B^2 + 4A^2} \tag{22}$$

$$A^2 = \frac{\gamma - 1}{2} M_\infty^2 \frac{T_\infty}{T_r} \tag{23}$$

$$B = \left(1 + \frac{\gamma - 1}{2} M_\infty^2\right) \frac{T_\infty}{T_r} - 1 \tag{24}$$

$$\gamma = .88 \tag{25}$$

$$\omega = .76 \tag{26}$$

The compressible turbulent flat plate method used here is that proposed by Van Driest (31) based on the Von Karman mixing length hypothesis in conjunction with the Squire-Young formulation for profile drag (29, chapter XXIV) as applied to a flat plate.

DISTRIBUTED ROUGH

$$\Delta X_1 = X_{TRAN} \tag{27}$$

$$C_{F_i} = \left(1.89 + 1.62 \log_{10} \frac{\Delta X}{K_S}\right)^{-2.5} / \left(1 + r \frac{\gamma - 1}{2} M_\infty^2\right) \tag{28}$$

$$(R_{\Delta X})_{i+1} = 2 R_{\theta_{TRAN}} / C_{F_i} \tag{29}$$

$$\Delta X_{i+1} = (R_{\Delta X})_{i+1} / R \tag{30}$$

$$l = L - X_{TRAN} + \Delta X \tag{31}$$

$$C_F' = \left(1.89 + 1.62 \log_{10} \frac{l}{K_S}\right)^{-2.5} / \left(1 + r \frac{\gamma - 1}{2} M_\infty^2\right) \tag{32}$$

$$C_F = C_F' \frac{l}{L} \tag{33}$$

$$C_F = MAX.\left(C_F/_{SMOOTH}, C_F/_{ROUGH}\right) \tag{34}$$

The turbulent flat plate method used here is that of Schlicting (29, chapter XXI) which is based on a transposition of Nikuradse's densely packed sand grain roughened pipe data. The effect of compressibility is due to the reduction in density at the wall as proposed by Goddard (32). The selection of the equivalent sand grain roughness for a given manufacturing surface finish is made with aid of Table I which was taken from Clutter(34).

TABLE I

Type of Surface	Equivalent Sand Roughness k (inches)
Aerodynamically smooth	0
Polished metal or wood	$0.02 - 0.08 \times 10^{-3}$
Natural sheet metal	0.16×10^{-3}
Smooth matte paint, carefully applied	0.25×10^{-3}
Standard camouflage paint, average application	0.40×10^{-3}
Camouflage paint, mass-production spray	1.20×10^{-3}
Dip-galvanized metal surface .	6×10^{-3}
Natural surface of cast iron	10×10^{-3}

THICKNESS CORRECTIONS

The foregoing evaluations produce an estimate of the shearing forces on a flat plate (at zero angle of attack) for a variety of conditions. As an actual aircraft has a nonvanishing thickness, an estimate of pressure gradient effects on skin friction and boundary layer displacement pressure drag losses is required. A common procedure for accomplishing this and the one which will be used here is based on nonlifting experimental correlations for symmetric two dimensional airfoils and axisymmetric bodies. The following relations derived by Hoerner (33, chapter VI) are used respectively.

$$K = \frac{C_d}{2C_f} = 1 + K_1 \frac{t}{c} + 60\left(\frac{t}{c}\right)^4 \tag{35}$$

$$K = \frac{C_D}{C_f} = 1 + 1.5\left(\frac{d}{L}\right)^{3/2} + 7\left(\frac{d}{L}\right)^3 \tag{36}$$

Hoerner recommends $K_1 = 2$ for airfoils with maximum thickness at 30 percent chord and $K_1 = 1.2$ for NACA 64 and 65 series airfoils. In this regard, the best information available to an analyst for his particular contour should be used. This is especially true for modern high performance shapes such as the supercritical airfoil, etc.

TOTAL VISCOUS DRAG

An aircraft total viscous drag coefficient is estimated by a sum of the preceding analysis over all components (i.e. wing, fuselage, vertical tail, etc.). That is

$$C_D = \sum_{J=1}^{N} C_{F_J} \left(\frac{S_J}{S_{REF}} \right) K_J \qquad (37)$$

The component length used in the calculation of the skin friction coefficient is the mean aerodynamic chord for planar components or segments thereof and the physical length for bodies and nacelles.

SKIN FRICTION NOMENCLATURE

C_d	section drag coefficient
C_D	drag coefficient
C_{D_F}	flat plate skin friction drag coefficient
C_F	flat plate average skin friction coefficient
C^*	$\frac{\mu^*}{\mu_\infty} \frac{T_\infty}{T^*}$
K_s	equivalent distributed sand grain height
ℓ	effective length - ft
L	geometric length - ft
L/d	body fineness ratio
M	Mach number
Pr	Prandtl number
r	recovery factor
R	unit Reynolds number, U_∞/ν_∞ ft^{-1}
$R_{[\,]}$	Reynolds number based on [ ]
$\mathcal{R}$	gas constant, 1716 $ft^2\,{}^\circ R/sec$
S	surface area - ft^2
T	static temperature - $^\circ R$
T_r/T_∞	recovery temperature ratio, $1+ r \frac{\gamma-1}{2} M_\infty^2$
t/c	airfoil thickness ratio
U	velocity, $\sqrt{\gamma RT}\, M$ - ft/sec
x	longitudinal distance from beginning of component, ft
γ	ratio of specific heats
θ	boundary layer momentum thickness, ft

μ	absolute viscosity, lbf-sec/ft^2
ν	kinematic viscosity, μ/ρ ft^2/sec
ρ	density, P/RT ,lbf- sec^2/ft^4
τ	turbulence intensity

SUBSCRIPTS

i	iteration number
INST	instability
j	component number
r	recovery
TRAN	transition point
∞	free stream

SUPERSCRIPTS

	property based on effective origin
*	Eckert reference temperature condition

REFERENCES

1. Thwaites, B., Incompressible Aerodynamics. Oxford: Clarendon Press (1960)

2. Kuchemann, D. and J. Weber, The Subsonic Flow Past Swept Wings at Zero Lift Without and With Body, R&M No. 2908, (1956)

3. Weber, J., The Calculation of the Pressure Distribution Over the Surface of Two-Dimensional and Swept Wings With Symmetrical Aerofoil Sections, R&M No. 2918, (1956)

4. Brebner, G.G., The Calculation of the Loading and Pressure Distribution on Cranked Wings, R&M No. 2947, (1953)

5. Hunton, L.W. and J.K. Dew, The Effects of Camber and Twist on the Aerodynamic Loading and Stalling Characteristics of a Large-Scale 45° Swept-Back Wing, NACA RM A50J24, (1951)

6. Method for Predicting the Pressure Distribution on Swept Wings With Subsonic Attached Flow, British Transonic Data Memorandum 6312, (1963)

7. Liepmann, H.W. and A. Roshko, Elements of Gasdynamics. New York: John Wiley and Sons (1957)

8. Tulinius, J., Theoretical Prediction of Wing-Fuselage Aerodynamic Characteristics at Subsonic Speeds, NA-69-789, (To be published)

9. Kojima, J. Instructions for Use of the Douglas-Neumann Potential Flow Program for Axisymmetric Flow, NA-65-385, (1965)

10. Weber, J. and G. G. Brebner, Low-Speed Tests on 45-deg. Swept-Back Wings, R & M No. 2882, (1958)

11. Tulinius, J., Theoretical Prediction of Symmetrical Thick Wing Surface Pressures for Zero Angle of Attack and Subsonic Speeds, NA-70-374, (1970)

12. Blenk, H., Der Endecker Als Tragende Wirbelflache, Z.A.M.M., Vol. 5, (1925)

13. Betz, A., The Theory of Aerofoils, Proceedings of the German Scientific Society for Aeronautics, No. II, (1920)

14. Birnbaum, W., Die Tragende Wirbelflache Als Hilfsmittel Zur Behandlling Des Zebenen Problems Der Tragflugeltheorie, Z.A.M.M., Vol. III, (1923)

15. Wagner, S., On the Singularity Method of Subsonic Lifting-Surface Theory, A.I.A.A. Paper No. 69-37, (1969)

16. Falkner, V. M., The Calculation of Aerodynamic Loading on Surfaces of any Shape, R & M 1910

17. Kuchemann, D., The Distribution on Lift over the Surface of Swept Wings, The Aeronautical Quarterly, Vol. IV, (1953)

18. Goldstein, S., Approximate Two-Dimensional Aerofoil Theory, A.R.C. Technical Report, C.P. No. 68, (1951)

19. Tulinius, J., Subsonic Aerodynamic Load Theories for Wings of Polygonal Planform, NA-66-781, (1966)

20. Der, E. S., and M. Nagai, A Controlled Deviation Interpolation Method (Codim), NA-60-1604, (1960)

21. Householder, A. S., Unitary Triangularization of a Nonsymmetric Matric, J. Assoc. Comp. Mach. 5, (1958).

22. Kuchemann, D., Progress in Aeronautical Sciences, Pergramon Press, Vol. 8, (1967).

23. Tulinius, J., Theoretical Prediction of Thick Wing Aerodynamic Characteristics at Subsonic Speeds, NA-70-104, (1970).

24. Tulinius, J., Derivation of Thick Wing and Pylon-Fanpod-Nacelle Aerodynamic Influence Equations, NA-71-23, (1971).

25. Sears, W.R., General Theory of High Speed Aerodynamics, pp 222,-229, Princeton University Press, 1954.

26. Ashley, H. and Landahl, M., Aerodynamics of Wings and Bodies, p 134-136, Addison Wesley, 1965.

27. Eminton, E., "On the Minimization and Numerical Evaluation of Wave Drag," RAE Report Aero 2564, 1955.

28. Eminton, E., "On the Numerical Evaluation of the Drag Integral," British R&M 3341, 1963.

29. Schlichting, H., Boundary Layer Theory, Fourth Edition, McGraw-Hill Book Co. Inc., 1958.

30. Eckert, E.R.G., "Survey of Heat Transfer at High Speed," WADC TR-54-70, 1954.

31. Van Driest, E.R., "The Problem of Aerodynamic Heating," Aeronautical Engineering Review, October 1956, pp. 26-41.

32. Goddard, F.E., "Effect of Uniformly Distributed Roughness on Turbulent Skin Friction Drag at Supersonic Speed," Journal Aero/Space Sciences, January 1959, pp.1-15,24.

33. Hoerner, S.F., Fluid Dynamic Drag, Published by Author, 148 Busteed Drive, Midland Park, New Jersey, 1958.

34. Clutter, D.W., "Charts for Determining Skin Friction Coefficients on Smooth and Rough Plates at Mach Numbers up to 5.0 With and Without Heat Transfer," Douglas Aircraft Report No. ES-29074, 1959.

35. Labrujere, Th.E., et al, "An Approximate Model for the Determination of the Pressure Distribution on Wings in the Lower Critical Speed Range," NLR MP68005U, 1968.

36. Goebel, T.P. Wind Tunnel Data Analysis for the NR/VTOL 0.06-Scale Model, NA-72-17-2, (1972).